

General Disclaimer

One or more of the Following Statements may affect this Document

- This document has been reproduced from the best copy furnished by the organizational source. It is being released in the interest of making available as much information as possible.
- This document may contain data, which exceeds the sheet parameters. It was furnished in this condition by the organizational source and is the best copy available.
- This document may contain tone-on-tone or color graphs, charts and/or pictures, which have been reproduced in black and white.
- This document is paginated as submitted by the original source.
- Portions of this document are not fully legible due to the historical nature of some of the material. However, it is the best reproduction available from the original submission.

NATIONAL AERONAUTICS AND SPACE ADMINISTRATION

Technical Memorandum 33-434

Mariner Venus/Mercury 1973 Study



FACILITY FORM 602

N70-10224 (ACCESSION NUMBER)	1 (THRU)
144 (PAGES)	1 (CODE)
CE#106557 (NASA CR OR TMX OR AD NUMBER)	31 (CATEGORY)

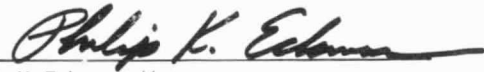
**JET PROPULSION LABORATORY
CALIFORNIA INSTITUTE OF TECHNOLOGY
PASADENA, CALIFORNIA**

August 1, 1969

NATIONAL AERONAUTICS AND SPACE ADMINISTRATION

Technical Memorandum 33-434

Mariner Venus/Mercury 1973 Study



P. K. Eckman, Manager
Mariner Venus/Mercury
1973 Study



C. W. Cole, Manager
Advanced Planetary
Missions Technology

JET PROPULSION LABORATORY
CALIFORNIA INSTITUTE OF TECHNOLOGY
PASADENA, CALIFORNIA

August 1, 1969

Acknowledgment

The principal contributors to this document include:

T. H. Bird	D. B. Nash
Dr. R. D. Bourke	M. V. Ohanesian
A. P. Bowman	W. A. Owen
W. F. Carroll	G. D. Pace
L. A. Couvillon	Dr. R. G. Ross
Dr. P. K. Eckman	D. K. Rubin
A. R. Eisenman	M. B. Simes
J. A. Fehsenfeld	F. L. Sola
G. E. Fleischer	J. M. Spiegel
G. W. Garrison	Dr. C. H. Stembridge
H. H. Gernandt	J. H. Stevens
T. E. Gindorf	F. M. Sturms
W. A. Hagemeyer	M. Swerdling
M. A. Herwald	D. Ting
W. J. Lane	J. L. Wolfe
D. R. Margetts	W. R. Woods
M. L. Moore	

Special acknowledgment should be given to C. A. Duarte and S. I. Plake for editorial assistance; F. J. Licher, art production; R. T. Chandler for typographic liaison; and especially to F. M. Hayward, who edited and supervised production of this document under strenuous circumstances.

Contents

I. Introduction	1
II. Mission Summary	2
A. Mission Description	2
B. Capabilities Summary	2
III. Objectives and Constraints	3
IV. Science Objectives	4
A. Specific Objectives—Mercury	4
B. Specific Objectives—Venus	5
C. Interplanetary Measurements	6
D. Two-Launch Mission Considerations	6
V. Mission Analysis	6
A. Introduction	6
B. Interplanetary Trajectories	7
C. Near-Planet Geometry	13
D. Navigation and Guidance	23
E. Launch Vehicle System	25
VI. Mission Description	29
VII. Spacecraft Description	32
A. Introduction	32
B. Configuration	32
C. <i>Mariner Venus/Mercury 1973</i> Baseline Sequence of Events	43
D. Weight Summary and Subsystem Development Status	47
E. Power Requirements and Subsystem Description	47
F. Telecommunications Subsystem Description and Performance	48
G. Data Handling	57
VIII. Spacecraft Subsystems Description	70
A. Structure	70
B. Radio Frequency Subsystem	72
C. Flight Command Subsystem	74

Contents (contd)

D. Power Subsystem	75
E. Central Computer and Sequencer	78
F. Telemetry Subsystem	85
G. Flight Control Subsystem	86
H. Pyrotechnic Subsystem	92
I. Propulsion Subsystem	96
J. Thermal Control Subsystem	98
K. Mechanical Devices	101
L. Data Storage Subsystem	102
M. Science Data Subsystem	102
N. Science Instrument Subsystems	104
Appendix A. 1970–1980 Mercury Opportunities (Direct and Venus Swingby)	109
Appendix B. Venus Entry Considerations	111
I. Introduction	111
II. Geometrical Constraints	111
III. Entry Heating and Aeroshell Considerations	112
IV. Flight Test Considerations	114
V. Summary of Mission Characteristics	115
Appendix C. Alternative Maneuver Turn Sequence	117
I. Introduction	117
II. Thermal Problems	117
III. Roll-A Turn Sequence Description	118
IV. Comparison of Turn Sequences	118
V. Maneuver Turn Sequence Tradeoff	121
VI. Conclusion	122
Appendix D. Alternate Solar Panel Configurations	123
I. Introduction	123
II. Types of Mirror Mosaic Designs	123
III. Alternatives to Mirror Mosaic Panels	123
IV. Tiltable Solar Panels	124

Contents (contd)

Appendix E. Alternate High-Gain Antenna Positioning for Extended Missions	127
I. Introduction	127
II. Circular 40-in. Paraboloid	127
III. Elliptical 33- X 66-in. Paraboloid	127
Appendix F. Solar Simulator Requirements	131
Nomenclature	134
References	136

PRE-SEPARATION (STOWED)

POST-SEPARATION

VENUS ENCOUNTER

MERCURY ENCOUNTER

Mariner Venus/Mercury 1973 Spacecraft (baseline configuration)

Mariner Venus/Mercury 1973 Study

I. Introduction

In the Fall of 1968, the NASA Office of Space Science and Applications (OSSA) requested the Advanced Planetary Missions Technology (APMT) Office of the Jet Propulsion Laboratory (JPL) to assess the feasibility of performing a 1973 Mercury flyby mission by way of Venus using the *Atlas/Centaur* launch vehicle.¹

The purpose of the study was to determine:

- (1) The gross capabilities and limitations of a 1973 Mercury flyby of the *Mariner* class.
- (2) The feasibility of Venus/Mercury trajectories other than the 1973 opportunity, and of direct Mercury trajectories.
- (3) The practicality of including a Venus entry probe with the 1973 mission.
- (4) The pacing state of the art and advanced development areas requiring early attention and support.

¹Letter to C. W. Cole (JPL) from N. W. Cunningham (NASA, Code SL), October 3, 1968.

The study benefited from substantial previous JPL work in flight mechanics, scientific objectives, and overall mission studies (Refs. 1-5).

The purpose of this report is to:

- (1) Document the work of the *Mariner* Venus/Mercury Study Team through June 1969.
- (2) Provide a basis for NASA mission planning in conjunction with members of the scientific community.
- (3) Provide the Project Office (if program approval is granted) with a mission description for purposes of planning, staffing, and resource allocation.
- (4) Identify critical research and advanced development problems.

The spacecraft configurations presented here are typical of those which might be flown for this mission. The reader is cautioned, however, that many subsystem interfaces and interactions have not yet been investigated in detail, so that alternate mechanizations may be required in some instances to satisfactorily accomplish system requirements. Some of these alternate approaches are discussed in the Appendices.

II. Mission Summary

The bulk of this report describes what is termed a "baseline" mission and a "baseline" spacecraft. Many deviations from the baseline mission, such as the Mercury arrival date, aiming point, and encounter geometry are possible. Some of these alternatives are described herein. Certain alternative spacecraft mechanizations and subsystem designs have also been considered in the study. Although some of these are mentioned in the text, most of these variations are discussed in the Appendices. Unless otherwise noted, all statements refer to the baseline mission and spacecraft configuration.

A. Mission Description

This section describes the characteristics of the 1973 Venus/Mercury mission considered in this study. A spacecraft is launched by an *Atlas (SLV-3C)/Centaur D* launching vehicle and placed on a trajectory that uses a gravity assist at Venus to carry it on to Mercury. The spacecraft is injected toward Venus from an earth parking orbit during October–November 1973. Three trajectory correction maneuvers are required. The first correction is performed approximately 8 days after injection to remove trajectory dispersions introduced by the launch vehicle guidance system. A second correction is performed 3 days before Venus encounter² to remove execution errors of the first maneuver.

For the baseline mission, Venus encounter occurs in the period February 3–4, 1974. At this time, the spacecraft is 0.70 AU from the sun and 43×10^6 km from earth. Earth occultation always occurs (i.e., the spacecraft passes behind Venus as seen from earth). The distance of closest approach to Venus ranges from 3600 to 5100 km.

A third trajectory correction is performed approximately 8 days after Venus encounter to remove errors due to navigation uncertainties at the time of the second maneuver. Sufficient accuracy is achievable to allow a variety of specific encounter geometries to be considered at Mercury, which satisfy a wide range of science objectives.

The baseline mission encounter at Mercury is a "dark-side" equatorial passage which provides both sun and earth occultation for the spacecraft. Encounter occurs during the period March 19–21, 1974; at this time, the probe is 0.47 AU from the sun and 132×10^6 km from earth. Encounters at Mercury are characterized by very high approach velocities, generally in the range of 13.5

13.5 km/sec. An attractive alternative encounter, a south polar pass which provides earth occultation, is described later in the text (section V-C).

B. Capabilities Summary

Figure 1 shows an isometric view of the baseline spacecraft configuration described in this report. The space-

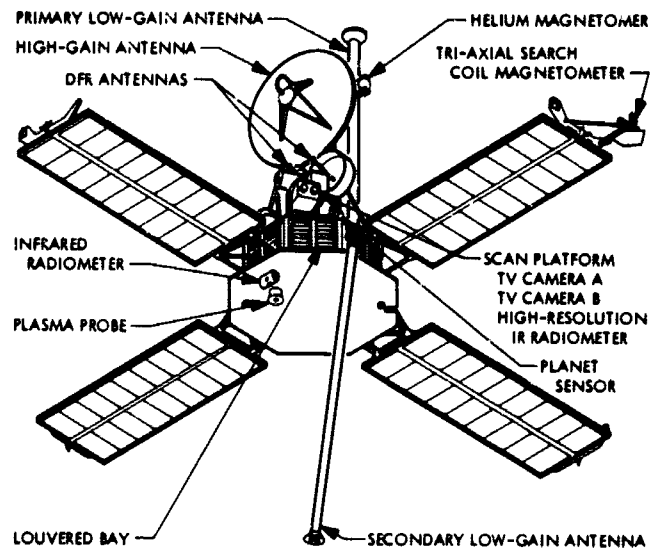


Fig. 1. Baseline spacecraft configuration

craft bears distinct resemblance to previous *Mariner* spacecraft from which it is derived. Four solar panels are mounted on outriggers to decouple them thermally from the spacecraft bus. Internal temperature of the bus is regulated by means of louvers on six of the bus' eight bays. One of the remaining bays is occupied by a liquid monopropellant propulsion subsystem, and the other has a high-emittance surface for maximum heat rejection. A sunshade and thermal blankets shield the spacecraft bus and most of the instruments. Attitude control torques during the cruise portion of the mission are provided by cold gas jets located at the ends of the solar panels. Two low-gain antennas provide communications coverage throughout the mission for all spacecraft attitudes. A high-gain directional antenna, designed to provide pointing toward earth with one degree of freedom, is shown at the top of the figure. When the solar panels are folded to their launch position, the spacecraft fits within a standard *Atlas/Centaur Surveyor* nose fairing.

Typical science instruments are shown in this configuration. On the sunlit side of the spacecraft are a plasma probe, which looks directly toward the sun, and

²Encounter (*E*) is defined as the time of closest approach.

a dark-side infrared radiometer (IRR) which is kept covered until the spacecraft reaches the vicinity of Mercury. A modest scan platform with two degrees of freedom carries two television (TV) cameras and a high resolution infrared radiometer (HRIR). Two dual-frequency receiver (DFR) antennas are mounted collinear with the high-gain antenna, and two magnetometers are mounted as far distant from the bus as possible.

Typical capabilities of this configuration are listed in Table 1.

Table 1. Mariner Venus/Mercury 1973 capabilities (baseline configuration)

Spacecraft injected weight	750 lb using Atlas (SLV-3C)/Centaur D (1130 lb allowable)
Science	8 experiments and 90 lb (6 are body fixed and 2 are on a two degrees-of-freedom scan platform)
Data storage	1.8×10^4 bits (32 pictures with other science). Three or more record/playback cycles at Mercury. Core buffer used for critical storage of fields and particles
Data rates	2 to 16.2 kbits/sec playback at encounter (high rate block coding), $8 \frac{1}{2}$ or $33 \frac{1}{2}$ bits/sec real-time engineering, $166 \frac{2}{3}$ bits/sec real-time encounter science
Antennas	One 40-in. steerable antenna and two low-gain antennas
RF power output	9 and 18 W
Altitude control	3-axis cold gas system using the sun and Canopus for reference.
Trajectory correction	4-maneuver capability with a total $\Delta v \approx 65$ m/sec
Spacecraft power	Solar panel 375 W near earth, 550 W near Mercury; 1350 W-hr battery capacity
Mission duration	20 days beyond Mercury encounter

III. Objectives and Constraints

The primary mission objective is a 1973 flyby investigation of Mercury using a Venus gravity-assist enroute. The investigation of Venus and interplanetary space is a secondary objective, primarily limited to those observations that can be performed with the Mercury science instruments.

At the outset of this study, certain constraints and design assumptions were made:

- (1) The launch vehicle is the Atlas (SLV/3)/Centaur D with a standard Surveyor aerodynamic fairing.
- (2) A single launch mission is assumed.

- (3) No planetary quarantine restrictions are assumed since the mission considered is several years distant, and present policy may well be modified in the meantime.
- (4) The spacecraft configuration is to make maximum use of Mariner Mars 1969 and Mariner Mars 1971 subsystem designs and technology.
- (5) The spacecraft is to be fully automatic, capable of performing all required functions, except for ground-based quantitative commands for trajectory correction maneuvers.
- (6) The mission extends from launch at earth through 20 days beyond Mercury encounter.
- (7) The Mercury science payload is based upon that suggested by NASA Headquarters guidelines.

The launch vehicle has a payload capability which exceeds that required by the spacecraft to support the sample science payload by at least 300 lb (sections V-B and V-E). The spacecraft configuration must fit within the allowable physical envelope of the launch vehicle; however, this constraint can be accommodated readily with minimum folding of the configuration.

Although only a single-launch mission is described, the indicated launch period of 25 days is probably sufficient to assure two launches, if desired. However, even for a two-launch mission with widely separated Mercury encounter dates, spacecraft launched anytime within the launch period must encounter Venus within a 4-day period in February 1974 (section V-B); the mission operations problems of conducting two planetary encounters and four trajectory maneuvers within 2 weeks have not been examined.

The requirement that the spacecraft be fully automatic is part of a larger goal, a design philosophy, embodied in all Mariner missions to date: that, wherever possible, every spacecraft action necessary for successful completion of the mission have at least one alternate functional mechanization. Thus, assumption (5) allows the spacecraft's receiver or command decoder to fail anytime after the last trajectory correction without causing loss of the mission.

The assumption that the mission end 20 days after Mercury encounter, while arbitrary, is more than sufficient to allow return of all Mercury science data. There is nothing inherent in the environment, or the spacecraft's trajectory or design, which prevents its continued opera-

tion beyond this time if there is reason to extend the mission (Appendix E). The mission could be extended to continue measurement of interplanetary fields and particles and to perform gravitational theory tests near solar conjunction.

The proposed inclusion of magnetometer instruments adds a general constraint that the spacecraft be magnetically clean. This constraint implies a number of special requirements such as material substitutions, and possible redesign, relocation or shielding of some components, since the *Mariner Mars 1969* spacecraft carried no magnetometers, nor will the *Mariner Mars 1971*.

Finally, the science payload incorporated in this study should be clearly understood as only an example. The payload suggested in the NASA study guidelines was described only as "typical." The instruments used for the spacecraft design were used because many of the requirements of these instruments were understood or could easily be developed at the beginning of the study, and because these instruments provided a broad test of spacecraft capability.

IV. Science Objectives

A. Specific Objectives—Mercury

Mercury has received relatively little observational study because of its small size and close proximity to the sun. However, for these reasons, it is one of the most important planets for more detailed study to obtain data bearing on the origin and history of the planetary solar system. (Ref. 6).

The basic scientific questions regarding Mercury are concerned with its bulk density and composition, and internal structure. These questions are discussed below in approximate order of their scientific importance. From these questions are derived a list of measurements that can be made by the type of flyby mission discussed in this report. The material contained in this section represents an updating of similar data presented in Ref. 7.

1. Average density of the planet. The latest reported density of Mercury is 5.44 g/cm^3 (Ref. 8). Since the size of the planet is too small and thus its internal pressure too low to induce low-to-high density phase changes, the high density of Mercury can be interpreted roughly in terms of chemical composition (Ref. 9). An uncompressed density of 5.44 g/cm^3 implies large amounts of free iron (Ref. 10). If the apparent high density of

Mercury is substantiated, then either (1) iron enrichment occurred by solar heating in the inner solar system matter prior to its accretion into planets, or (2) the sun had no influence, and the circum-solar cloud was chemically heterogeneous at time of planetary accretion. If Mercury contains free iron, this lends support to the theory that the earth has an iron core.

The average density is determined from the mass and average diameter of the planet. The present data on the mass of Mercury are internally consistent only to within 2% (Refs. 8 and 11). Analysis of the trajectory of the flyby spacecraft will greatly improve the mass determination (Ref. 12) and should resolve any questions about systematic errors in mass determinations based on radar ephemeris measurements from earth.

Optical results indicate the average diameter of the planet is not known to better than approximately 10% (Ref. 13). Radar results indicate an accuracy of 0.1% assuming no systematic error. Imaging from a flyby spacecraft should permit determination of the diameter to better than 1%. Occultation measurements will independently give the radius of the planet at the points of entry and emergence, both for the sun and earth occultations. These radii, however, may not exceed the accuracy of future earth-based radar measurements made prior to the 1973 flyby.

2. Mass distribution. Since the apparent high density of Mercury implies a high iron content, determining the internal mass distribution will indicate the extent to which the planet has differentiated, and thus to what extent surface material represents the average composition.

Mass distribution is determined from principal moments of inertia which are calculated from determination of the angular rotation rate, mass, radii, and the dynamical flattening of the planet. Search for a magnetic field may be inconclusive to establish the existence of a liquid core since the rotation rate of the planet may be too low to produce a field from a liquid core, even if one is present.

The determination of the mass distribution of Mercury probably cannot be obtained by this mission. An orbiting spacecraft is indicated.

3. Shape of the planet. The shape or oblateness indicates two things about the planet: (1) inequalities of figure not attributable to rotation indicate the rigidity of the interior; e.g., whether molten or solid; (2) large asymmetries of figure may indicate a fission origin, i.e.,

that Mercury separated from a differentiated or otherwise non-uniform parent object.

Shape can be best determined by both polar and equatorial radius measurements. (The baseline flyby trajectory by its occultation measurements will give only equatorial radii.) Determination of shape is an important factor supporting a second (polar pass) mission. Whole disk images from the TV may indicate asymmetry or bulges. A quantitative assessment of this measurement should be made.

4. Composition of the surface. The gross chemical and mineralogical composition of the surface is related to the average density and mass distribution in that a highly differentiated planet will have a surface composition quite different than the bulk planetary composition. If the surface composition is high in potassium, uranium, and thorium, it would imply low iron in the surface and high iron toward the core, both of which in turn indicate differentiation since the apparent high bulk density requires abundant iron in the planet as a whole.

Some indication of the gross surface elemental composition can be obtained from a flyby by measurement of characteristic gamma or X-radiation emitted by radioactive isotopes or produced by solar excitation of surface elements if the atmosphere is < 1 mb and background from intense solar irradiation can be accounted for. The gross mineralogical composition can be inferred from spectral measurements of the visible and near-IR reflectance.

5. Surface morphology. Determining the gross morphological and topographical nature of the surface of Mercury should indicate directly the type and extent of internal and external processes that have operated on the planet. For example, a highly cratered surface similar to the moon would suggest: (1) a tectonically inactive planet since accretion, (2) little differentiation, and (3) absence of an iron core. Whereas basin, continent, and mountain structures, as on earth, would suggest active tectonic activity and indicate that differentiation and possible core formation may have gone on after accretion of the planet. Possible surface fractures associated with thermal bulges ("hot poles") will be sought.

Surface morphology will best be visible in television coverage of the terminator regions. Both polar and equatorial coverage are desired.

6. Atmosphere composition and density. There is no evidence for an atmosphere on Mercury, only estimates of a probable upper limit of about 1 mb. The mass of

Mercury is too low to retain a significant atmosphere because of intense solar heating and solar wind sweeping. Any possible atmosphere, however, may be interpreted in terms of (1) present and past outgassing history of Mercury and (2) solar wind interactions.

Photometry at the limb of the planet at large phase angles, in the violet near-ultraviolet spectral region, would be a sensitive test of the presence of an atmosphere, reducing the least upper bound on surface pressure as inferred from terrestrial measurements. Comparison of the amount of polarization in the near-UV on the limb and on the center of the disk can yield a detection threshold approaching 10^{-5} bars. Radio frequency occultation measurements can detect the presence of an ionosphere with great sensitivity.

In summary, this baseline Mercury mission can make important contributions toward answering many questions bearing on the origin of the terrestrial planets. The following are useful measurements and quantities to determine: mass, radii, shape, magnetic field, surface morphology, surface characteristics, and atmosphere density and composition.

B. Specific Objectives—Venus

Venus is similar to the earth in size and density—hence it is reasonable to presume some similarity in gross composition. The atmospheric conditions on Venus, however, are very different from those of earth and we naturally suppose the surface conditions to be different. Other questions regarding Venus concern the bulk properties of the planet and are similar to those discussed above for Mercury.

Although such basic data as the atmospheric composition, pressure, temperature profiles, and surface temperature are known approximately, some of the most important questions to be answered by observation during a flyby mission concern the surface morphology, the cloud composition, and the structure and composition of the outermost atmosphere.

1. Surface morphology. The nature of the solid surface of Venus is essentially unknown. Earth-based radar observations indicate a number of extensive features on the surface of the planet which give especially strong return signals. Such observations suggest that these are areas of high surface roughness, but nothing is known about their relative elevations. Some indication of extreme topographic variation was obtained by comparison of the results from *Venera 5* and *6*. Our thoughts on

these matters are of course speculation. Broad areas that have very different reflectivity may be found to be analogous to our (granodioritic) continents and (basaltic) ocean basins on earth. Correlation of large compositional domains such as these with elevation may reflect isostatic equilibrium or an approach to it. Planetary orogeny analogous to what is considered to represent sea-floor spreading on earth may be more obvious on Venus in the absence of an ocean. An important objective, therefore, is to determine the topography and reflectivity of the solid surface to a resolution of at least 100 m.

2. Distribution and composition of clouds. The measurements of *Mariner V* and *Venera 4, 5, and 6* have proven the atmosphere of Venus to be very extensive and quite opaque. Optical frequency measurements can only provide data from the uppermost layers of clouds and the thin atmosphere above them. Photography at several wavelengths, with a resolution of better than 1 km, should delineate structure in the upper clouds. Information on the nature of cloud particles could be constructed from cloud photometry which includes a wide range of wavelengths and those phase angles very difficult of access from earth (i.e., especially those near superior conjunction, phase angles 140-180 deg).

3. Outermost atmosphere. Determination of the outermost atmospheric temperature, density, and molecular weight are important boundary conditions on models of the Venus atmosphere. Ultraviolet and visible spectroscopy at good spectral and high spatial resolution would give much-needed data on the neutral and ionic composition from atmosphere in and above the uppermost haze or cloud layer. Such measurements, giving distribution of components, are difficult and in many cases impossible to carry out from present earth-based observations.

C. Interplanetary Measurements

The mission will offer the first fields and particles measurements in the region sun-ward of 0.7 AU. These measurements will provide a much greater range of relative solar distances over which solar wind, solar flare particles, and cosmic rays are measured, and also will enter a region where direct measurements can be compared with radio-astronomical indications of solar-corona properties.

The microstructure of the interplanetary magnetic field, its temporal and spatial variations, is of great interest. The existence of these variations is a direct consequence of the interaction between magnetic field and solar plasma,

making the measurement of the magnetic field a sensitive indicator of changes in the flow of the solar wind. Simultaneous direct measurements of plasma changes in direction, particle energy distribution (and mass distribution, if possible), would yield important information on shock wave propagation and other plasma phenomena. Correlation of particle behavior with solar coronal filament streaming should be easier at 0.7 AU than at larger distances from the sun.

D. Two-Launch Mission Considerations

The scientific value of a second launch during this opportunity may be examined relative to each of the planetology questions for Mercury as follows:

- (1) This mission will probably add little to the question of the mass.
- (2) The earth occultation will give radii at different points to compare with those radii determined by the first flight and thus give a measure of the flattening and inferences of internal mass distribution. This measurement is a unique contribution in that radii away from the equator cannot be determined with comparable precision by earth-based radar.
- (3) A thermal scan near the sunset terminator will give information on the thermal inertia and thus on the porosity of the surface material. This information would seem to be more supportive than of fundamental interest.
- (4) The strongest contribution of this mission would be to examine a different portion of the surface of Mercury. A different pass will allow systematic comparison of the imagery of areas which experience different thermal regimes. New information on the composition of the surface should also be obtained from a second flyby.
- (5) The question of an atmosphere would appear to be reasonably well resolved by the first mission.

The value of a second flyby in regard to Venus would be maximized if a different set of instruments were flown. If the same instruments were flown on a second spacecraft, the value, with respect to Venus, of a second mission is unknown.

V. Mission Analysis

A. Introduction

The opportunity to go to Mercury via a close encounter with Venus was first identified by Minovitch in Ref. 14.

There it was shown that the advantages of a Venus swingby trajectory were twofold: First, considerably lower launch energy is required than for direct missions to Mercury³, and second, close-up scientific investigations of Venus may be possible while in the vicinity of that planet. The 1973 Venus/Mercury opportunity is unique: in that year an *Atlas/Centaur* can launch a 1200-lb spacecraft to Mercury passing by Venus at an altitude of 1000 to 6000 km. Furthermore, a considerable range of arrival conditions is available at Mercury so that a variety of scientific measurements are possible. This section discusses the available possibilities for conducting a 1973

mission, the factors influencing trajectory selection, and the baseline mission design chosen.

B. Interplanetary Trajectories

1. *Characteristics of the opportunity.* Trajectory data for the 1973 Venus opportunity have been published previously by Sturms in Ref. 1 where the flyby of Venus was emphasized. Since emphasis of the current study is on Mercury, this report presents the trajectory information in a form more suitable for Mercury mission design. Figures 2-6 show the basic trajectory data.

³A comparison of requirements for direct versus swingby trajectories to Mercury is given in Appendix A.

Figure 2 shows contours of constant launch energy on a Mercury arrival date versus earth launch date grid. The

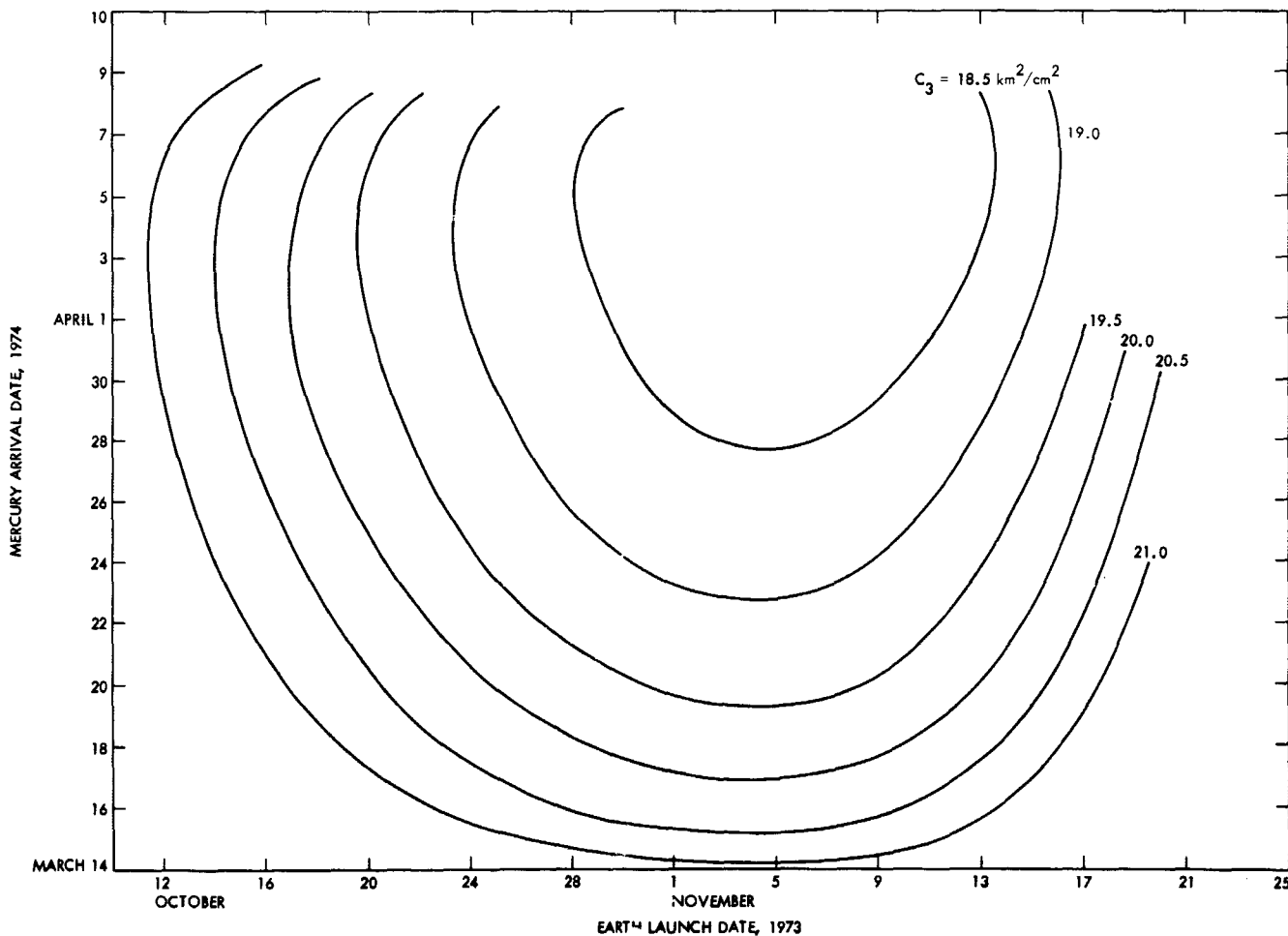


Fig. 2. Launch energy, C_3 , km^2/sec^2

launch energy (C_3) is defined as twice the energy per unit mass of the spacecraft at earth escape (in km^2/sec^2) and is related to the spacecraft weight that can be flown with the particular launch vehicle. For instance, an *Atlas-Centaur*⁴ can launch a spacecraft up to 1200 lb on a trajectory with $C_3 \leq 21 \text{ km}^2/\text{sec}^2$; hence this vehicle can launch a 1200-lb spacecraft on all combinations of launch and arrival dates inside the $C_3 = 21 \text{ km}^2/\text{sec}^2$ contour. Each pair of earth launch and Mercury arrival dates completely specify the flyby conditions at Venus; i.e., no flexibility in the Venus encounter is available. Figure 3 shows two of these conditions. The red curves, with contours of constant Venus arrival date, show that there

is a reasonably small spread in the date of Venus passage (February 2-7) corresponding to a large spread in Mercury arrival dates. The green curves show the altitude of closest approach at Venus (the radius is taken as 6200 km, a value known to be above the sensible atmosphere). This parameter represents a hard boundary to the available trajectories at zero altitude. A practical boundary is an altitude of 1000 km; below this value ground and quarantine requirements may be difficult to meet.

In Fig. 4 the red curves show contours of constant V_∞ (hyperbolic excess speed, km/sec) at Venus. The values of 8-9 km/sec are considerably greater than usually found at Venus-only missions; these high values bear

⁴Launch vehicle characteristics are discussed in detail in section V-E.

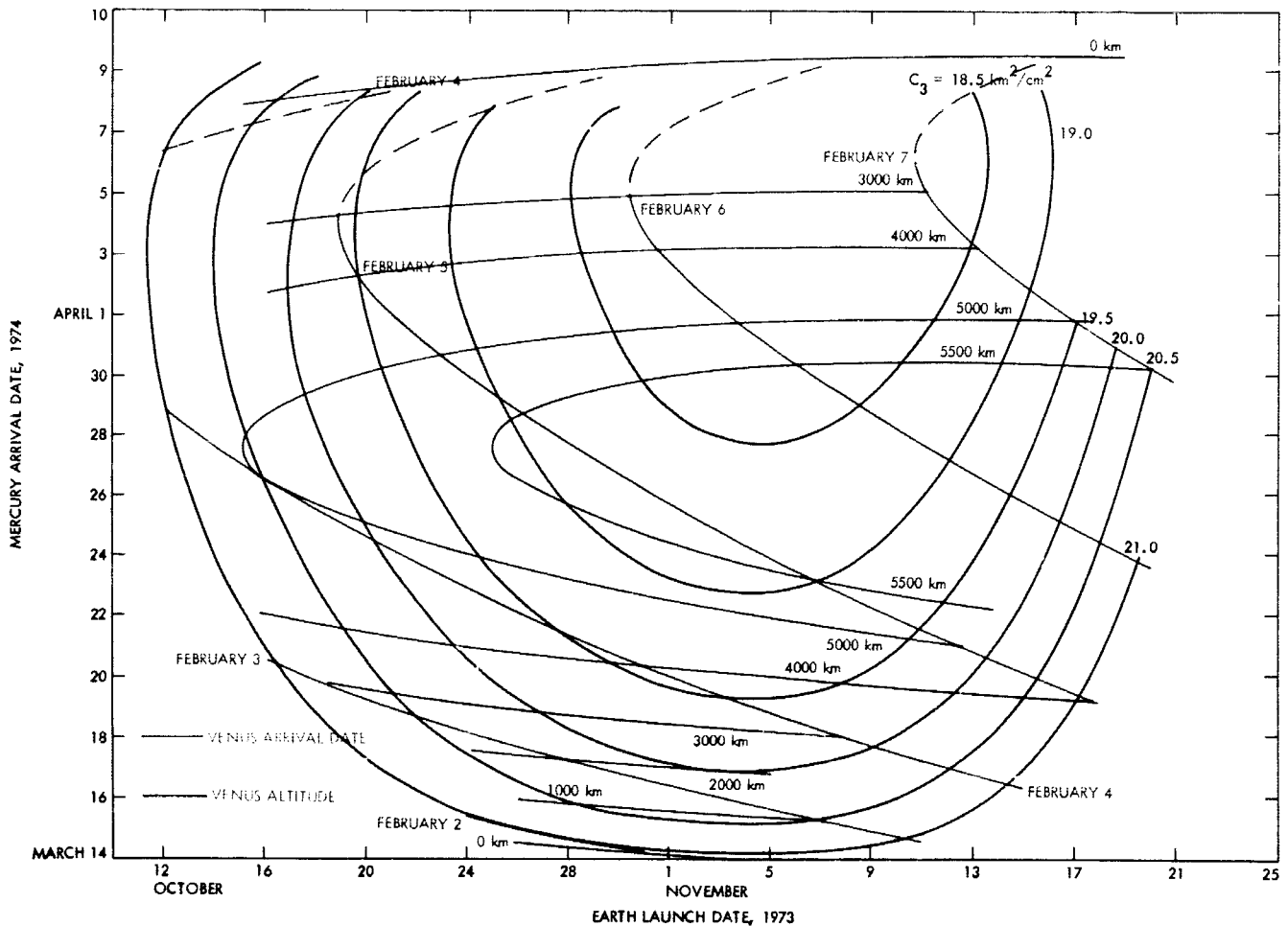


Fig. 3. Altitude at Venus and Venus arrival date

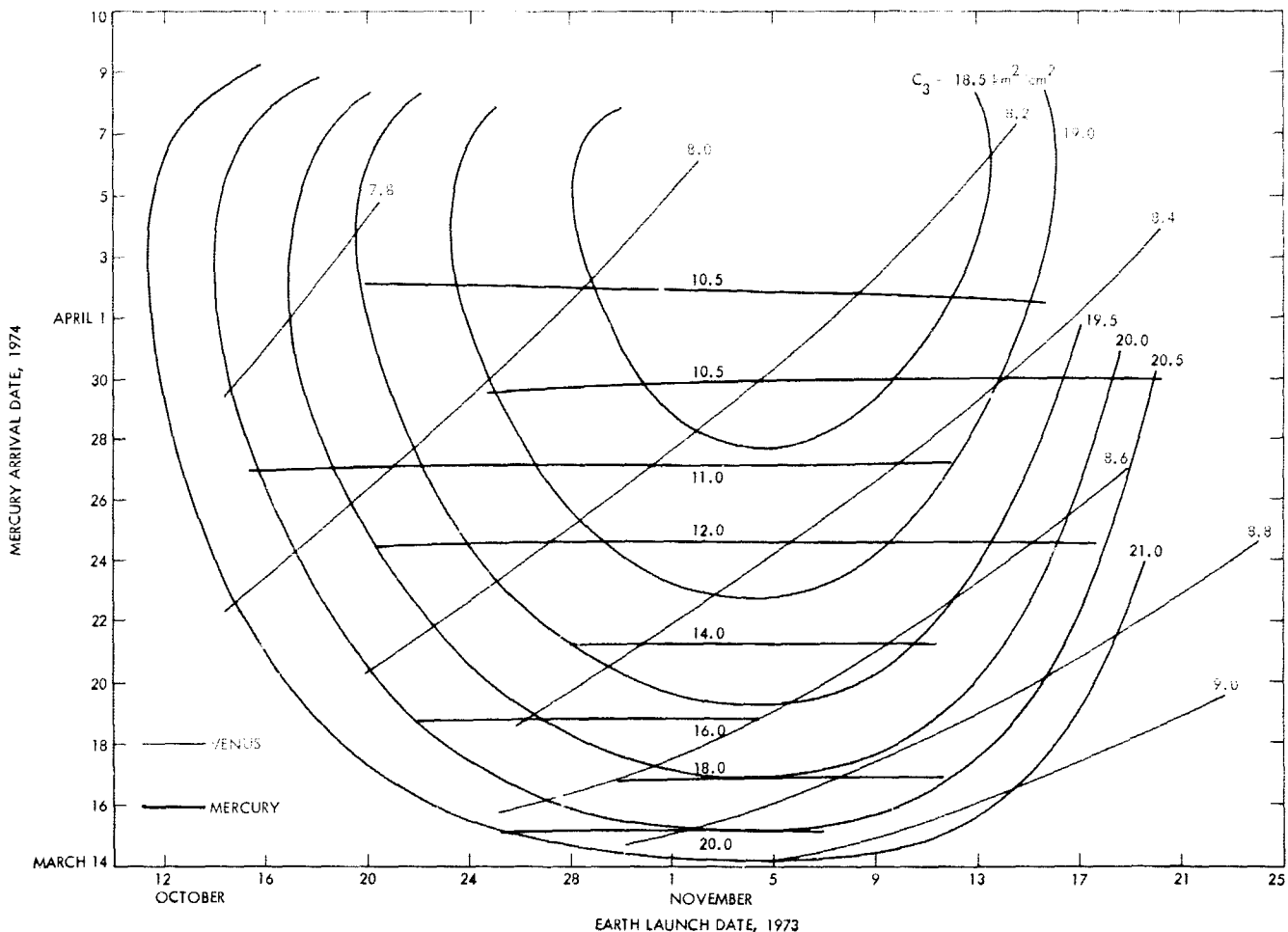


Fig. 4. Hyperbolic approach speeds at Venus and Mercury, km^2/sec^2

directly on the requirements of a Venus entry probe on this mission (Appendix B). In this figure, the green curves show contours of constant V_∞ at Mercury. The lowest available value over the whole opportunity is 10.4 km/sec , substantially higher than for missions to Venus and Mars.

Figures 5 and 6 show the orientation of the direction vectors to the earth and sun relative to the Mercury centered coordinate system shown in Fig. 7. Here **S** is along the incoming asymptote, **T** lies in the plane of the ecliptic and **R** completes a right-handed RST system. The aiming point at the target planet is designated by **B** and θ as shown in Fig. 7. The angle ζ_E between **S** and the Mercury-to-earth vector is plotted in Fig. 5 (the red

curves), and the green curves show the angle η_E from **T** to the projection of the earth-to-Mercury vector in the **R-T** plane. The definition of ζ and η for a generalized body (subscript **B**) may be seen in Fig. 8. Figure 6 shows similar quantities, ζ_s and η_s , for the sun. The centerlines of the earth and sun occultation zones are given by $\theta = \eta_E$ and $\theta = \eta_s$, respectively.

Note that over the range of the plots all the pertinent Mercury quantities are nearly constant with earth launch date⁵. Because of a few days spread in Venus passage date,

⁵F. M. Sturms, Jr., JPL Systems Analysis Section, has surveyed this opportunity for $C_3 \leq 30 \text{ km}^2/\text{sec}^2$ (rather than $21 \text{ km}^2/\text{sec}^2$ as shown here) and has found this generalization still to be valid.

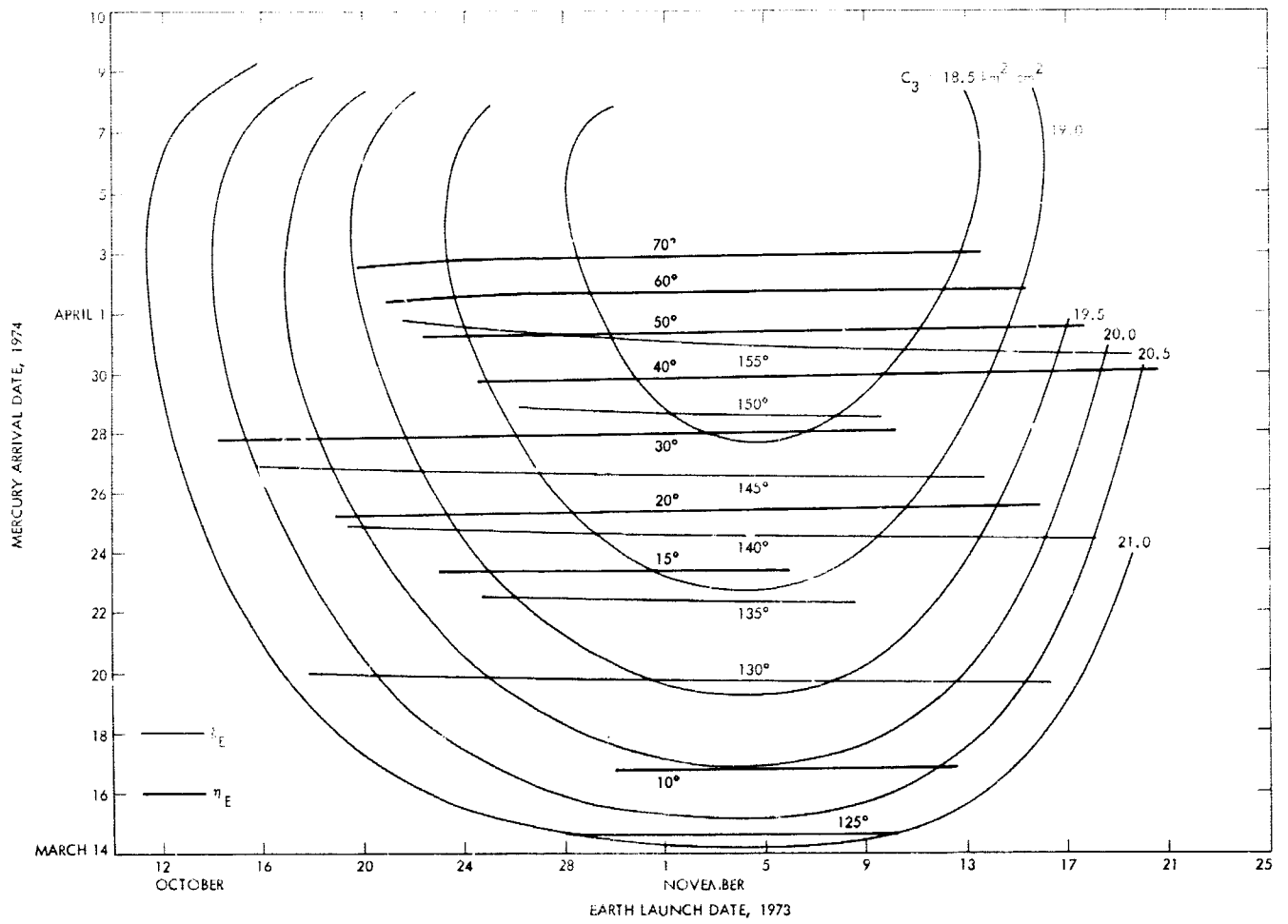


Fig. 5. Direction vectors to earth relative to Mercury-centered coordinate system

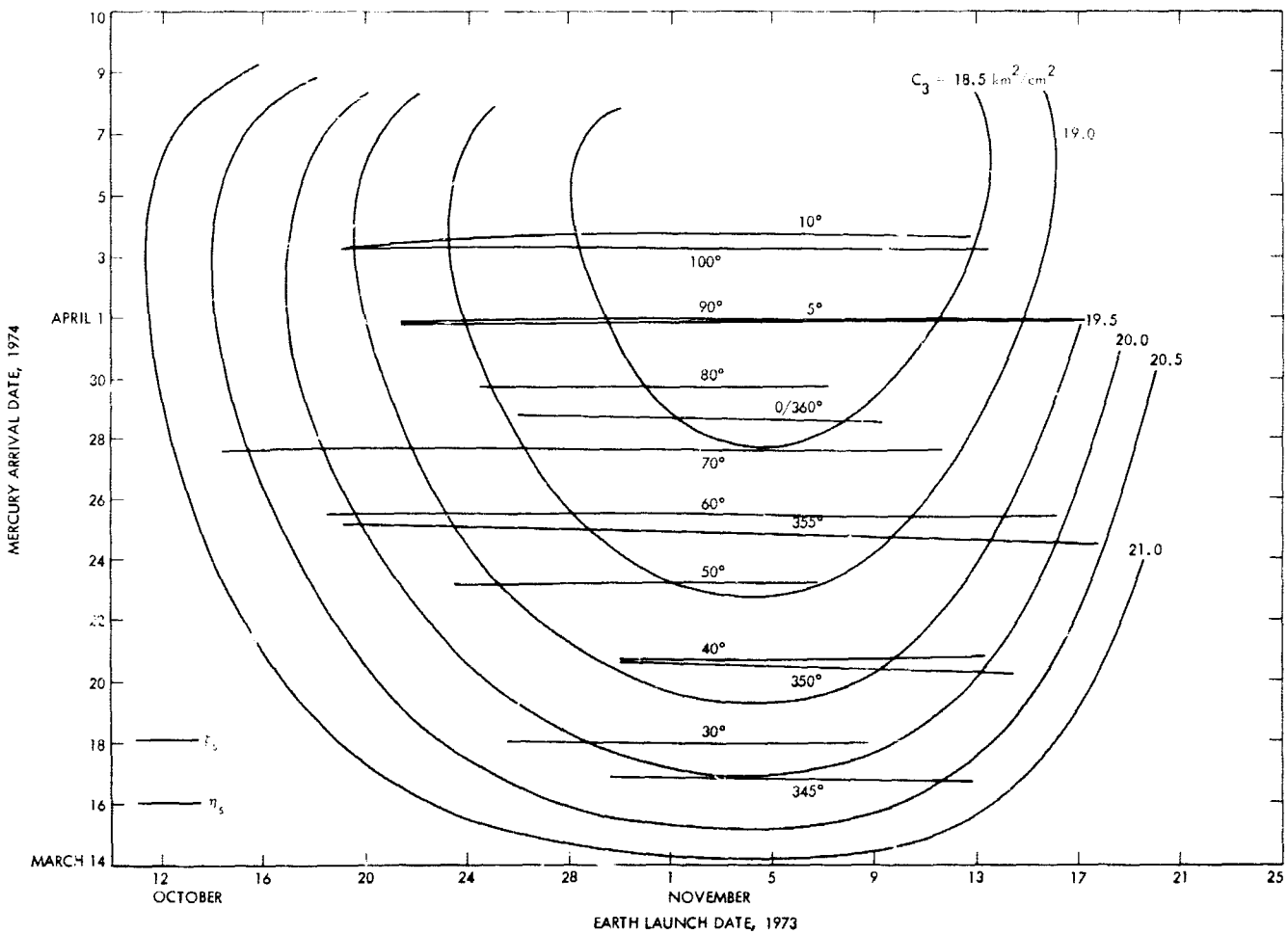


Fig. 6. Direction vectors to sun relative to Mercury-centered coordinate system

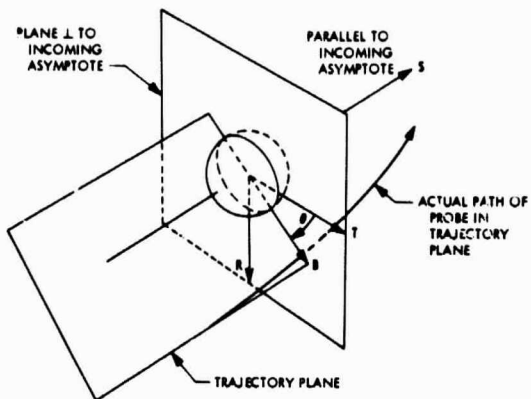


Fig. 7. Aiming zone parameter definition

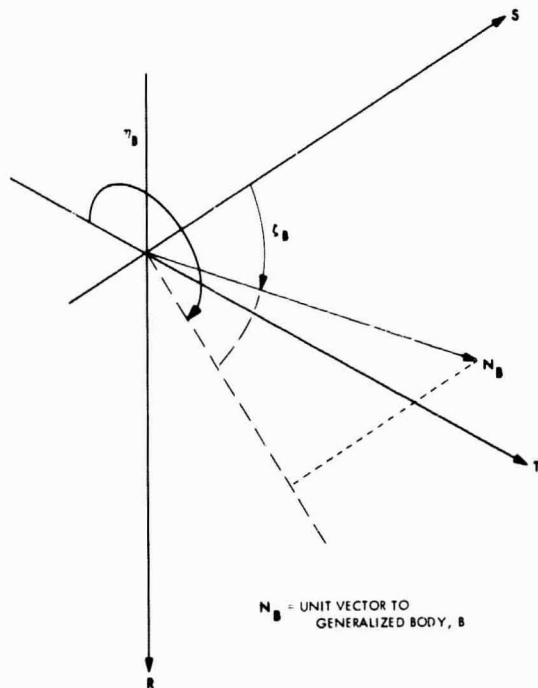


Fig. 8. Geometry for aiming point angles

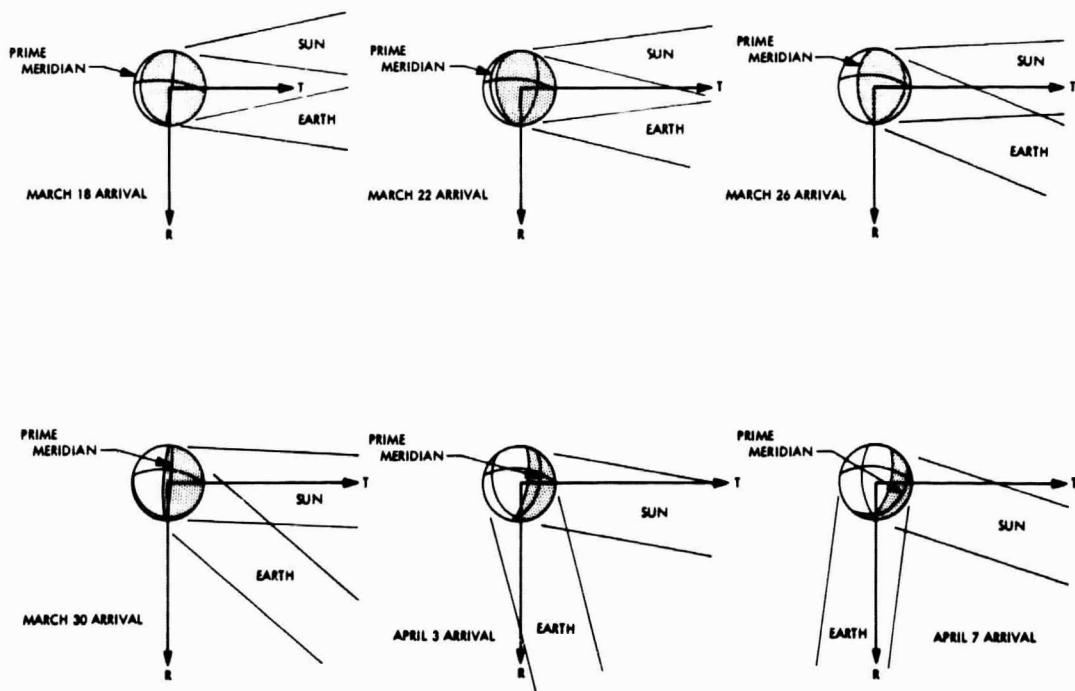


Fig. 9. Mercury arrival conditions

this results in all trajectories arriving at Mercury at a particular time having nearly identical Venus-to-Mercury legs. Accordingly, Mercury approach conditions on a particular arrival date are representative of all trajectories arriving on that date.

Figure 9 shows the appearance of Mercury from the approach asymptote on six arrival dates. For progressively later arrivals, the earth occultation zone moves from alignment with **T** to alignment with **R** (i.e., η_R increases from ≈ 0 to ≈ 90 deg), the planet becomes more illuminated (as seen from the approach asymptote), and the prime meridian moves into the dark. On March 26, 1974, Mercury is at aphelion and, because of the rotational-orbital synchronism, the prime meridian lies on the terminator.

2. Trajectory selection criteria. In selecting the baseline and alternate mission profiles, certain constraints and preferences were assumed:

- (1) Prime emphasis is on Mercury so that arrival conditions are selected which are favorable to imaging and other experiments.
- (2) Venus closest approach altitude is constrained to be greater than 1000 km.
- (3) A launch period ≥ 15 days is deemed adequate for a single spacecraft.
- (4) Venus and Mercury encounters are constrained to be in view of Goldstone so that facilities there and at similar longitudes in the United States could be used.

3. Selected launch period. The reference trajectory is that launched October 26, 1973, and arriving at Mercury March 20, 1974, 1800 GMT. A "dark side" flyby was chosen providing both sun and earth occultation, and generally following the equator (Fig. 9). The lighted hemisphere becomes visible to the spacecraft shortly after encounter, and conditions are favorable for imaging continuously thereafter until resolution is limited by range.

An alternate trajectory which arrives April 3 and approaches a nearly half-illuminated planet was studied. Targeting was along **R** in the earth occultation zone so that the spacecraft flies under the South Pole and follows

^{*}The prime meridian definition is taken from Ref. 15, viz, passing through the subsolar point at the instant of perihelion passage on May 1, 1968.

the terminator, affording favorable imaging throughout the near-encounter phase. Details of these two trajectories and the near-Venus phase are covered in section V-C.

Having assumed the Mercury arrival date of March 20, 1974, the launch period was designed to conform with the above constraints. Figure 10 shows the Goldstone view periods of Venus on a launch date versus Mercury arrival date grid. The baseline launch period is indicated by the X's and the alternate by the O's. Table 2 gives the details of the launch period. Note that the baseline consists of two continuous 10-day segments separated by a 5-day gap and that the desire for constant Mercury arrival conditions (i.e. constant arrival date) has been tempered by the requirement to have Venus encounter over Goldstone. The alternate launch period is broken into three segments running 5, 5, and 4 days, respectively.

C. Near-Planet Geometry

1. Mercury. The approach conditions at Mercury for the reference trajectory are such that both sun and earth occultation are possible if passage is sufficiently close to the planet (Fig. 9). A closest approach altitude of approximately one radius provides adequate imaging and is well within the two occultation zones. Hence the reference trajectory was targeted for the center of the overlap region ($\theta = 0$ deg) with a periapsis altitude of 2500 km. Figure 11 shows the planet with the occultation zones and the aiming point as seen from the approach asymptote. Figure 12 shows the planet and flyby trajectory in the trajectory plane. Note the small amount of bending compared to previous planetary flybys. This is due to the high approach speed and relatively small mass of Mercury.

Figure 13 shows the planet as seen from various points along the trajectory. The intersections of the equator and longitudes 0° , 90° , 180° and 270° are termed "hot" and "warm poles," so named because of the nonuniform solar heating experienced by various points on the equator (Ref. 15). These "poles" are designated in Fig. 13 as:

HP0	Hot pole at 0° longitude
WP90	Warm pole at 90° longitude
HP180	Hot pole at 180° longitude
WP270	Warm pole at 270° longitude

The drawings in Fig. 13 are in true perspective (i.e. focal plane projection) so that the earth (indicated by the "E") and sun (indicated by "S" in actual apparent diameter) may be seen in the background. The scale is

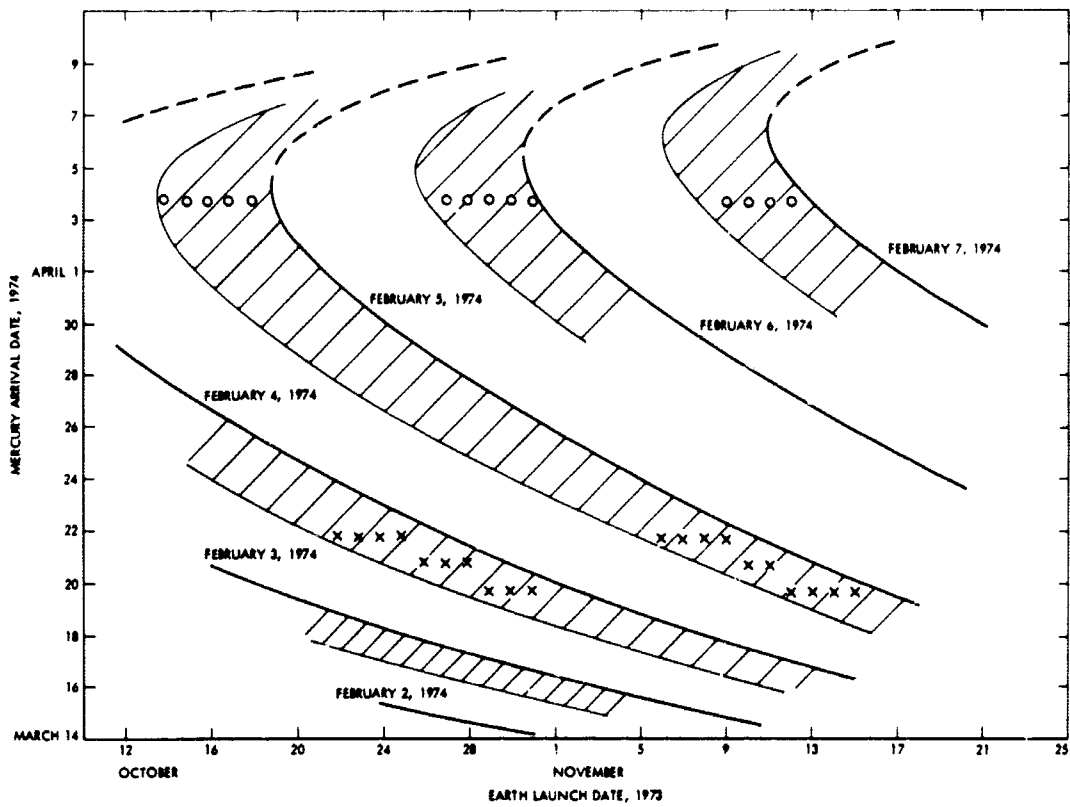


Fig. 10. Goldstone view periods of Venus at encounter

Table 2. 1973 earth-Venus/Mercury trajectory characteristics

Earth launch	Venus arrival, GMT	Mercury arrival, GMT	Venus closest approach altitude, km	Launch energy, C_2 , km^2/sec^2	
Baseline launch period					
Reference trajectory →	10/22/73	2/3/74 ~ 1400	3/21/74 ~ 1800	4200	20.0
	10/23/73	2/3/74 ~ 1700	3/21/74 ~ 1800	4300	19.9
	10/24/73	2/3/74 ~ 1900	3/21/74 ~ 1800	4300	19.8
	10/25/73	2/3/74 ~ 2100	3/21/74 ~ 1800	4400	19.7
	10/26/73	2/3/74 ~ 1700	3/20/74 ~ 1800	4000	19.8
	10/27/73	2/3/74 ~ 1900	3/20/74 ~ 1800	4000	19.7
	10/28/73	2/3/74 ~ 2100	3/20/74 ~ 1800	4100	19.6
	10/29/73	2/3/74 ~ 1600	3/19/74 ~ 1800	3600	19.7
	10/30/73	2/3/74 ~ 1900	3/19/74 ~ 1800	3700	19.6
	10/31/73	2/3/74 ~ 2100	3/19/74 ~ 1800	3700	19.5
	Five-day gap				
	11/6/73	2/4/74 ~ 1500	3/21/74 ~ 1800	5000	19.2
	11/7/73	2/4/74 ~ 1800	3/21/74 ~ 1800	5000	19.2
	11/8/73	2/4/74 ~ 2000	3/21/74 ~ 1800	5000	19.3
	11/9/73	2/4/74 ~ 2200	3/21/74 ~ 1800	5100	19.4
	11/10/73	2/4/74 ~ 1800	3/20/74 ~ 1800	4700	19.5
	11/11/73	2/4/74 ~ 2000	3/20/74 ~ 1800	4800	19.6
	11/12/73	2/4/74 ~ 1600	3/19/74 ~ 1800	4100	19.9
	11/13/73	2/4/74 ~ 1800	3/19/74 ~ 1800	4200	20.1
	11/14/73	2/4/74 ~ 2000	3/19/74 ~ 1800	4200	20.3
	11/15/73	2/4/74 ~ 2200	3/19/74 ~ 1800	4300	20.5
Alternate launch period					
	10/14/73	2/4/74 ~ 1430	4/3/74 ~ 1800	3000	20.3
	10/15/73	2/4/74 ~ 1630	4/3/74 ~ 1800	3100	20.4
	10/16/73	2/4/74 ~ 1830	4/3/74 ~ 1800	3100	20.2
	10/17/73	2/4/74 ~ 2030	4/3/74 ~ 1800	3200	20.0
	10/18/73	2/4/74 ~ 2230	4/3/74 ~ 1800	3200	19.8
Eight-day gap					
	10/27/73	2/5/74 ~ 1500	4/3/74 ~ 1800	3600	18.6
	10/28/73	2/5/74 ~ 1700	4/3/74 ~ 1800	3600	18.5
	10/29/73	2/5/74 ~ 1900	4/3/74 ~ 1800	3700	18.5
	10/30/73	2/5/74 ~ 2100	4/3/74 ~ 1800	3700	18.4
	10/31/73	2/5/74 ~ 2300	4/3/74 ~ 1800	3800	18.4
Eight-day gap					
	11/9/73	2/6/74 ~ 1600	4/3/74 ~ 1800	3800	18.3
	11/10/73	2/6/74 ~ 1800	4/3/74 ~ 1800	3800	18.3
	11/11/73	2/6/74 ~ 2000	4/3/74 ~ 1800	3900	18.4
	11/12/73	2/6/74 ~ 2200	4/3/74 ~ 1800	3900	18.4

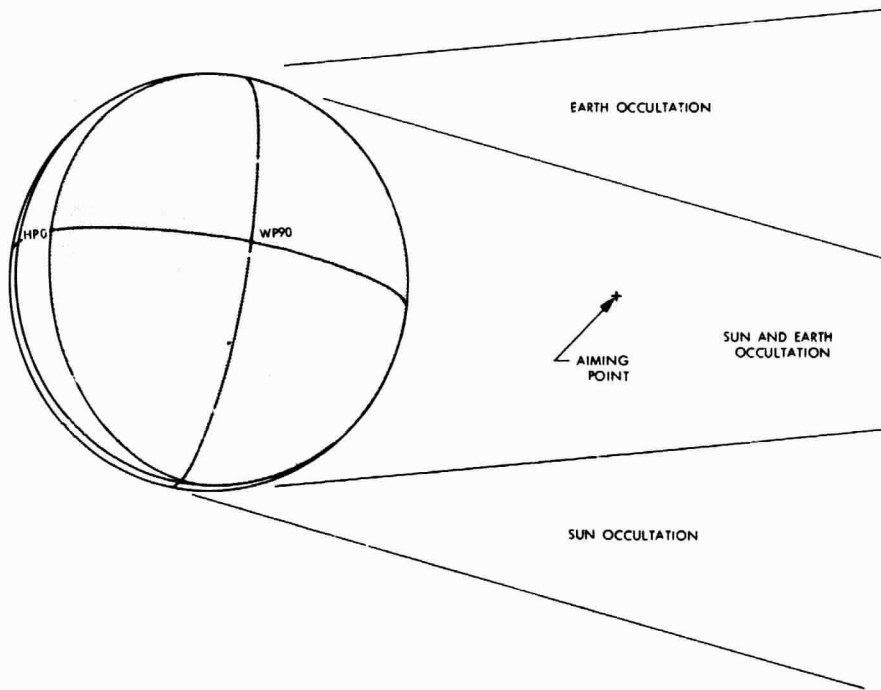


Fig. 11. Mercury aiming plane (reference trajectory)

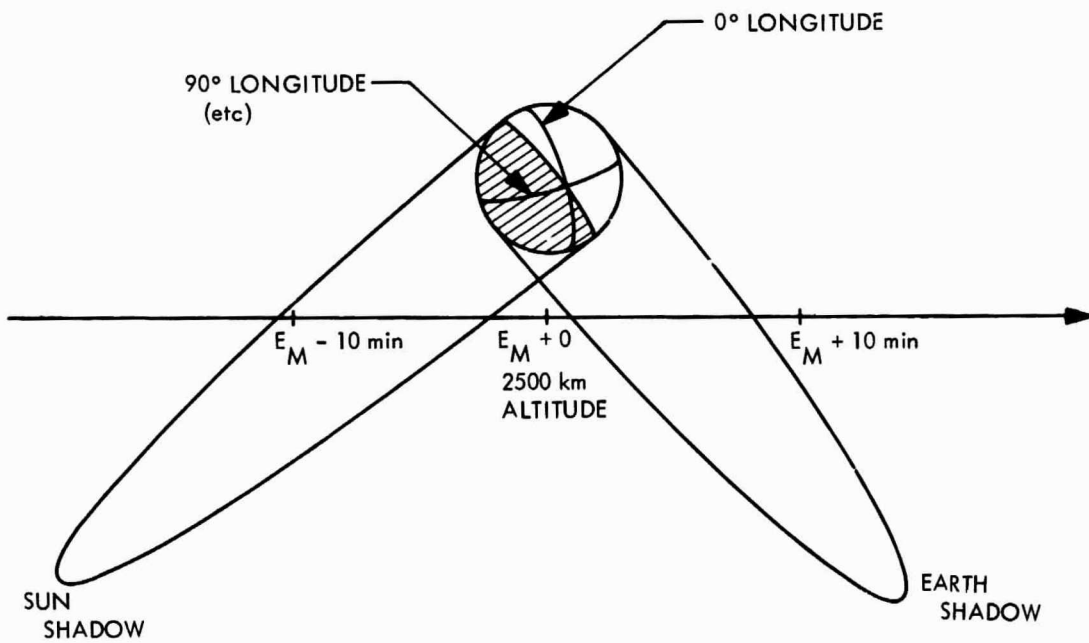


Fig. 12. Reference Mercury flyby trajectory

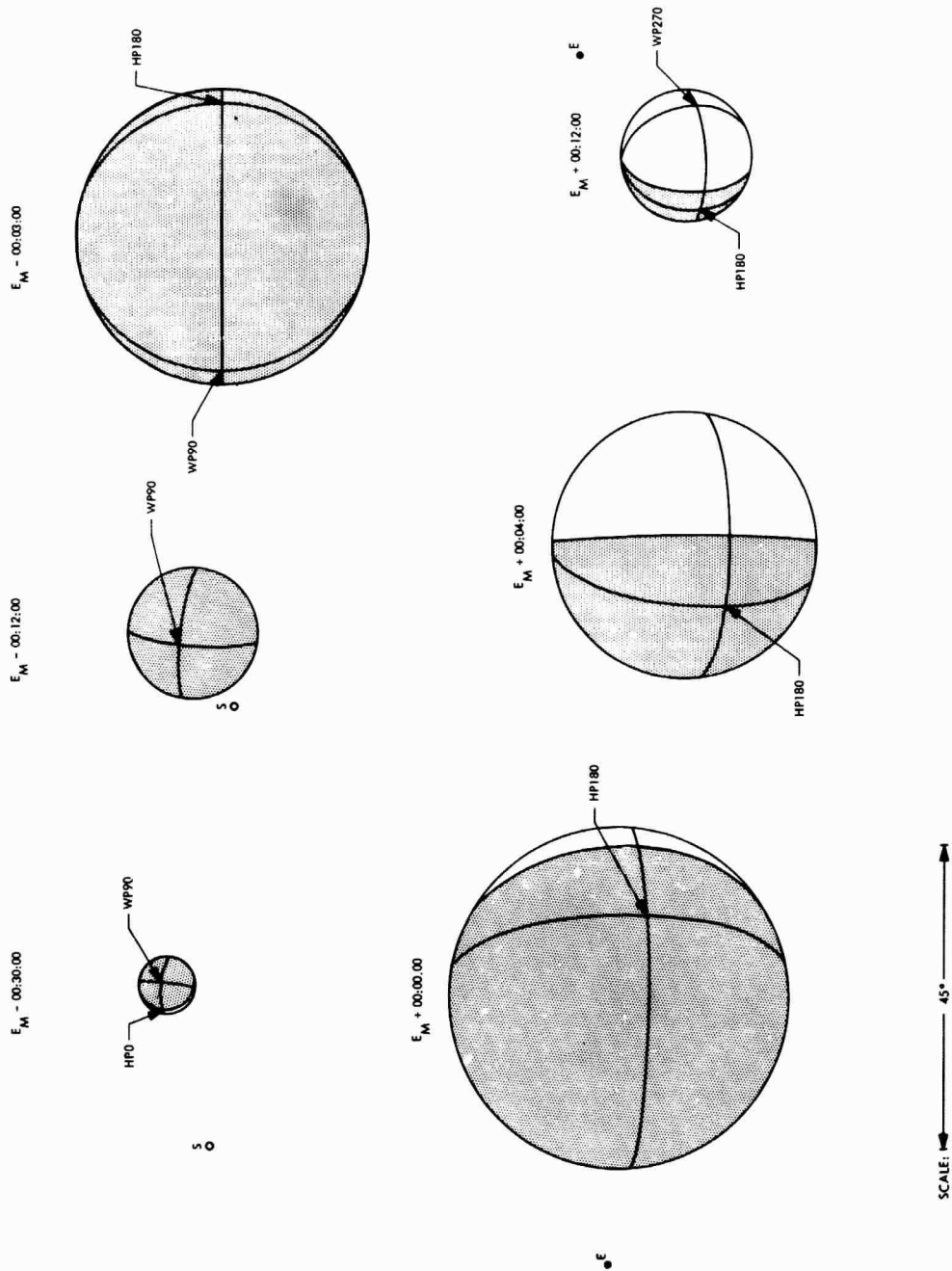


Fig 13. Mercury as seen from reference flyby trajectory

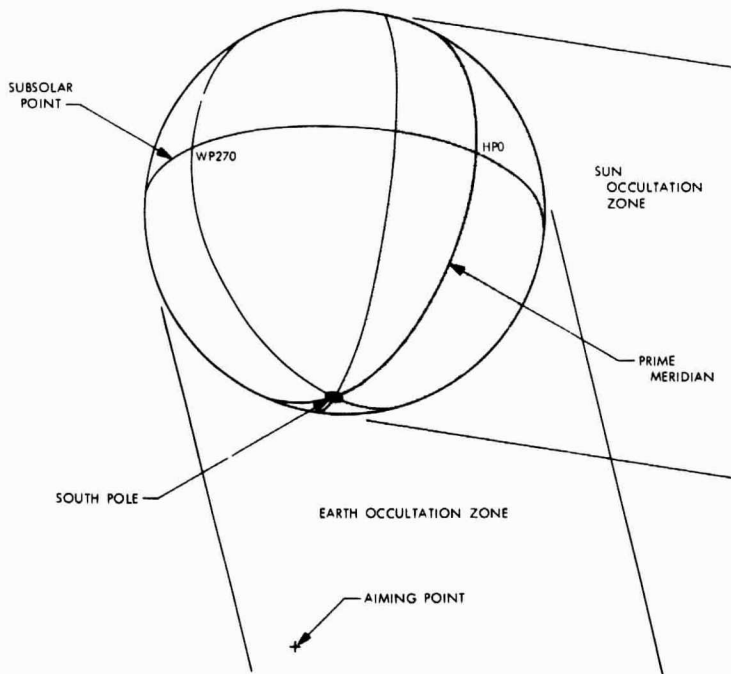


Fig. 14. Mercury aiming plane (alternate trajectory)

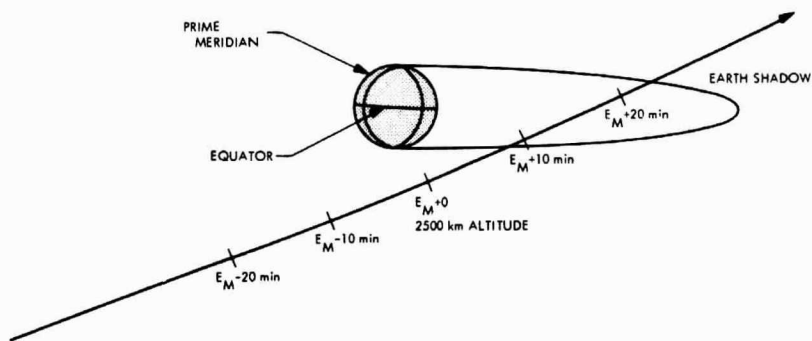


Fig. 15. Alternate Mercury flyby trajectory

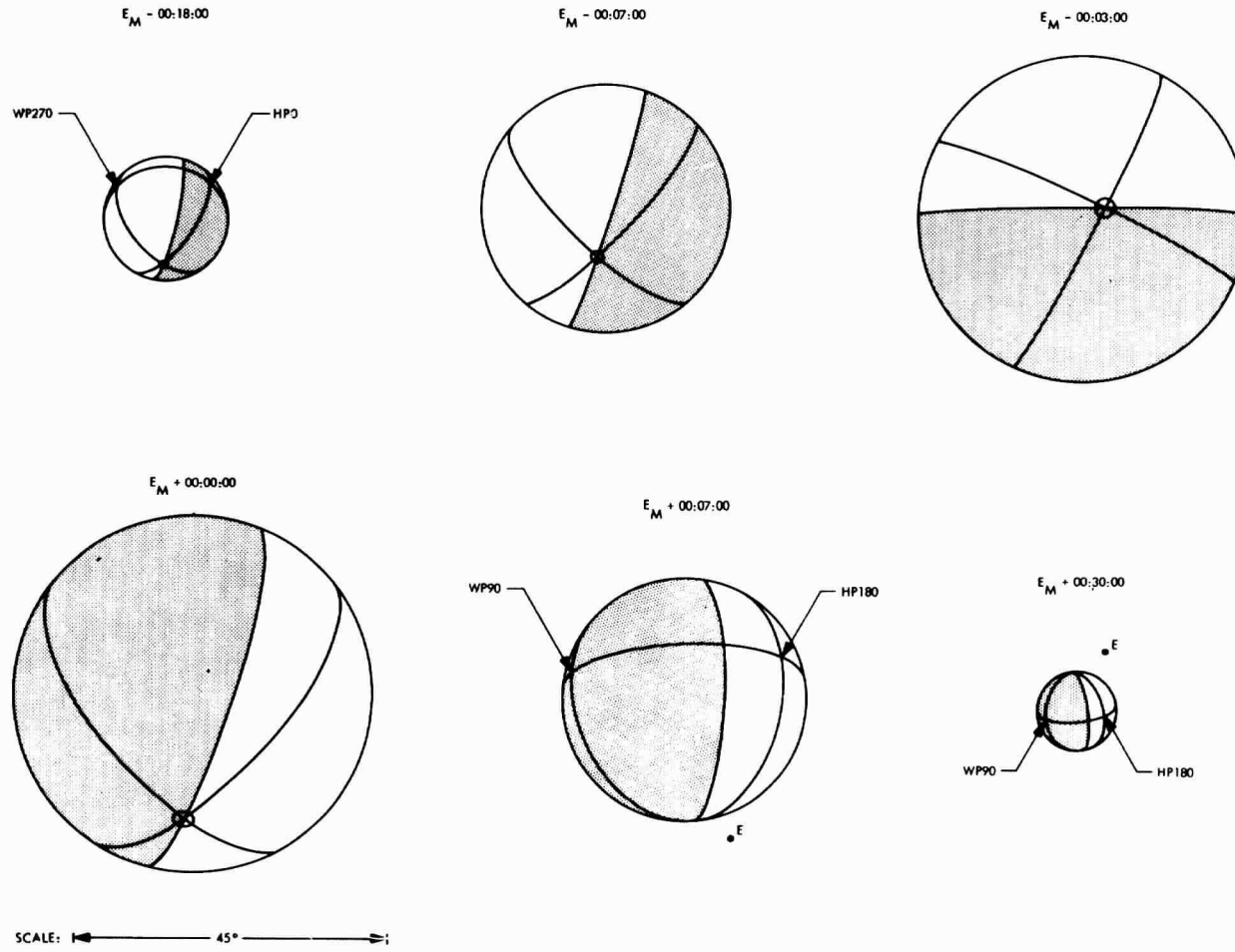


Fig. 16. Mercury as seen from alternate flyby trajectory

such that the time blocks in each corner are approximately $6.8 \text{ deg} \times 25.6 \text{ deg}$. It should be pointed out that the instruments on the spacecraft are not necessarily viewing the planet at the times shown. The actual event sequence is discussed in section VII-C, and scan platform limitations in section VII-B.

For the April 3 arriving alternate trajectory, there is no significant overlap of the two occultation zones in the aiming plane, and earth occultation was selected as preferable. The aiming point was chosen nearly on the **R** axis with a closest approach altitude of 2500 km. Figure 14 shows the planet with the occultation zones and aiming point as seen from the approach asymptote. Figure 15 shows the flyby trajectory in the trajectory plane; the planet is nearly completely shaded when seen in this view as one is looking nearly directly into the sun. Figure 16 is analogous to Fig. 13, but for the alternate trajectory and at different times. Note that since targeting is well away from the sun occultation zone (and hence the trajectory is quite far from the sun's shadow) the sun never comes into the field of view.

2. Venus. As noted above, conditions at Venus are uniquely specified once the Mercury arrival and earth launch dates are chosen. Also, there is only a small variation in the Venus flyby since the arrival date is confined to 2 days for the baseline case and 3 days for the alternate case. The largest variation is in periapsis altitude which ranges from 3600 to 5100 km over the baseline launch period and 3000 to 3900 km over the alternate (Table 2).

Aiming plane diagrams at Venus are shown in Ref. 1, Figs. 32-35. These show that the aiming points for the trajectories surveyed lie within the earth occultation zone but outside the sun occultation zone.

Figure 17 shows the reference flyby trajectory at Venus (launch October 26, 1973, Venus arrival February 3, 1974 and Mercury arrival March 20, 1974). Because of the narrow range of Venus passage conditions, this is typical of Venus flybys for both the baseline and alternate missions. Meridians 0° , 60° , 120° , 180° , 240° and 300° , and the earth's shadow (the region of the earth occultation) are shown on the figure. Closest approach altitude is 4038 km. The longitude convention takes the prime meridian through radar identified feature α' which is 40° to the east (measured on the celestial sphere) of the meridian which faces the Earth at inferior conjunction.

Figure 18 shows the appearance of Venus from the flyby trajectory between $E_V - 30 \text{ min}$ (Venus encounter minus 30 min) and $E_V + 30 \text{ min}$. The scale is the same as that used in Figs. 13 and 16. On the approach, the planet presents a nearly fully dark face with the sun in the background. The radar identified feature α , the prime meridian, and the subearth point are on the side facing the spacecraft. Earth occultation begins at $E_V + 6 \text{ min}$ and ends at $E_V + 20 \text{ min}$. In the course of the flyby, the

The meridian and longitude definitions are taken from Ref. 11, pp. 28 and 29, where the North Pole is adopted along the angular momentum vector, and longitude increases to the east (measured on the planet surface). The feature locations are taken from Ref. 16.

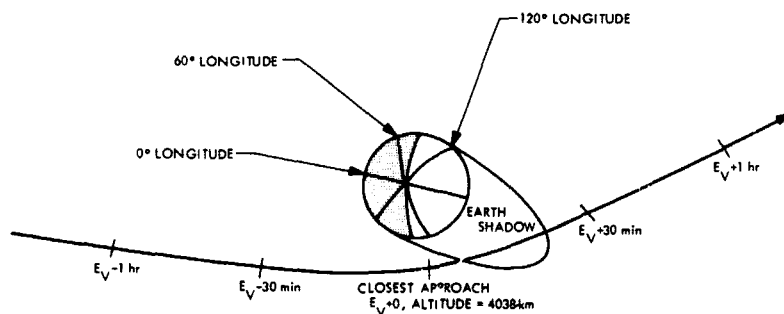


Fig. 17. Reference Venus flyby trajectory

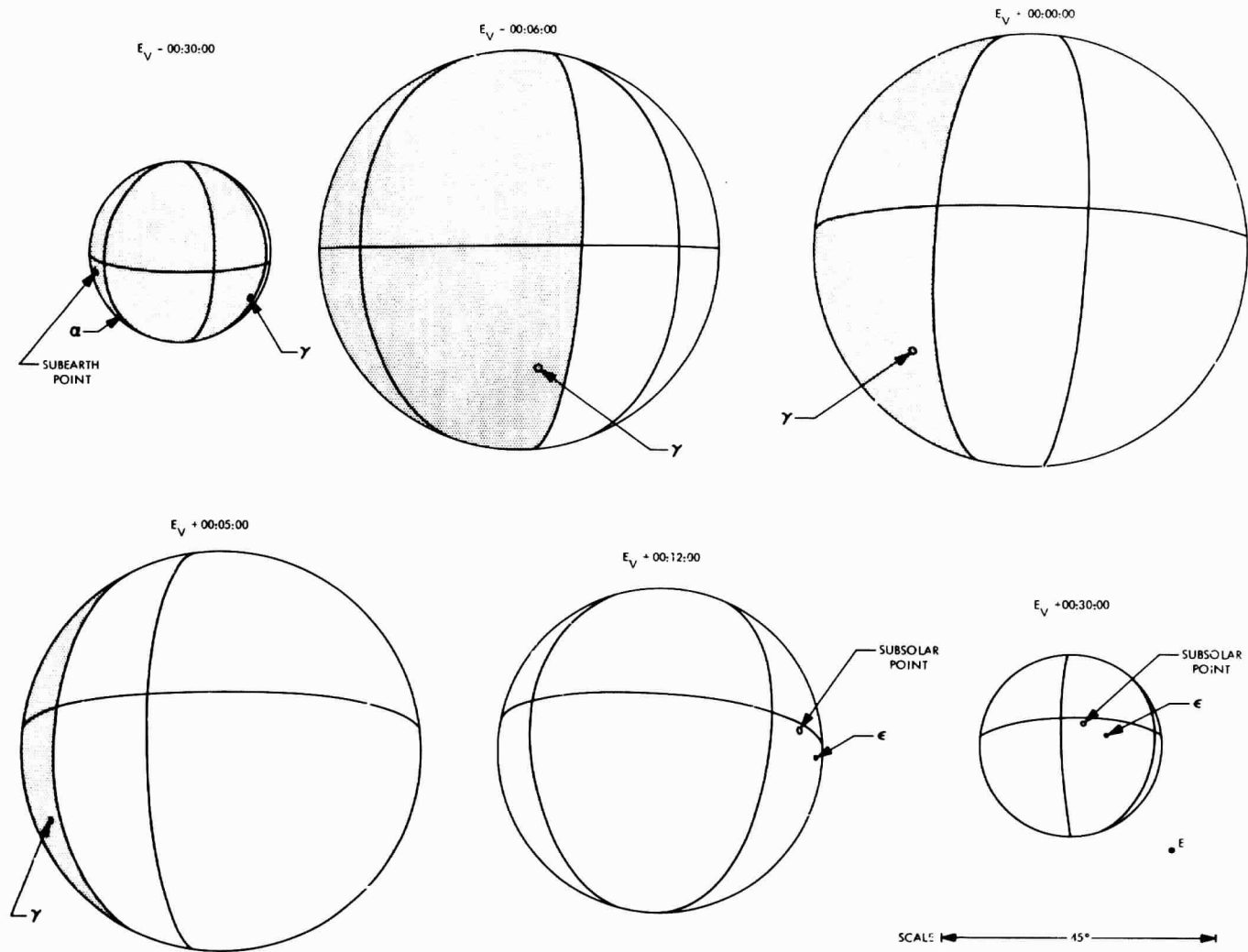


Fig. 18. Venus as seen from flyby trajectory

spacecraft passes close to features γ and ϵ . Feature γ is a few degrees into the dark, whereas ϵ is near the subsolar longitude. Features β and δ can never be seen. An active radar investigation was performed during the Spring 1969 opposition and numerous additional features are expected to be identified as a result of that study.⁸

D. Navigation and Guidance

An analysis of guidance requirements for the 1973 mission was published by Sturms in Ref. 1. Although the basic guidance policy presented there is still applicable, navigation advances and revised projections since Sturms' analysis cause the quantitative results to be revised appreciably. The remainder of this section presents the basis and results of the revised analysis.

The *Atlas/Centaur* launch vehicle has, through *Surveyor* and *Mariner* Mars 1969 flight experience, proven to be exceptionally accurate. Using an injection covariance matrix characteristic of a planned *Mariner* Mars 1969 launch at approximately the same value of C_3 , the rms Venus dispersion following injection is 31,900 km and the rms first maneuver is 3.13 m/sec (section V-E). Because the injection characteristics are similar for the entire launch period, a single rms first maneuver magnitude is assumed throughout. Table 3 summarizes the characteristics of the first maneuver.

Table 3. First maneuver characteristics

Reference trajectory: Launch October 26, 1973,
Mercury arrival March 20, 1974

Dispersion at Venus due to launch errors	
Semimajor axis, km	31,380
Seminor axis, km	5,735
Orientation angle, deg ^a	174.7
First maneuver magnitude (performed at launch + 8 days)	
Rms value, m/sec	3.13
Mean, m/sec	2.77
Sigma, m/sec	1.45
Dispersion at Venus following first maneuver	
Semimajor axis, km	388
Seminor axis, km	101
Orientation angle, deg ^a	171
Three dimensional rms miss, km	439
^a See Fig. 19 for definition.	
Note: Rayleigh approximation used for maneuver statistics (Ref. 17).	

⁸R. M. Goldstein, JPL Communications Research Section, personal communication.

In sizing the first maneuver, no consideration was given to biasing the launch trajectory for planetary quarantine purposes, because the planetary quarantine policy for a 1973 Venus/Mercury mission is not yet established. Furthermore, the results of the Soviet missions in 1967 and 1969 will probably influence this policy. If an injection bias is necessary, the effect will be to increase the rms first maneuver.

Pointing and shut-off errors in the first maneuver will cause a dispersion at Venus which must be reduced by a second maneuver. Pointing errors are discussed in section VII-G-2 and shut-off errors in section VIII-I. The results stated in these sections imply a proportional pointing error of 0.7% 1σ and a proportional velocity error of 0.2% 1σ . The simplified execution error model given in Ref. 18 requires equal proportional errors in all directions; a conservative estimate is that the total 1σ proportional error is 0.7%. The simplified model assumes a spherical velocity error distribution following a maneuver which may be mapped to the target, and the model allows the use of the midcourse execution accuracy data generated by a conic trajectory program.

The rms value of the second maneuver may be approximated by taking the three-dimensional rms miss at the target and dividing by the time between the second maneuver and Venus encounter. This result compares favorably to that found in Ref. 1 using integrated values. Characteristics of the second maneuver are shown in Table 4 for the reference trajectory. The values are essentially the same as for the other candidate trajectories because of the nearly constant Venus arrival date.

The residual error following the second maneuver is almost entirely due to the orbit determination uncertainty at the time of its execution. The level of orbit determination (OD) accuracy depends on several factors discussed by Melbourne in Ref. 19. The principal factors are relative station location, location of the Earth spin axis relative to the crust, charged particle density between the station and the spacecraft, timing synchronization errors between stations, and ability to determine the spacecraft-station range rate. All but the last of these can be lumped into an equivalent station location accuracy. These equivalent accuracies are quoted in Ref. 19 for two eras of Deep Space Network (DSN) development and are repeated in Table 5.

The multi-planet mission requires precise determination of the spacecraft position relative to the intermediate

Table 4. Second maneuver characteristics

Reference trajectory: Launch October 26, 1973,
Mercury arrival March 20, 1974

Dispersion at Venus following first maneuver	
Semimajor axis, km	388
Semiminor axis, km	101
Orientation angle, deg	171
Three dimensional rms miss, km	439
Second maneuver magnitude (performed at encounter - 3 days)	
Rms value, m/sec	1.7
Mean, m/sec	1.5
Sigma, m/sec	0.7
Residual dispersion at Venus due to orbit determination uncertainties (1972 DSN capability)	
Semimajor axis, km	27.2
Semiminor axis, km	5.0
Orientation angle, deg	125

Note: Rayleigh approximation used for maneuver statistics (Ref. 17).

Table 5. Equivalent DSN Station location and range rate uncertainties

All statistical values one sigma

Parameter uncertainty	DSN capability date (Ref. 19)	
	1969	1972
Distance from earth's spin axis	2 m	0.8 m
Longitude	4 m	1.6 m
Range rate	3 mm/sec	1 mm/sec

planet, hence that planet's ephemeris must be well known. Knowledge of the ephemeris of Venus has improved dramatically over recent years. The current ephemeris uncertainty is described in Ref. 11. This uncertainty has been estimated for 1973 based on discussions with W. G. Melbourne and the position error of the center of mass of Venus was assumed to be between 1 and 5 km.

Orbit determination uncertainties in the Venus impact plane are shown in Fig. 19 along with the execution error dispersion from the first maneuver. Parameter values of interest are summarized in Table 6.

Table 6. Navigation parameter uncertainties

All statistical values one sigma

Parameter uncertainty	DSN capability date (Ref. 19)			
	1969	1972		
A priori spacecraft position (spherical), km	200.	150.		
A priori spacecraft velocity (spherical), km/sec	2×10^{-5}	10^{-5}		
GM Venus, km ³ /sec ²	0.8	0.4		
Venus position (spherical), km	5.	1.		
Station spin axis distance, m	2.0	0.8		
Station longitude, m	4.0	1.6		
Range rate data noise, mm/sec	3.0	1.0		
B-plane				
Tracking span, E - 30 days to	$E_V - 8$ days	$E_V - 4.5$ days	$E_V - 8$ days	$E_V - 4.5$ days
Semimajor axis, km	71.7	66.2	29.8	27.2
Semiminor axis, km	15.7	13.4	5.9	5.0
Orientation angle, deg	125.3	125.0	125.3	124.8
Rms error, km	73.4	67.6	30.4	27.2

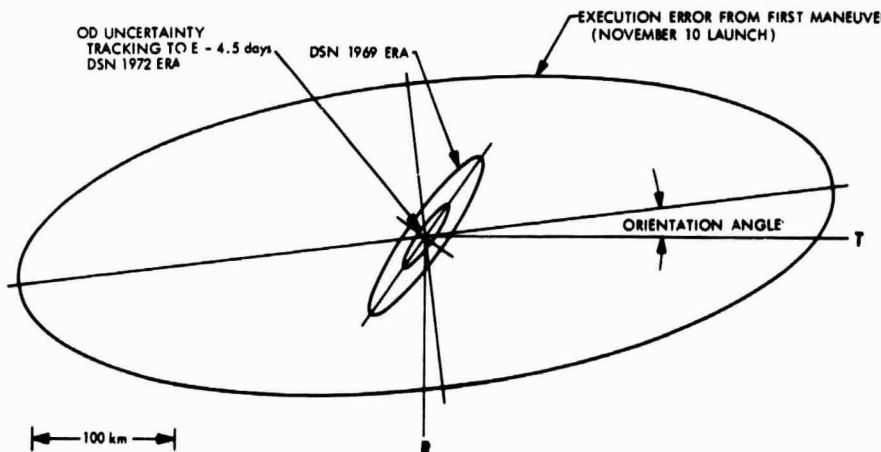


Fig. 19. One-sigma Venus B-plane dispersions

The magnitude of the third maneuver is directly proportional to the impact plane miss at Venus, hence its value depends on the DSN navigation capability. The rms magnitude is 26 m/sec for the current capability and 11 m/sec for that expected in 1972.

Following the third maneuver, the residual dispersion is due to execution errors. The dispersion at Mercury depends strongly on the flight time from Venus to Mercury and, therefore, on the Mercury arrival date. Hence the results are quite different for the reference and alternate trajectories, as may be seen from Figs. 20 and 21 where 3σ dispersion ellipses are plotted about the nominal aiming points. Two levels of DSN capability and two levels of proportional execution errors are shown. The standard deviation of the proportional execution errors, σ_e (due to pointing and magnitude) are taken to be 0.008 (slightly larger than those quoted in section VII-G-2) and 0.005 (an optimistic projection to 1973 capa-

Table 7. Dispersion at Mercury following third maneuver (1 sigma)

Mercury arrival date	3/20/74	4/3/74
Orientation angle, deg	138	167
1969 DSN capability		
1σ dispersion for 1σ execution = 0.008		
major axis, km	545	1630
minor axis, km	462	301
1σ dispersion for 1σ execution = 0.005		
major axis, km	347	1018
minor axis, km	289	188
1972 DSN capability		
1σ dispersion for 1σ execution = 0.008		
major axis, km	235	655
minor axis, km	195	121
1σ dispersion for 1σ execution = 0.005		
major axis, km	147	409
minor axis, km	128	76

Table 8. Total midcourse fuel requirements, m/sec

Parameter	DSN capability date (Ref. 19)	
	1969	1972
RMS value	30	15
Mean	27	13
Sigma	12	5
Mean + 3 sigma	64	29

Note: Rayleigh approximation used for maneuver statistics (Ref. 17).

bility). For the late arrival, only the most optimistic guidance parameters (the 1972 DSN capability and $\sigma_e = 0.005$) assure success with a single post-Venus maneuver for the aiming point chosen. One-sigma dispersion values are given in Table 7.

The total midcourse fuel requirements are given in Table 8; the values are essentially identical for both the reference and alternate trajectories. Note that the requirements are sufficiently small, especially for the assumed 1972 DSN navigation capability, that *Mariner Mars 1969* midcourse velocity capability will be adequate (section VIII-I).

A summary of the guidance parameters is given in Table 9. The major conclusion is that the dispersion at Mercury following the last maneuver is generally adequate to assure occultation(s) and avoid planetary impact, assuming current navigation and guidance performance. Improved performance will assure occultation for the alternate south-polar trajectory.

Table 9. Guidance summary, baseline mission

Earth-based radio navigation		
Maneuver time	Rmr size, m/sec	Purpose
Launch + 8 days	3.1	Remove launch vehicle dispersions
Venus encounter - 3 days	1.7	Remove execution errors from first maneuver
Venus encounter + 8 days	11 - 26	Compensate for navigation errors at second maneuver
Total mean-plus-three-sigma fuel load		29 - 64 m/sec
Rms residual dispersion at Mercury		
1969 DSN capability		750 km
1972 DSN capability		200 km

E. Launch Vehicle System

The launch vehicle assumed for the *Mariner Venus/Mercury 1973* is the *Atlas (SLV-3C)/Centaur D*. Similar vehicles have been successfully used to launch a number of spacecraft, i.e., the last three *Surveyor* spacecraft, the *Orbiting Astronomical Observatory (OAO)* spacecraft, and two *Mariner Mars 1969* spacecraft. Many of the requirements and constraints for the *Mariner Venus/Mercury 1973* mission are similar to those of the *Mariner Mars 1969* mission; therefore, much of the material in Ref. 20 is appropriate and has been used for the current baseline study.

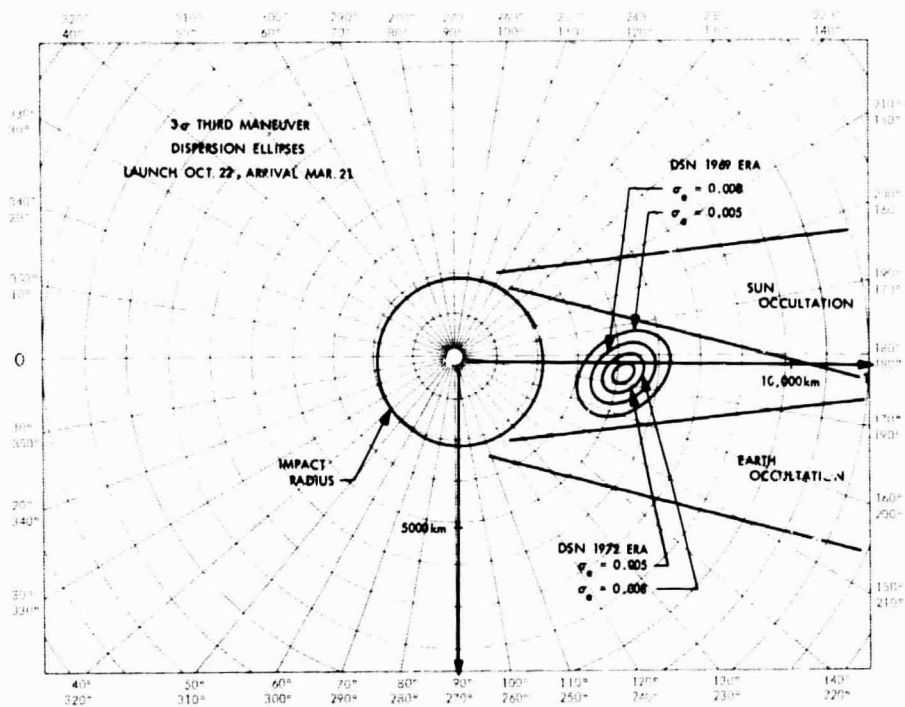


Fig. 20. Reference trajectory third maneuver dispersion ellipses (3- σ)

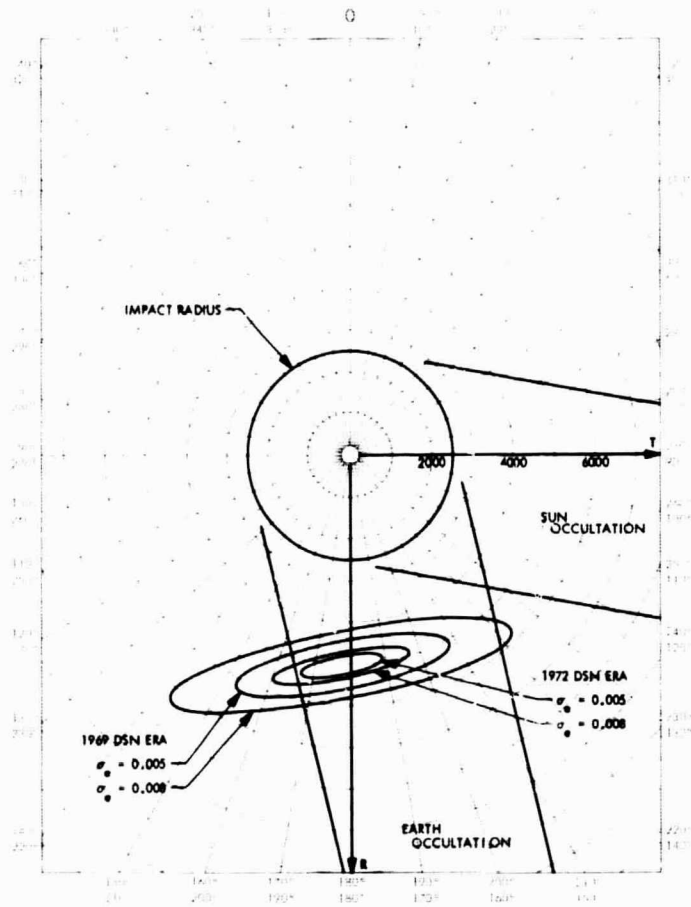


Fig. 21. Mercury impact plane for November 3, 1973 launch and April 3, 1974 arrival showing 3- σ dispersion ellipses

1. *Nose fairing payload envelope.* Figure 22 shows the standard version of the *Centaur* nose fairing. The standard fairing was used for *Surveyor*, *Mariner Mars 1969*, and is planned for *Mariner Mars 1971*. The baseline *Mariner Venus/Mercury 1973* configuration will fit within this standard payload envelope.

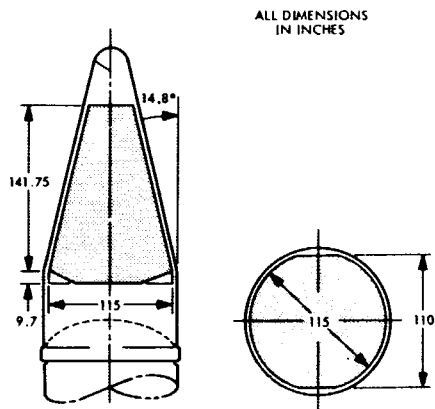


Fig. 22. Surveyor payload envelope

The nose fairing is constructed of honeycomb fiberglass and is made in four sections, i.e., two half-conical sections and two half-cylindrical sections. The spacecraft is encapsulated in the two half-conical sections at the launch area Explosive Safe Facility (ESF) assembly area, transported to the launch complex, and mated to the launch vehicle, to which the two half-cylindrical sections have been previously installed. When the launch vehicle

is out of the earth's lower atmosphere and still accelerating, the nose fairing is jettisoned by separation of two clamshell halves, each comprising one half-cylindrical and one half-conical section. Separation of the two halves is accomplished by pyrotechnic release devices and two gas jets located in the forward end of the nose fairing.

2. *Injection capability.* As discussed in section V-B, the launch energy C_3 required for the mission is 19.2 to 20.5 km^2/sec^2 (Table 2). Adequate launch windows may be obtained with an allowable maximum launch azimuth of 114° . Figure 23 indicates a maximum allowable separated spacecraft weight of 1180 lb for *Mariner Venus/Mercury 1973* assuming a launch azimuth of 90° . The payload capabilities shown for *Mariner Venus/Mercury 1973* are 100 lb greater than those shown for *Mariner Mars 1969* since the configuration of *Mariner*

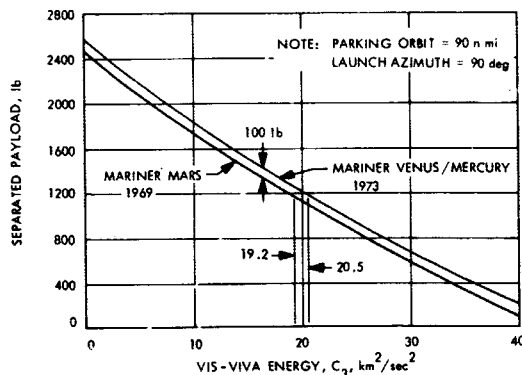


Fig. 23. Parking orbit ascent payload capability

Table 10. Injection covariance matrices

	X, m	R, m	V, m/sec	Γ , mrad	W, m	\dot{W} , m/sec
$\Delta_{OD/C-}$	1.202E 05	-1.192E 05	2.624E 02	-7.237E 01	-5.711E 04	-2.148E 02
		2.455E 05	-3.588E 02	1.261E 02	-1.026E 05	-7.367E 01
			8.689E-01	-2.006E-01	1.871E 02	1.548E-01
		Symmetric		7.006E-02	-2.885E 01	3.049E-02
					9.474E 05	2.694E 03
						9.642E 00
Δ_{JPL-}	0.1202E 00	-0.1192E 00	0.2624E-03	-0.9123E-04	-0.5711E-01	0.2148E-03
		0.2455E 00	-0.3588E-03	0.1448E-03	-0.1026E 00	-0.7367E-04
			0.8689E-06	-0.2417E-06	0.1871E-03	0.1548E-06
		Symmetric		0.9571E-07	-0.1989E-04	-0.3191E-08
					0.9474E 00	0.2694E-02
						0.9642E-05

Mars 1969 included a second telepak on the *Centaur*, weighing approximately 100 lb, which is not required for this mission. Figure 24 indicates a payload loss of 50 lb for a launch azimuth of 114° (worst case), thus the net separated spacecraft weight capability would be 1130 lb. This estimate does not include an estimated 70 lb for spacecraft adapter which is normally included with payload weight for launch, but which is not injected into

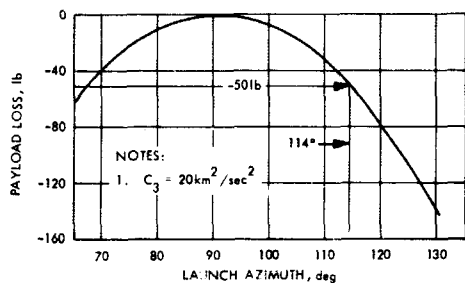


Fig. 24. Payload loss vs launch azimuth

orbit with the spacecraft. There are other possible contingency allowances and improvements for the *Atlas/Centaur* which could be used to increase payload weight capability, but the present capability already exceeds that required for the *Mariner Venus/Mercury 1973* baseline mission.

Because of the small declination ($<4.5^\circ$) of the launch asymptote for the *Mariner Venus/Mercury 1973* mission, the distance between launch and perigee is too large to permit a direct ascent launch profile. The *Mariner Venus/Mercury 1973* mission will therefore require the use of a parking orbit. For the baseline reference trajectory selected (section V-B-3), the 2-hr window opens at 0546 GMT October 26, 1973, with azimuth of 90° (opening) to 114° (closing) and a maximum coast time of 1739 sec. The coast time decreases with increasing azimuth. However, for the opening day of the selected baseline period (October 22, 1973) the maximum coast time is 1754 sec, which is considered the maximum required for the entire launch period. The maximum coast time successfully used to date on any *Centaur* mission is 25 min (1500 sec). However, an increase of coast time to meet the *Mariner Venus/Mercury 1973* requirements should not be unduly difficult.

*JPL, personal communication to P. Eckman from F. M. Sturms, Jr., January 22, 1969; subject: Launch Window for *Mariner Venus/Mercury 1973*.

3. *Injection accuracy.* The injection accuracy is a function of many trajectory variables such as launch azimuth, flight profile, injection energy, payload weight, and coast time.

Since a reference trajectory was not available for this mission, specific accuracy data could not be generated. However, for the purposes of the guidance analysis and sizing the first midcourse maneuver (section V-D), an injection covariance matrix from *Mariner Mars 1969* was used. A direct ascent trajectory at a C_3 of $18.2 \text{ km}^2/\text{sec}^2$ was taken as representative. Table 10 gives the injection covariance matrix in both the General Dynamics/Convair (GD/C) and JPL forms. Table 11 summarizes the injection errors from the first matrix in Table 10 and compares them to those from *Surveyor* and the *Applications Technology Satellite (ATS)*. The values shown for *Mariner Venus/Mercury 1973* were used in sizing the first midcourse maneuver shown in Table 3.

Table 11. One-sigma injection errors*

Mission	Coast time, min	σ_X , m	σ_R , m	σ_V , m/sec	σ_Γ , mrad	σ_W , m	$\sigma_{\dot{W}}$, m/sec
<i>Mariner Venus/Mercury 1973</i>	30	347	499	0.94	0.267	980	3.13
<i>Surveyor</i>	25	4100	1000	1.0	0.48	1100	3.0
<i>Applications Technology Satellite (ATS)</i>	60	5400	1600	2.6	0.67	2200	3.7

*These errors are not statistically independent.
 σ_X = Down-range position error
 σ_R = Radius error from the center of the earth
 σ_V = Inertial velocity magnitude error
 σ_Γ = Flight path angle error
 σ_W = Cross-range position error
 $\sigma_{\dot{W}}$ = Cross-range velocity error

VI. Mission Description

The baseline mission sequence for *Mariner Venus/Mercury 1973* is similar to previous *Mariner* missions, with two notable exceptions. The spacecraft encounters two planets, Venus and Mercury, and performs three midcourse trajectory correction maneuvers. The first midcourse correction occurs 8 days after launch. The second and third maneuvers occur 3 days before Venus

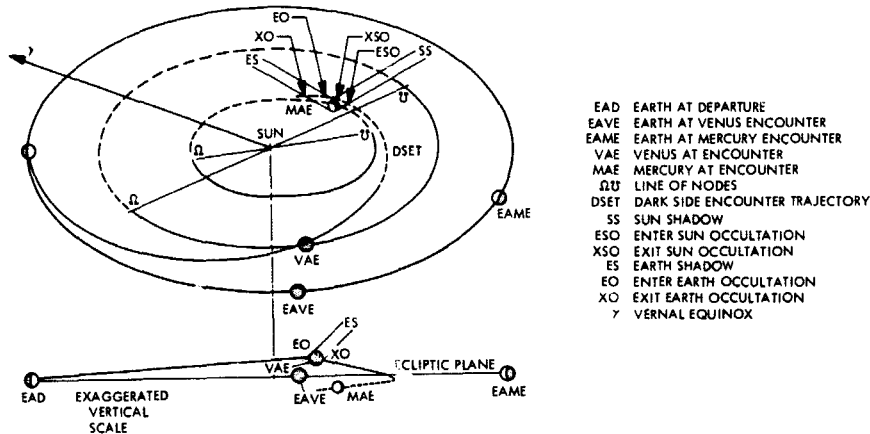


Fig. 25. Mariner Venus/Mercury 1973 trajectory and sequence

encounter, and 8 days after Venus encounter, respectively. The baseline mission is depicted in Fig. 25. The spacecraft approaches the dark side of Venus above the ecliptic plane, passes the planet approximately 100 days after launch (the actual number of days depends on the launch day), and travels through the earth occultation zone. The spacecraft then passes downward through the ecliptic plane and proceeds toward Mercury. At Mercury, the spacecraft travels through the sun occultation zone, passes within 2500 km of the surface of Mercury, and travels through the earth occultation zone in rapid succession. The baseline mission is terminated 20 days past Mercury encounter.

The Mariner Venus/Mercury 1973 baseline capabilities were indicated in Table 1. A significant difference from recent Mariner spacecraft is the inclusion of a one degree-of-freedom, high-gain steerable antenna. In addition, the baseline spacecraft has the capability for four midcourse trajectory corrections; however, only three maneuvers are anticipated. The Mariner Venus/Mercury 1973 spacecraft will pass approximately 0.43 AU from the sun after Mercury encounter, which is closer than any previous Mariner spacecraft. This is a most important difference because the thermal environment will be significantly more severe.

Interplanetary cruise science and engineering rates are 166% bits/sec and 66%, 33% or 8% bits/sec, respectively. Interplanetary science and engineering data are trans-

mitted over the primary low-gain antenna until approximately 65 days before Venus encounter. The high-gain antenna is used subsequently for communications except during maneuvers. The baseline antenna configuration results in a few weeks loss of cruise science data near earth for early launch dates, because the spacecraft is optimized to acquire data primarily during planetary encounters, and secondarily, between Venus and Mercury.

A buffer has been added to the baseline science data subsystem (SDS) to augment the tape recorder. The intent of the buffer is to store real-time fields and particles data during critical periods of the mission near planetary encounter when the data storage subsystem (DSS) is in the record or playback mode.

The baseline spacecraft has the primary objective of obtaining data in the vicinity of Mercury; however, some of the Mercury-peculiar experiments can perform a useful science mission at Venus and during interplanetary flight. The instruments applicable at Venus are the TV, high resolution infrared radiometer (HRIR), and the dual frequency receiver (DFR). The playback data rate at Venus is 16.2 kbits/sec. The playback rate at Mercury is 8.1 kbits/sec. The baseline mission requires at least one 210-ft antenna.

Figure 26 indicates the Venus encounter science sequence. The tape recorder must be stopped for approx-

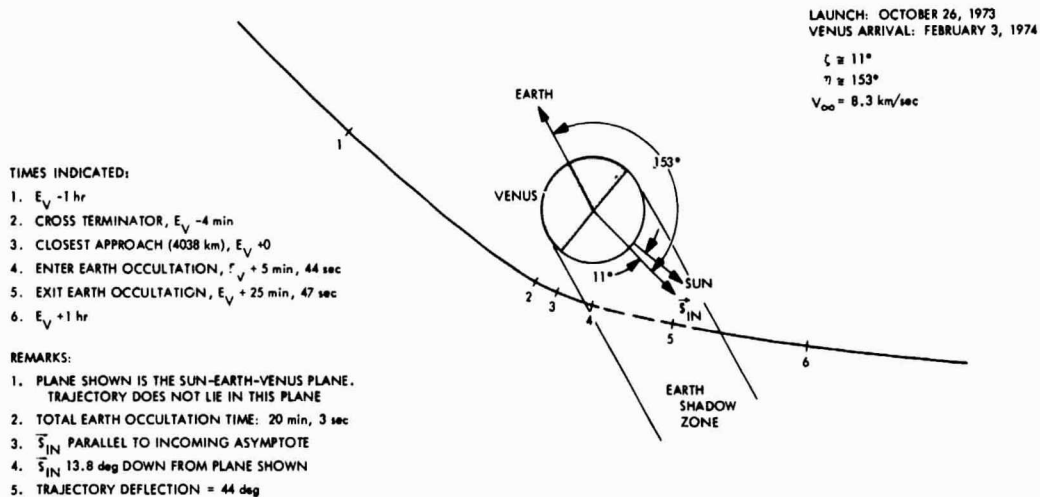


Fig. 26. Venus encounter sequence

imately 10 min during earth occultation at Venus, since the maximum recording time is approximately 20 min and data immediately before and immediately after earth occultation is desired. The tape recorder is partially unloaded and pictures taken alternately for approximately 16 hr past closest approach, when Venus subtends approximately a 1-deg field of view.

The Mercury encounter sequence is indicated in Fig. 27. The encounter sequence for Mercury is initiated 7 days prior to closest approach. Periodically, a sequence of eight TV pictures is taken and transmitted back to Goldstone or one of the other two 210-ft sites planned. Record and playback of pictures will occur up to 12 min before closest approach. The pre-encounter science ex-

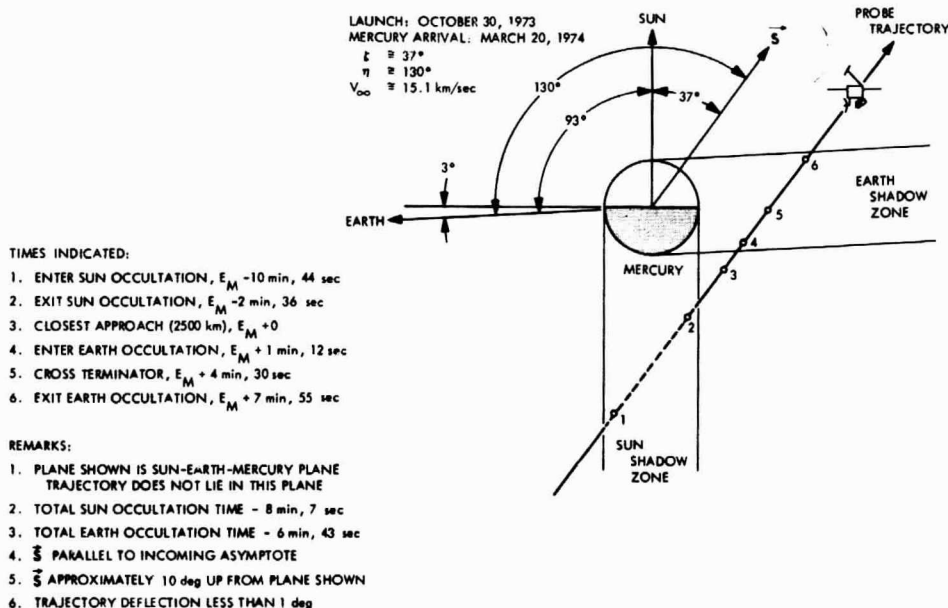


Fig. 27. Mercury encounter sequence

periments consist primarily of TV and HRIR. The cruise science instruments are also of interest during the pre-encounter as well as the post-encounter and occultation periods. The near-encounter sequence starts at sun occultation which begins 10 min before closest approach for the baseline mission. The infrared radiometer (IRR) scans the dark side of Mercury during sun occultation. Solar occultation ends approximately 2 min before closest approach. The DFR is switched into its high data rate mode at this time for earth occultation measurements. The TV and HRIR sequence is initiated 3 min after closest approach during earth occultation, and prior to the spacecraft crossing the Mercury terminator at $E_M + 4$ min, 30 sec. The spacecraft exits earth occultation about 8 min after closest approach. The TV and HRIR near-encounter sequence ends approximately 19 min after closest approach, when the DSS is filled to capacity. At this point, the spacecraft is commanded into the post-encounter science sequence in which the DSS alternately plays back encounter data previously stored and records additional TV pictures taken between these playbacks. The spacecraft is returned to the far-encounter mode approximately 3 hr after encounter, after which periodic picture taking and cruise science measurements will continue until 7 days after encounter. From 7 days until the end of the mission, cruise science measurements will be taken.

Section III referred to the possibility of extending the mission duration. The primary impact of extending the mission is a requirement that the high-gain antenna track the earth through solar opposition, requiring the antenna to function in full sun illumination at high solar intensity.

VII. Spacecraft Description

A. Introduction

The baseline spacecraft configuration resulted from consideration of the objectives and constraints described in section III, and various alternatives that arose during the study period. Some of the more significant alternatives are (baseline selections in *italics*):

- (1) *Early arrival* (March 20) at Mercury versus late arrival (sections IV, and V-C)
- (2) Sunny side, versus polar, versus *dark side pass* for early arrival (sections IV, and V-C)
- (3) Venus entry capsule versus *flyby only* (Appendix B)

- (4) Maneuver sequence; *pitch-roll* versus roll-A turn (Appendix C)
- (5) Solar cell temperature control; *4 panel mirror mosaic* versus 2 tiltable panels (Appendix D)
- (6) *Termination of mission at 20 days past Mercury* versus an extended mission (Appendix E)
- (7) Encounter record and playback data handling; *core buffer* versus other methods (to avoid loss of fields and particles data) (section VII-G).
- (8) Optimization of data return *near Mercury* versus earth/Venus interplanetary flight region (sections VII-F and Appendix E).

In the following sections, descriptions are given of the baseline spacecraft configuration, sequence of events, weight estimates, power requirements and subsystem telecommunications performance and subsystem, and data handling.

B. Configuration

1. Guidelines and constraints. Those elements of the mission which significantly impact the configuration are listed here for reference even though they may have been presented in earlier sections of the report (section III).

a. Mission parameters

Atlas/Centaur launch vehicle

Standard *Centaur (Surveyor)* shroud (Fig. 22)

Mariner-class spacecraft

Maximum utilization of *Mariner* Mars 1969 and 1971 hardware and technology

1130-lb maximum injected spacecraft (not including launch vehicle/spacecraft adapter)

b. Design requirements

Survive 5.4 solar constants experienced near Mercury at a distance of 0.43 AU from the sun

Provide maximum visibility of Mercury (and Venus) for the imaging and other planet-oriented experiments

Provide satisfactory data return throughout mission, especially from Venus encounter until 20 days after Mercury encounter

Provide spherical command-link capability.

2. Spacecraft description. The *Mariner* Venus/Mercury 1973 spacecraft configuration is based on *Mariner* Mars

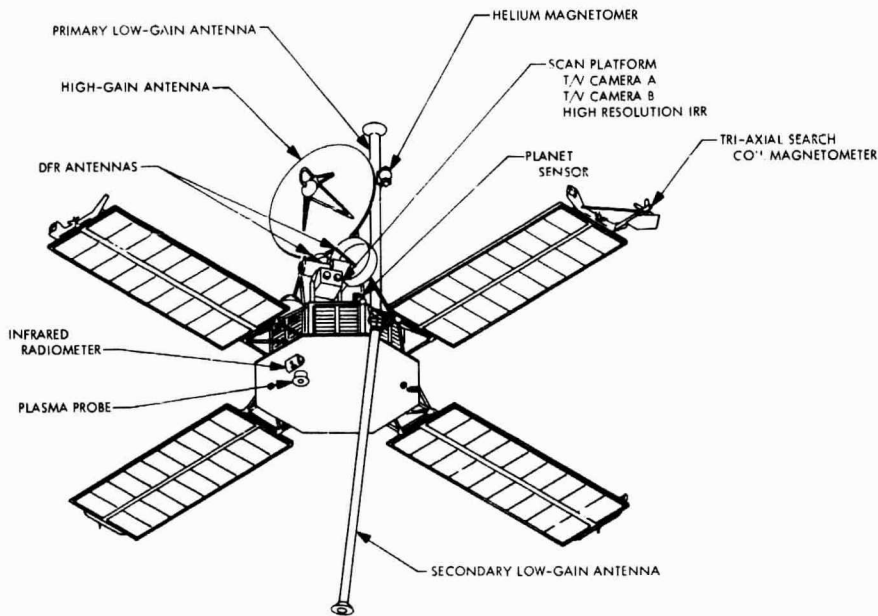


Fig. 28. Mariner Venus/Mercury 1973 spacecraft, sunlit side

1969 and 1971 hardware and technology and is identical except where unique mission parameters dictate modification or replacement of components. Figure 28 depicts the baseline spacecraft resulting from the study effort. Although the configuration pictured is not necessarily the optimum spacecraft, it serves to indicate potential problem areas and to suggest alternate approaches needing additional study. Several of these areas are discussed in the Appendices.

The spacecraft consists of the standard *Mariner* octagonal bus with six louvered bays, a *Mariner* Mars 1969 propulsion module in the seventh bay, and a high-emission, fixed radiating surface in the eighth. Four modified *Mariner* Mars 1971 solar panels are mounted on outriggers. Figure 29 is a *Mariner* Venus/Mercury 1973 configuration drawing showing subsystem and component arrangement. The panels and outriggers are inverted to face the sun in a direction opposite from that on flights to Mars. The *Mariner* Mars 1969 high-gain antenna has been placed on the shade side of the spacecraft; an instrument scan platform is shown which is considerably smaller than that used on either *Mariner* Mars 1969 or 1971. Neither the antenna nor the platform is exposed to

the sun except during maneuvers. The launch vehicle adapter along with its V-band assembly and separation mechanism remain unchanged. However, the adapter will be virtually empty since there is no scan platform on the forward face of the spacecraft. Succeeding paragraphs will cover the spacecraft and its subsystem in more detail.

a. Coordinate convention. Conventional *Mariner* coordinate systems and bay locations have been used without regard to weight, CG, or thermal considerations. A tabulation of bay locations is given below.

Bay No.	Equipment
I	Power conversion and pyro
II	Propulsion
III	Attitude control and CC&S
IV	Telemetry and command
V	Data storage
VI	RF communications
VII	Science
VIII	Power regulator and battery

Figure 30 defines the spacecraft coordinate systems. Though the coordinates are consistent with previous *Mariner* Mars spacecraft, it should be noted that the direction to the sun from the spacecraft has changed to the +Z direction. The relationship between spacecraft and launch-vehicle coordinate systems is given in Fig. 31.

b. Solar panels. Four solar panels similar structurally to those used on *Mariner* Mars 1971 are mounted on inverted *Mariner* Mars 1971-type outriggers to minimize thermal input to the spacecraft. The panels fold up for storage within the *Surveyor* fairing with the active surface facing outward. The panels slope inward slightly as they rise from the outrigger hinge points to the upper tips (Fig. 29). The upper corners are attached to one another through the *Mariner* Mars 1971 damper and latching mechanisms.

The panels provide approximately 83 ft² of surface area, one-third of which is covered with solar cells. The remainder is covered with second-surface mirrors arranged in a mosaic pattern among the cells. The mirrors reduce the panel temperature near Mercury by reflecting most of the solar energy incident to them and by emitting the heat from the solar cells conducted to them through the substrate. The substrate thickness will be increased from the 5 mils used in *Mariner* Mars 1969 and 1971 panels to perhaps as much as 20 mils for an improved conductive path. This solar panel design concept was chosen for the baseline configuration; some alternatives are discussed in Appendix D.

c. High-gain antenna. A *Mariner* Mars 1969, 40-in.-diameter, parabolic high-gain antenna is mounted on a truss structure within the stowed solar panels and does not require deployment. Except during maneuvers, the antenna remains in the shade throughout the mission. The location and height of the antenna are such that an unobstructed field of view (a 30-deg included angle cone frustum emanating from the face of the dish) is provided from $E_V - 65$ days to $E_M + 20$ days. The antenna has one degree of freedom articulation and rotates through 150 deg about a "hinge" axis defined later in section VII-F, Fig. 40.

The baseline antenna and its support structure obscure a portion of the scan platform field of view in the present configuration (Fig. 29). Additional effort will be required to restructure and relocate the antenna to minimize or eliminate interference. Field-of-view obscuration

is covered in greater detail in the next section.

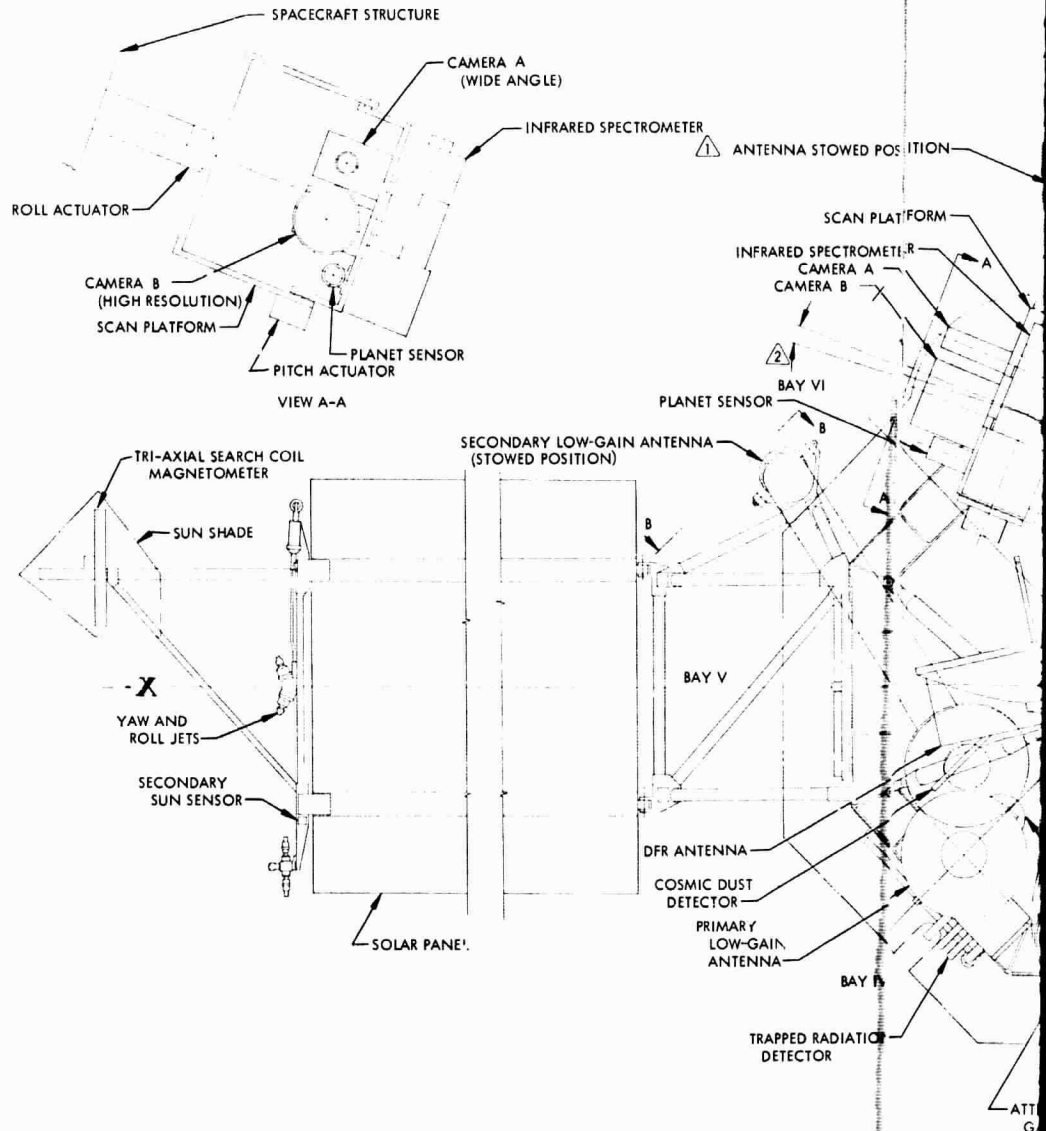
d. Low-gain antenna. A pair of *Mariner* Mars 1969 low-gain antennas provide spherical command-link capability regardless of spacecraft attitude. The antennas are mounted on top of identical 93-in. wave guides. Each antenna has an unobstructed 2.2π steradian spherical sector field of view. The primary omni is body fixed on the centerline of bay IV near the edge of the bus on the shade side of the spacecraft, with its axis parallel to the 180-deg cone vector. The secondary low-gain antenna rotates from a stowed position within the solar panels through approximately 200 deg to a deployed position on the sunlit side of the spacecraft; the deployment position is at 80 deg clock and 20 deg cone angle. The deployment hinge is attached to the bay V solar panel outrigger and protrudes into the area in front of bay VI.

e. Thermal shield and sun shade. The entire sunlit face of the spacecraft is covered by a thermal blanket which extends beyond the edges of the bus to form a shade. The edges of the shade are rigidized and supported by a stand-off structure attached to the outriggers. The extension for bays II and VIII is approximately 10 in. to protect the propulsion module and Canopus sensor, respectively. The extension is 6 in. for the remaining bays.

f. Scan platform. Science instruments which require articulation are mounted on a 2-degrees-of-freedom scan platform with complete rotational freedom (360 deg) about mutually perpendicular axes. The platform is located near the edge of the spacecraft, at the corner between bays VI and VII on the shade side, and is not exposed to the sun except during maneuvers.

The platform has the physical ability to point the cameras toward any point on a spacecraft centered celestial sphere. However, the spacecraft bus, sun shade, solar panels, and antennas do obscure some portions of the sphere. The platform location has been chosen to limit the obscuration to noncritical or least-critical areas. As located and mechanized for the baseline configuration, the platform provides for a post-encounter sequence at Venus, and both pre- and post-encounter sequences for the Mercury baseline and alternate south polar trajectories. The following section will cover the capabilities and limitations in greater detail.

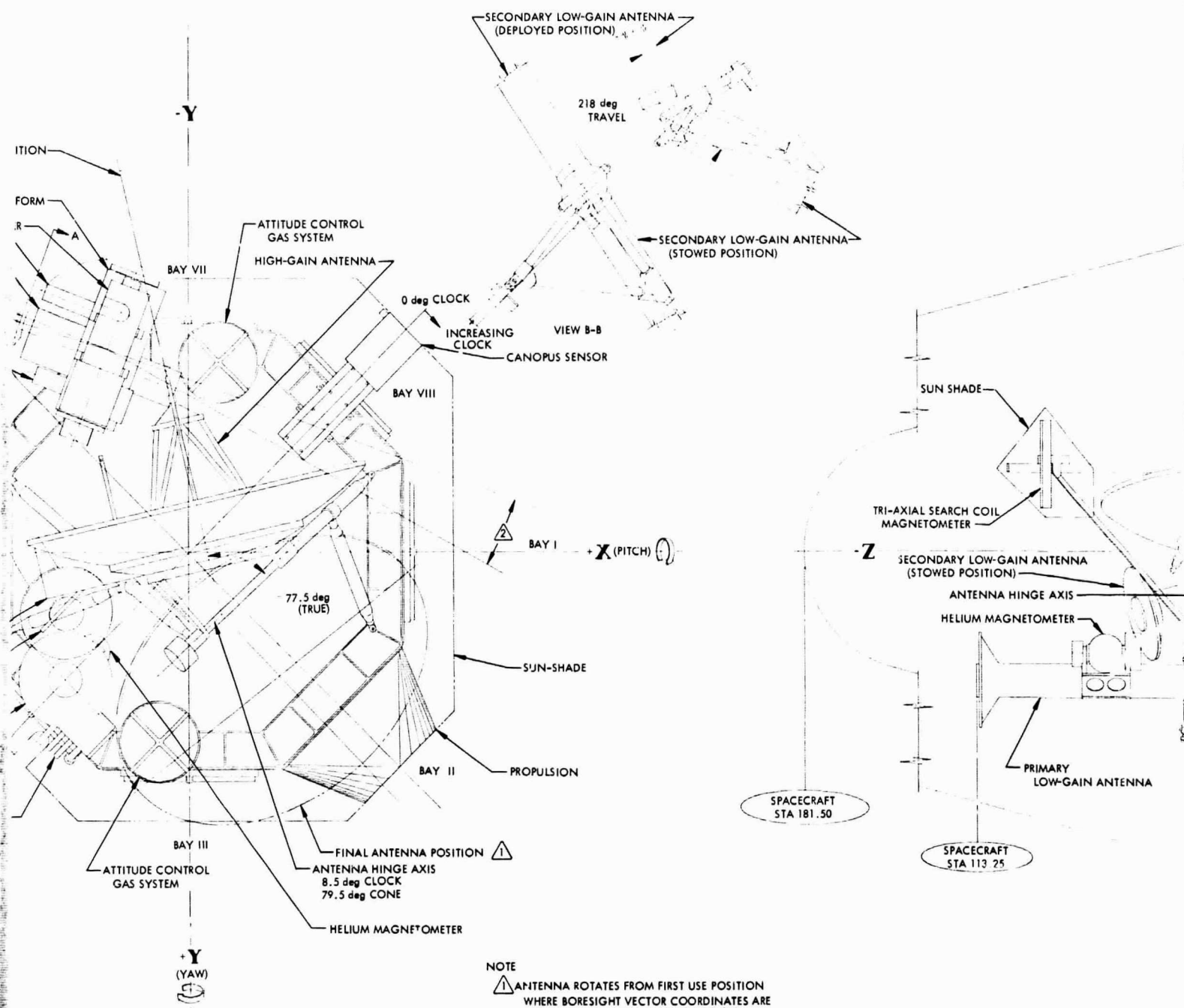
3. Scan platform pointing and obscuration. To determine the capabilities and limitations of the scan platform,



JPL TECHNICAL MEMORANDUM 33-434

FOLDOUT FRAME

A

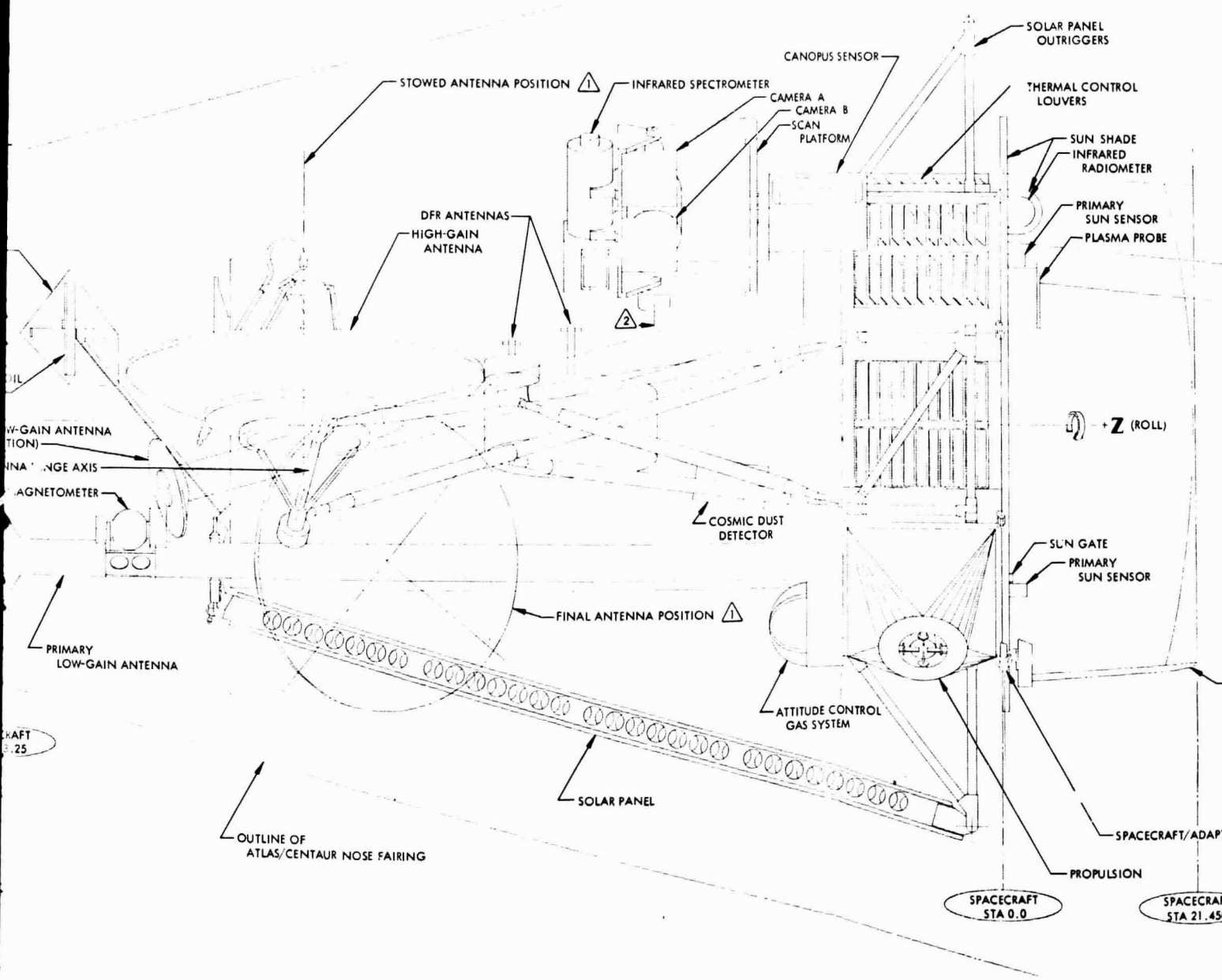


NOTE

△ ANTENNA ROTATES FROM FIRST USE POSITION WHERE BORESIGHT VECTOR COORDINATES ARE APPROXIMATELY 150 deg CONE AND 300 deg CLOCK THROUGH AN ANGLE OF 155 deg TO A FINAL POSITION OF APPROXIMATELY 45 deg CONE AND 90 deg CLOCK

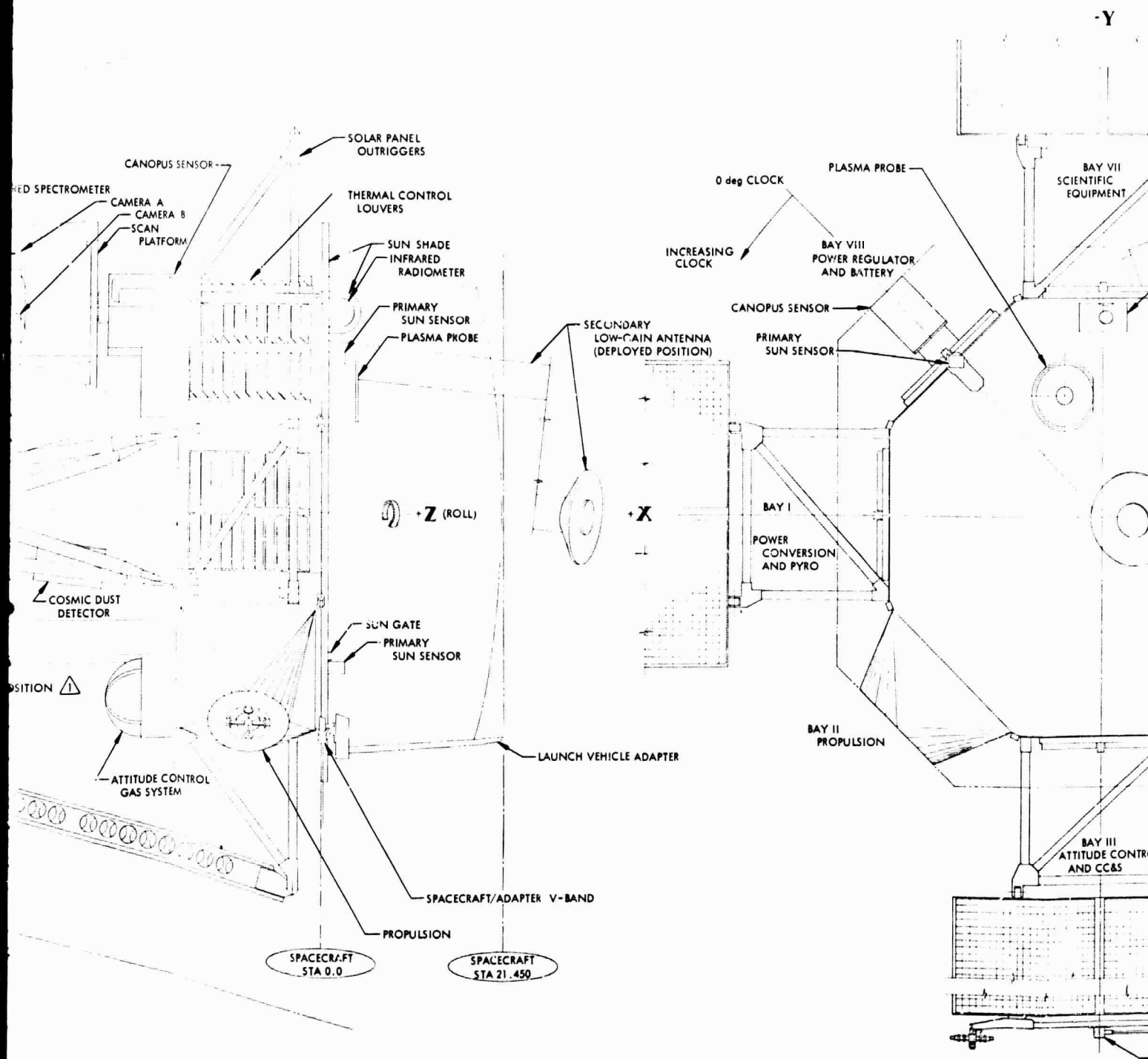
△ FOR CONE AND CLOCK VALUES OF SCAN PLATFORM POINTING VECTOR AND SPACECRAFT MASKING SEE FIGS. 32 - 36

FOLDOUT FRAME
B



FOLDOUT FRAME





FOLDOUR FRAME

D

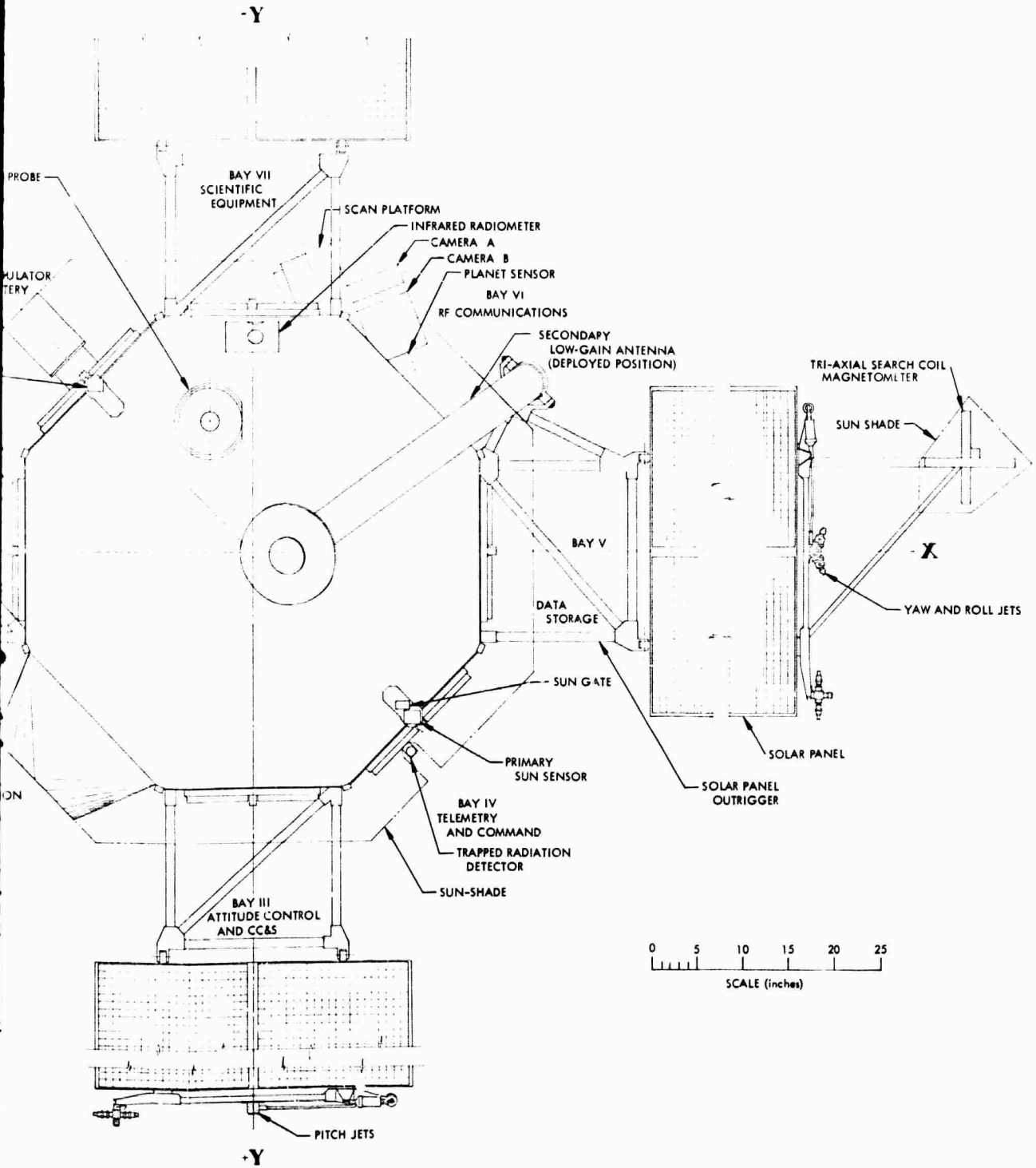


Fig. 29. Mariner Venus/Mercury 1973 configuration

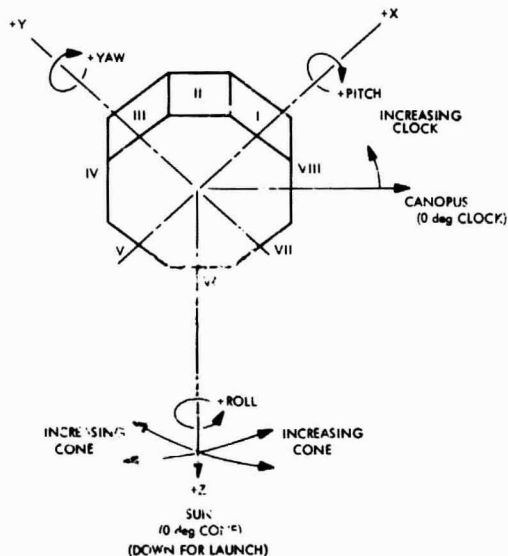


Fig. 30. Spacecraft coordinate system

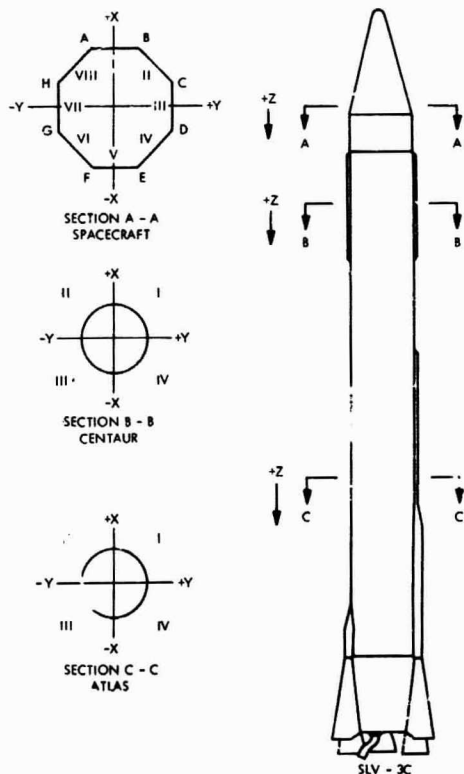


Fig. 31. Spacecraft/launch vehicle coordinate system relationship

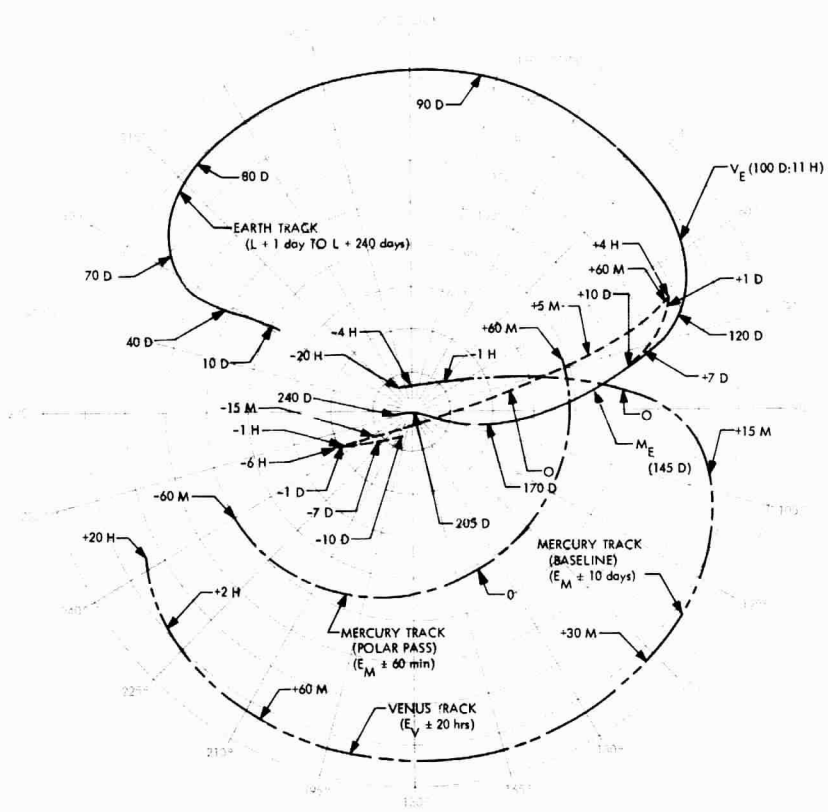
a series of figures was generated which shows the interaction between the scan platform pointing vector, the spacecraft, and the high-gain antenna.

a. *Pointing vector.* Figure 32 is a polar coordinate presentation of the apparent track of the center of planets Venus, Mercury and earth as seen from the spacecraft. The plots are given in the spacecraft coordinates of cone and clock angles with tic marks providing a time reference. (The presentation does not show the effect of planet size. At closest approach, both Venus and Mercury subtend an angle of ~ 90 deg)

The traces shown in Fig 32 are:

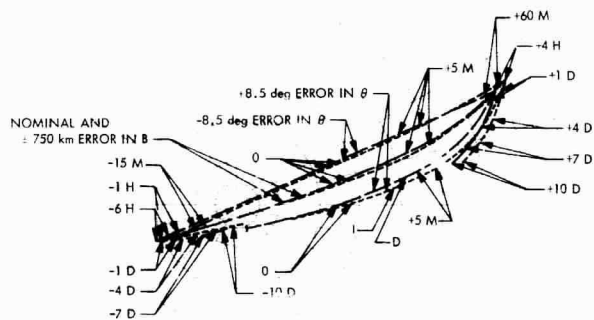
- (1) Earth (10/16/73 launch) $L + 1$ day to $L + 240$ days
- (2) Venus (10/22/73 launch) $E_V \pm 20$ hr
- (3) Mercury (10/22/73 launch)
 - (a) Reference trajectory (equatorial pass) $E_M \pm 10$ days
 - (b) Alternate trajectory (south polar pass) $E_M \pm 60$ min

b. *Pointing vector dispersions.* For the baseline mission, the effect of varying launch dates and B-plane errors on the nominal trace for the Mercury equatorial pass was also evaluated. Examination of the range of launch dates indicates that launch day 1 (10/22/73 launch; 3/21/74 arrival) and launch day 8 (10/29/73 launch; 3/19/74 arrival) give the extremes in cone and clock angle. For each of these, arbitrarily sized perturbations of ± 750 km in B and ± 8.5 deg in θ were applied to the nominal aiming point ($B = 5000$ km, $\theta = 0$ deg). (Refer to sections V-B and V-D for coordinate definitions and anticipated trajectory dispersions.) The resulting scan platform pointing vector dispersions are plotted in Fig. 33.



O = CLOSEST APPROACH
M = MINUTES (-) BEFORE, (+) AFTER, CLOSEST APPROACH
H = HOURS (-) BEFORE, (+) AFTER, CLOSEST APPROACH
D = DAYS (-) BEFORE, (+) AFTER, CLOSEST APPROACH

Fig. 32. Cone and clock coordinates of planet centers



- - - - - OCTOBER 22, 1973 LAUNCH
 MARCH 21, 1974 ARRIVAL
 - - - - - OCTOBER 29, 1973 LAUNCH
 MARCH 19, 1974 ARRIVAL
 O = CLOSEST APPROACH
 M = min (-) BEFORE, (+) AFTER, CLOSEST APPROACH
 H = hr (-) BEFORE, (+) AFTER, CLOSEST APPROACH
 D = days (-) BEFORE, (+) AFTER, CLOSEST APPROACH

Fig. 33. Dispersions to baseline Mercury track resulting from varying launch date and B-plane errors

c. *Scan platform capability.* Figures 34 and 35 show the degree to which masking limits the platform capabilities.¹⁰ The irregular outline superimposed on planet traces represents the limits to which the platform can be rotated in cone and clock while maintaining a *totally* unobstructed field of view. The center of rotation of the platform is taken as the origin in these figures.

Also presented in the figures are the relative positions and shapes of the high-gain antenna, and the scan platform fields of view at various critical times near encounter. It may be seen that the view of the center of Mercury is not obstructed by the antenna (Fig. 35) though masking of Venus from $E_V + 7$ min to $E_V + 30$ min does occur (Fig. 34). Masking caused by the baseline high-gain support structure has not been presented in these figures. Restructuring will be necessary to eliminate the masking which results from the structure shown in Fig. 29.

In summary, the platform provides an unobstructed field of view for both cameras when pointed at the planet centers for at least the following intervals:

- (1) Venus encounter
 $E_V - 10$ min to $E_V + 7$ min; and $E_V + 30$ min to $E_V + 20$ hr
(view obstructed by high-gain antenna from $E_V + 7$ min to $E_V + 30$ min).
- (2) Baseline trajectory (Mercury equatorial pass)
 $E_M - 7$ days to $E_M - 15$ min; and, $E_M + 3.5$ min to $E_M + 10$ days
(view obstructed by spacecraft from $E_M - 15$ min to $E_M + 3.5$ min).
- (3) Alternate trajectory (Mercury south polar pass)
 $E_M - 60$ min to $E_M + 60$ min

4. *Science instruments.* At this point in the program, a science payload has not been selected. However, evaluation of interface problems such as instrument placement, look angles, fields of view, and temperature control can only be accomplished using instruments for which data and requirements exist. Therefore, a representative

¹⁰Geometric considerations and physical aspects assumed in determining the masked area are shown in Fig. 36. For convenience in constructing the mask, a fixed shape for the field of view was used throughout. The shape used is conservative except at the outer ends of the solar panels, where interference does not occur in the baseline mission.

science payload as suggested by NASA, was used, and, where appropriate, parameters of prior *Mariner* instruments were assumed.

The instruments are: wide-angle camera, narrow-angle camera, high-resolution infrared radiometer, dark-side infrared radiometer, helium magnetometer, tri-axial search coil magnetometer, dual-frequency receiver, energetic particle detector, plasma probe, and cosmic dust detector.

The two cameras and the HRIR are located on the scan platform which has a $4\text{-}\pi$ steradian pointing capability, though portions of the field of view are obscured, as discussed in section VII-B-3.

The IRR is mounted on the sunlit face of the spacecraft. The sensor is partially submerged within bay VII and is mounted against a louvered wall. The sensor is covered by the forward thermal blanket except for the view ports. A removable sun shade will cover the port area until solar occultation occurs.

The helium vapor magnetometer mounts on the primary low-gain antenna mast 80 in. above the spacecraft as in previous *Mariner* spacecraft designs.

The tri-axial search coil magnetometer sensor consists of three mutually perpendicular bar shaped elements. The sensor is located 10 ft from the spacecraft on a 2-ft fixed boom which is attached to the end of a solar panel. A shade is provided to protect the sensor from the sun.

A pair of cupped turnstile DFR antennas (423.3 and 1294.8 MHz) are attached to, and move with, the high-gain antenna. This articulation provides for an occultation experiment at Venus and Mercury without the necessity of separate repositioning of the DFR antennas at the two planets. The DFR antennas may require relocation if unacceptable interference with the scan platform field of view occurs.

The plasma probe, energetic particle detector, and cosmic dust detector of the types used on previous *Mariner* spacecraft were also evaluated. These instruments should require no special attention with the exception of the plasma probe, where materials changes in the sensor will be required to withstand the thermal environment near Mercury.

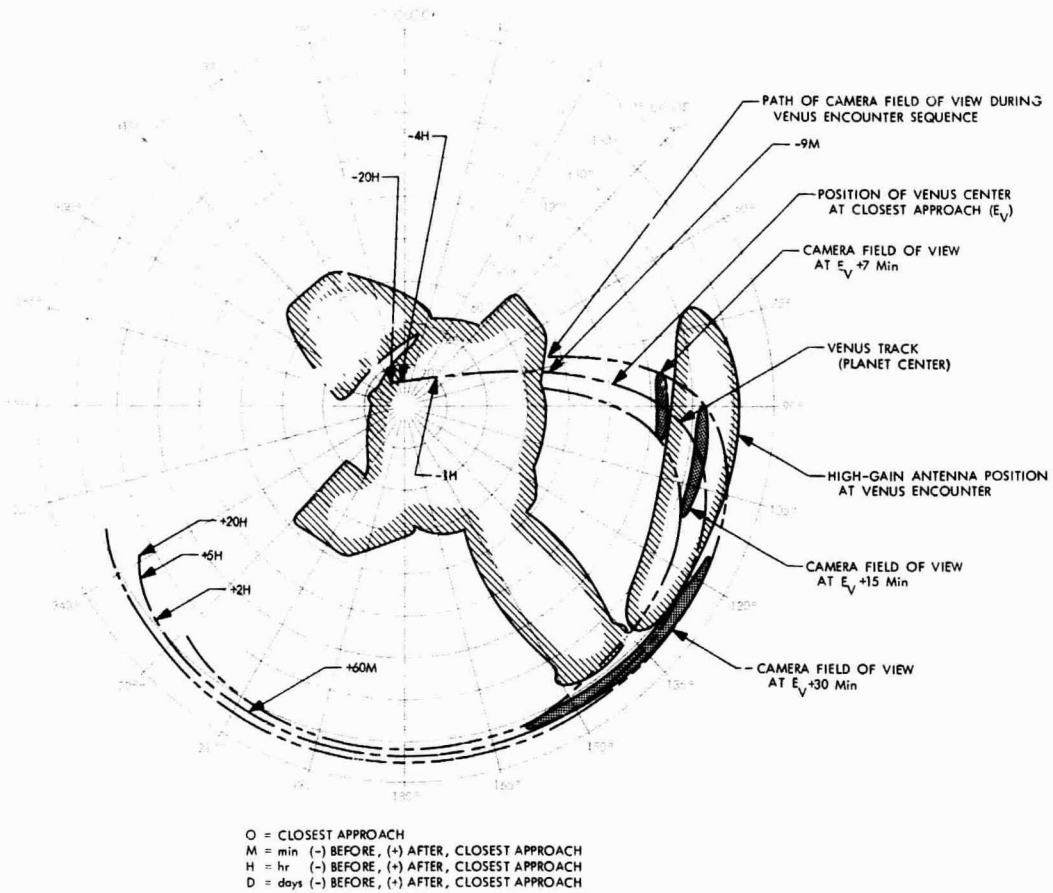
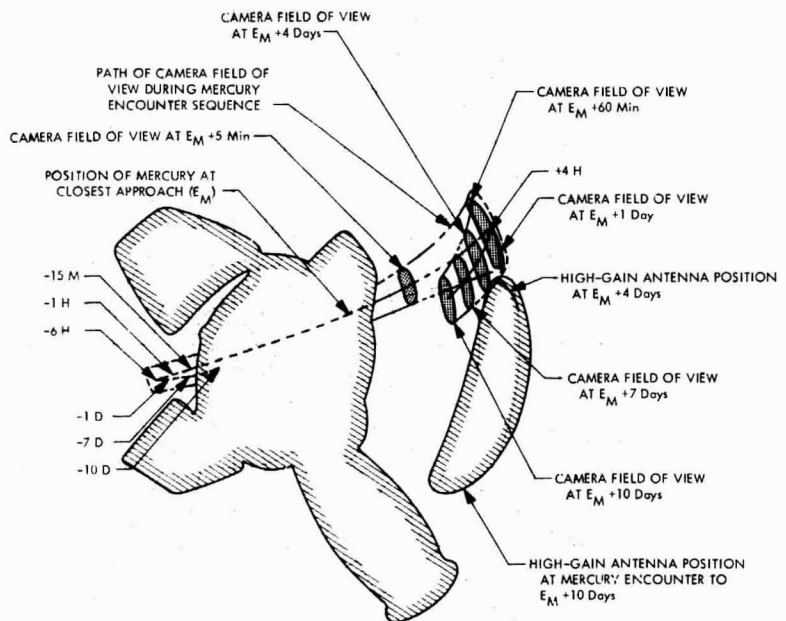


Fig. 34. Scan platform view limitations at Venus



O = CLOSEST APPROACH
 M = min (-) BEFORE, (+) AFTER, CLOSEST APPROACH
 H = hr (-) BEFORE, (+) AFTER, CLOSEST APPROACH
 D = days (-) BEFORE, (+) AFTER, CLOSEST APPROACH

Fig. 35. Scan platform view limitations at Mercury

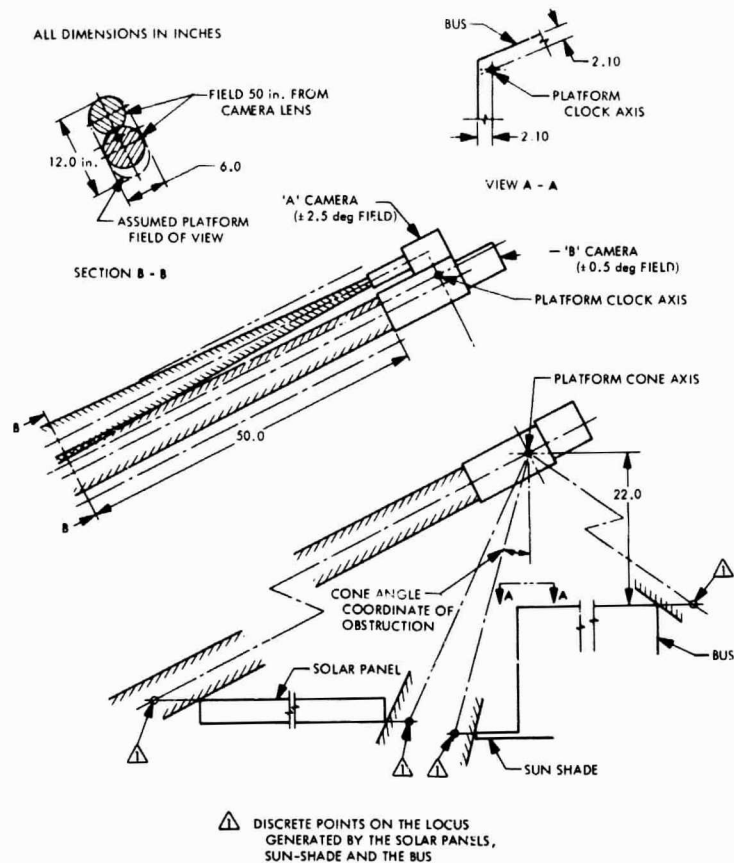


Fig. 36. Spacecraft mask determination

C. Mariner Venus/Mercury 1973 Baseline Sequence of Events

The sequence of events that follows was generated to provide a nominal mission outline. The reference trajectory was assumed with Venus arrival February 3, 1974 (1700 GMT) and Mercury arrival March 20, 1974 (1800 GMT). The launch date is October 26, 1973. The baseline mission assumed is an equatorial pass with dual (sun and earth) occultation at Mercury.

The level of detail presented is only that which is necessary to assist the technical disciplines in initial design of subsystems. The source and destination of commands necessary to implement the sequence of events are not considered here.

Definitions used in this sequence are:

- $L + 0 =$ liftoff (2-in. rise)
- $S + 0 =$ spacecraft separation from launch vehicle
- $M_n + 0 =$ start of n th trajectory correction maneuver ($n = 1,2,3$)
- $E_V + 0 =$ closest approach to Venus
- $E_M + 0 =$ closest approach to Mercury

The nominal operational telemetry modes referred to in this section are described in section VII-G. Performance predictions are discussed in section VII-F.

A time-line diagram of some of the key maneuver and encounter events is shown in Fig. 37.

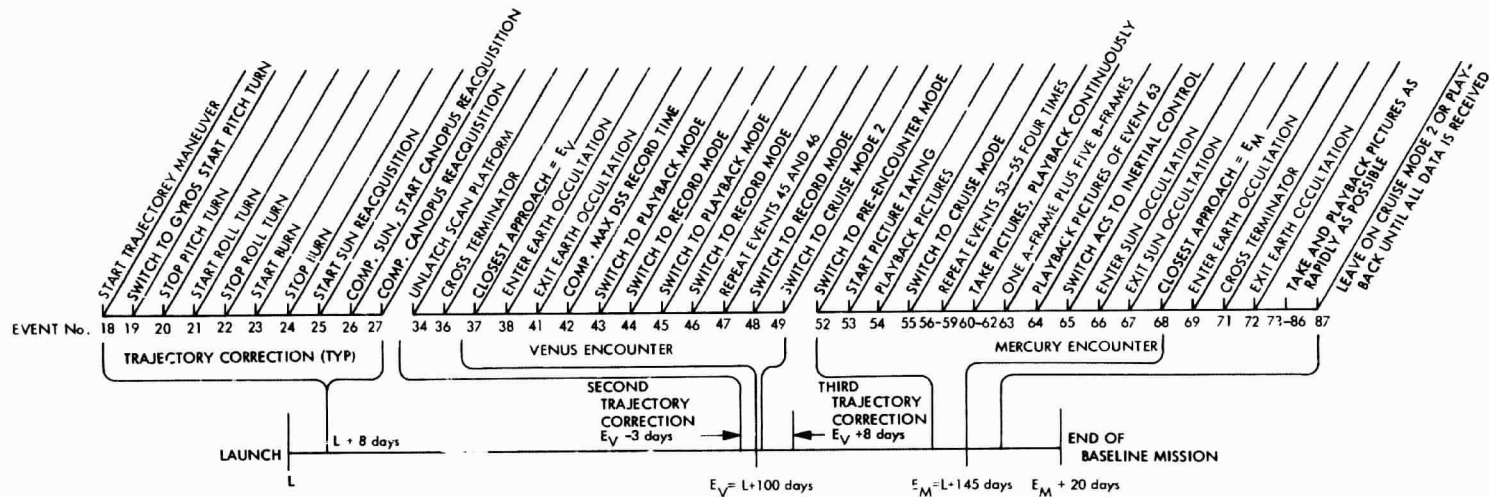


Fig. 37. Time-line sequence of events, baseline mission

Major events with their associated nominal times follow:

EVENT	TIME
1. Start final spacecraft countdown checkout. RF power on, cruise mode I. TWT low power. Transmitting and receiving on primary low-gain antenna.	L - 4 hr
2. Clear, load, and verify CC&S.	L - 1 hr
3. Start one-way communications (downlink only).	L - 1 hr
4. Switch spacecraft to internal power and verify.	L - 7 min
5. Start CC&S sequence.	L - 4 min
6. Liftoff.	L + 0 (Oct. 26, 1973) 0546 GMT
7. Aerodynamic fairing separation.	To be determined
8. Second Centaur burn cutoff (injection). ¹¹	L + 39 min (1739 sec coast time)
9. Separate spacecraft.	S + 0 (L + 40 min)
10. Turn on active attitude control ACS. Start acquiring sun.	S + 0
11. Start two-way communications. Transmitting and receiving on primary low-gain antenna. 85-ft d' h. Low-power TWT.	S + 0
12. Deploy solar panels and secondary low-gain antenna.	S + 3 min, 10 sec
13. CC&S backup to verify turn-on of ACS, (deployment of solar panels and secondary low-gain antenna.	S + 25 min (L + 65 min)
14. Sun acquisition complete. Switch to solar panel power.	Event 10 + 0 min to event 10 + 45 min
15. Switch to cruise mode II. Start calibration of magnetometers.	Event 14 + 0 min
16. Complete magnetometer calibration. Turn on Canopus sensor and initiate roll search about the sunline axis.	Event 14 + 10 hr
17. Complete Canopus acquisition. Terminate roll search.	Event 16 + 0 min to event 16 + 120 min

¹¹All powered flight trajectories require a parking orbit. A typical value of 39 min includes 29 min coast time and 10 min from launch to start of parking orbit.

¹²The baseline turn sequence for all *Mariner Venus/Mercury* 1973 maneuvers is a pitch turn followed by a roll turn (referred to as a pitch-roll maneuver). The above times are typical values for any of the four possible trajectory-correction maneuvers. The roll-A maneuver turn sequence is discussed in Appendix C and appears to be a possible alternative to the pitch-roll maneuver turn sequence as some thermal problems are alleviated.

¹³Launch-date dependent.

EVENT	TIME
18. Initiate first trajectory correction maneuver. Switch to cruise mode I. Gyros turned on. Low-power TWT, primary low-gain antenna, 210-ft dish not mandatory. Ranging turned off.	M ₁ + 0 (L + 8 days)
19. Switch to inertial reference. Set polarity. Start pitch turn ¹² (0.18 deg min to 180 deg max).	M ₁ + 68 min, 16 sec
20. Stop pitch turn.	Event 19 + 1 sec to event 19 + 2000 sec
21. Set polarity. Start roll turn (0.18 deg min to 180 deg max).	Event 20 + 256 sec
22. Stop roll turn.	Event 21 + 1 sec to event 21 + 2000 sec
23. Start burn.	Event 22 + 1024 sec
24. Stop burn.	Event 23 + 0.0 ^o sec to event 23 + 102.35 sec
25. Start sun reacquisition.	Event 24 + 256 sec
26. Complete sun reacquisition. Switch to cruise mode II. Start Canopus reacquisition.	Event 25 + 0 sec to event 25 + 1200 sec (M ₁ + 93 min, 54 sec to M ₁ + 182 min, 14 sec)
27. Complete Canopus reacquisition. Gyros turned off.	Event 26 + 1 hr to event 26 + 4 hr
28. Switch TWT to high-power. TWT will remain in high power for remainder of mission.	L + 10 days
29. Switch to cruise mode I. Science loss due to blackout. (Will not occur for late launches.)	L + 15 days ¹³ (Oct 26 launch)
30. Unlatch high-gain antenna.	Between events 29 and 31
31. Switch to high-gain spacecraft antenna. Spacecraft receiving over primary low-gain antenna. Switch to cruise mode II. Resume ranging desired.	L + 35 days ¹³ (Oct 26 launch)
32. Initiate second trajectory maneuver. ¹² Switch to cruise mode I. Gyros turned on. Switch spacecraft transmission to primary low-gain antenna. 210-ft dish may be mandatory depending on value of turns. Repeat events 19-27.	M ₂ + 0 (E ₁ - 3 days) January 31, 1974 (L + 97 days) ¹³
33. Switch spacecraft transmission back to high-gain antenna. Switch to cruise mode II. 85-ft dish.	M ₂ + 93 min, 54 sec to M ₂ + 182 min, 14 sec
34. Unlatch scan platform.	Between events 33 and 35
35. Switch to pre-encounter mode.	E ₁ - 1 hr
36. Cross terminator.	E ₁ - 3 min, 59 sec
37. Closest approach. DSS on. Picture taking commences. Switch to record mode I. DFR begins high rate data transmission.	E ₁ + 0, 1700 GMT Feb 3, 1974 (L + 100 days) ¹³

EVENT	TIME
38. Enter earth occultation. Engineering data will be lost throughout occultation. Switch to record mode II.	$E_1 + 5 \text{ min, } 44 \text{ sec}$
39. Switch to record mode III in order to conserve storage capacity for occultation exit. Time will be determined by actual picture sequence as frame time varies depending on whether same camera, alternating cameras, or a combination is the picture order desired.	To be determined
40. Switch to record mode II.	$E_1 + 21 \text{ min, } 0 \text{ sec}$
41. Exit earth occultation. Switch to record mode I.	$E_1 + 25 \text{ min, } 47 \text{ sec}$
42. Completion of maximum DSS recording time. Time required of actual recording (not counting gap from event 39 to 40) will vary from 16.6 to 21.4 min, depending on camera sequence chosen. 32 pictures have been taken.	To be determined
43. Switch to playback mode. Play back two pictures which will take 10 min, 57 sec.	To be determined
44. Switch to record mode I. Take one picture.	Event 43 + 0
45. Switch to playback mode. Play back two pictures (most recent picture and one encounter picture).	Event 44 + 31 sec
46. Switch to record mode I. Take one picture.	Event 45 + 10 min, 57 sec
47. Repeat steps 45 and 46 until recorder is empty and all encounter and far encounter pictures have been transmitted. Minimum time (no gap in picture taking) to do this would be approximately 6 hr.	
48. Switch to record mode I. TV will take 32 more pictures at appropriate times until $E_1 + 16 \text{ hr}$. These pictures will be stored on DSS until 210-ft dish comes into view again. Fields and particles data will be received by 85-ft dish whenever 210-ft dish is not in view. Cruise mode II will be used when TV pictures are not being recorded or played back.	To be determined 'approx. $E_1 + 7 \text{ hr}$
49. Switch to cruise mode II.	$E_1 + 16 \text{ hr}$
50. Initiate third trajectory maneuver. ¹² Switch to cruise mode I. Gyros turned on. Switch spacecraft transmission to low-gain antenna. 210-ft dish mandatory unless turns very small. Repeat events 19-27.	$M_3 + 0 (E_1 + 8 \text{ days})$
51. Switch to cruise mode II. Switch spacecraft transmission back to high-gain antenna.	$M_3 + 93 \text{ min, } 54 \text{ sec}$ $M_3 + 182 \text{ min, } 14 \text{ sec}$
52. Switch to pre-encounter mode.	$E_M - 7 \text{ days}$

EVENT	TIME
53. Switch to record mode I. ¹⁴ Start picture taking when camera B resolution equals 500 km. Record 7 B frames and one A frame. Will take 4 min, 58 sec if A frame is between two B frames. HRIR remains off.	$E_M - 7 \text{ days}$
54. Switch to playback mode. Transmit 8 pictures taken in event 53; will take 87 min, 36 sec.	Event 53 + 0 min, 58 sec
55. Switch to cruise mode II.	Event 54 + 87 min, 36 sec
56. Repeat events 53-55.	$E_M - 4 \text{ days}$
57. Repeat events 53-55.	$E_M - 2 \text{ days}$
58. Repeat events 53-55.	$E_M - 1 \text{ day}$
59. Repeat events 53-55.	$E_M - 12 \text{ hr}$
60. Switch to record mode I. Begin when B field of view is approximately one planet diameter. Record one B frame. Requires 31 sec. HRIR on.	$E_M - 6 \text{ hr, } 54 \text{ min}$
61. Switch to playback mode. Transmit picture taken in event 60; will take 11.2 min.	$E_M - 6 \text{ hr, } 53 \text{ min, } 29 \text{ sec}$
62. Begin repeating events 60-61 (continuously).	$E_M - 5 \text{ hr, } 42 \text{ min, } 17 \text{ sec}$
63. Switch to record mode I. Record one A frame followed by five B frames.	$E_M - 1 \text{ hr, } 22 \text{ min, } 58 \text{ sec}$
64. Switch to playback mode. Transmit 6 pictures taken in event 63; will take 67 min, 12 sec.	$E_M - 1 \text{ hr, } 19 \text{ min, } 12 \text{ sec}$
65. Switch to cruise mode II. Switch ACS to inertial control (gyros on).	$E_M - 12 \text{ min}$
66. Enter sun occultation. Take cover off IRR. Begin IRR operation.	$E_M - 10 \text{ min, } 44.5 \text{ sec}$
67. Exit sun occultation. Turn IRR off. Put cover back on.	$E_M - 2 \text{ min, } 36.8 \text{ sec}$
68. Closest approach.	$E_M + 0, 1800 \text{ GMT}$ March 20, 1974 ($L + 145 \text{ days}$) ¹³
69. Switch to record mode III. Enter earth occultation. Lose engineering data throughout occultation.	$E_M + 1 \text{ min, } 12 \text{ sec}$
70. Switch to record mode II. Record A and B frames until DSS capacity is filled; will take 16 min, 33 sec.	$E_M + 3 \text{ min}$
71. Cross terminator.	$E_M + 4 \text{ min, } 30 \text{ sec}$
72. Exit earth occultation. Switch to record mode I. Switch ACS back to celestial reference (gyros off).	$E_M + 17 \text{ min, } 55.2 \text{ sec}$
73. Switch to playback mode. DSS now full. Transmit 2 pictures.	$E_M + 19 \text{ min, } 33 \text{ sec}$
74. Switch to record mode I. Take one B frame.	$E_M + 43 \text{ min, } 57 \text{ sec}$
75. Repeat events 73 and 74 three times for a total of four cycles. (28 pictures on DSS at completion of cycles.)	$E_M + 44 \text{ min, } 28 \text{ sec}$

¹⁴For the baseline configuration, there are two cameras, A and B, which are discussed in section VIII-N.

EVENT	TIME
76. Switch to playback mode. Transmit 8 pictures (20 pictures on DSS).	$E_M + 1 \text{ hr, } 59 \text{ min, } 13 \text{ sec}$
77. Switch to record mode I. Record one B frame.	$E_M + 3 \text{ hr, } 28 \text{ min, } 49 \text{ sec}$
78. Repeat events 76 and 77 three times for a total of four cycles. At completion DSS will be empty.	$E_M + 3 \text{ hr, } 29 \text{ min, } 20 \text{ sec}$
79. Switch to cruise mode II.	$E_M + 7 \text{ hr, } 59 \text{ min, } 41 \text{ sec}$
80. Switch to record mode I. Record 7 B frames and one A frame; will take 4 min, 58 sec if A frame is between two B frames. HRIR off.	$E_M + 12 \text{ hr}$
81. Switch to playback mode I. Transmit 8 pictures taken in event 80. Will take 87 min, 36 sec.	$E_M + 12 \text{ hr, } 4 \text{ min, } 58 \text{ sec}$
82. Switch to cruise mode II.	$E_M + 13 \text{ hr, } 32 \text{ min, } 34 \text{ sec}$
83. Repeat events 80-82.	$E_M + 1 \text{ day}$
84. Repeat events 80-82.	$E_M + 2 \text{ days}$
85. Repeat events 80-82.	$E_M + 4 \text{ days}$
86. Repeat events 80-82.	$E_M + 7 \text{ days}$
87. Leave on cruise mode II or playback mode until all desired data are obtained.	$E_M + 7 \text{ days}$
88. End of baseline mission. ¹⁵	$E_M + 20 \text{ days}$

D. Weight Summary and Subsystem Development Status

The *Mariner Venus/Mercury 1973* subsystem weights and status are shown in Table 12 for the baseline Mercury flyby. The total spacecraft weight is 829 lb, which includes 71 lb for the *Mariner Mars 1969* spacecraft adapter. Thus, the separated (injected) spacecraft weight is 758 lb. The launch energy C_3 required for the baseline opportunity is $20.5 \text{ km}^2/\text{sec}^2$, which corresponds to a separated spacecraft capability of approximately 1130 lb for the *Atlas (SLV-3C)/Centaur D* launch vehicle. Therefore, an additional 372 lb of separated spacecraft payload capability exists for the baseline opportunity.

The propulsion weight shown includes the capability for a fourth midcourse trajectory correction maneuver. The SDS weight shown includes 7 lb for the core buffer discussed in section VII-G and VIII-M. The science payload, given in section VIII-N, weighs 90 lb, approximately 12% of the separated spacecraft weight. The power subsystem weight breakdown is discussed in section VIII-D. The DSS, FTS, FCS and RFS subsystem weights are based on tentative *Mariner Mars 1971* values.

¹⁵Refer to section III and Appendix E for extended mission considerations.

The design and technology status of each subsystem is as indicated.

E. Power Requirements and Subsystem Description

The *Mariner Venus/Mercury 1973* power subsystem consists of a primary and a secondary power source, solar panels and silver zinc batteries, and (tentatively selected) silver zinc batteries, respectively. In addition, power conditioning components are provided for conditioning and conversion of unregulated solar panel and battery outputs as required by user subsystems. A functional block diagram of the *Mariner Venus/Mercury 1973* baseline power subsystem is shown in section VIII, Fig. 64. A combination of the *Mariner Mars 1969/1971* power subsystems was used as the baseline system. The sizing of the primary and secondary power source and conditioning equipment is based on the total power demand from each source and component in addition to the efficiencies of these components which vary throughout the mission. Component efficiencies and their effect on the total power demand are shown in section VIII, Table 18.

The distance of the spacecraft from the sun must be taken into consideration when sizing the solar panel. On April 2, 1974 (13 days after arrival at Mercury), the spacecraft is at its closest approach to the sun, assumed as 0.43 AU. Solar intensity is increased from 140 mw/cm^2 at earth to approximately 757 mw/cm^2 . Associated with the increase in solar intensity is a significant increase in temperature. Because of this, a newly designed solar panel is required, limiting maximum panel temperature to 135 to 140°C. As a result, near-Mercury output may drop to approximately 19 Vdc (Appendix D), which is below the minimum input voltage allowance of 25 Vdc (maximum 50 Vdc) for operation of the power conditioning, battery charger, and battery. However, the switching of four solar panels from a parallel condition at 35 Vdc (temperature approaches 60°C) to a two-panel parallel-series operation (shown in section VIII, Fig. 65), will alleviate this condition. Available solar panel power will vary from approximately 375 W at near-earth to approximately 550 W at Mercury (Appendix D). A detailed discussion of this approach is presented in section VIII-D-2 and -4.

Table 13 summarizes the total raw power required for the key operational modes (section VII-C) which occur from launch through a Mercury-sun occultation mode. Included is the power source required and assigned for each mode of operation. A detailed breakdown of power requirements is shown in section VIII, Table 18.

Table 12. Weight summary and subsystem development status

Subsystem	Weight, lb	Design	Technology
Adapter	71	Mariner Mars 1969	Mariner Mars 1969
Structure	170	Major modification	Mariner Mars 1969
RFS	55	Mariner Mars 1971	Mariner Mars 1971
FCS	9	New	Current
CC&S	20	Minor modification	Mariner Mars 1969
FTS	21	Major modification	Current
ACS	69	Minor modification	Mariner Mars 1969
Pyro	10	Minor modification	Mariner Mars 1969
Cabling	58	New	Current
Propulsion	50	Minor modification	Mariner Mars 1969
TC	26	Major modification	Mariner Mars 1969/1971 ^a
Devices	24	Minor modification	Mariner Mars 1969/1971
DSS	20	Mariner Mars 1971	Mariner Mars 1971
SDS	25	New	Mariner Mars 1971
Scan control	20	New	Mariner Mars 1969
Power	90	Minor modification	Current ^b
TV	49	Major modification	Mariner Mars 1971
HRIR	11	Major modification	Nimbus
IRR	5	Major modification	Mariner Mars 1969
Magnetometers	7	Major modification	Mariner Mars 1971 & OGO
Plasma probe	7	Minor modification	Mariner Mars 1971
Energetic particle detector	3	Minor modification	Mariner Mars 1971
Cosmic dust detector	3	Minor modification	Mariner Mars 1964
DFR	6	Minor modification	Mariner Venus 67
Total spacecraft weight	829		
Spacecraft adapter weight	71		
Separated spacecraft weight	758		

Atlas-Centaur separated spacecraft capability approximately 1130 lb for $C_3 = 20.5 \text{ km}^2/\text{sec}^2$

^aREAD required for sun side insulation
^bREAD required for solar arrays

F. Telecommunications Subsystem Description and Performance

1. *Mission requirements.* The following telecommunications subsystem requirements were assumed:

- (1) Engineering telemetry and command capability are required during the near-earth phase after sun acquisition, once roll stabilization has been achieved.
- (2) Engineering telemetry and command coverage is required during the motor burn of all trajectory correction maneuvers. It is also highly desirable that communications be maintained through all turns prior to the burn, then during sun acquisition after the maneuvers are completed. Use of the 210-ft DSIF antenna is required for spherical coverage of the second and third maneuvers.
- (3) Engineering telemetry and command capability are required during all other phases of the mission not covered in (1) and (2) above.

- (4) Cruise science data is desired over as much of the mission as possible. However, performance at Mercury and Venus has priority.
- (5) High-rate telemetry at 8.1 kbits/sec is required at $E_M - 7$ days to $E_M + 7$ days. High-rate telemetry at 4.1 kbits/sec is desired to 20 days after E_M .

2. *Baseline and alternate systems.* An overall block diagram of the Mariner Venus/Mercury 1973 telecommunications subsystem is shown in Fig. 38. The major components of the telecommunications subsystem are the antennas, spacecraft radio subsystem, spacecraft command subsystem, data storage subsystem, and the spacecraft telemetry subsystem.

a. *Antennas*

Primary low-gain antenna. The primary low-gain antenna is used for both transmitting and receiving from launch until the point where the high-gain antenna is usable for transmission. The primary low-gain antenna is then used for command reception until approximately

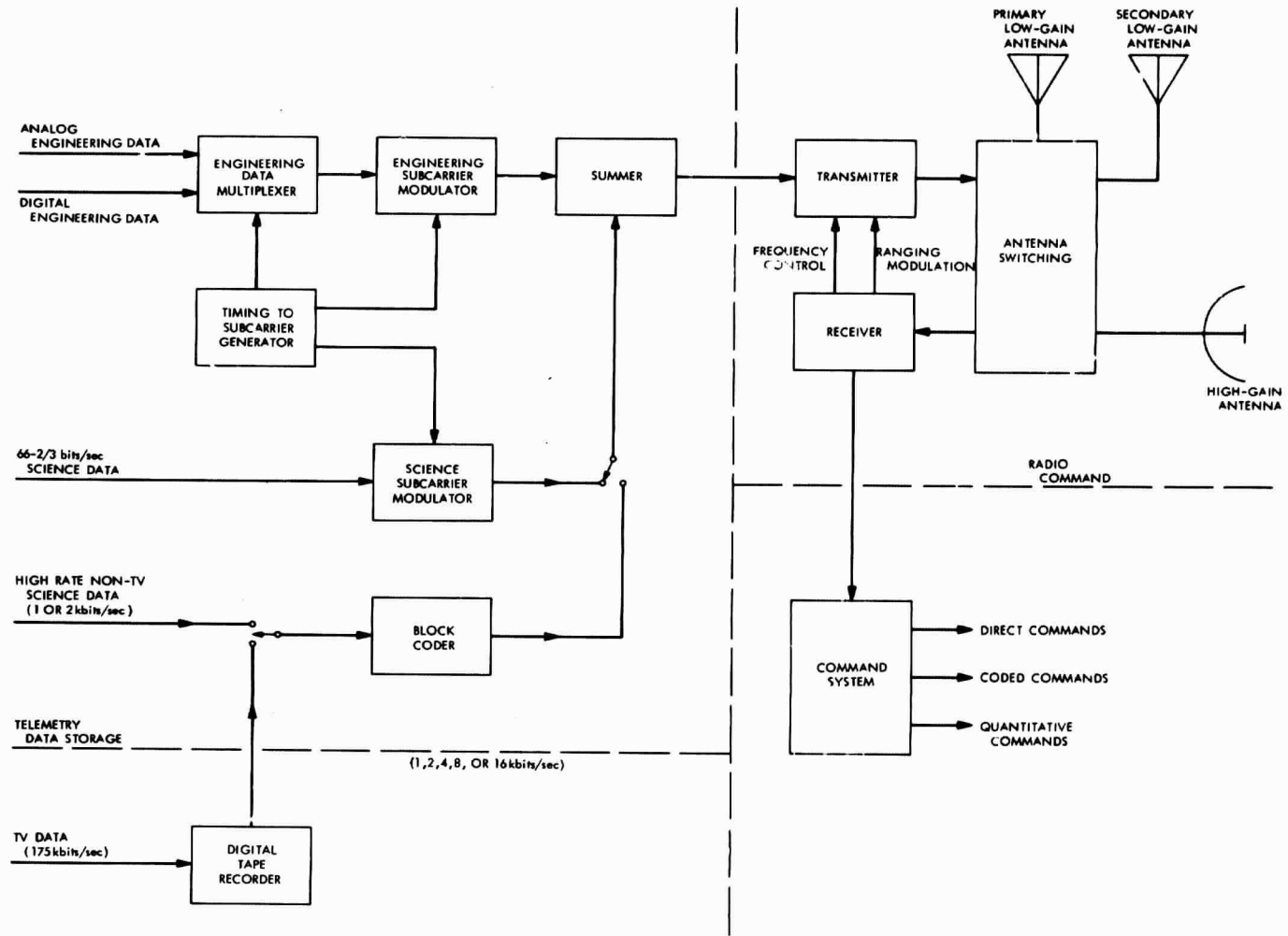


Fig. 38. Telecommunications subsystem block diagram

Table 13. Preliminary power profile (baseline)

Key operational modes	Raw power required, W	Power source assigned
1. Launch	279	Battery
2. Sun acquisition	289	Battery
3. Roll calibration and Canopus acquisition	324	Solar panel
4. Cruise mode II: Battery charging, low-power TWT	322	Solar panel
5. Cruise mode I: first maneuver	338	Battery
6. Cruise mode II: Battery charging, high-power TWT	359	Solar panel
7. Cruise mode I: blackout	266	Solar panel
8. Cruise mode I: second and subsequent maneuver	362	Battery
9. Pre-encounter	377	Solar panel
10. Record mode I and II	349	Solar panel
11. Record mode III	343	Solar panel
12. Playback mode I	271	Solar panel
13. Cruise mode II: Sun occultation (near Mercury)	325	Battery

Mercury encounter, after which time the command reception is through the secondary low-gain antenna. The antenna proposed for the *Mariner Venus/Mercury 1973* mission is a modified *Mariner Mars 1969* design which will provide a pattern similar to that furnished by the *Mariner Venus 67* low-gain antenna. The proposed antenna pattern is shown in Fig. 39. The primary low-gain antenna is located at 180-deg cone angle (Fig. 29).

Secondary low-gain antenna. The secondary low-gain antenna is identical to the primary low gain. The secondary mast size could probably be reduced in length, and still meet its requirements for command reception past Mercury and telemetry and command usage during some maneuvers. The secondary antenna is located at 20-deg cone angle, 80-deg clock angle. In this position, it provides the best performance at Mercury with minimum variation of the roll pattern symmetry. Mounting of this antenna is also illustrated in Fig. 29. At launch, the secondary low-gain antenna is in a stowed position, and it is deployed after launch to an operating position.

High-gain antenna. A *Mariner Mars 1969/1971* high-gain antenna, which is a 40-in. circular paraboloid with boresight gain of 25.6 dB, is adequate to meet the mission requirements, if it is mounted so as to move with one degree of freedom.

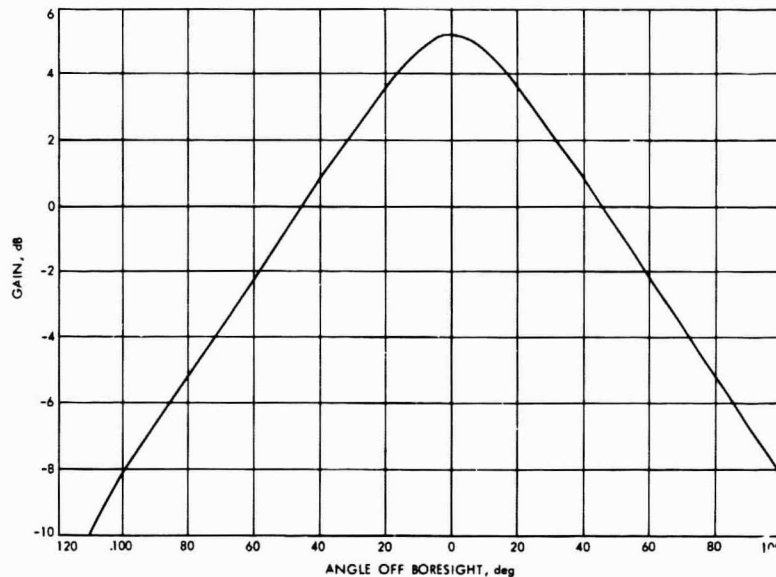


Fig. 39. Radiation pattern of low-gain antennas

The antenna is mounted in the shade to withstand high temperature environment encountered late in the mission. The baseline location chosen for the antenna hinge axis is: $\theta = 8.5$ deg and $\phi = 10.5$ deg. The antenna rotates about the hinge axis in such a way that its boresight axis makes an angle $\psi = 77.5$ deg with respect to the hinge axis. Figure 40 illustrates the angles defining the antenna hinge axis and the antenna boresight axis.

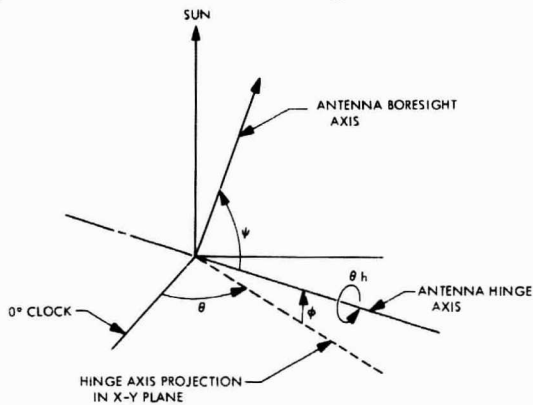


Fig. 40. Antenna hinge and boresight axis location in spacecraft coordinates

The pointing error versus flight time, which is the angle from the antenna boresight axis to the earth vector is shown in Fig. 41 for the baseline hinge axis location. Curve 1 in Fig. 41 illustrates the pointing error if the antenna were mounted perfectly and ignores the attitude control limit cycling. Curve 2 in Fig. 41 considers the effects of an error in mechanical mounting location of the antenna, and the effects of the attitude control limit cycling. The baseline hinge location provides usable antenna pointing over a large portion of the mission, and provides a cruise science capability of 66% bits/sec early in the mission.

An alternate antenna location was considered which provided better antenna pointing during the Venus/Mercury portion of the mission. The pointing error versus time for this position is shown in Fig. 42.

The antenna is positioned by CC&S commands such that the desired antenna hinge-angle time-function is approximated by straight-line segments which are programmed into the CC&S. The number of positions required for the antenna has not been evaluated, but would be approximately 20 with the position increments becom-

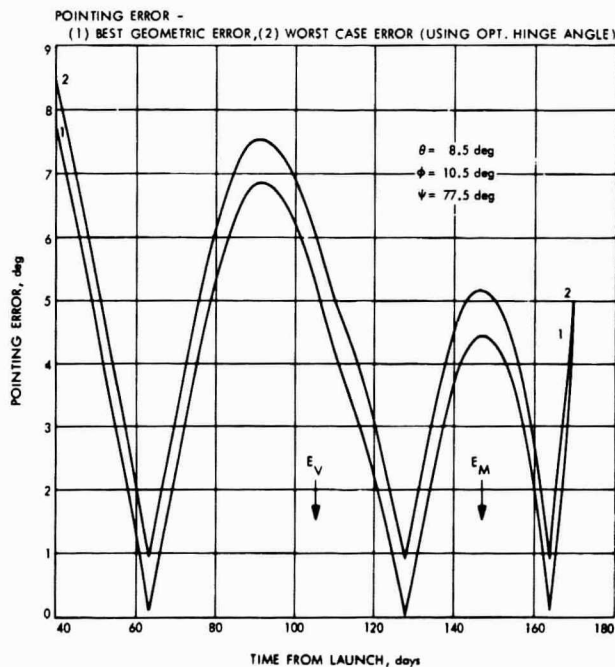


Fig. 41. Pointing error (baseline position, October 21, 1972 launch)

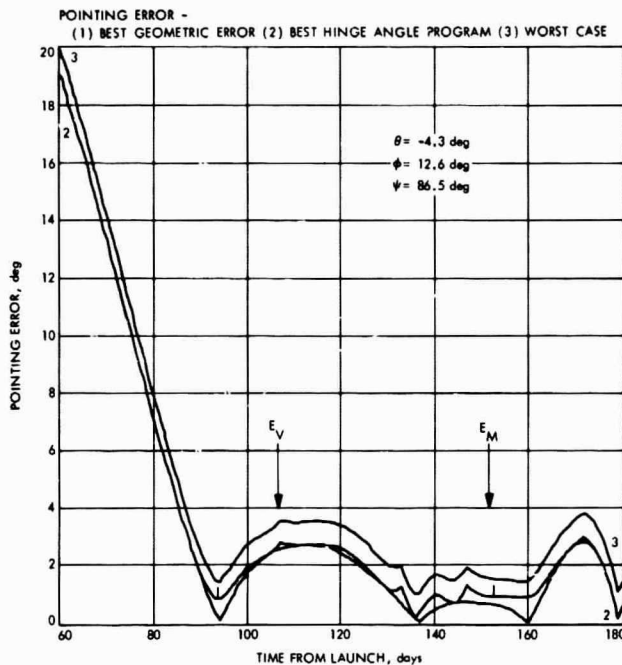


Fig. 42. Pointing error (alternate position, October 21, 1973)

ing finer later in the mission. The high-gain antenna is launched in a latched position and is unlatched at approximately 20 days after launch.

b. Spacecraft radio subsystem. The only change from the *Mariner Mars 1971* radio frequency subsystem (RFS) is the addition of a circular switch to allow switching between the two low-gain antennas.

c. Spacecraft command subsystem. A single channel command subsystem operating at 4 bits/sec is assumed. This command subsystem is a new design from the command subsystems previously used in *Mariner Mars 1969* and 1971.

d. Data storage subsystem. Plans are to fly one digital recorder, similar to one of the *Mariner Mars 1971* recorders. Data storage capability is to be 1.8×10^8 bits. The record rate desired is 175 kbits/sec and playback rates are 16.2, 8.1, 4.05, 2.025, and 1.0125 kbits/sec.

e. Spacecraft telemetry subsystem. The telemetry subsystem is redesigned from the *Mariner Mars 1969/1971* configuration due to the unavailability of the integrated circuits used in the 1969/1971 design. Data rates used

on these spacecraft are considered in the baseline configuration.

3. Telemetry and command capability for baseline design. Telemetry and command performance predictions were made using the baseline communication subsystems described in the preceding section. The performance predictions are presented as curves relating performance margin versus time. The performance margin is the magnitude by which the received signal level exceeds the specified threshold level. The thresholds for the various communications modes used in this study, are:

Mode	Bit error rate	ST/N ₀ , dB
Engineering telemetry	5×10^{-3}	5.2
Low-rate science	5×10^{-3}	5.2
Command	1×10^{-5}	11.0 ± 1
High-rate telemetry*	1×10^{-2}	3.0

*Word error rate.

ST/N₀ is the ratio of the received power (S) per bit time (T) to the noise power per unit bandwidth (N₀). It

is a convenient parameter used to define system performance.

In the performance description, the terms grayout and blackout are used. Grayout is the point at which the performance margin is equal to the summation of negative tolerances of all link parameters. Blackout is the region below the point where the performance margin is 0. Thus the system is below threshold if it is in the blackout region.

a. Trajectory geometry. Figures 43 and 44 give the earth clock angle and earth cone angles, respectively, for an early launch (October 21, 1973) and late launch (November 10, 1973).

b. Cruise mode I performance. Cruise mode I is one of two cruise modes used in the baseline design. During cruise mode I operation only engineering telemetry is to be transmitted, either at $8\frac{1}{2}$ or $33\frac{1}{2}$ bits/sec.

Figures 45 and 46 show the cruise mode I telemetry performance using the primary low-gain antenna. Cruise mode I reaches grayout at $8\frac{1}{2}$ bits/sec on the 210-ft DSIF antenna 2 wk after Venus encounter with the spacecraft in low power. In the high-power mode, essentially spherical coverage is provided for the second maneuver, using the 210-ft DSIF antenna. For the third maneuver, on the 210-ft antenna, telemetry grayout at $8\frac{1}{2}$ bits/sec with the spacecraft in high power occurs when the earth vector is 63 deg off boresight of either low-gain antenna. Data used in deriving Figs. 45 and 46 is shown in Table 14.

c. Cruise mode II (science at $66\frac{2}{3}$ bits/sec, engineering at $8\frac{1}{2}$ bits/sec performance). In the telemetry cruise mode II, engineering data and science data are transmitted simultaneously. Figure 47 illustrates cruise mode II performance margin on both the primary low-gain antenna and the high-gain antenna. For the October 21

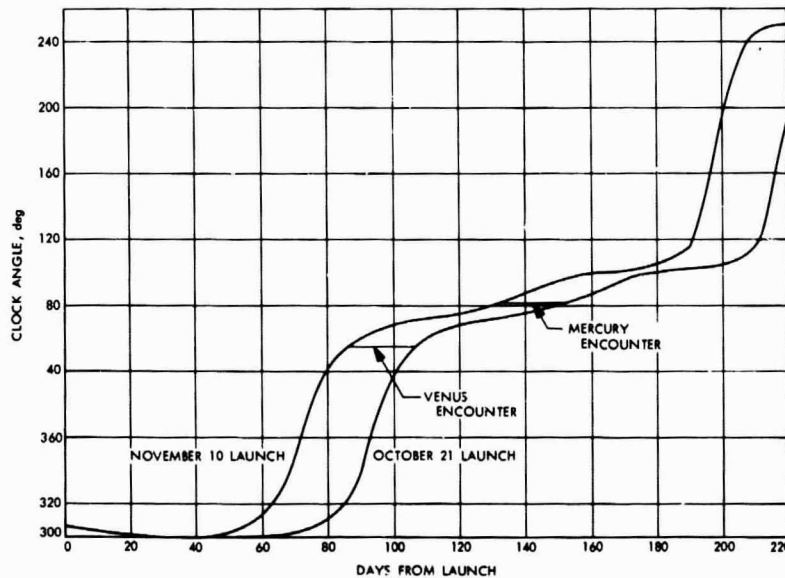


Fig. 43. Clock angle of earth (with respect to Canopus)

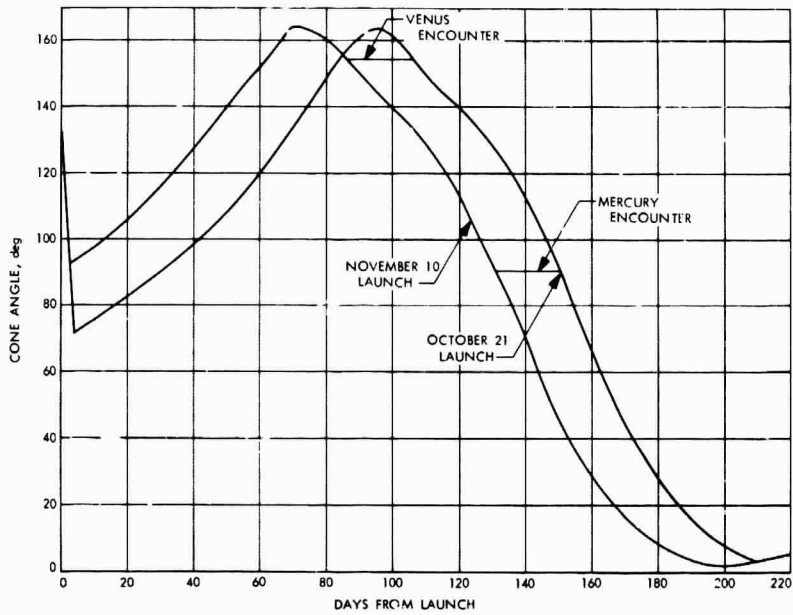


Fig. 44. Cone angle of earth (earth-probe-sun angle)

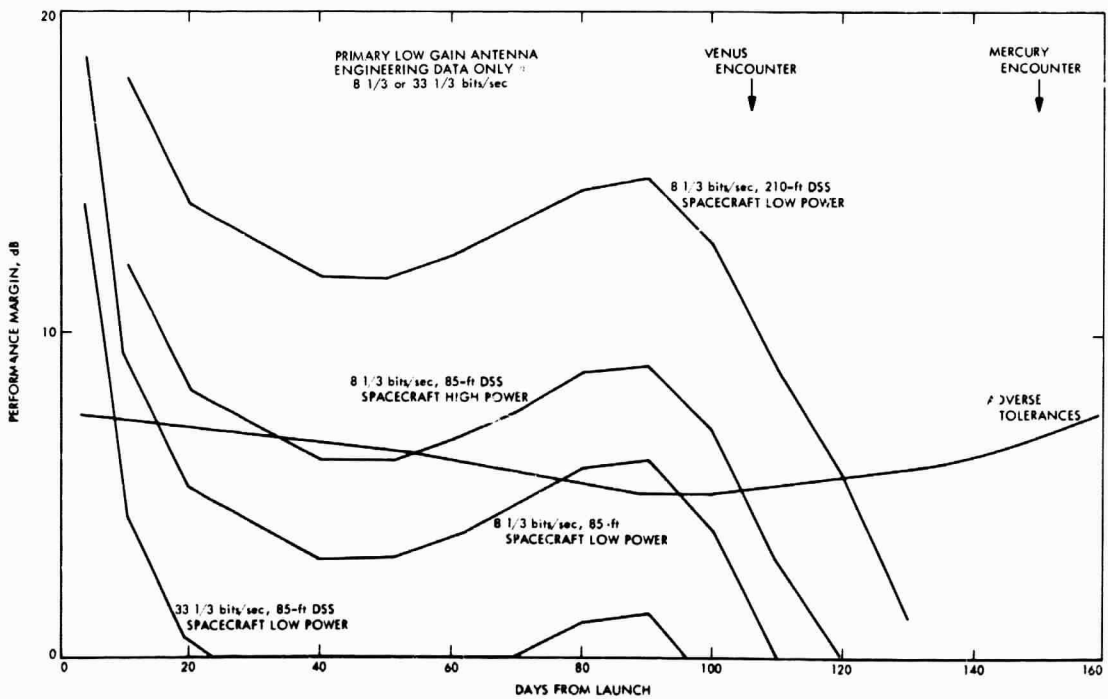


Fig. 45. Cruise mode I performance, October 21, 1973 launch

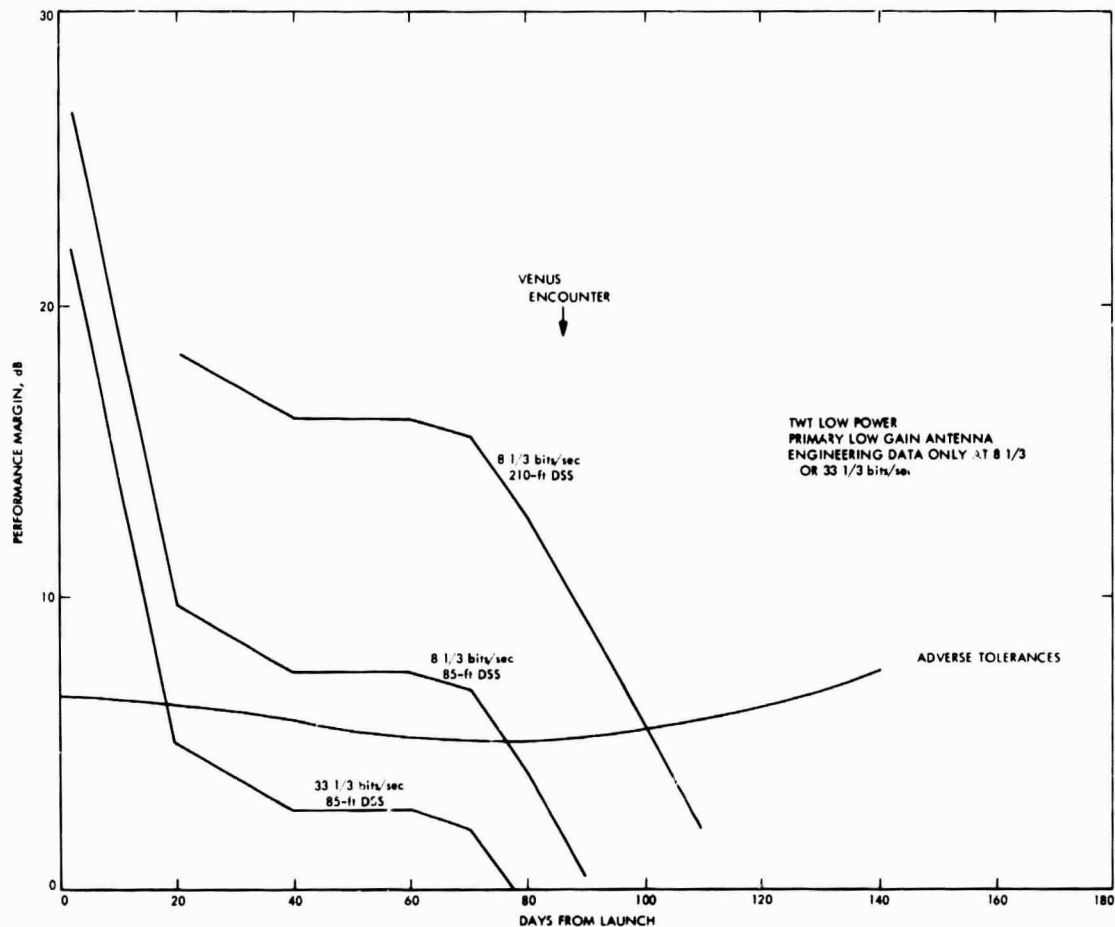


Fig. 46. Cruise mode I performance, November 10, 1973 launch

launch, there is a 10- to 20-day period early in the mission when cruise mode II data is below threshold. For the November 10 launch, cruise mode II can be received continuously. Data used in deriving these figures is shown in Table 15.

d. High-rate performance. High-rate telemetry, in which each 6 bits of telemetry data are block-coded into a 32-bit word, can be transmitted at data rates from 1 to 16 kbits/sec nominally. In the plots shown for the high-rate performance at various bit rates, the engineering channel, which is transmitted simultaneously with the high rate, is not shown. The modulation indices will

be chosen, however, such that the engineering performance margin is equal to or, in some cases, better than the high-rate performance.

Figures 48 and 49 illustrate high-rate performance for the October 21 and November 10 launch dates, respectively, for the baseline antenna hinge position. For this orientation, the maximum data rate above grayout at Mercury encounter is 4.05 kbits/sec. Note that the parameters chosen for the 210-ft antenna are quite conservative (elevation angle 10 deg), so that the 4.05 kbit/sec performance will normally be well above grayout, and the 8.1 kbits/sec performance well above blackout, almost approaching the grayout level.

Table 14. Telemetry design control table: cruise mode I

Engineering channel: 8 1/2 bits/sec
Science channel: none

DSS: 85-ft antenna
Spacecraft: primary low-gain antenna

TWT: low power
Launch: 10/21/73

Arrival: 4/1/74
Time in mission: L + 160 days

No.	Parameter	Nominal value	Tolerance	
			Favorable	Adverse
1	Total transmitter power, dBmW	39.020	1.100	0.000
2	Transmitting circuit loss, dB	-1.990	0.360	-0.360
3	Transmitting antenna gain, dB	5.200	1.500	-1.500
4	Transmitting antenna pointing loss, dB	-15.700	2.637	-2.637
5	Space loss, dB F = 2297 MHz, R = 158 × 10 ⁶ km	-263.755	0.000	0.000
6	Polarization loss, dB	-2.057	0.190	-0.198
7	Receiving antenna gain, dB	53.500	0.600	-0.600
8	Receiving antenna pointing loss, dB	0.000	0.000	-0.250
9	Receiving circuit loss, dB	0.000	0.000	0.000
10	Net circuit loss, dB (2+3+4+5+6+7+8+9)	-224.803	5.287	-5.546
11	Total received power P(T), dBmW (1+10)	-185.783	6.387	-5.546
12	Receiver noise spectral density, dBmW/Hz	-181.220	-0.870	+0.727
13	Carrier power/total power, dB	-2.440	0.560	-0.660
14	Received carrier power, dBmW (11+13)	-188.223	6.947	-6.206
15	Carrier threshold noise BW, dB/Hz	10.800	-1.000	0.000
Carrier tracking (one-way)				
16	Threshold SNR in 2B _{L0} , dB	0.000	0.000	0.000
17	Threshold carrier power, dBmW (12+15+16)	-170.420	-1.872	0.727
18	Performance margin, dB (14-17)	-23.803	8.819	-6.933

No.	Parameter	Nominal value	Tolerance	
			Favorable	Adverse
Data channel				
19	Data power/total power, dB	-3.660	0.750	-0.880
20	Waveform distortion loss, dB	0.000	0.000	0.000
21	Loss through radio system, dB	-1.950	0.200	-0.200
22	Subcarrier demod loss, dB	-0.400	0.100	-0.100
23	Bit sync/detection loss, dB	-0.100	0.100	-0.100
24	Receiver data power, dBmW (11+19+20+21+22+23)	-191.893	7.537	-6.826
25	Threshold data power, dBmW (12+25a+25b)	-166.811	-0.872	0.727
a	Threshold PT/N ₀ , dB (BER = 1 × 10 ⁻⁴)	5.200	0.000	0.000
b	Bit rate, dB bits/sec	9.208	0.000	0.000
26	Performance margin, dB (24-25)	-25.081	8.409	-7.553
Data channel				
27	Data power/total power, dB	-3.660	+0.750	-0.880
28	Waveform distortion loss, dB	0.000	0.000	0.000
29	Loss through radio system, dB	-0.750	0.100	-0.100
30	Subcarrier demodulation loss, dB	-0.250	0.100	-0.100
31	Bit sync/detection loss, dB	0.100	0.100	-0.100
32	Received data power, dBmW (11+27+28+29+30+31)	-190.543	7.437	-6.726
33	Threshold data power, dBmW (12+33a+33b)	-160.791	-0.872	0.727
a	Threshold PT/N ₀ , dB (BER = 1 × 10 ⁻⁴)	5.200	0.000	0.000
b	Bit rate, dB bits/sec	15.228	0.000	0.000
34	Performance margin, dB (32-33)	-29.752	8.309	-7.453

High-rate performance for the alternate antenna position is shown in Fig. 50. For this hinge position, 8.1 kbits/sec is above grayout after encounter, and the performance margin curve is generally smoother, since the antenna pointing is optimized over a smaller portion of the trajectory. Note that the high-gain antenna is not useful until approximately 1 mo before Venus encounter. This means about 2 mo of cruise science data is discarded in favor of better pointing late in the mission, if the alternate antenna hinge orientation is chosen. Data used in the high rate calculations are shown in Table 16,

for a multiplex using high rate at 4.05 kbits/sec and engineering at 8 1/2 bits/sec.

e. *Command performance.* Figure 51 shows command performance margin for the October 21 launch using the 35-ft antenna DSIF. For the 85-ft antenna, command performance is above grayout for 34 days after Venus encounter. After that time, one must either (1) command through the 210-ft antenna which provides considerable margin with 20 kW transmitter power, (2) modify the high-gain antenna on the spacecraft to allow reception

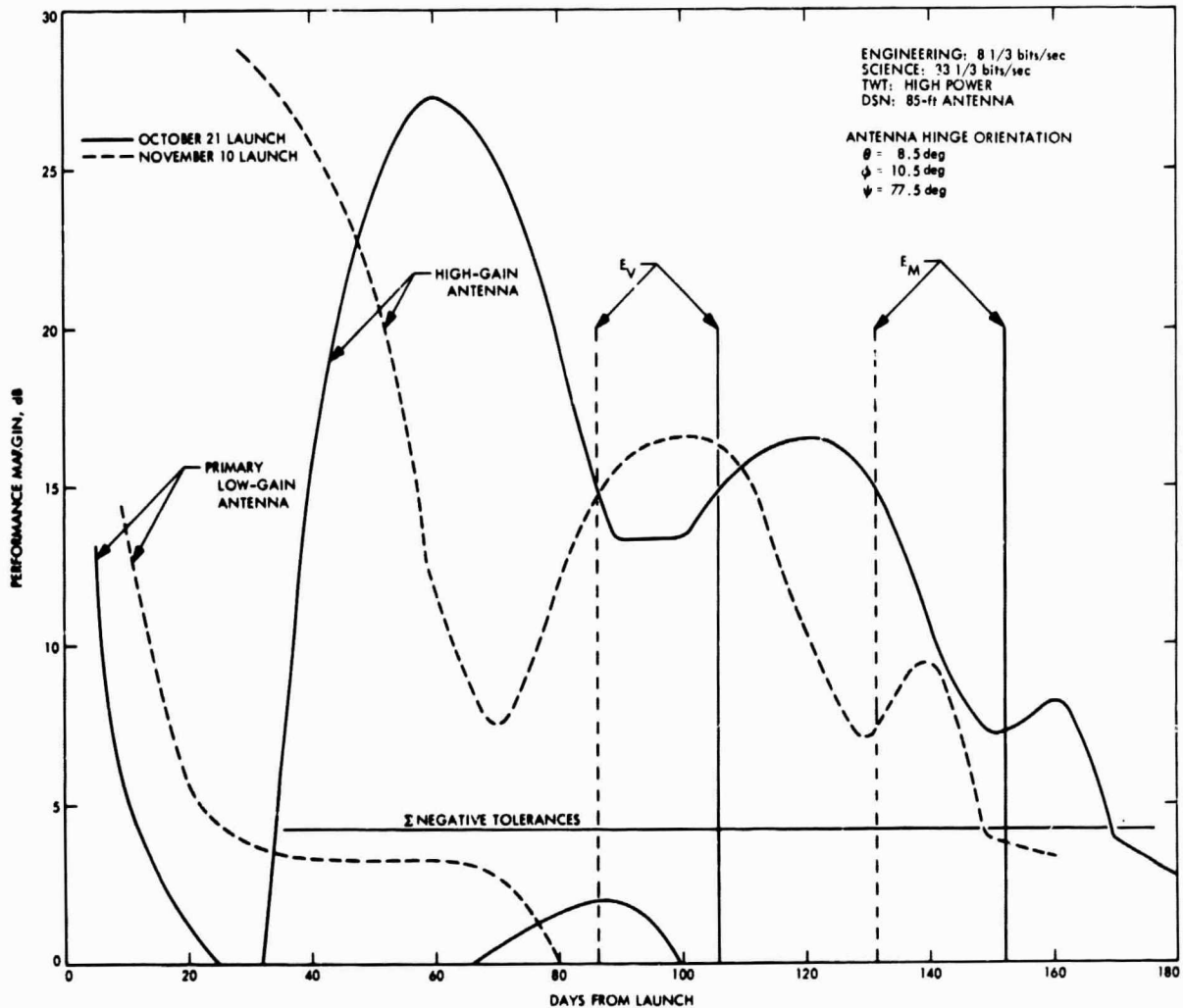


Fig. 47. Cruise mode II telemetry performance

of these command signals, or (3) modify the command system to provide 1-bit/sec operation. This latter modification could either allow the command system to operate only at 1 bit/sec, or could provide a dual capability of operating at either 4 or 1 bits/sec.

Performance for the November 10 launch is virtually identical to that for the October 21 launch. Command parameters used in these calculations are given in Table 17.

G. Data Handling

1. Introduction. The *Mariner Venus/Mercury 1973* data handling is similar to previous *Mariner* missions with few major exceptions. A core buffer has been incorporated into the SDS to enable continuous coverage

of fields and particles data during critical intervals. The DSS is assumed to be similar to the *Mariner Mars 1971* DSS, but with a higher record rate. The SDS would have to be modified slightly to accept the *Mariner Venus/Mercury 1973* data stream and the incorporation of the core buffer.

2. Telemetry mode descriptions. The six data handling modes considered as a baseline to the current design and utilized in the development of the flight sequence of events in section VIII-C are delineated in the subsequent paragraphs of this section. The telecommunications constraints and requirements were discussed in section VII-F, from which the data rates discussed for each mode below originate. The data rates possible are a function of the spacecraft position, TWT power, antenna implementa-

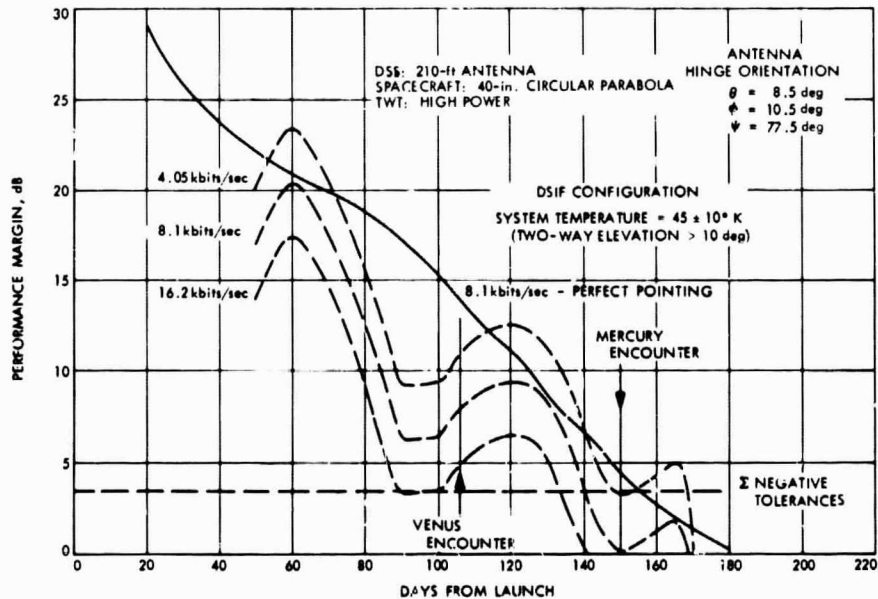


Fig. 48. High-rate performance, October 21, 1973 launch

tion, coding procedure, etc. Each mode listed represents a particular combination of the above, which is outlined as the data modes are individually developed.

a. Cruise mode I. This is the mode normally used during interplanetary cruise to transmit only engineering data over a single channel. Transmission is assumed over the high-gain antenna except early in the mission when high-gain performance is below threshold, and during the three midcourse trajectory correction maneuvers, when spherical coverage is desired. The primary low-gain antenna is used early in the mission and the primary and/or secondary low-gain antenna will be used during maneuvers. For the third maneuver, telemetry grayout at 8½ bits/sec occurs with the spacecraft in high power when the earth is 63 deg off boresight of either low-gain antenna. Except for this, a minimum telemetry capability of 8½ bits/sec exists for the mission duration; if desired, 33½ bits/sec could be utilized early in the mission and during periods of high-gain antenna operation. An 85-ft antenna would be sufficient for all times when cruise mode I occurs, except during the second and third midcourse trajectory correction maneuvers when a 210-ft antenna might be required. The configuration corresponding to cruise mode I is shown in Fig. 52.

b. Cruise mode II. This mode is normally used to transmit engineering data over one channel and cruise science data over another channel. Transmission is assumed over the high-gain antenna except early in the mission when high-gain performance is below threshold. The engineering channel data rate is 8½ or 33½ bits/sec as discussed under cruise mode I. The cruise science channel data rate is 33½ or 66½ bits/sec, except near planetary encounters where a data rate of 166½ bits/sec is assumed. This performance (166½ bits/sec) is marginal at Mercury encounter (grayout). The data rate of 166½ bits/sec would be possible from a performance standpoint at other mission times, but is not considered necessary based on estimates of cruise instruments assumed for the baseline spacecraft design. An 85-ft antenna would be sufficient for all times cruise mode II occurs, except possibly during Mercury encounter when a 210-ft dish might be necessary for a cruise science rate of 166½ bits/sec. Figure 53 shows a schematic of cruise mode II.

c. Pre-encounter mode. This mode is normally used near planetary encounter. The data handling rates are the same as those discussed under cruise mode II. The chief distinction is that encounter data handling related instrumentation is being prepared for use, which affects the spacecraft power requirements.

Table 15. Telemetry design control table: cruise mode II

Engineering channel: 8 1/2 bits/sec
 Science channel: 66 2/3 bits/sec

DSS: 85-ft antenna
 Spacecraft: high-gain antenna

TWT: high power
 Launch: 11/10/73

Arrival: 3/21/74
 Time in mission: L + 160 days

No.	Parameter	Nominal value	Tolerance	
			Favorable	Adverse
1	Total transmitter power, dBmW	42.320	0.580	0.000
2	Transmitting circuit loss, dB	-1.450	0.250	-0.250
3	Transmitting antenna gain, dB	25.600	1.000	-1.200
4	Transmitting antenna pointing loss, dB	0.000	0.000	0.000
5	Space loss, dB F = 2297 MHz, R = 210 × 10 ⁶ km	-266.120	0.000	0.000
6	Polarization loss, dB (10 deg)	-0.020	0.000	-0.110
7	Receiving antenna gain, dB	53.300	0.600	-0.600
8	Receiving antenna pointing loss, dB	0.000	0.000	-0.250
9	Receiving circuit loss, dB	0.000	0.000	0.000
10	Net circuit loss, dB (2 + 3 + 4 + 5 + 6 + 7 + 8 + 9)	-188.690	1.850	-2.410
11	Total received power P(1), dBmW (1 + 10)	-146.370	2.430	-2.410
12	Receiver noise spectral density, dBmW/Hz Noise temperature, 55 ± 10 °K	-181.220	-0.872	+0.727
13	Carrier power/total power, dB	-4.766	+1.000	-1.000
14	Received carrier power, dBmW (11 + 13)	-151.370	2.430	-3.410
15	Carrier threshold noise BW, dB/Hz	10.800	-1.000	0.000
Carrier tracking (one-way)				
16	Threshold SNR in 2B _{LO} , dB	0.000	0.000	0.000
17	Threshold carrier power, dBmW, (12 + 15 + 16)	-170.420	-1.872	+0.727
18	Performance margin, dB (14-17)	19.050	5.302	-4.137

No.	Parameter	Nominal value	Tolerance	
			Favorable	Adverse
Data channel B				
19	Data power/total power, dB	-11.39	1.000	-1.000
20	Waveform distortion loss, dB			
21	Loss through radio system, dB	-1.300	0.400	-0.400
22	Subcarrier demod loss, dB			
23	Bit sync/detection loss, dB			
24	Received data power, dBmW (11 + 19 + 20 + 21 + 22 + 23)	-158.910	3.830	-3.810
25	Threshold data power, dBmW (12 + 25a + 25b)	-166.812	-0.872	+0.727
a	Threshold PT/N ₀ , dB (BER = 5 × 10 ⁻³)	5.200	0.000	0.000
b	Bit rate, dB bits/sec	9.208	0.000	0.000
26	Performance margin, dB (24-25)	7.902	4.702	-4.537
Data channel A				
27	Data power/total power, dB	-3.119	+0.800	-0.800
28	Waveform distortion loss, dB			
29	Loss through radio system, dB	-1.05	0.300	-0.300
30	Subcarrier demodulation loss, dB			
31	Bit sync/detection loss, dB			
32	Received data power, dBmW (11 + 27 + 28 + 29 + 30 + 31)	-150.539	3.530	-3.510
33	Threshold data power, dBmW (12 + 33a + 33b)	-157.781	-0.872	+0.727
a	Threshold PT/N ₀ , dB (BER = 5 × 10 ⁻³)	5.200	0.000	0.000
b	Bit rate, dB bits/sec	18.239	0.000	0.000
34	Performance margin, dB (32-33)	+7.242	4.402	-4.237

d. *Record mode I.* This mode occurs at planetary encounter and uses the DSS for storage of high-rate science data. The record rate is 175 kbits/sec. TV data, HRIR data and, if desired, IRR data (at Mercury only), and fields and particles data are being recorded. Engineering data are being transmitted in real time over one channel and fields and particles data, IRR data (at Mercury only), DFR data and, if desired, HRIR data over the other channel. Thus all science (except TV and

possibly HRIR) is being recorded and sent in real time, except when the same camera is taking a succession of pictures; during the latter case the DSS would be off for the 10-sec picture erase time. During this 10-sec interval, science will be sent in real time and stored in a core buffer, if desired, for transmission during a noncritical interval. Record mode I nominally utilizes the high-gain antenna near planetary encounters. The engineering channel data rate is 8 1/2 or 33 1/3 bits/sec as discussed

Table 16. Telemetry design control table: high rate

Engineering channel: 8 1/2 bits/sec
Science channel: 4.05 kbits/sec

DSS: 210-ft antenna
Spacecraft: high-gain antenna

TWT: high power
Launch: 11/10/73

Arrival: 3/21/74
Time in mission: L + 160 days

No.	Parameter	Nominal value	Tolerance	
			Favorable	Adverse
1	Total transmitter power, dBmW	42.320	0.580	0.000
2	Transmitting circuit loss, dB	-1.450	0.250	-0.250
3	Transmitting antenna gain, dB	25.600	1.000	-1.200
4	Transmitting antenna pointing loss, dB	0.000	0.000	0.000
5	Space loss, dB F = 2297 MHz, R = 210 × 10 ⁶ km	-266.120	0.000	0.000
6	Polarization loss, dB	-0.020	0.0000	-0.110
7	Receiving antenna gain, dB	61.400	0.300	-0.300
8	Receiving antenna pointing loss, dB	0.000	0.000	0.000
9	Receiving circuit loss, dB	0.000	0.000	0.000
10	Net circuit loss, dB (2+3+4+5+6 +7+8+9)	-180.590	1.550	-1.860
11	Total received power P(T), dBmW (1+10)	-138.270	2.130	-1.860
12	Receiver noise spectral density, dBmW/Hz (elev. = 10 deg). Noise temperature, 45 ± 10°K	-182.068	-1.091	0.872
13	Carrier power/total power, dB	-7.67	1.570	-2.050
14	Received carrier power, dBmW (11+13)	-145.940	3.120	-3.910
15	Carrier threshold noise BW, dB/Hz	10.800	-1.000	0.000
16	Carrier tracking (one-way) Threshold SNR in 2B _{LO} , dB	0.300	0.000	0.000
17	Threshold carrier power, dBmW (12+15+16)	-171.268	-2.091	0.872
18	Performance margin, dB (14-17)	25.328	5.211	-4.782

No.	Parameter	Nominal value	Tolerance	
			Favorable	Adverse
Data channel C 16,200 bits/sec				
19	Data power/total power, dB	-1.040	0.310	-0.390
20	Waveform distortion loss, dB	0.000	0.000	0.000
21	Loss through radio system, dB	-0.100	0.100	-0.100
22	Subcarrier demod loss, dB	-0.100	0.000	-0.100
23	Bit sync/detection loss, dB	-0.200	0.000	-0.100
24	Received data power, dBmW (11+19+20+21+22+23)	-139.710	2.440	-2.500
25	Threshold data power, dBmW (12+25a+25b)	-142.998	-1.091	0.872
a	Threshold PT/N, dB (WER = 1 × 10 ⁻²)	3.000	0.000	0.000
b	Bit rate, dB bits/sec	36.070	0.000	0.000
26	Performance margin, dB (24-25)	+3.288	3.531	-3.372
Data channel B 8 1/2 bits/sec				
27	Data power/total power, dB	-21.200	0.960	-1.510
28	Waveform distortion loss, dB	0.000	0.000	0.000
29	Loss through radio system, dB	-0.800	+0.200	-0.200
30	Subcarrier demodulation loss, dB	-0.250	+0.100	-0.100
31	Bit sync/detection loss, dB	-0.100	+0.100	-0.100
32	Received data power, dBmW (11+27+28+29+30+31)	-160.770	+3.490	-3.770
33	Threshold data power, dBmW (12+33a+33b)	-167.660	-1.091	0.872
a	Threshold PT/N ₀ , dB (BER = 1 × 10 ⁻⁵)	5.200	0.000	0.000
b	Bit rate, dB bits/sec	9.208	0.000	0.000
34	Performance margin, dB (32-33)	+6.890	4.581	-4.642

for cruise mode I. The science channel data rate would have a maximum data rate of 166% bits/sec as discussed for cruise mode II, except if HRIR data were desired in real time (assumed 1000 bits/sec). During the 10-sec picture erase time (when the DSS is off) the core buffer will accept fields and particles data for later playback to earth. If HRIR data were desired in real time, a 210-ft antenna would be necessary. An 85-ft

dish would be sufficient for all other times record mode I occurs. This mode is depicted in Fig. 54.

e. Record mode II. This mode is used for high-rate science data at planetary encounters during earth occultation, when no real-time data can be sent to earth. This mode also requires the DSS to be on and in the record state. The record rate is 175 kbits/sec. TV data, HRIR

Table 17. Command design control table: single channel

Data channel: 4 bits/sec
 Sync channel: not used

DSS: 85-ft antenna
 Spacecraft: primary low-gain antenna

Launch: 10/21/73
 Arrival: 4/1/74

Time in mission: L + 130 days

No.	Parameter	Nominal value	Tolerance	
			Favorable	Adverse
1	Total transmitter power, dBmW	70.000	0.500	0.000
2	Transmitting circuit loss, dB	0.000	0.000	0.000
3	Transmitting antenna gain, dB	51.800	0.900	0.900
4	Transmitting antenna pointing loss, dB	0.000	0.000	0.000
5	Space loss, dB F = 2116 MHz, R = 80 × 10 ⁶ km	-257.022	0.000	0.000
6	Polarization loss, dB	-0.057	0.027	-0.027
7	Receiving antenna gain, dB	5.200	0.400	-0.400
8	Receiving antenna pointing loss, dB	-5.947	0.999	-0.999
9	Receiving circuit loss, dB	-0.080	0.010	-0.010
10	Net circuit loss, dB (2+3+4+5+6 +7+8+9)	-206.136	2.336	-2.337
11	Total received power P(T), dBmW (1+10)	-136.136	2.836	-2.337
12	Receiver noise spectral density, dBmW	-165.675	-0.700	0.700
13	Carrier power/total power, dB	-3.000	0.250	-0.250
14	Received carrier power, dBmW (11+13)	-139.136	3.086	-2.587
15	Carrier threshold noise BW, dB/Hz	11.460	-0.850	0.150

No.	Parameter	Nominal value	Tolerance	
			Favorable	Adverse
Carrier tracking (one-way)				
16	Threshold SNR in 2B _{LO} , dB	0.000	0.000	0.000
17	Threshold carrier power, dBmW (12+15+16)	-154.215	-1.550	0.850
18	Performance margin, dB (14-17)	15.578	4.636	-3.437
Data channel				
19	Data power/total power, dB	-3.000	0.250	-0.250
20	Waveform distortion loss, dB	0.000	0.000	0.000
21	Loss through radio system, dB	-1.500	0.200	-0.200
22	Subcarrier demod loss, dB			
23	Bit sync/detection loss, dB			
24	Received data power, dBmW (11+19+20+21+22+23)	-140.636	3.286	-2.787
25	Threshold sync power, dBmW (12+25a+25b)	-148.655	-0.700	0.700
a	Threshold PT/N ₀ , dB (BER = 1 × 10 ⁻⁵)	11.000	1.000	-1.000
b	Bit rate, dB bits/sec	6.020	0.000	0.000
26	Performance margin, dB (24-25)	8.019	4.986	-4.487

data, and fields and particles data are being recorded. No data (science or engineering) is being sent in real time since the earth is not in view. Since engineering data is not assumed to be recorded, it is being lost. During the assumed 10-sec picture erase time, if the same camera were taking a succession of pictures, the DSS would be off. During this 10-sec interval, while the spacecraft is occulted by the earth, real-time science can be stored in a core buffer, if desired, for transmission during a non-critical interval. During the 10-sec picture erase time (when the DSS is off) the core buffer will again accept fields and particles data for later transmission to earth. The spacecraft may or may not be able to distinguish record mode II from record mode I; however, the distinction is made here to simply encounter discussions. Figure 55 is a schematic of record mode II.

f. *Record mode III.* This mode occurs during earth occultation when no high-rate science data needs to be

recorded. The DSS is off. Critical fields and particles are being stored in a core buffer for later transmission during a noncritical interval. No data (science or engineering) is being sent in real time since the earth is not in view. Because engineering data are not assumed to be recorded or the core buffer, such data are being lost. The core buffer will accept fields and particles data during critical occultation intervals for later transmission to earth. Figure 56 is a schematic of record mode III.

g. *Playback mode.* This mode shown in Fig. 57 allows playback of previously stored science data and uses the DSS in the playback state. The playback rates are assumed to be up to 16.2 and 8.1 kbits/sec at Venus and Mercury, respectively. Previously stored data are being transmitted over one channel at the above rates and engineering data are being sent over the other channel as discussed under cruise mode I. Playback mode nominally makes use of the high-gain antenna near planetary en-

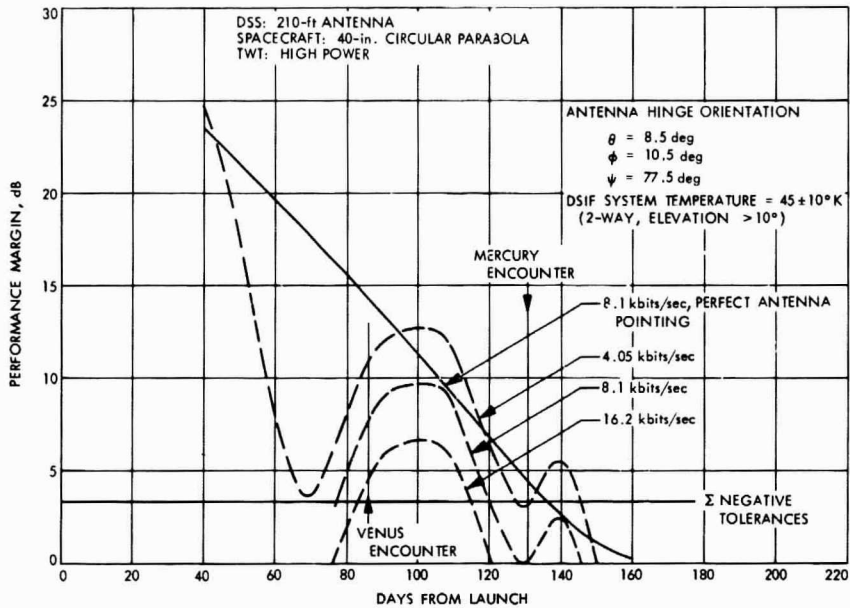


Fig. 49. High-rate performance, November 10, 1973 launch

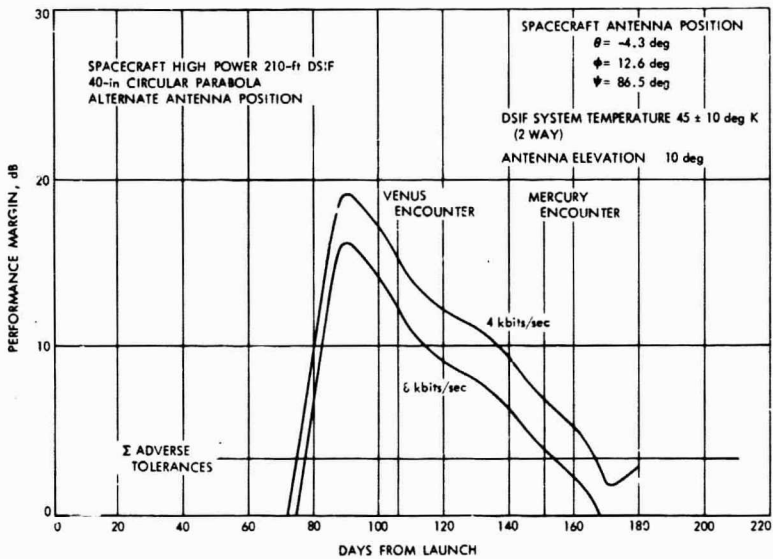


Fig. 50. High-rate performance, October 21, 1973 launch, alternate position

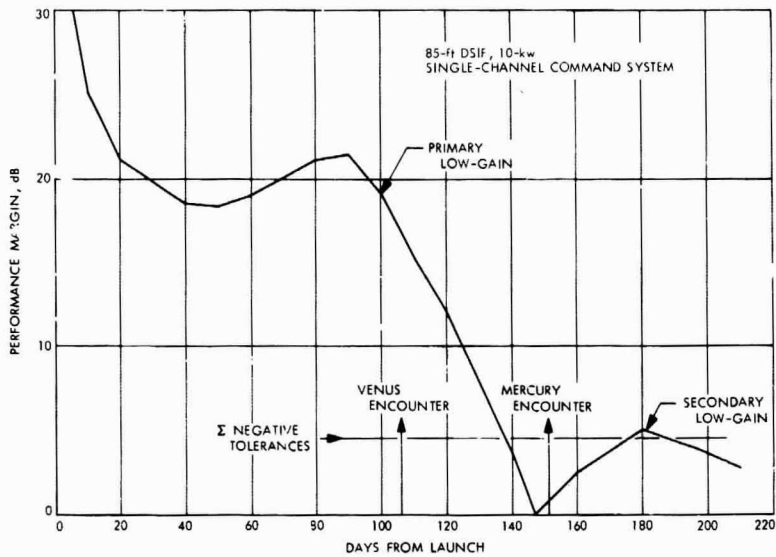


Fig. 51. Command performance, October 21, 1973 launch

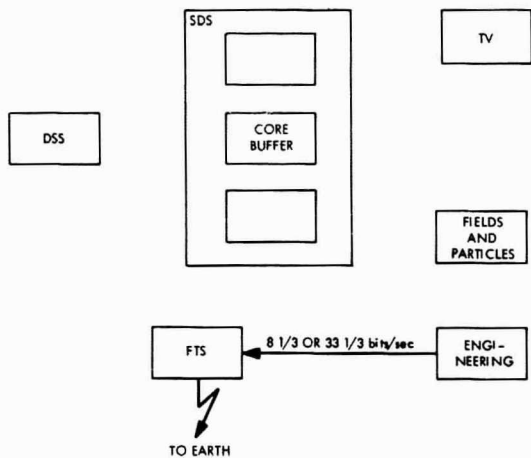


Fig. 52. Schematic representation of cruise mode I

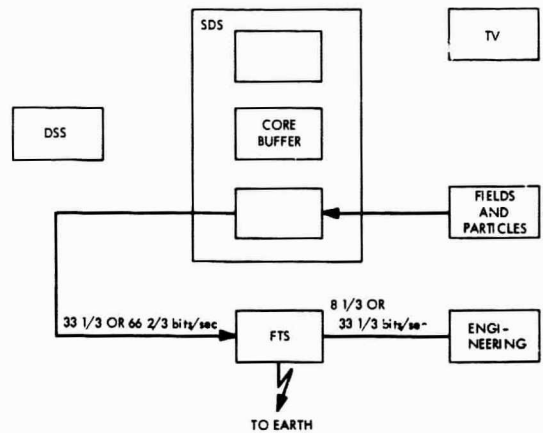


Fig. 53. Schematic representation of cruise mode II or pre-encounter mode

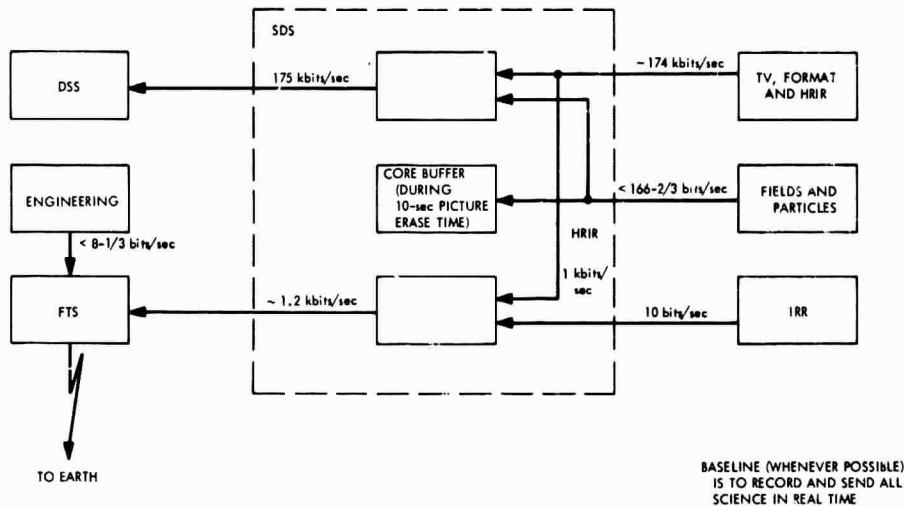


Fig. 54. Schematic representation of record mode I

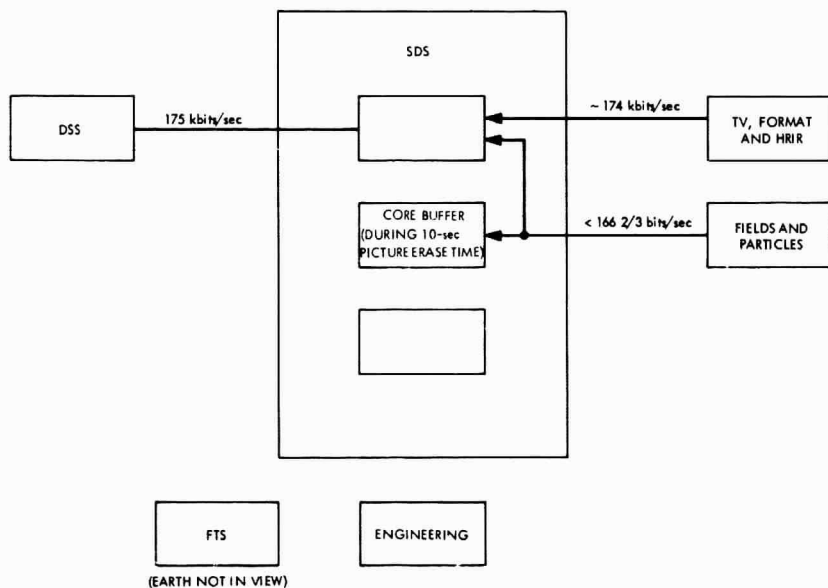


Fig. 55. Schematic representation of record mode II

counters. Real-time fields and particles cannot be sent in real time since two channels are already occupied. Critical fields and particles may be stored in a core buffer, if desired, for later transmission to earth during a noncritical interval. The core buffer will accept fields and particles data during critical intervals when the DSS

is in the playback mode. A 210-ft dish would be mandatory to receive on earth at the higher playback rates.

3. Record modes I, II, and III and playback mode discussion. The purpose of this discussion is to describe the parameters related to data handling for *Mariner*

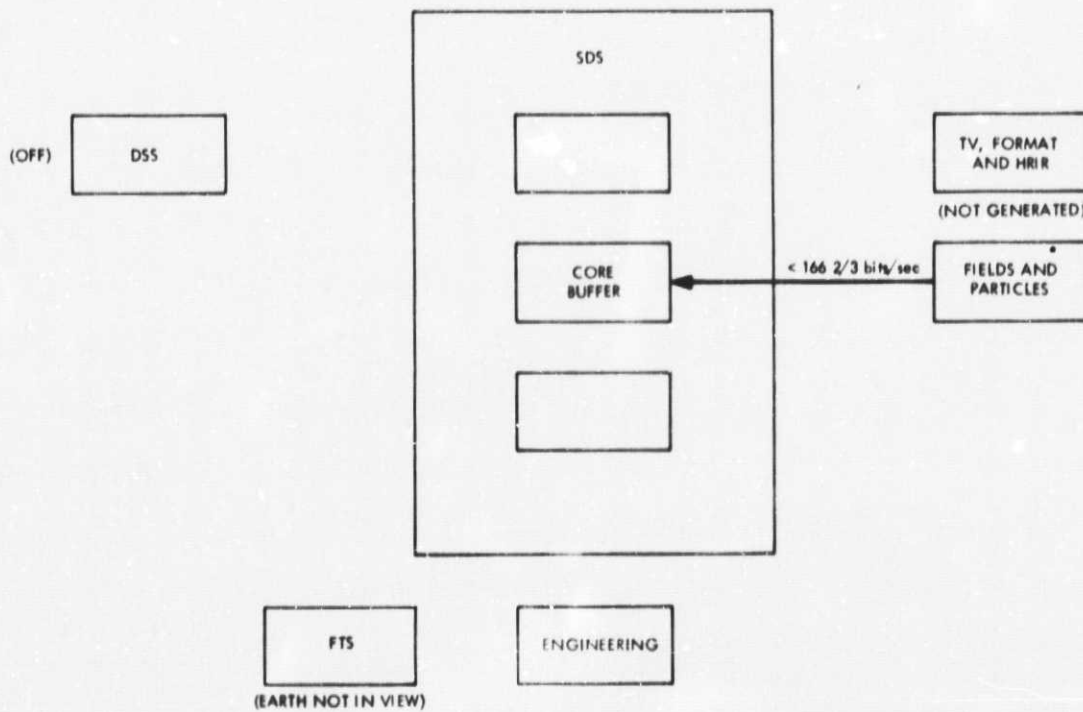
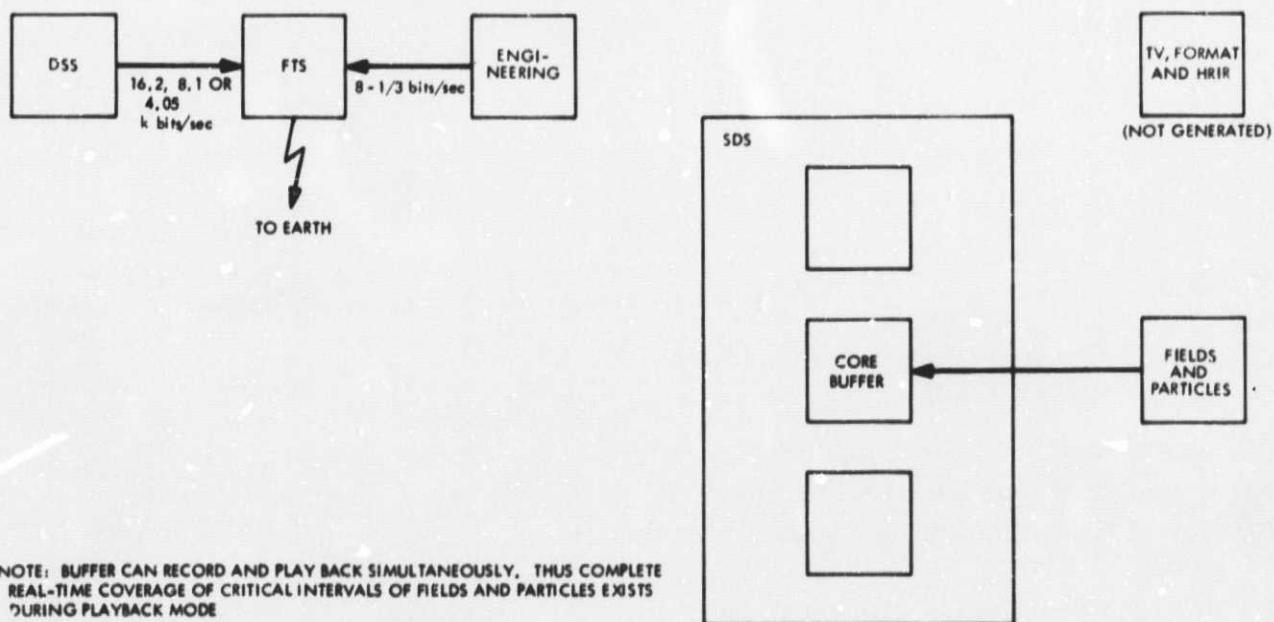


Fig. 56. Schematic representation of record mode III



NOTE: BUFFER CAN RECORD AND PLAY BACK SIMULTANEOUSLY. THUS COMPLETE REAL-TIME COVERAGE OF CRITICAL INTERVALS OF FIELDS AND PARTICLES EXISTS DURING PLAYBACK MODE

Fig. 57. Schematic representation of playback mode

Venus/Mercury 1973 during record and playback conditions. Picture format, data storage, etc., will be discussed, followed by the means of recording and playing back data.

Initially, some of the parameters must be constrained; then the remaining parameters can be derived. One possible method of generating necessary parameters is outlined below.

An initial assumption is the picture size which was fixed at 704 lines, 945 pixels/line and 8 bits/pixel, which is equivalent to 5.322×10^6 bits/picture. This corresponds to the present *Mariner* Mars 1969 TVS (not *Mariner* Mars 1971) which has $700 \times 832 \times 9 = 5.25 \times 10^6$ bits/picture.

Following an assumed picture size, it will be necessary to fix the maximum encounter science data rate, excluding TV video information. This rate is to be buffered by the SDS with TVS data for DSS recording. For the baseline mission, the following data rates, except for TV video information are assumed for the instruments:

Instrument	Data rate bits/sec
Cosmic dust detector	1
DFR	10
Energetic particle detector	3
Plasma probe	100
Magnetometers	40
IRR (sun occultation)	10
HRIR	1000
Minimum instrument requirements	1164

The 1164 bits/sec rate is well within the 2000 bits/sec assumed, allowing a contingency which might be necessary as detailed design of the instruments proceeds.

To determine the maximum encounter science bit rate, excluding TV video information, a total TV formatting rate must be assumed. The following data rates are assumed:

TV formatting	Bits/line
Picture count	6
Real-time frame count	16
Line count	10
PN sync	31
Contingency	10
Camera ID	1
	74 bits/line
	× 704 lines/frame
	= 52,096 bits/frame
$\frac{52,096 \text{ bits/frame}}{31.065 \text{ sec/frame}}$	= 1.68×10^3 bits/sec = 1680 bits/sec
∴ Total science	= 3680 bit/sec (average)

Before proceeding, the distinction between a frame and a picture should be emphasized. A picture is defined as video information only and a frame is defined as video information plus TV formatting and instrument data other than TV. Thus a frame, for the purposes of this discussion, would include 3680 bits/sec (average) of information in addition to TV (pure picture) video information.

Finally a DSS record rate must be assumed. Ideally this would be determined by locating on the planet's surface a desired swath and then extrapolating backwards to a necessary frame time. Given the bits/picture, the effective picture record rate would be defined as shown in Fig. 58. To this effective record rate, the maximum encounter science data rate would be added (to this case 3680 bits/sec) and the resultant would be the total record rate necessary. We have assumed a record rate of 175 kbits/sec. This record rate is higher than the value for *Mariner* Mars 1971, utilizing the same DSS, but was felt necessary due to the high approach velocities at Venus (8.3 km/sec) and Mercury (15.1 km/sec).

With the above assumptions, the following parameters can be derived:

(1) Pure picture time =

$$\frac{5.322 \times 10^6 \text{ bits/picture}}{175 \times 10^3 \text{ bits/sec}} = 30.411 \text{ sec/picture}$$

This represents the time necessary to record one pure picture excluding TV formatting and other instruments.

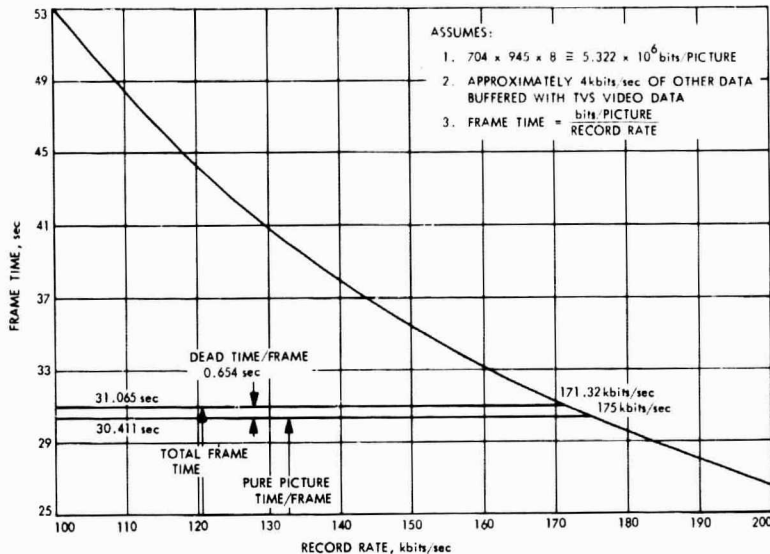


Fig. 58. Frame time versus record rate

- (2) Effective picture record rate = $175 \text{ kbits/sec} - 3.68 \text{ kbits/sec} = 171.32 \text{ kbits/sec}$

This represents an average picture record rate. One line of pure TV data would be recorded at 175 kbits/sec and then formatting and instrument data would be recorded in an interval before the next line of pure TV data was recorded. The effective picture record rate is the average rate from the beginning of one line to the beginning of the next. If there were no TV formatting or other instruments, the effective picture record rate would be identical to the DSS assumed rate of 175 kbits/sec .

- (3) Total picture time (frame time) =

$$\frac{5.322 \times 10^6 \text{ bits/picture}}{171.32 \text{ kbits/sec}} = 31.065 \text{ sec/picture}$$

This represents the time necessary to record one pure picture at an effective record rate of 171.32 kbits/sec . Thus, since the record rate of the DSS is 175 kbits/sec , TV formatting and instruments would be recorded at an effective rate of 3680 bits/sec , which corresponds to the value assumed. The time above is the amount of time necessary to

record one pure picture with TV formatting and instruments interleaved on a line-by-line basis.

- (4)
$$\begin{aligned} \text{Dead time/picture} &= 31.065 \text{ sec/picture} \\ &- 30.411 \text{ sec/picture} \\ \hline &0.654 \text{ sec/picture} \end{aligned}$$

This represents the portion of time of one total picture devoted to TV formatting and other instruments.

- (5) Dead time/line =

$$\frac{0.654 \text{ sec/picture}}{704 \text{ lines/picture}} = 0.9289 \text{ ms/line}$$

This represents the time from the end of one line of pure picture information to the beginning of the next line of pure picture information.

- (6) Pure picture time/line =

$$\frac{30.411 \text{ sec/picture}}{704 \text{ lines/picture}} = 43.197 \text{ ms/line}$$

This represents the time to record one line of pure picture information.

$$\begin{aligned}
 (7) \text{ Total line time} &= 43.197 \text{ ms/line} \\
 &+ \frac{0.9289 \text{ ms/line}}{44.120 \text{ ms/line}}
 \end{aligned}$$

This represents the time to record one line of pure picture information and TV formatting and other instrument data and to be ready to record the next line.

$$\begin{aligned}
 (8) \text{ Bits/frame of TV formatting and other instrument data} &= 0.654 \text{ sec} \times 175 \times 10^3 \text{ bits/sec} \\
 &= 0.1145 \times 10^6 \text{ bits}
 \end{aligned}$$

$$\begin{aligned}
 (9) \text{ Bits/picture} &= \\
 \frac{44.126 \text{ ms}}{43.197 \text{ ms}} \times 5.322 \times 10^6 \text{ bits/picture} &= 5.436 \times 10^6 \text{ bits/picture}
 \end{aligned}$$

This represents the total number of bits per picture. The above parameters are depicted in Fig. 59.

Before data implications for mission sequence can be examined, two other parameters must be assumed:

- (1) Vidicon erase time = 10 sec
- (2) DSS capacity = $1.8 \pm 5\% \times 10^8$ bits
 \therefore worst case = 1.71×10^8 bits

The number of frames/track is:

$$\begin{aligned}
 &\frac{1.8 \times 10^8 \pm 5\% \text{ bits}}{5.43 \times 10^6 \text{ bits/frame} \times 4 \text{ tracks}} \\
 &= 8.27 \pm 0.41 \text{ frames/track}
 \end{aligned}$$

The above calculations assume that cameras A and B are alternating and that while picture information from one camera is being recorded, the vidicon on the other camera is being erased. This is depicted in Fig. 60 for a sequence of 8 frames. It will be assumed that each track can store 8 frames, i.e., the nominal case above.

Figure 61 shows the case of one camera (A or B) taking a succession of pictures. The DSS will be shut off during the 10-sec vidicon erase time. One second of tape will be lost by turning on and off the DSS during each 10-sec vidicon erase time. Therefore, if we assume that 7 sec of tape are lost for one track, we can derive the number of bits lost per track and the DSS storage capability in the following manner:

Assume 8 frame/track results in 7 sec of tape lost if cameras cycle continuously:

$$\begin{aligned}
 \text{Bits lost/track} &= 7 \text{ sec/track} \times 175 \times 10^3 \text{ bits/sec} \\
 &= 0.1225 \times 10^7 \text{ bits/track}
 \end{aligned}$$

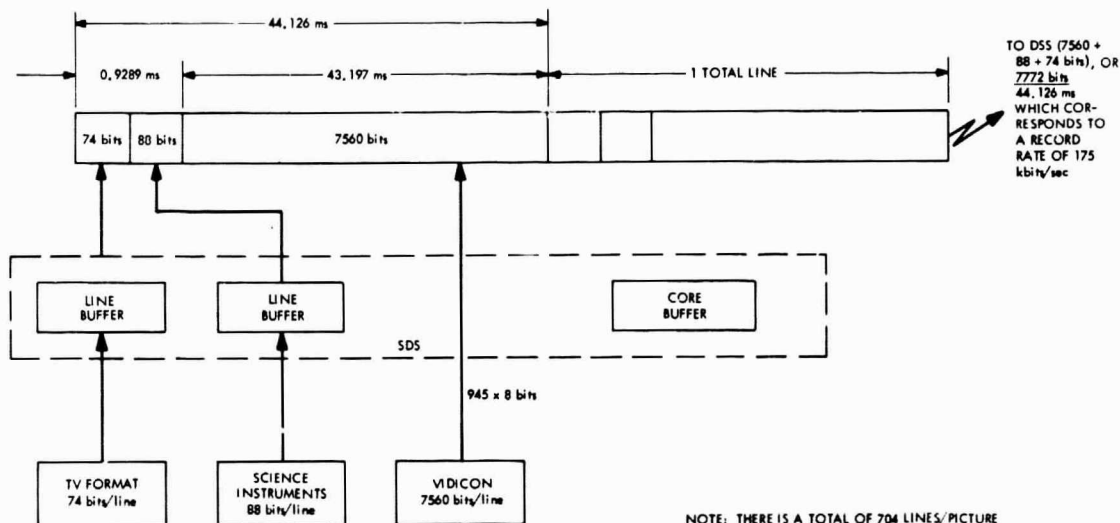


Fig. 59. Data handling on a line basis at encounter

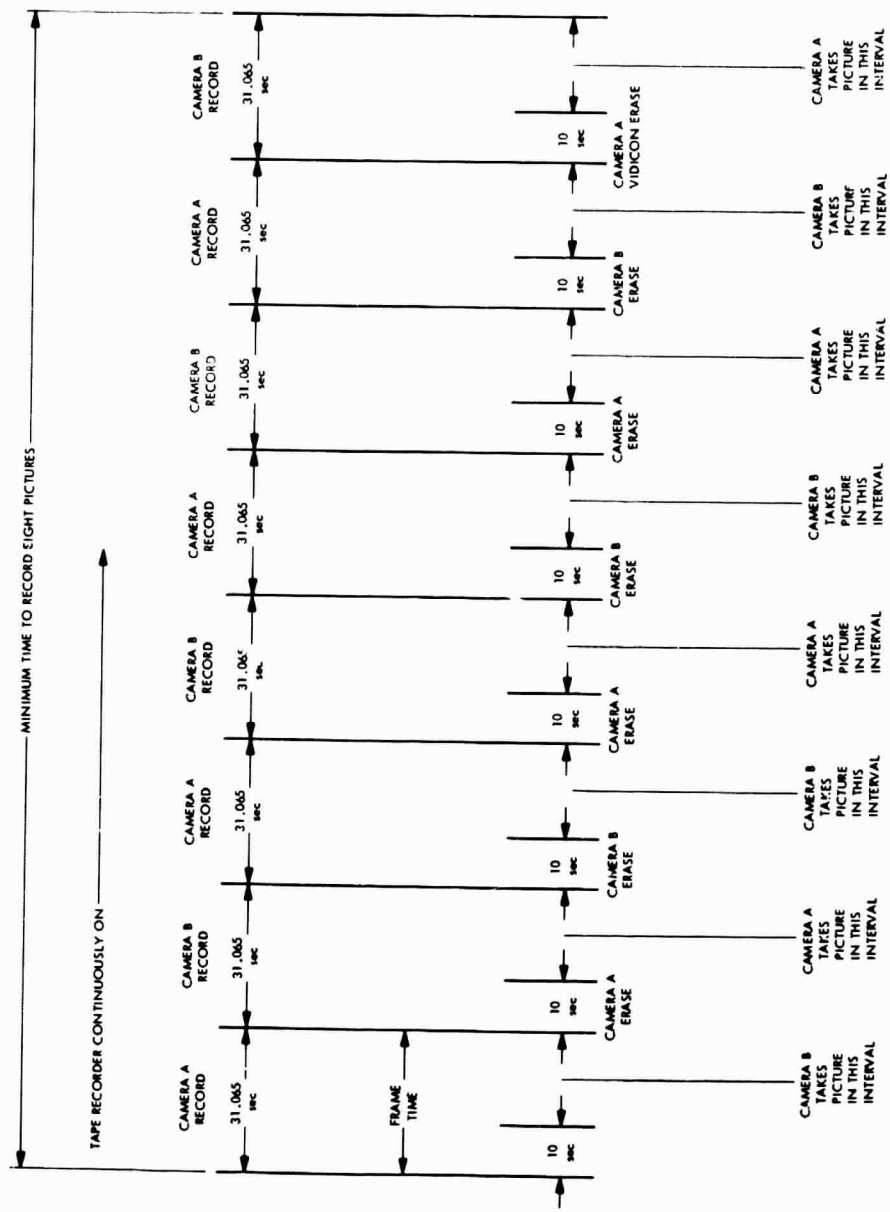


Fig. 60. Frame sequence, cameras alternating

$$\begin{aligned} \text{Total bits/track} &= 1.8 \pm 5\% \times 10^8 \text{ bits}/4 \text{ tracks} \\ &= (4.5 \pm 0.225) \times 10^7 \text{ bits/track} \end{aligned}$$

$$\begin{aligned} \text{Effective bits/track} &= 4.5 \pm 0.225 \times 10^7 \text{ bits/track} \\ &\quad - 0.1225 \times 10^7 \text{ bits/track} \\ &= (4.377 \pm 0.225) \times 10^7 \text{ bits/track} \end{aligned}$$

$$\begin{aligned} \text{Frames/track} &= \frac{(4.377 \pm 0.225) \times 10^7 \text{ bits/track}}{5.43 \times 10^6 \text{ bits/frame}} \\ &= 8.05 \times 0.41 \text{ frames/track} \end{aligned}$$

Thus the assumption of 8 frames/track is justified if we assume the nominal case. The above parameters have been used to provide a baseline mission sequence.

The data handling depicted occurs when all science data are to be recorded with TV data simultaneously. However, if all science data are not being recorded with TV data simultaneously on the DSS, the total frame time will remain the same; i.e., there would be a gap on the tape where other encounter science data would have been.

The record mode discussed here was chosen since it appeared to best satisfy the constraint that fields and particles data be retained over the entire critical interval during the near-encounter period. During a portion of the Venus and Mercury encounter period, the DSS would be off (section VII-C) during earth occultation. To avoid loss of fields and particles data during this critical interval before pictures are taken, fields and particles data are stored in a core buffer that can read and write simultaneously (record mode III). Once DSS operation is initiated during earth occultation (i.e., pictures being taken), fields and particles data are interleaved on a line-by-line basis with TV data. During the 10-sec picture erase periods between pictures (when the DSS is stopped and the same camera is being used repeatedly as illustrated in Fig. 61) the core buffer also functions to prevent loss of fields and particles data during critical intervals (record mode II).

Once earth occultation ends, fields and particles data are again recovered over the direct link (the buffer's function is now redundant).

Note that the HRIR is assumed to produce data only when TV pictures are being recorded. Therefore, HRIR data is always interleaved with TV data on a line-by-line basis.

IRR data will be produced only near or during solar occultation at Mercury (when earth is in view).

During the critical near-encounter period, it is also imperative that no fields and particles data be lost during playback. Therefore, during playback, fields and particles data are stored in a core buffer that can record and playback simultaneously. After one frame of DSS data is played back, the DSS will stop and the buffer will play back information acquired while the frame was being played back. The DSS then will back up to compensate for the tape that was lost while shutting off and then will play back the next frame stored on the tape (playback mode). This process will be repeated during encounter playback periods.

Other possible means of receiving critical real-time fields and particles during playback would be to: (1) send real-time and particles interleaved with engineering over the engineering channel, (2) send real-time fields and particles into a second DSS with a low record rate for playback after the critical near encounter period, and (3) increase the capacity of the present DSS so that playback wouldn't be necessary during the critical encounter period.

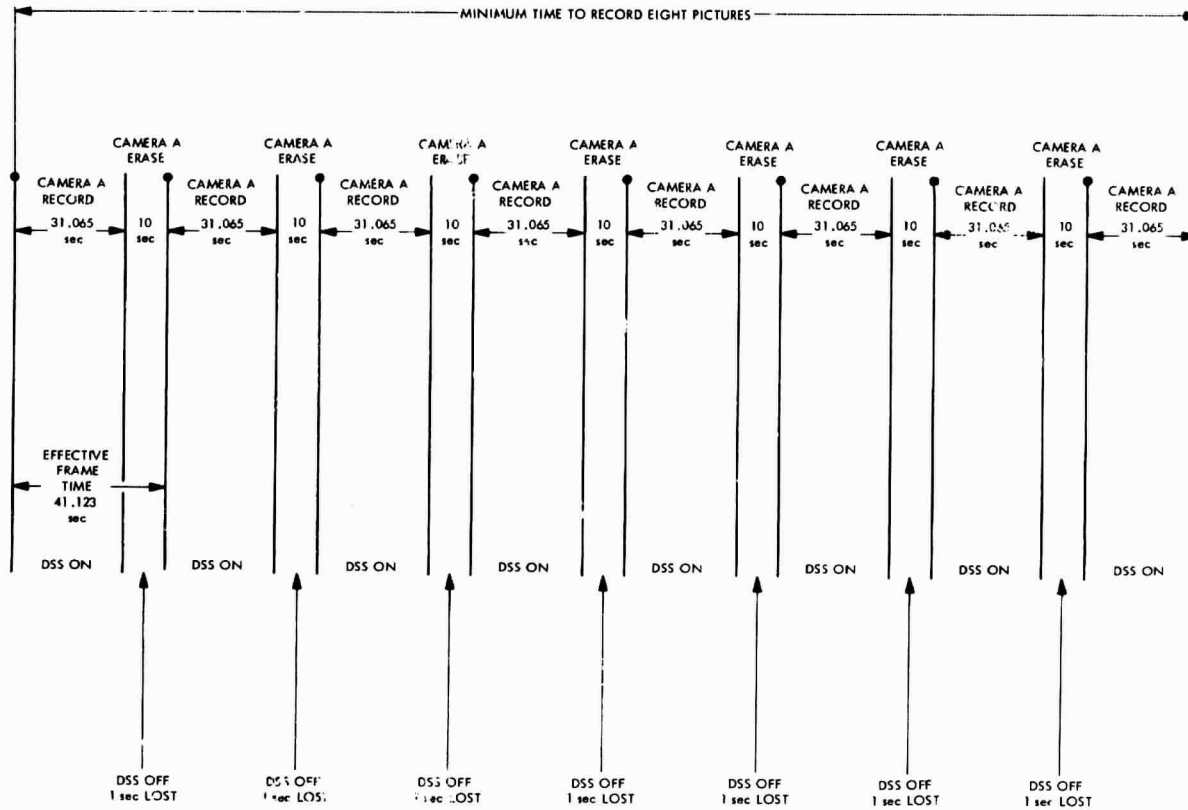
VIII. Spacecraft Subsystems Description

A. Structure

Primary function of the spacecraft structure is to integrate mechanically the subsystems which comprise a functioning spacecraft. As such, the structure provides support and alignment for all flight equipment.

The basic structure is an electronic compartment 54.5 in. across the diagonals and 18 in. high, consisting of upper and lower octagonal rings, connected at each corner by longerons. Seven of the bays contain electronic assemblies and the eighth bay houses the propulsion subsystem. The electronic assemblies are packaged in chassis which, when installed in the spacecraft structure, serve as load carrying members.

Pedestals and brackets are attached to the basic structure as necessary to support and align sensors, scientific instruments, primary low-gain antenna, and attitude control components. The electronic cabling is supported by a trough which also provides for mounting of cable-end connectors at each bay.



NOTE: DOTS INDICATE WHEN PICTURE BEING TAKEN (TAKES ≤ 20 ms).
 THIS TIME HAS NOT BEEN TAKEN INTO ACCOUNT BUT IS
 ASSUMED PART OF ERASE TIME OF 10 sec.
 IDENTICAL FOR CAMERA B

ENCOUNTER SCIENCE LOST IN 10 sec
 GAP AT PRESENT UNLESS SENT
 IN REAL TIME OR STORED ON
 BUFFER. HRIR ONLY ON WHEN
 TV IS ON.

Fig. 61. Frame sequence, same camera

The high-gain antenna is mounted on top of a tubular truss structure approximately 5 ft tall. This structure, which attaches to the corners of the upper ring, provides the one degree-of-freedom antenna with an unobstructed view of earth during appropriate portions of the mission.

The solar panels are mounted on 18-in.-long outriggers to thermally decouple them from the spacecraft. Each of the outriggers is made up of five tubular members which provide longitudinal and transverse stability. The outrigger in bay V incorporates provisions for mounting the deployable secondary low-gain antenna.

The spacecraft is attached to the launch vehicle through the spacecraft adapter. The adapter mates with the *Centaur* adapter and is attached to the lower ring of the spacecraft structure by a V-band assembly at the eight corners of the octagon.

All major structural components are similar if not identical to those used on previous *Mariner* spacecraft. The most notable structural changes are: (1) addition of high-gain antenna superstructure, (2) relocation of the scan platform, and (3) inverting of the *Mariner* Mars 1971 solar panel outriggers.

B. Radio Frequency Subsystem

The radio frequency subsystem (RFS) receives the uplink command and ranging signals transmitted by the Deep Space Instrumentation Facility (DSIF) and transmits the telemetry and ranging signals to the DSIF. A block diagram of the RFS is shown in Fig. 62. Both the received and transmitted frequencies are in the S-band. In the one-way mode of operation (downlink only), the transmitted frequency of 2295 MHz (nominal) is controlled by an on-board crystal oscillator (called the auxiliary oscillator) contained within the exciter. When the spacecraft receives an uplink signal, and the receiver acquires phase-coherence with that signal, the spacecraft-transmitted frequency is controlled by the uplink frequency and is 240/221 times the received frequency of 2115 MHz (nominal). If the spacecraft is in a one-way mode, the DSIF can provide for only one-way doppler tracking of the spacecraft. In the two-way mode of operation, the DSIF can accomplish two-way doppler tracking and ranging. The receiver and exciter portions of the RFS are functionally similar to those utilized for *Mariner* Mars 1969 and 1971.

The spacecraft receiver demodulates the command signal and the ranging information from the uplink signal. The command data is then sent to the flight com-

mand subsystem for processing. The ranging code, when present in the uplink signal, is remodulated on the downlink to provide the turn-around ranging data. This ranging function may be turned on or off in the radio by means of a ground command, and is also turned off periodically by a CC&S timing function. The downlink is also modulated in one of several modes by a composite telemetry signal from the flight telemetry subsystem.

The receiver, which operates continuously, is a narrow-band, automatic phase-tracking, double conversion super-heterodyne receiver. The receiver input stage is a balanced mixer, using hot carrier diodes. The spacecraft transmitter has redundancy by having two exciters and two traveling wave tube (TWT) amplifiers. Either exciter may be used with either amplifier, thus providing full redundancy. Switching between exciters and amplifiers is accomplished automatically by circuits which periodically test exciter and amplifier outputs. If the exciter outputs are below a specified threshold, automatic transfer to the redundant equipment is accomplished. Switching may also be performed by ground commands. The present design is for either of the power amplifiers to operate in a 10- or 20-W power output mode. Power output switching may be performed either automatically by CC&S commands or by ground command, and is accomplished by the adjustment of operating voltages. Input power to the TWTs is held constant.

The RFS uses three antennas. The high-gain antenna, used only for transmitting, is a 40-in.-diameter circular paraboloid, identical to that used on *Mariner* Mars 1969 and 1971. Two low-gain antennas which are modified *Mariner* Mars 1969 designs, are mounted approximately diametrically opposed on the spacecraft. The primary low-gain antenna, used during the early portion of the mission, is mounted at 180 deg cone angle, and the secondary antenna, used after Mercury and during maneuvers, is mounted at 20 deg cone angle, 80 deg clock angle.

A summary of the nominal RFS parameters is:

Uplink frequency: 2115 MHz

Downlink frequency: 2295 MHz

RF power output: 10 or 20 W

Antennas:

- (1) High-gain, 40-in.-diameter circular paraboloid, right-hand, circularly polarized
- (2) Two low-gain antennas, modified *Mariner* Mars 1969 design, right-hand circularly polarized

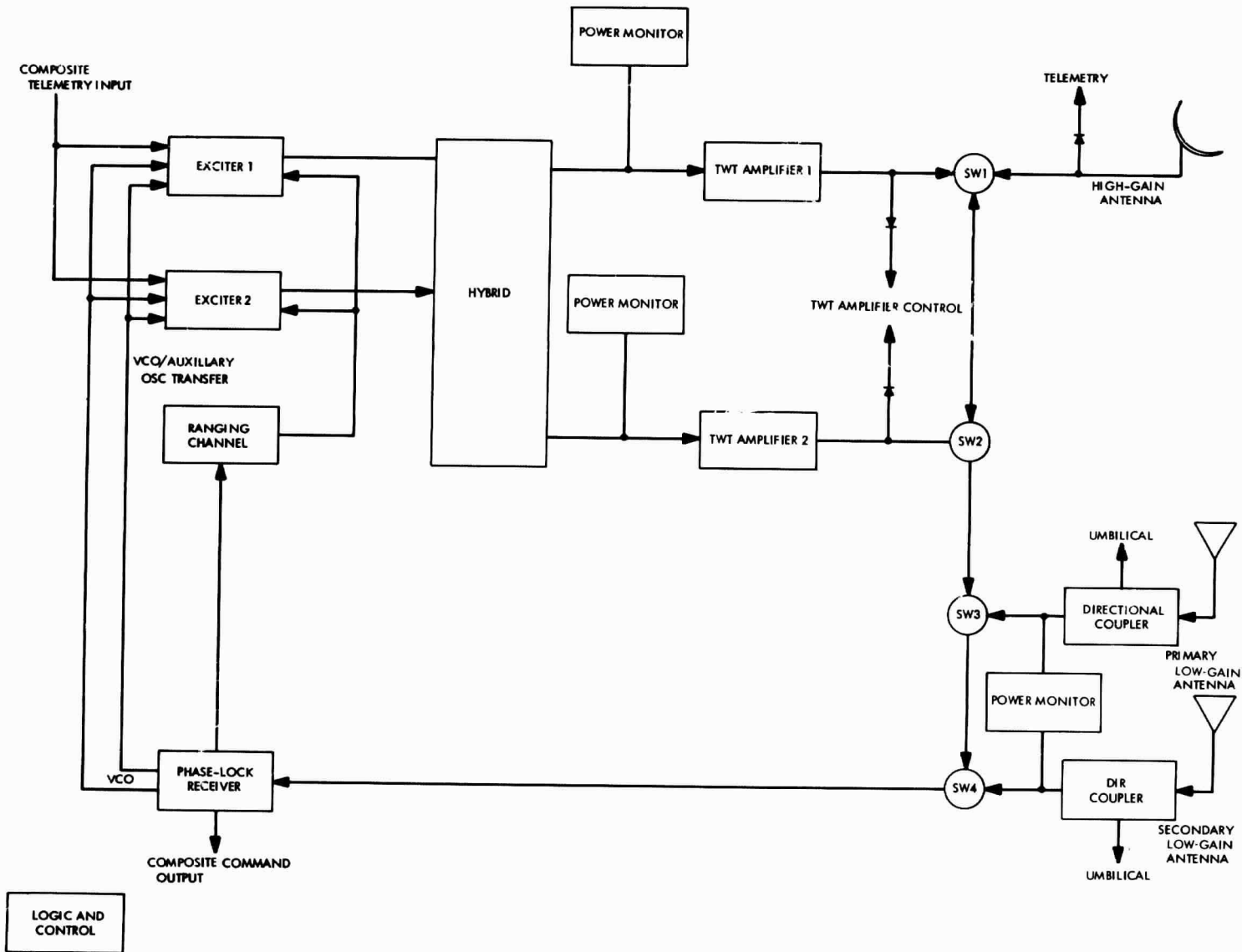


Fig. 62. Radio frequency subsystem block diagram

Weights:

RFS, 55.1 lb

High-gain antenna system, 16.5 lb (includes boom and actuator)

Low-gain antennas, 10 lb (includes both primary and secondary antennas, but does not include actuating mechanism for the secondary low-gain antenna)

Power Requirements:

2.4 kHz power, 28 W continuously

TWT low power, 57 W of dc power

TWT high power, 93 W of dc power

C. Flight Command Subsystem

The flight command subsystem recommended for *Mariner Venus/Mercury 1973* is a single subcarrier PCM/PSK/PM type, using a bit synchronizer. PCM/PSK/PM indicates that the data is pulse-code modulated, the data then phase-shift keys a subcarrier, and the subcarrier phase modulates the RF carrier. Such a system has substantial data rate, error rate, and acquisition time advantages over the *Mariner Mars 1969* and *1971* implementation. It is also amenable to multiple bit rates, if this feature is needed by the mission. For the baseline configuration a single bit rate, 4 bits/sec, system is described.

The block diagram of the command subsystem is shown in Fig. 63, from which it is seen that the subsystem performs several functions:

- (1) Accept a narrow-band PSK subcarrier from the transponder receiver
- (2) Acquire sync and synchronously demodulate the subcarrier
- (3) Acquire sync and synchronously detect the PCM bits
- (4) Detect a word START code in the PCM data, using this detection to resolve all ambiguities
- (5) Decode direct commands (DCs) and provide isolated switch closures to the command output
- (6) Recognize and decode coded commands (CCs) and channel the serial bits and bit sync to the CC&S
- (7) Similarly, recognize and then decode quantitative commands (QCs), and channel these commands to the scan subsystem.

Direct commands are commands which provide a single-switch closure to the user subsystem in order to cause some function to be activated in real time. Coded commands and quantitative commands provide quantitative information to either the CC&S or the scan subsystem to furnish timing information used later in the mission.

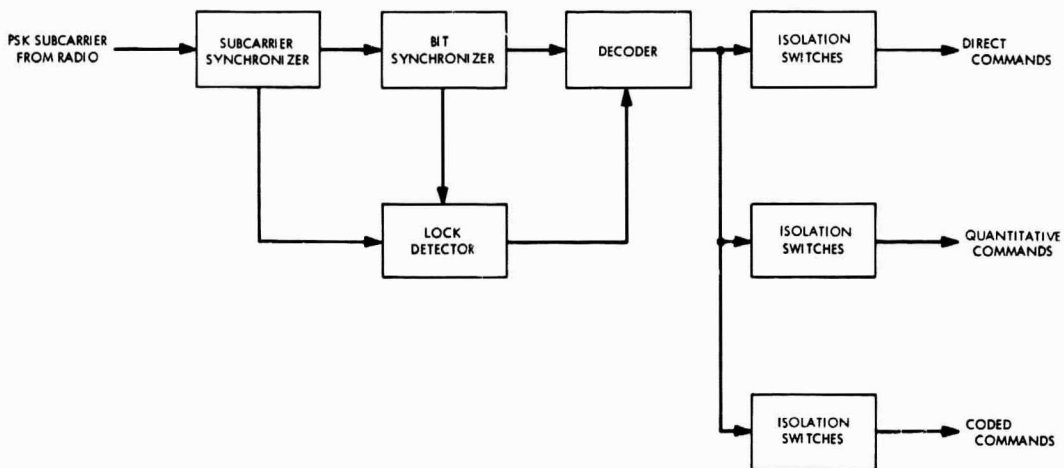


Fig. 63. Flight command subsystem

Performance parameters for the command subsystem are:

Required ST/N_0 : 11.0 \pm 1.0 dB

Bit rate: 4.0 bits/sec

Error rates: (at $ST/N_0 = 11.0$ dB)

Bit error rate less than 1×10^{-5}

False start less than 1×10^{-6}

False abort less than 1×10^{-3}

Sync acquisition time: 150 bit times (35 sec with probability of acquisition = 0.99)

Command word length: less than 32 bits

Weight: 8.7 lb

Power: 2.5 W

D. Power Subsystem

The *Mariner* Venus/Mercury 1973 spacecraft power subsystem is essentially a modification of the *Mariner* Mars 1969 and 1971 power subsystems. Modifications are due primarily for operation near earth and Mercury, as well as for a revised science payload. The following text describes why these changes are required, alternate solutions to the problem, and a preliminary description of the overall power subsystem.

1. Power requirements. A mission power profile depicting the subsystem power requirements as compared to the key operational modes is shown in Table 18. Total raw power required during the complete mission will vary from 266 to 377 W. Duration of time (for battery sizing) is also shown.

2. Solar panel. Because a significant increase in temperature associated with an increase in solar intensity is anticipated at Mercury, a newly designed solar panel is required. With the increase in temperature expected at Mercury, panel output voltage may be reduced from 50 Vdc near earth to 19 Vdc depending on the operating temperature of the panels. Zener diodes are provided for clamping of panel output voltage at 50 Vdc when colder operating temperatures prevail. However, in considering operation at Mercury, the newly designed panel is expected to limit maximum temperatures in the range of 135 to 140°C. At some predetermined operating temperature (approximately 60°C), equivalent to a panel output voltage of approximately 35 Vdc, the switching of the four solar panels operating in parallel to a two-panel parallel-series condition will occur. The Zener

diodes will clamp the panel output voltage at 50 Vdc. Further explanations of this approach are discussed in the power conditioning and distribution section that follows.

The worst case design considers four 21-ft² solar panels operating in parallel near earth and providing a total of approximately 375 W. For operation at Mercury, four panels operating in parallel-series condition will provide approximately 550 W.

A detailed discussion of the solar panel configuration and alternate approaches are provided in section VII-E and in Appendix D, respectively.

3. Battery. The worst case energy demand requirement may vary up to 500 W-hr. This demand may occur during any of the three planned maneuvers, each of which may last up to 80 min. With the addition of the launch mode, sun occultation at Mercury and a possible fourth maneuver, a total of six battery discharge/charge cycles is required. Preliminary testing of the *Mariner* Mars 1969, 18-cell 1350 W-hr silver zinc battery has shown that this battery is capable of providing the above required cycles and is therefore (tentatively) selected for this mission.

The *Mariner* Mars 1969 battery charger may be used for battery charging which occurs immediately after acquiring solar panel power. The charger provides a maximum charging current of less than 1 A with a maximum output voltage of 34.6 ± 2 Vdc at 5 mA. The charger has the capability of accepting an input voltage varying from 25 to 50 Vdc.

4. Power conditioning and distribution. A preliminary functional block diagram of the *Mariner* Venus/Mercury 1973 spacecraft power subsystem is shown on Fig. 64. Four solar panels provide power to the dc bus located in the power source logic subassembly. During the early phases of the mission, the four panels are operating in parallel at 50 Vdc. For operation at Venus and Mercury, or when excessive temperatures reduce the solar panel output voltage to 35 Vdc, two panels operating in parallel are automatically switched in series with the remaining two panels also operating in parallel as shown in Fig. 65. In this manner, the battery will never be required to supplement the solar panels. In effect, battery operation will be identical to that of the *Mariner* Mars 1969 system. In addition, no modifications to *Mariner* Mars 1971 power conditioning components and *Mariner* Mars 1969 battery

Table 18. Mariner Venus/Mercury 1973 mission power profile

Key operational modes	Power source	Duration of event (worst case), min
1. Launch	Battery	38
2. Sun acquisition	Battery	45
3. Roll calibration and Canopus acquisition	Solar panel	
4. Cruise mode II: battery charging. Low-power TWT	Solar panel	
5. Cruise mode I: First maneuver	Battery	80
6. Cruise mode II: battery charging. High-power TWT	Solar panel	
7. Cruise mode I: telemetry blackout	Solar panel	
8. Cruise mode I: second and subsequent maneuver	Battery	80
9. Pre-encounter	Solar panel	
10. Record mode I and II	Solar panel	
11. Record mode III	Solar panel	
12. Playback mode	Solar panel	
13. Cruise mode II: sun occultation (near Mercury)	Battery	8

Subsystem	Key operational modes												
	1	2	3	4	5	6	7	8	9	10	11	12	13
Main inverter 2.4 kHz (avg)													
Science:													
HRIR	0								5.0	5.0	5.0	0	0
TV	6.0								38.0	38.0	38.0	6.0	6.0
IRR	0												2.5
DFR	0								2.5	2.5	2.5	2.5	2.5
Magnetometers	0	0	5.0	5.0	0	5.0	0	0	5.0				
Plasma probe	0	0	6.5	6.5	0	6.5	0	0	6.5				
Energetic particle detector	0	0	1.0	1.0	0	1.0	0	0	1.0				
Cosmic dust detector	0	0	0.2	0.2	0	0.2	0	0	0.2				
SDS (includes I W for buffer)	0	0	22.0	22.0	0	22.0	0	0	22.0	23.0	23.0	23.0	22.0
Total science	6.0	6.0	40.7	40.7	6.0	40.7	6.0	6.0	80.2	81.2	81.2	44.2	45.2
Engineering:													
Scan electronics	4.0								18.5	18.5	18.5	4.0	4.0
Data storage	10.0								18.0	22.0	18.0	19.0	18.0
Flight telemetry system	15.0												
Flight command	2.5												
RFS	28.0												
Pyrotechnic	0	1.0											
Thermal control heater (No. 1)	38.5	26.0	26.0	26.0	38.5	26.0	26.0	38.5	0				
CC&S	29.0	16.0											
Attitude control	13.0	25.0	25.0	4.0	52.0	4.0	4.0	52.0	4.0				25.0
Gyro No. 1	8.0	8.0	8.0	0	8.0	0	0	8.0	0				8.0
Power distribution	2.25												
Total engineering (2.4 kHz)	150.25	140.75	140.75	119.75	180.25	119.75	108.75	177.25	105.25	109.25	105.25	87.75	119.95
Total 2.4 kHz inverter output	156.25	146.75	181.45	160.45	186.25	160.45	114.75	183.25	184.45	190.45	186.45	132.95	164.95
Efficiency	0.903	0.900	0.910	0.903	0.911	0.903	0.870	0.911	0.911	0.912	0.912	0.88	0.904

Table 18 (contd)

Subsystem	Key operational modes (contd)												
	1	2	3	4	5	6	7	8	9	10	11	12	13
Total 2.4 kHz inverter input	166.38	163.05	199.39	177.35	204.4	177.35	125.0	194.56	202.46	208.82	204.44	150.62	182.46
Scan motor (400 Hz-1 ϕ) incl eff 0.797	0	—————→							11.79	11.79	11.79	0	0
Gyro No. 2 (400 Hz-3 ϕ) including efficiency 0.775	11.6	11.6	11.6	0	11.6	0	0	11.6	0	—————→			11.6
Total boost reg output requirement	177.98	174.65	210.99	177.35	216.0	177.35	125.0	206.16	214.25	220.61	216.23	150.62	194.06
Efficiency	0.878	0.877	0.908	0.905	0.878	0.905	0.892	0.883	0.909	0.910	0.909	0.900	0.883
Total boost regulator input requirement	202.71	199.14	232.4	195.96	246.0	195.96	140.13	233.47	235.7	242.42	237.88	167.4	219.77
Unreg dc power requirement													
Boost regulator input	202.71	199.14	232.4	195.96	246.0	195.96	140.13	233.47	235.7	242.42	237.88	167.4	219.77
Battery charger	0.5	0.5	0.5	3.5	0.5	3.5	0.5	0.5	3.5	0.5	—————→		
TWT	57.0	—————→					93.0	—————→					
Boost regulator fail sensor	1.5	—————→											
Thermal control heater (No. 2)	9.3	22.5	—————→										
Subtotal	271.0	280.6	313.86	310.96	327.5	347.96	257.6	350.97	365.2	337.42	332.88	262.4	314.77
Power source and logic efficiency	0.97	—————→											
Total raw power requirement	279	289	324	322	338	359	266	362	377	349	343	271	325

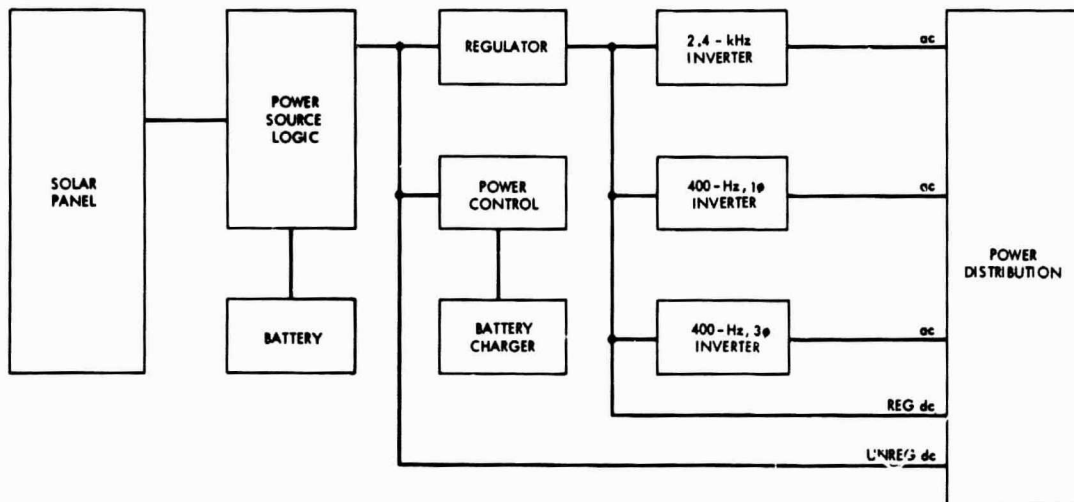


Fig. 64. Power subsystem functional block diagram

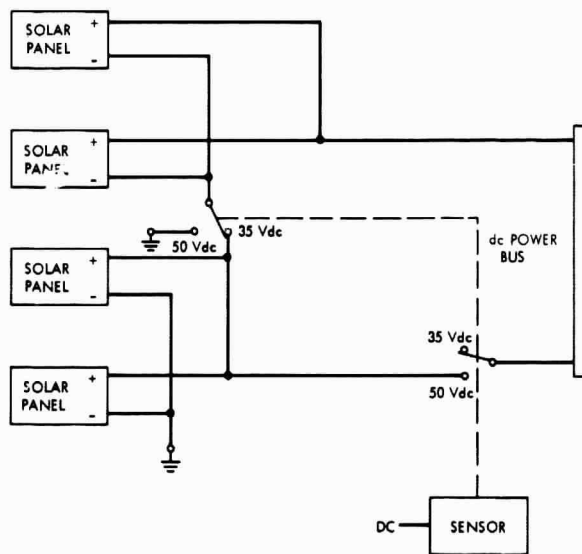


Fig. 65. Solar panel functional schematic switching diagram

will be required. Mechanization of the above sensing and switching logic and components requires further study.

An alternate approach eliminating the above solar panel switching philosophy would be to redesign the boost regulator and battery charger for accommodating lower solar panel input voltages. In addition, the present number (18) of battery cells in series would have to be reduced. As a consequence, the ampere hour capacity of the battery cells may have to be increased. However, this approach tends to be more costly than the solar panel switching scheme.

The main booster regulator converts solar panel voltage to a regulated 56 Vdc at a tolerance of $\pm 1\%$. An identical standby booster regulator serves as a backup to the main booster regulator and will provide power in case of failure of the main booster regulator. Switchover is controlled by on-board detection of over-or-under voltage at the output of the main booster regulator. The maximum power output of both the main and standby booster regulators is 300 W.

The main inverter output is designed to provide 2.4 kHz $\pm 1\%$ single-phase, square-wave power at 50 Vrms $\pm 3\%$ from a regulated 56 Vdc $\pm 1\%$ input. Timing signals to the central computer and sequencer are provided from the main inverter. In event of failure of the main inverter, the system will switch to a standby inverter with identical

output characteristics. The maximum power output of the main and standby inverters is 250 W.

The 400-Hz inverter consists of both single-phase and three-phase outputs. The output characteristics of the single-phase portion, including both amplitude and frequency, are 28 Vrms $\pm 5\%$ square wave and 400 Hz $\pm 0.01\%$ in the normal mode, respectively. Average power output is 15 W at 28 V with a peak loading of 21 W for a maximum of 60 sec. The 400-Hz three-phase power output characteristics, including both frequency and amplitude, are 400 Hz $\pm 0.01\%$ in the normal mode and 27.2 Vrms $\pm 5\%$ line-to-line, quasi square wave, respectively. Average power of the three-phase output is 12 W with a peak of 15 W.

5. Power system weight. The following is a weight breakdown of the *Mariner Venus/Mercury 1973* power subsystem and current design status:

	Weight, lb	Design status
Solar cells (not including structure, mirrors)	18.5	New
Battery, including chassis, <i>Mariner Mars 1969 AgZn</i>)	34.58	<i>Mariner Mars 1969</i>
Battery charger	2.14	<i>Mariner Mars 1969</i>
Main inverter (2.4 kHz) (2)	5.86	<i>Mariner Mars 1971</i>
Boost regulator (2)	11.70	<i>Mariner Mars 1971</i>
Inverter (400 Hz, 1 ϕ and 3 ϕ)	3.51	<i>Mariner Mars 1969</i>
Power control	2.33	<i>Mariner Mars 1969</i>
Power source logic	8.5	<i>Mariner Mars 1969 (modified)</i>
Power distribution	1.8	<i>Mariner Mars 1969 (modified)</i>
Heater dc power	1.2	<i>Mariner Mars 1969 (modified)</i>
Total	90.17	

E. Central Computer and Sequencer

1. Introduction. The Central Computer and Sequencer (CC&S) will be a modified *Mariner Mars 1969* CC&S. It is a stored-program, special-purpose digital computer

with a fixed sequencer for maneuver redundancy. Two changes are recommended for increased reliability and flexibility, ease of programming, and simplification of in-flight reprogramming. One is an increase in memory size to 512 words from the 128 words in the *Mariner* Mars 1969 CC&S. The second is a modification to the instruction list. The subtract operation is altered to include a compare and skip option, and some operation codes are altered and expanded to accommodate an execute event instruction. The two changes will be discussed in a later section.

The characteristics of the *Mariner* Venus/Mercury 1973 CC&S are summarized in Table 19. The reliability is a recent estimate based on parts count, constant component failure rates, and independent failures.¹⁶

During the trajectory correction maneuvers, the CC&S operates in one of three modes: tandem, computer only, or fixed sequencer only. Normally, the tandem mode is used since this results in maximum CC&S reliability. In the tandem mode, the fixed sequencer controls the maneuver events. The computer outputs are compared to the sequencer outputs by on-board logic. If they do not agree, the maneuver is automatically aborted. DC commands can switch the CC&S to either of the other two modes if difficulty with the computer or fixed sequencer is encountered before or during a maneuver.

2. Functional requirements. The purpose of the CC&S is to provide timing and sequencing functions for other spacecraft subsystems throughout the flight. The complete flight program is stored in the CC&S on the launch pad 1 hr before launch (refer to the baseline sequence of

events). At any time, subject to a restriction (section VIII-E-4-c), during the flight the contents of the memory can be read out or altered one word at a time. If the program is altered in flight, the CC&S can perform an automatic check to insure that the alteration was made properly.

All CC&S events, except those which occur during trajectory correction maneuvers and earth occultations, are backed up by ground commands. Some CC&S events, in turn, back up the timed events of other subsystems, particularly during earth occultations.

3. Sequence of events. This section contains a discussion of the functioning of the CC&S during the flight. To facilitate the discussion, the sequence of events is divided into six subsequences: prelaunch, launch, cruise, the trajectory correction maneuvers, Venus encounter, and Mercury encounter.

a. Prelaunch. The prelaunch sequence starts when the CC&S memory is loaded 1 hr before liftoff ($L - 1$ hr) and ends with separation of the spacecraft ($S + 0$). The loaded program includes a supplementary diagnostic routine which perform a simple check on the memory contents.

Immediately following the loading of the memory, the diagnostic routine computes the sum of all words in the program and compares it with a stored value. A zero difference between the computed and stored values signifies that the memory has been loaded properly and the CC&S is operating. A verify output signal is produced. At $L - 4$ min, after the spacecraft has been switched to internal power, the CC&S main program is started by release of a CC&S inhibit. Three minutes later the CC&S produces a second verify output that indicates proper operation.¹⁷

For the remainder of the mission the CC&S keeps track of the passage of time. It counts time in increments of 1 hr. In addition, when necessary, it subdivides any hour into minutes and seconds. Time is measured from the start of CC&S operation; that is, 4 min before launch.

Until the spacecraft is separated, the CC&S outputs (except for the verify signal) are disabled by a relay hold current. At separation the current is removed and all CC&S outputs are enabled.

¹⁷Since the fixed sequencer does not operate except during a maneuver, there is no verification of its readiness. If desirable, its readiness could be verified. Such verification will take about 2 hr to accomplish.

Table 19. Characteristics of *Mariner* Venus/Mercury 1973 CC&S

Type	Digital, bit-serial, stored program special purpose
Memory size	512 words of 22 bits each
Reliability (estimated mean time before failure)	Computer: 53,800 hr Fixed sequencer: 130,000 hr CC&S in tandem: 141,000 hr
Weight	20 lb (excluding cables)
Power	29 W (Launch), 16 W (average cruise), 18 W (peak)
Volume	600 in. ³ (excluding cables)

¹⁶Personal communications, David Rubin (JPL), September 27, 1968 and October 10, 1968.

b. *Launch.* The launch sequence extends from the time the spacecraft is separated until it is fully attitude stabilized. There will be from five to seven events in the launch sequence. The times of their occurrence can be specified to the nearest minute. The initial spacecraft events (solar panel unlatch, etc.) are initiated by a counter not associated with the CC&S. The CC&S provides a backup capability for these events. The remaining events in the launch sequence are initiated by CC&S outputs and are backed up by ground command.

The time of occurrence of any CC&S event in this sequence, as in any other, may be modified in flight by appropriate transmission of CC commands.

c. *Cruise.* The cruise sequence begins with the start of CC&S operation and continues through the entire flight. The other sequences are "superimposed" on the cruise sequence. The computer interleaves the timing of cruise events with the timing of events in the other sequences. Typical of the types of events occurring in the cruise sequence are Canopus sensor updates, changes in RF power, high-gain antenna pointing corrections, as well as events that recur periodically, called cyclics. The total number of cruise events (excluding cyclics, which may occur tens or hundreds of times) is estimated to be between 25 and 60 depending on the required number of antenna pointing events.

Cruise event times are normally specified to the nearest hour. If necessary, events can be timed with 1-min resolution but this is discouraged because it tends to reduce mission reliability. Events that are specified with higher resolution cause the CC&S to access the computer memory more often. The memory, containing the flight sequence of events, is volatile only when it is being accessed; thus it is susceptible to any sizable (greater than $\pm 20\%$) power transient at those times. The CC&S contains circuits to sense this condition and will stop its time-keeping while notifying the ground via the FTS. But the memory contents can no longer be trusted. They have to be examined and corrected if necessary.

All cruise events are backed up by ground (DC) command.

d. *Trajectory correction maneuvers.* Four trajectory correction maneuvers are possible although three is the more likely number. The three will occur at the following approximate times: $L + 8$ days, $E_V - 3$ days, and $E_V + 8$

days. Since all the baseline maneuvers are similar, only one will be discussed here.

A maneuver can be performed with the CC&S in any one of its three maneuver modes. With the CC&S in the tandem mode, two sets of CC commands are transmitted to the spacecraft to establish durations for pitch and roll and the motor burn. One set is routed to the CC&S computer and one set is supplied to the fixed sequencer. In either of the other two modes, only one set of CC commands is required. It is stored in the CC&S unit that is operating.

Storage of the CC commands can be accomplished at any time before the start of the maneuver. The command format requires two command words for each CC being stored in the computer. The first word specifies the memory address, into which the subsequent information is to be inserted. It also contains the first 7 bits of the 22-bit word to be stored. The second command word contains the remaining 15 bits. A CC command to be stored in the fixed sequencer requires only one command word.

The maneuver is initiated by a DC command. The maneuver sequence will consist of nine events. This number includes both the starting and stopping of the turns, and motor burn. Maneuver events may be timed with 1-sec resolution. Spacecraft turns are also timed to the nearest second, but motor burn duration is controlled to within one accelerometer pulse.

The events initiated by the CC&S during a maneuver are not normally backed up by RF command. Except for the first maneuver, the round-trip communication time delays virtually eliminate the effectiveness of any emergency measures initiated from the ground. Therefore, the maneuver is normally executed with the CC&S in the tandem mode. Any discrepancy between the computer outputs and the sequencer outputs will immediately cause a maneuver abort and celestial references will be reacquired.

e. *Venus encounter.* The Venus encounter sequence begins at $E_V - 1$ hr and ends at $E_V + 16$ hr. The 20 to 40 events in this sequence will be programmed with 1-sec resolution.

f. *Mercury encounter.* The Mercury encounter sequence begins at $E_M - 7$ days and ends at $E_M + 7$ days. The 80 to 120 events in this sequence will be timed with 1-sec resolution.

4. CC&S Description.

a. Functional description

General description. As previously mentioned, the CC&S is a special purpose computer with a fixed sequencer for redundancy during maneuvers. Figure 66 is a block diagram of the CC&S, illustrating its organization.

The computer unit. Approximately 80% of the CC&S subsystem is composed of the computer unit shown in the upper part of Fig. 66. The processor controls memory transfers; performs logic, control, and arithmetic operations; senses external and internal interrupts; and routes event addresses to the event decoder at appropriate times.

Memory transfers can occur only during a memory scan, which is normally performed once every hour. The memory scan consists of executing instructions sequentially unless the program specifies a jump. Encountering a halt instruction ends the scan. Flags that may be set as a result of instructions encountered and executed during a scan can call for another scan to follow in 1 sec or 1 min rather than an hour later. This will be the rule for scans in launch, maneuver, and encounter sequences. In the cruise sequence, however, hourly scans will normally occur.

The processor's arithmetic capability is limited to adding and subtracting any two 22-bit words in memory, and subtracting 1 from a selected portion of any single 22-bit word in memory. The processor's logic and control capability includes conditional and unconditional program jumps, instruction operation code modifications and word transfers. The processor also contains flip-flops that allow external (ground command) control of the computer operation. These flip-flops are interrogated periodically by an instruction that causes a program jump if the flag is set.

The baseline memory consists of 512 words (22 bits per word) of ferrite core storage, and input/output, address and control circuits. Each bit of a word is stored in one core. Words may be randomly addressed but the bits of a word are read out sequentially. Reading a bit destroys it, and it must be restored in the core if it is to be retained unaltered. Therefore, the memory operates in a "read/restore" cycle. The memory also contains a 1-word register for transferring memory contents to the FTS during a ground-commanded memory readout. It is also used as an input buffer and as an accumulator.

The input decoder accepts and controls CC command data from the FCS for insertion into the memory and also controls the transfer of memory information to the FTS.

The computer clock converts the 2.4-kHz square wave from the power subsystem into clock pulses for timing the operations of the processor, memory and event decoder.

The event decoder and event actuators receive and decode the event addresses from the processor. The event decoder is capable of decoding 72 discrete states from a 9-bit address. It is mechanized so that from one to three of these discrete states can be simultaneously selected. This capability, subject to certain restrictions, allows a variety of output actuator combinations to be implemented as the need arises during the flight.

Fixed sequencer unit. The fixed sequencer is shown in the lower portion of Fig. 66. It provides redundant maneuver capability within the CC&S. Prior to the start of a maneuver, the duration values and polarity for pitch and roll, and the number of accelerometer pulses desired during motor burn, are supplied to the input decoder from the FCS. The input decoder routes this information to the appropriate duration register (pitch turn, roll turn or motor ΔV) via the switch logic. Once the maneuver starts, each duration register is counted to overflow in turn. The counting and the suitable intervening delays are controlled by the switch logic.

Modal operation. The tandem mode provides an on-board check of the critical maneuver turns and motor burn. In this mode the sequencer is the prime maneuver element with the computer programmed to follow along and check its operation. Except during the motor burn, if the computer outputs do not match the sequencer outputs during a maneuver, the maneuver is automatically aborted. During motor burn, the computer monitors elapsed time. If the motor burn length exceeds a maximum value it is terminated. This arrangement protects against incorrectly executed turns—wrong direction or magnitude—and excessive motor burns. Short motor burns that might result can be corrected by subsequently executing another maneuver.

In the event of problems with the tandem mode, either CC&S unit can be selected for a maneuver on the basis of diagnosis of the problem. Mode control is obtained by DC commands. The tandem mode is automatically assumed in the absence of DC commands to the contrary.

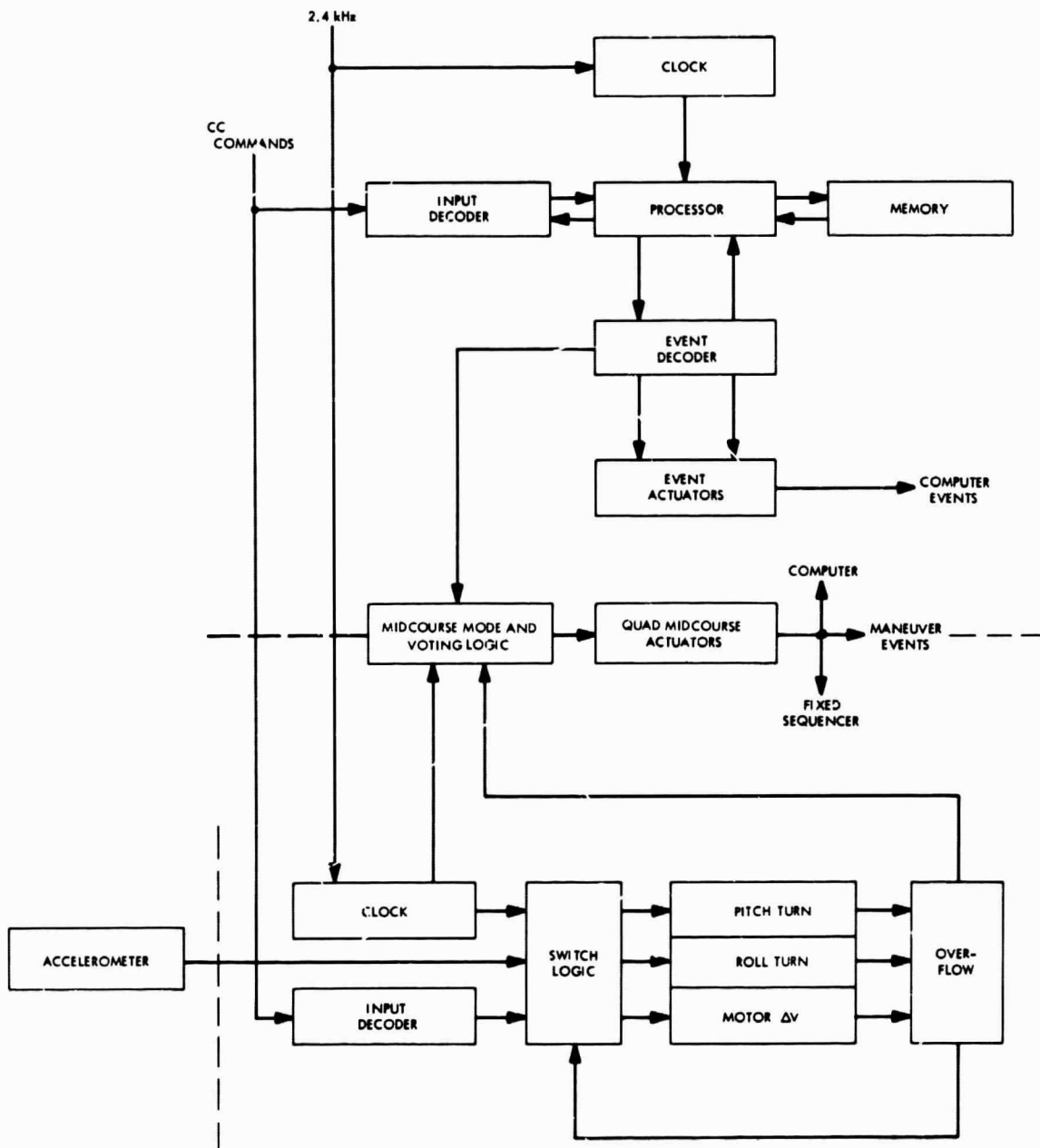


Fig. 66. CC&S organization block diagram

The maneuver event actuators are separated from the other actuators. They are quad redundant for high reliability.

Instruction list. The computer instruction list consists of 16 instructions. The operation code in the instruction word is limited to 4 bits. Therefore, 16 instructions is the maximum ordinarily permissible with the *Mariner Mars 1969* design. To increase this number in a straightforward manner would precipitate a major redesign effort and this is not contemplated for the *Mariner Venus/Mercury 1973* mission. However, some changes, discussed later in section VIII-E-5 b, are recommended to save some memory space and to simplify the programming.

The 16 instructions can be categorized as:

- Arithmetic: 1—add; 1—subtract
- Jump: 1—unconditional jump,
1—reset operation code to zero and unconditional jump;
1—flag unconditional jump;
1—count 1 and conditional jump;
1—decrement address by 1 and conditional jump;
4—decrement time by 1 and conditional jump;
- Other: 1—no operation; 1—program halt;
2—word transfer and halt;
1—transfer word

The limited number of instructions available complicates the programming. Development of a high-level compiler that would allow a general purpose computer to convert a given mission sequence directly to machine language is quite difficult and, therefore, has not been attempted. However, programs written for *Mariner Mars 1969* have been simulated and checked on a general purpose computer. Once the "tricks" of programming with these instructions become familiar, programming becomes a relatively straightforward task. Fortunately, errors, to which machine language programming is prone, can be eliminated by the above-mentioned simulations.

b. Interface description. This description is essentially that of the *Mariner Mars 1969* CC&S and is offered here as a guide.

Input boundaries exist for primary power, command subsystem signals, telemetry subsystem signals, data auto-

mation subsystem signals, inhibit/enable signals from the spacecraft separation connector, blockhouse launch complex equipment (LCE) signals, and direct access signals via the CC&S operation support equipment (OSE).

Output boundaries exist for event outputs to spacecraft users, engineering telemetry to the telemetry subsystem, performance and control signals to the blockhouse LCE, and performance and control signals to the CC&S-OSE.

The CC&S receives primary 2.4-kHz square-wave power with $\pm 0.01\%$ frequency stability from the power subsystem. This input also serves as the basic CC&S clock frequency.

The CC&S receives the following signals from the FCS:

- i. Reset the fixed maneuver sequence and switch the maneuver logic to the non-tandem standby mode.
- ii. Start the maneuver sequence (two independent signals).
- iii. Halt computer operation and inhibit computer output actuators.
- iv. Restart computer operation and enable computer output actuators.
- v. Switch maneuver output actuators to computer-only and start the maneuver sequence.
- vi. Switch the CC&S maneuver logic to the tandem standby mode and enable operation of the power transient detector.
- vii. Coded commands of 18 bits separately to the computer and fixed sequencer portions of the CC&S along with alert and data sync.

The CC&S receives an alert signal from the FTS to start a memory readout cycle and a train of synchronization pulses to synchronize the shifting of data back to the FTS for transmission.

The CC&S receives a signal from the SDS each time a TV picture is taken and another signal at the start of the near-encounter sequence to initiate programmable delays which are used to fix the time of clock angle slow down-encounter terminate, analog recorder stop, and digital recorder stop.

From the spacecraft separation connector the CC&S receives an input enabling its logic and removing relay hold at spacecraft separation.

The CC&S receives from the blockhouse LCE the CC&S inhibit, relay hold, CC&S clear, data sync, data alert, data and OSE +28 Vdc interface power.

All CC&S timed events to other spacecraft subsystems are isolated relay contact openings or closures.

To the FTS the CC&S provides the following outputs: data; an end-of-data-readout signal at the completion of a requested readout mode; an event indication output whenever a CC&S event is output, or a command is received by the CC&S, or certain other logic functions are executed within the CC&S; logic status indication.

The CC&S delivers the data verify, relay hold monitor, and operation verify signals to the blockhouse LCE.

c. Event timing accuracy. While the frequency source that the CC&S uses to accumulate time is highly stable, over a period of several months an appreciable error can be expected. However, it is anticipated that this error will be compensated for under CC&S program control. Event times can be modified as a result of calibration of the flight frequency source either before or during flight.

As for maneuvers, the motor burn will be controlled by spacecraft acceleration rather than by accumulated time. On the other hand, any turn duration is ± 0.5 sec of the desired interval in the worst case. In addition, in the computer-only maneuver mode, the intervals between the turns and between the last turn and the motor burn are in-flight modifiable and are timed to ± 0.5 sec.

The transmission of CC commands can cause a temporary interruption of the normal time-keeping routines in the computer. Therefore, if time losses and/or subsequent reprogramming are to be avoided, CC command loading should be restricted to intervals when the CC&S is in cruise mode (1-hr operation cycles). CC command loading may be accomplished without difficulty if it is done between the hourly scans. This loading restriction saves considerable circuitry within the CC&S without unduly penalizing the spacecraft or mission operations since all loading can normally occur during the cruise mode.

A timed interlock is provided in the CC&S to return the computer to real-time operation if any CC word should be interrupted before its completion.

5. Changes to Mariner Mars 1969 CC&S

a. Increased memory size. The Mariner Mars 1969 flight program occupies the entire 128 words of memory. Approximately 75 locations are needed for event time processing and executive routines, and about 50 locations are now being used for event times. In estimating the size of the Mariner Venus/Mercury 1973 flight program, we have to add the 80 to 120 events anticipated for Mercury encounter, about 55 instructions for the added antenna pointing task, and about 20 words for the diagnostic routine. The total anticipated program length in the worst case is therefore about 320 words. The memory size is restricted to powers of two because the CC&S is a binary machine. Therefore, the required memory size is 512 words.

This increase in memory capacity can be reduced if an "overlay" technique is used to conserve memory space. The flight program can be divided into two segments. One segment would be loaded before launch. Then, sometime during the flight, the second segment would be loaded in the same locations formerly occupied by the first segment. If the two segments are of similar length they will each be about 160 to 200 words long. Therefore the Mariner Mars 1969 memory size need be increased to only 256 words.

Memory reloading would probably take place following the third maneuver. This is approximately 108 days after launch. The CC&S input decoder must function properly until then. If the input decoder fails before the memory is loaded with the second segment, the remaining mission events would have to be commanded from the ground. Therefore, although the overlay approach is a feasible alternative to increasing the memory size, it results in a small decrease in mission reliability. Furthermore, a 512-word memory is also slated for the 1971 Mars orbiter CC&S.

b. Instruction modification. As a result of extensive programming exercises in preparation for, and during, the Mariner Mars 1969 flights, it became apparent that a means for comparing the magnitudes of two numbers would be desirable. It would be helpful in reducing the length of the diagnostic routine. Another attractive feature would be the ability to execute any particular event repeatedly over a period of time with one instruction. These supplements to the computer's capability would simplify the programming and save storage space.

However, as previously mentioned, the operation code capacity of 4 bits cannot be increased without an extensive redesign of the CC&S. To circumvent this costly alternative, it was decided that the compare-and-skip option could be added to the subtract instruction. In addition, the operation codes of two instructions could be combined, thus allowing for the introduction of an execute event instruction.

The two instructions whose operation codes could be combined are the halt and no operation. These instructions have no operands associated with them. Some of the bit positions that normally specify the operand addresses in the instruction word can then be easily used to expand the operation code for these two instructions. They would effectively have 5-bit operation codes. The 4-bit parts would now be identical, thus freeing one operation code. The freed code would serve for the execute event instruction.

The modification to the subtract instruction is as follows. If the subtrahend and minuend in a subtraction are not equal, the next instruction would follow in the program execution. If they were equal, the instruction after the next would follow. With this feature, a subtract (with no comparison) is performed by inserting two identical instructions following the subtract. To perform a subtract and compare, two different instructions are entered in the program. A subtract and compare operation in the *Mariner Mars 1969* CC&S requires a 3-word subroutine. Thus one word position is saved each time this is required in the program. On the other hand, the subtract operation would now require an additional word. The net result would be a saving because the subtract and compare is needed much more often than the subtract alone.

The execute event instruction is useful for periodic events such as cyclics and planetary platform slew commands. It would supplement the count 1 and conditional jump instruction. The latter executes an event once after a given time interval has elapsed and causes a program jump. The former instruction would do the inverse. It would execute an event repeatedly throughout a given time interval, causing a program jump each time, and at the end of the interval would continue with the next instruction. This instruction would save approximately three memory locations whenever it appeared in a program.

Both of the proposed instruction list modifications can be accomplished with a minimum of hardware changes. An estimate of the extra hardware needed is one flip-flop

and perhaps three to seven logic gates. The exact quantity depends on the number of gates that can be shared between the count 1 and conditional jump and the execute event instructions. Of course, some rewiring of other logic gates will be required to accommodate the operation code changes.

F. Telemetry Subsystem

The telemetry subsystem design recommended for *Mariner Venus/Mercury 1973* is a wired sequence tree-commutator with several data modes (Fig. 67). Convolution or block encoding may be applied to its output, depending upon specific data requirements and DSN plans. The general philosophy of subcarrier multiplex of engineering and scientific data will be followed, since this has proved to be a clean and operationally practical technique.

The tree switch approach was selected, rather than the traditional *Mariner* decimal-deck structure, because of the substantial reliability, due to the reduced parts count advantage of the former. This change is especially attractive because the Texas Instruments series 51 integrated circuits are no longer manufactured, and therefore, a redesign of the 1969/1971 telemetry subsystem is mandatory. A wired (fixed) sequence rather than program is recommended for this baseline. Further studies should investigate the potentially substantial advantages of a stored program commutator.

Performance parameters for the telemetry system are:

Inputs: 100 analog, 50 serial digital, 100 parallel digital.

Outputs: 2 PCM/PSK subcarriers, mixed, precision waveforms.

Subcarrier frequencies: unresolved. Minor impact for a selection of subcarriers between 10 and 400 kHz.

Data Rates:

(1) Overall capability: 5-500 bits/sec for low-rate channels; 500-100,000 bits/sec for high rate.

(2) Considered in this study:

Engineering at 8½ or 33½ bits/sec

Low rate science (uncoded) at 66½ bits/sec

High rate science (block-coded) at 1.0125, 2.025, 4.05, 8.1, or 16.2 kbits/sec

Coding: convolutional, block or uncoded

Weight: 21 lb (estimated)

Power: 15 W (estimated)

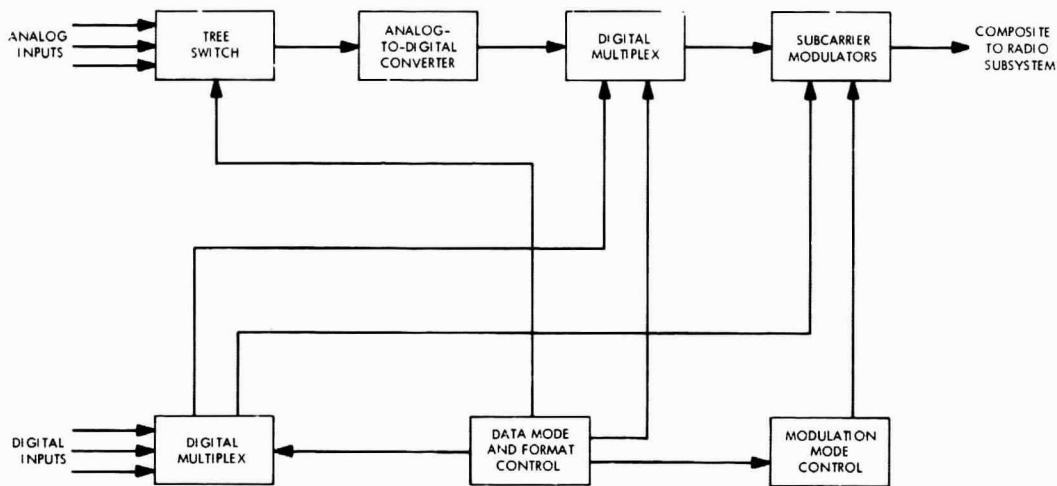


Fig. 67. Telemetry subsystem

G. Flight Control Subsystem

1. *Attitude control subsystem requirements.* The attitude control subsystem (ACS) is required to orient the spacecraft automatically with respect to the lines of sight to the sun and Canopus after separation from the launch vehicle and after each of the three trajectory correction maneuvers. Upon receipt of commands from the CC&S, the ACS must orient the spacecraft to align the propulsion system thrust axis in the direction commanded for the trajectory correction maneuver and must control the direction of the velocity change imparted during the trajectory correction maneuver. In addition, it must provide cruise attitude stabilization for 165 days.

a. Attitude Control Subsystem.

Introduction. The attitude control subsystem is essentially the same as the *Mariner* series ACS, which consists of a cold gas "bang-bang" reaction jet system which stabilizes the spacecraft about all three axes. This system has the capability to reduce the initial launch vehicle tip-off rates and acquire the sun and Canopus. During cruise, the spacecraft axes are aligned relative to the sun and Canopus through the use of celestial sensors (Fig. 68). When other orientations are required, i.e., for trajectory correction maneuvers, an inertial reference is provided by gyroscopes. The spacecraft is initially in the cruise attitude and then rotations are made, about the spacecraft axes, to the new desired attitude. An autopilot control subsystem is provided to stabilize the spacecraft during

trajectory corrections (motor burn). This control system uses the gyros as the error sensors and employs jet vane actuators to control the direction of the thrust vector (Fig. 69). In addition, an integrating accelerometer is used to control the velocity increment imparted during motor burn.

The required modifications to a *Mariner* Mars 1969/1971-type ACS system for the Venus/Mercury Mission consist of: (1) logic changes to provide for sun occultation at Mercury, and (2) sun sensor protection against a high-temperature environment near Mercury. Also, nitrogen cold-gas required has increased slightly (about 2 lb) based on anticipated increases in solar torques for this inner planet mission and contingencies such as scan platform interactions, etc. While the baseline maneuver turn sequence is that of *Mariner* Mars 1969, i.e., pitch-roll, it appears that an alternate sequence (described in Appendix C) could offer some advantages from a temperature control standpoint. For any of the *Mariner* Venus/Mercury 1973 maneuvers, the maximum time spent in a fixed attitude (of great importance from a temperature control standpoint) is expected to be 23 min. The maximum time the spacecraft will not be sun-acquired during a maneuver is expected to be 97 min.

Figure 70 illustrates the *Mariner*-type dual gas system to be used. Placement of the pitch, yaw, and roll valves is indicated; also shown is the high- and low-pressure gas system hardware and the valve lever arm length.

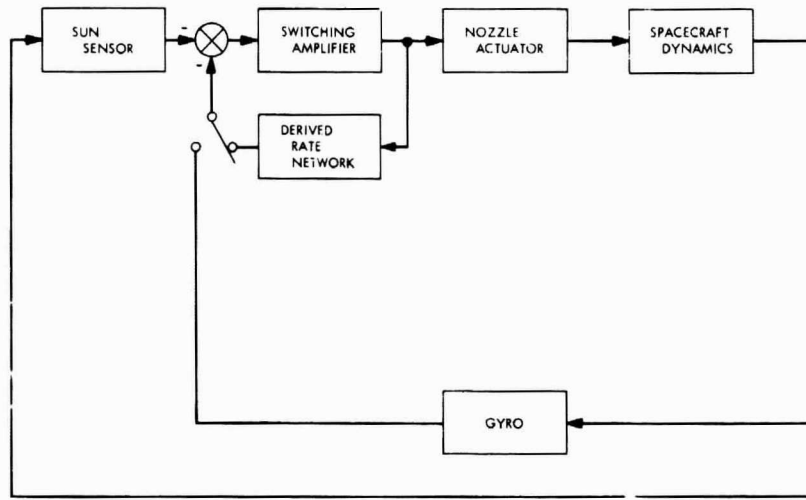


Fig. 68. Roll cruise control configuration

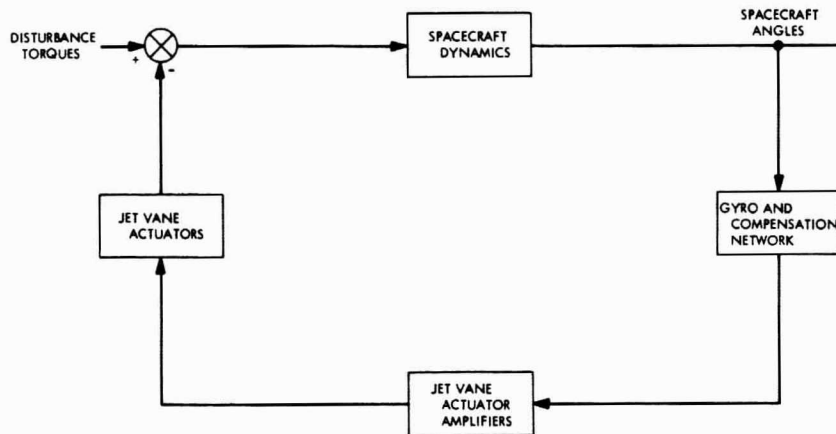


Fig. 69. Pitch and yaw autopilot configuration

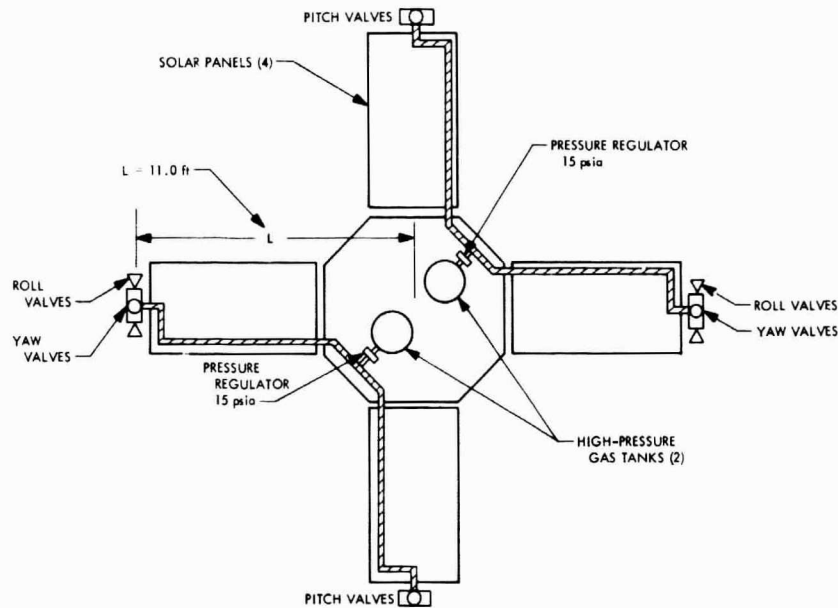


Fig. 70. Attitude control gas system

A summary of the *Mariner Venus/Mercury 1973* flight control mechanization as compared to *Mariner Mars 1969* and *1971* designs is indicated in Table 20. Included in the summary is a planet sensor(s) similar to that (those) used on *Mariner Venus 67*, which may be required to provide on-board sensing of impending encounters with either Venus or Mercury.

Table 21 shows the ACS weight breakdown, and a mission power profile for the ACS is given in Fig. 71.

2. Maneuver pointing error. As part of the current *Mariner Venus/Mercury 1973* study, the rms value of the maneuver pointing error was estimated. The maneuver pointing error is defined as the angle between the commanded maneuver velocity and the actual maneuver velocity. The rms value is simply the square root of the expected value of the square of this angle.

To make this estimate, the *Mariner Mars 1969* maneuver sequence was assumed with two exceptions. The waiting time between the pitch and roll turns and the waiting time between the end of the burn and start of sun reacquisition were each reduced to 256 sec. The 512 sec saved were added to the waiting time between

Table 20. *Mariner Venus/Mercury 1973* flight control system mechanization

Flight control unit	Comparison with mechanization for other <i>Mariner</i> missions
Attitude control electronics and logic	Minor changes in logic to provide for sun occultation. Minor changes in parameters
Celestial sensors	Planet sensor(s) (if required) similar to <i>Mariner Venus 67</i> . Changes to sun sensors for thermal control. Canopus tracker similar to <i>Mariner Mars 1971</i>
Autopilot electronics and jet vane actuators	Similar to <i>Mariner Mars 1969</i> . Minor changes in parameters
Inertial reference unit	Gyros and accelerometer similar to <i>Mariner Mars 1971</i> . Realignment of accelerometer sensitive axis. Minor changes in parameters
Reaction control system	Similar to <i>Mariner Mars 1969/1971</i>
Scan control electronics and logic	Similar to <i>Mariner Mars 1969/1971</i>
Antenna hinge control electronics and logic	New design

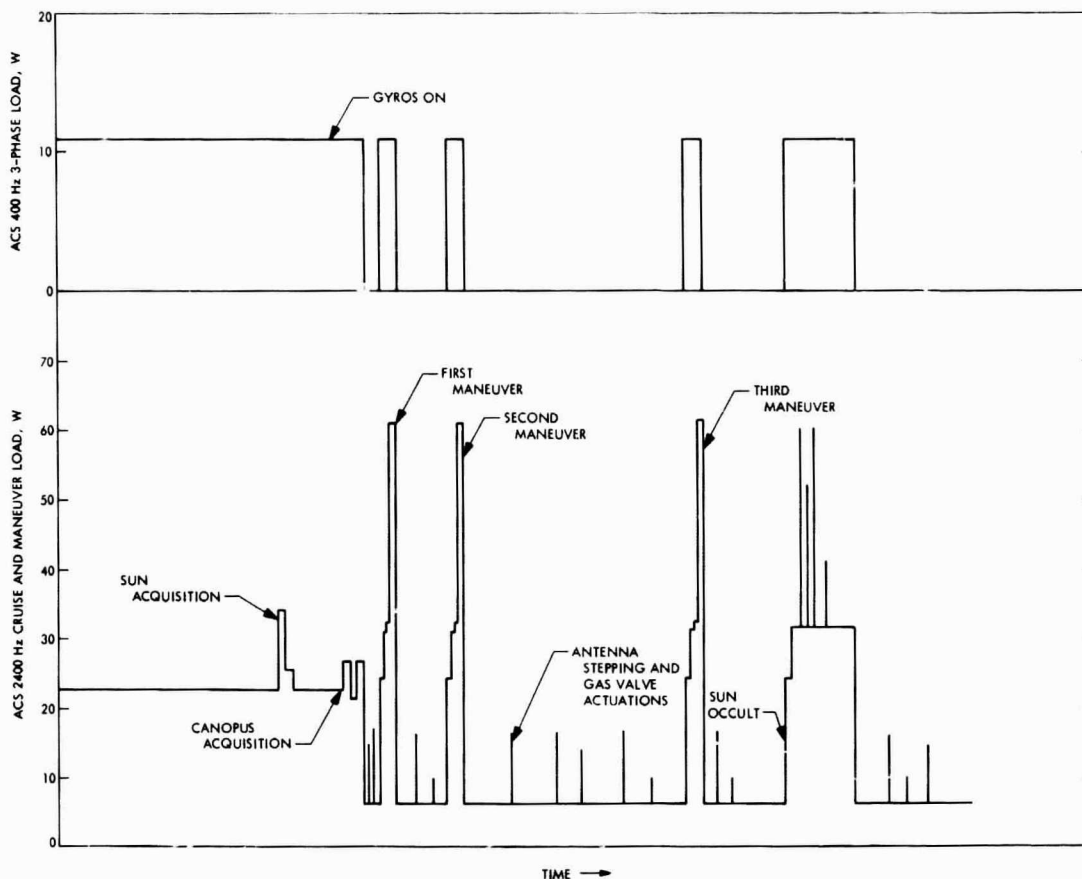


Fig. 71. ACS power profile

Table 21. Attitude control subsystem weight breakdown

Item	Weight, lb
+X, +Y gas system assembly	12
-X, -Y gas system assembly	12
Nitrogen gas	7
Antenna hinge actuator	3
Antenna hinge control electronics	2
Sensors (sun, Canopus, etc.)	10
Inertial reference unit	11
Midcourse propulsion bay	4
ACS electronics	8
Total:	69

the end of the roll turn and the start of the burn. This allows 1024 sec to evaluate the engineering data telemetered during the turns and, if necessary, to abort the maneuver.

A list of the sources of error considered, the estimated 3σ values of these errors, and the percentage of the square of the rms value of the pointing error contributed by each error are shown in Table 22. The estimated rms value of the pointing error is also included.

3. Antenna articulation subsystem. This section describes the subsystem used for controlled pointing of the high-gain antenna. The antenna pointing subsystem is based on a function describing the antenna's position in a single rotational degree of freedom. This angular

function of time is stored in the central computer, prior to launch, in the form of connected line segments and is subsequently used to update the antenna's pointing direction toward earth by means of a pulsed stepper motor. Pointing errors associated with a one degree-of-freedom system are evaluated in addition to the effects of spacecraft attitude errors, structural misalignments, and stored program approximations.

a. High-gain antenna articulation control subsystem.

Trajectory characteristics. A plot of earth's apparent position in a spacecraft-centered coordinate system is

given in Fig. 72 for the launch on October 21. It is apparent that the earth track is reasonably close to a planar curve. However, in examining the feasibility of using a single degree-of-freedom articulation system, the degree to which the earth track is nonplanar is critical. If the earth track cannot be closely approximated by a single-axis rotation within the pointing error requirements, the alternatives are a communication system redesign or a two degrees-of-freedom antenna mechanization.

Pointing errors for a one degree of freedom articulation system. The geometry involved in determining a best

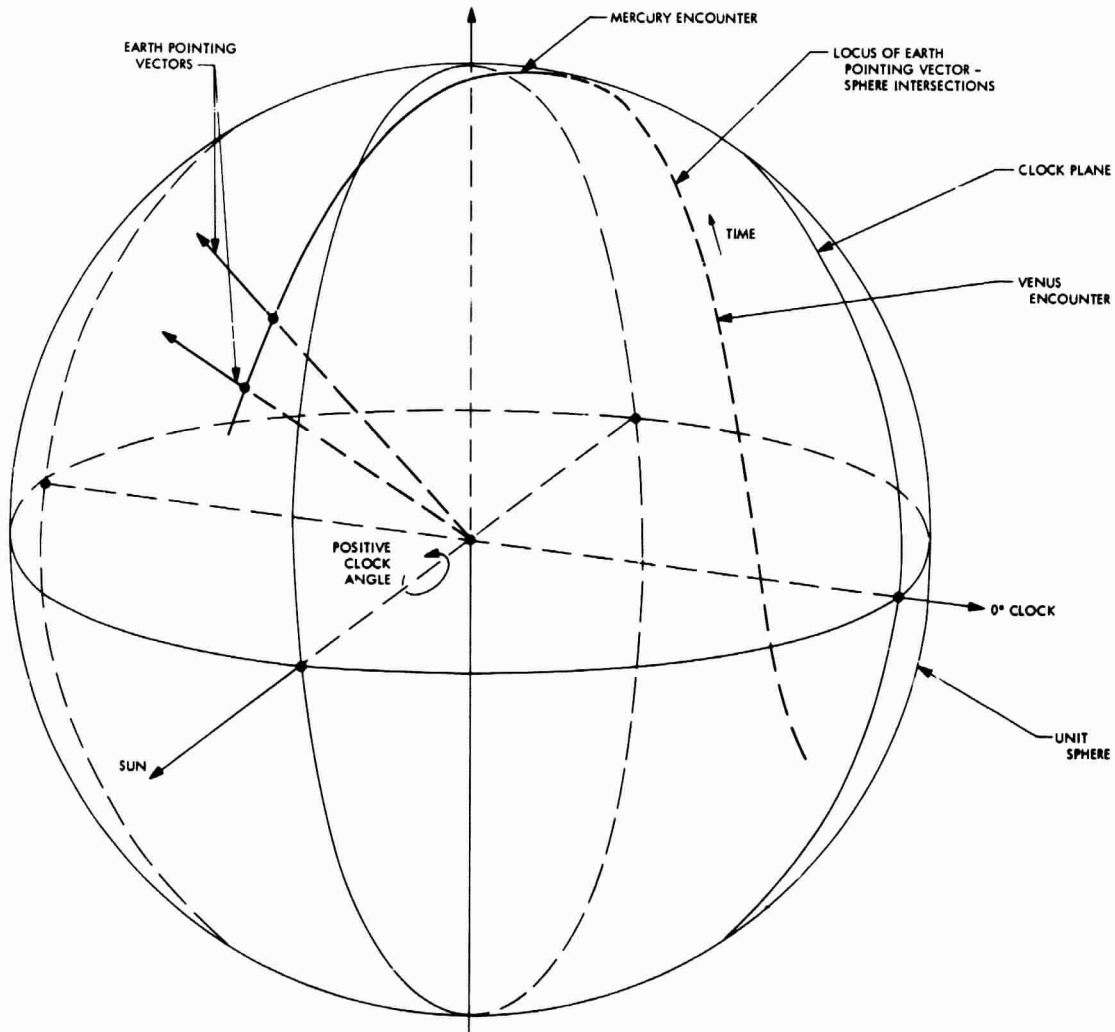


Fig. 72. Earth vector loci on spacecraft-centered sphere, October 21, 1973 launch

Table 22. Contributions to the maneuver pointing error^a

Error source	3 σ Value (per axis)	Percent variance contributed
Gyro and integrator drift	2.61 μ rad/sec	10.6
Gyro misalignment	5.25 mrad	30.3
Limit cycle (± 4.4 mrad)	7.62 mrad	27.7
Sun sensor misalignment and null offset	5.43 mrad	10.8
Canopus sensor misalignment and null offset	4.71 mrad	2.4
Switching amplifier null offset	1.71 mrad	5.3
Turn time resolution (± 0.5 sec)	0.867 sec	2.4
Turn rate calibration	3.3 μ rad/sec	0.9
Thrust vector misalignment	8.67 mrad	1.1
CG offset from the design thrust vector	3.144 mrad	8.5

^a Total rms value of the pointing error = 7.12 mrad.

location for a single axis of antenna rotation is illustrated in Fig. 73. Angles θ and ϕ uniquely locate the rotational or hinge axis of the antenna with respect to the spacecraft pitch, yaw, and roll axes X, Y, and Z. Later discussion will indicate the earth pointing errors to be expected when the spacecraft attitude is not perfect.

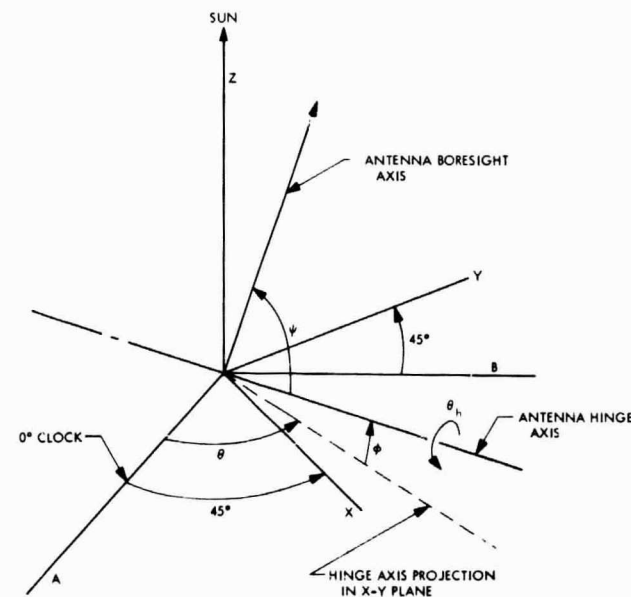


Fig. 73. Antenna hinge and boresight axis location in spacecraft coordinates

Additional freedom in directing the antenna boresight axis on an optimum path is obtained by varying ψ , the angle of the boresight axis cant to the hinge axis. Thus it is possible to obtain an antenna pointing vector track on the spacecraft-centered sphere (Fig. 72) which is not an arc of a great circle. However, θ , ϕ , and ψ are all absolutely fixed in flight, and only the hinge angle, θ_h , can be changed by preprogrammed commands from the CC&S and/or direct single step commands from earth. The design philosophy also assumes a single antenna orientation, θ , ϕ , and ψ , is acceptable for all launch days in the period from October 22 to November 15.

In addition to the pointing error due to out-of-plane movement of the earth track, sources of pointing errors are:

- (1) Spacecraft attitude misalignments
- (2) Spacecraft and antenna structural misalignments
- (3) Antenna control system hysteresis and nonlinearities
- (4) Pointing program approximations

The maximum (worst case) contribution to pointing error by the attitude control system is obtained by a vector summation of maximum pitch, yaw, and roll deviation, each 0.25 deg, which gives a total error of 0.43 deg. Structural misalignments are difficult to specify since they include the effects of thermal gradients over the spacecraft and antenna dish, antenna mounting errors (reflected by errors in θ , ϕ and ψ), and antenna electrical-to-mechanical boresight calibrations. However, these have been assumed to result in tolerances on the values of θ , ϕ , and ψ which are ± 0.25 , ± 0.25 , and ± 0.1 deg, respectively. Antenna actuator drive-train hysteresis and potentiometer nonlinearities have been added to the effects of an approximate, CC&S generated, antenna hinge angle program resulting in a maximum pointing error contribution of about 0.25 deg. This error is quite dependent on the out-of-plane errors at a particular point in the mission.

As a result of these uncertainties, a pointing error specification should include approximately a 1.0 deg margin over and above the purely geometrical errors resulting from earth position deviations out of a plane (as seen from the spacecraft). This is a conservative specification since the errors described are taken in a worst case sense.

Baseline design and resulting pointing errors. The choice of a single antenna-to-spacecraft orientation which meets the pointing error requirement for all launch days is of primary concern. Figure 74 illustrates the resulting pointing error for a launch October 21 using the baseline antenna position. This antenna hinge axis orientation was chosen to allow the cruise science data to be transmitted on the high-gain antenna as early as possible, as well as to provide high-rate telemetry (up to 5.1 kbits/sec) to Mercury encounter plus 20 days. The lower curve represents the least pointing error obtainable at each point in time, assuming a perfectly aligned antenna, no spacecraft attitude errors, and including the effects of trajectory geometry only. The upper curve describes the worst possible error when spacecraft attitude control deadzones (± 0.25 deg all axes) and antenna mounting tolerances ($\theta = 8.5 \pm 0.25$ deg, $\phi = 10.5$ deg ± 0.25 deg, $\psi = 77.5 \pm 0.1$ deg) are also included.

A plot of the ideal antenna hinge angle time function and its approximation by six connected, straight-line segments is shown in Fig. 75. The line segment type of approximation to the desired antenna rotation function is easily obtained and is readily mechanized in terms of on-board computer hardware and a stepper-motor drive mechanism. Although the function shown corresponds to an alternate antenna position ($\theta = -4.3$ deg, $\phi = 12.6$ deg, $\psi = 86.5$ deg) (Appendix E), it is almost identical to the function required for the baseline position; i.e., the same number of segments are required and only slight variations would occur.

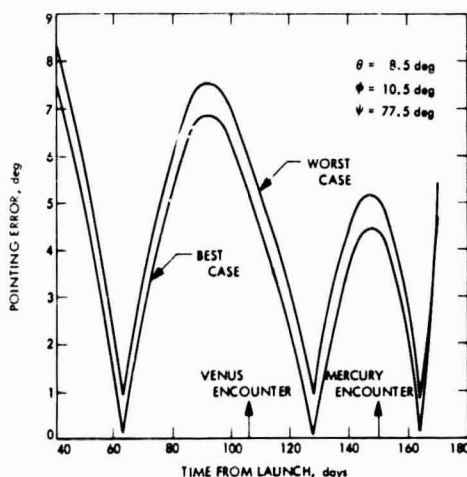


Fig. 74. Antenna pointing error versus time

Articulation control subsystem functional description. In summary, the antenna pointing control subsystem is a one degree-of-freedom mechanization capable of meeting pointing error requirements (section VII-F). The spacecraft antenna is rotated by a stepper motor and a reducing gear-train combination at a nominal step size of 0.1 deg along the programmed line segments. Maximum rate of change in the hinge angle is about 2.5 deg per day, resulting in a maximum stepping rate of about 1 step per hour.

A functional block diagram of the subsystem is shown in Fig. 76. The stepper motor is pulsed directly as long as the commanded position differs from the actual antenna position by more than a minimum resolution increment (0.1 deg, as an example). Both CC&S and ground backup commands are provided for stowing or deploying the antenna, starting the hinge angle program, and one-step incrementing of the hinge angle independent of the stored program.

H. Pyrotechnic Subsystem

1. General description. The pyrotechnic subsystem for the *Mariner Venus/Mercury 1973* spacecraft is based upon proven techniques and design philosophy employed in previous *Mariner* spacecraft subsystems. Improvements in circuitry and components that enhance reliability will be incorporated. The design is essentially that of the *Mariner 1969* subsystem, modified only to the extent required to accommodate the increased number of propulsion events and any added pyrotechnic functions.

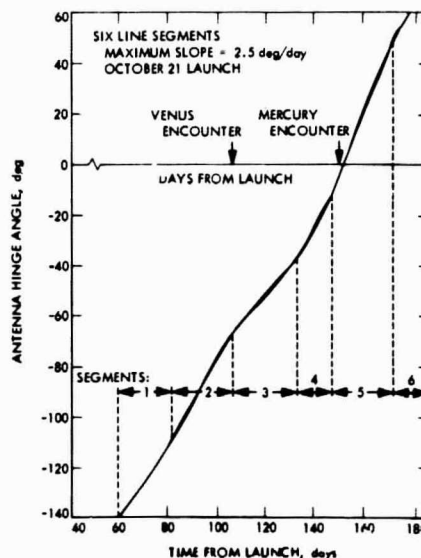


Fig. 75. Antenna hinge angle program

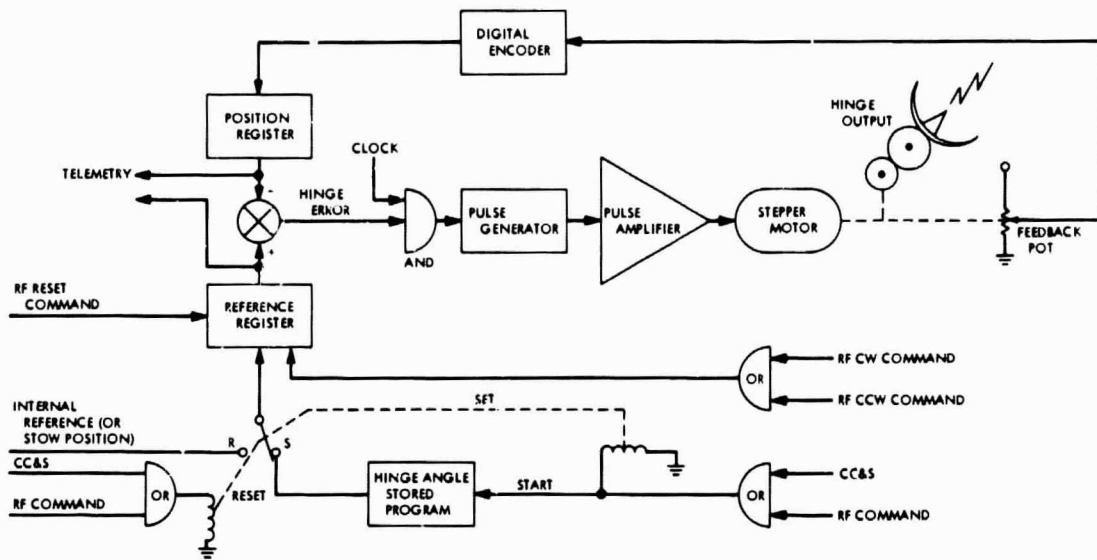


Fig. 76. High-gain antenna hinge control block diagram

2. **Functions.** The subsystem performs functions such as release of the *Centaur* spacecraft separation device; firing of squibs associated with the propulsion subsystem explosive valves; release of the science scan platform, solar panels, and antennas. Redundancy in critical functions is employed through the use of redundant commands, circuitry, squibs and devices. The subsystem block diagram with functions and interfacing subsystems is shown in Fig. 77.

3. **Subsystem elements.** Hardware elements included in the pyrotechnic subsystem are:

(1) Pyrotechnic switching unit (PSU), an electronic unit that contains an electroexplosive device firing

section and an instrumentation section. Capacitor banks are used to store squib firing energy; silicon controlled rectifiers (SCR) switch the energy upon command to squib loads. Unijunction transistors (UJT) are used to generate gate pulses for the SCRs. Advantages of such a circuit include lowered command current, assured triggering over a wide range of ambient temperatures, and reduction of false triggering due to noise. A schematic of a typical firing channel is shown in Fig. 78.

(2) Electroexplosive devices (EED) associated with the following functions:

- (a) Spacecraft/launch vehicle separation device
- (b) Release of low-gain antenna

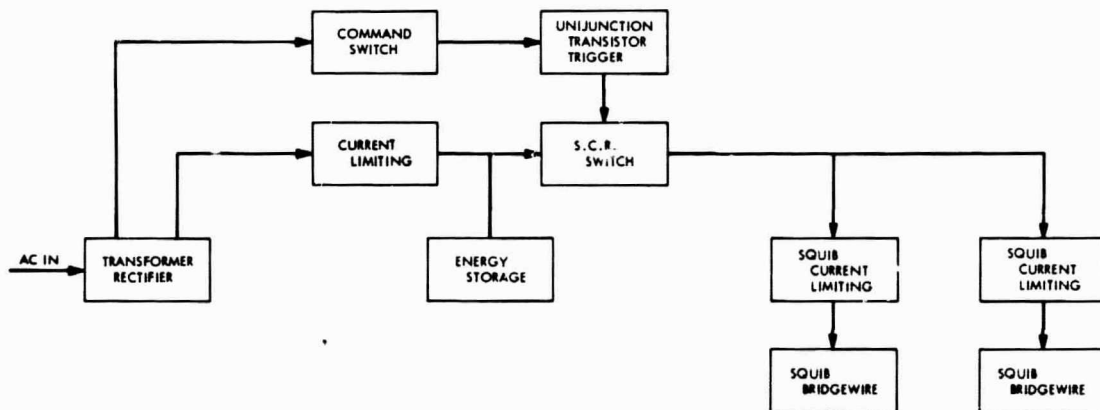


Fig. 77. Pyrotechnic subsystem block diagram

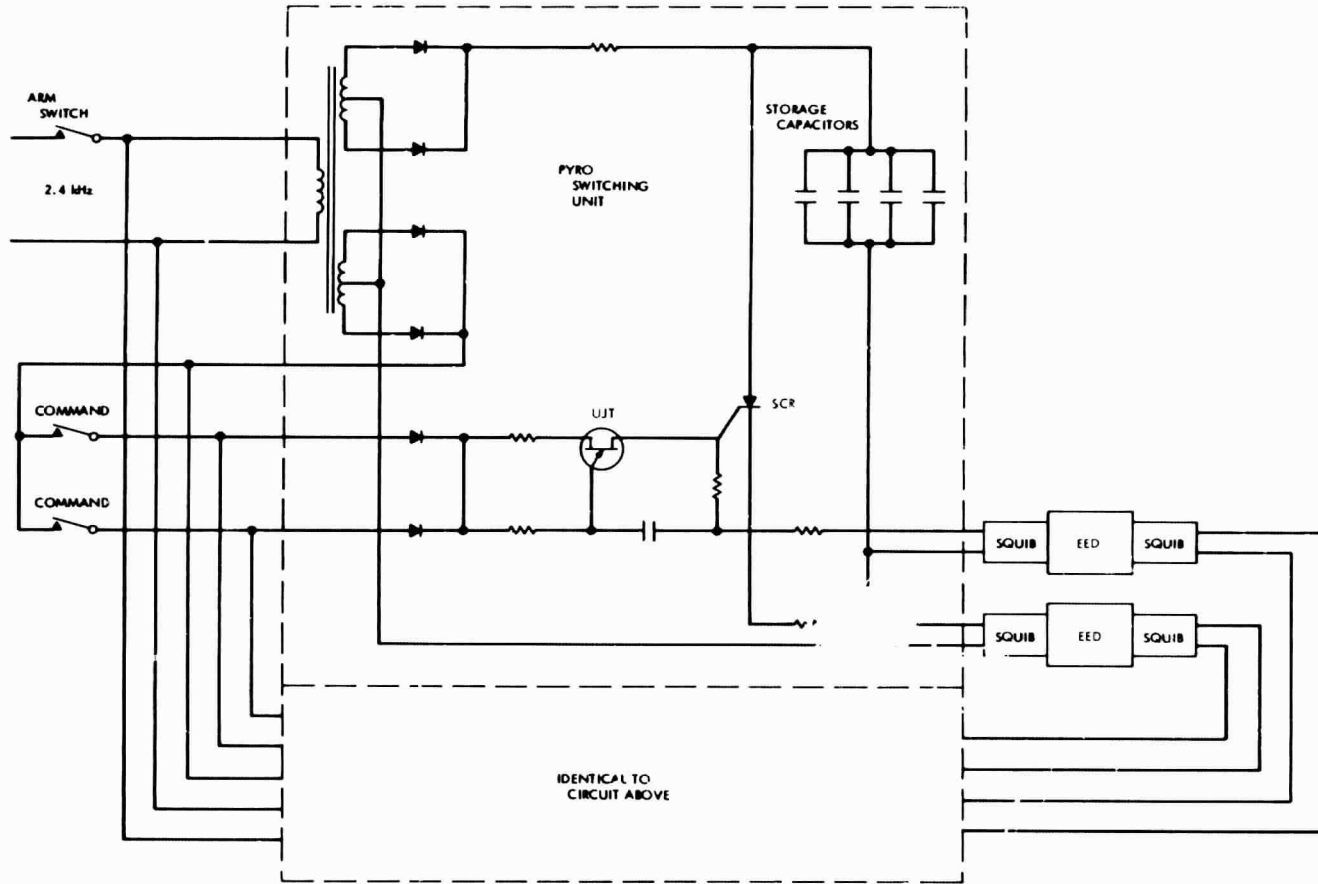


Fig. 78. Typical squib firing circuit for PSU

- (c) Release of science scan platform
- (d) Release of solar panels
- (e) Release of high-gain antenna
- (f) Propulsion and pressurant explosive valves capable of at least four maneuvers

4. Subsystem inputs.

a. *Power input.* The ac power supplied to the subsystem consists of a 2.4-kHz square wave having an amplitude of 50 Vrms $\pm 3\%$. The average power demand is 1 W. The peak power demand occurs with storage capacitor charging, and since capacitor charging current is limited, the demand never exceeds 10 W.

Multiple dc secondary voltages are provided for capacitor bank charging and pyrotechnic command excitation through transformation and rectification. The command excitation is distributed from the PSU to each subsystem required to provide pyrotechnic event commands.

Since the ac power to the subsystem is interrupted by the separation initiated timer or pyrotechnic arming switch, located on the spacecraft adjacent to the *Centaur* spacecraft adapter, the subsystem is not excited (armed) until separation has occurred.

b. *Command signal inputs.* PSU command signals consisting of a momentary switch closure of between 10 msec and 10 sec are supplied by:

- (1) Separation initiated timer (SIT)
- (2) Central computer and sequencer (CC&S)
- (3) Flight command subsystem (FCS)

5. *Subsystem outputs.* Outputs from the PCU are:

- (1) Command excitation power (not to exceed 35 Vdc) distributed to each spacecraft command source.
- (2) Electroexplosive device firing pulses having a minimum amplitude of 5 A for at least 10 msec delivered to each squib bridgewire upon receipt of the proper command. Multiple bridgewires are fired simultaneously in some pyrotechnic events, in which case, current limiting resistors in series with each bridgewire limit the peak current to the bridgewire, provide isolation in the event individual squib shorts, and provide a means for measurement of delivered squib current with ground operation support equipment (OSE).

(3) OSE instrumentation outputs consist of the aforementioned squib firing current outputs, capacitor bank voltages, and command excitation voltage. These outputs are made available at an easily accessible connector when the PSU is installed in the spacecraft.

(4) Telemetry outputs from the PSU to the flight telemetry subsystem are provided to obtain in-flight diagnostic information. The data consists of an event signal indicating the delivery of firing current to squib loads at each pyrotechnic firing.

6. *Electroexplosive devices.* Electroexplosive devices are used in the spacecraft to perform the functions previously listed. The EED consists of a squib and a mechanical device. The squib contains a pyrotechnic mixture that is electrically initiated. The resulting chemical reaction produces a rapid release of energy that is utilized by the mechanical device to perform its function, i.e., pull pins, open valves, release clamps, etc.

Characteristics of the electroexplosive devices used are:

- (1) Squibs have an electrical connector; the connector being an integral part of the squib body.
- (2) Squibs have redundant bridgewires.
- (3) Squibs used in the EED are hot-wire gas generating types that will withstand 1-A, 1-W, without firing. The squibs will be capable of withstanding a static discharge of 25 kV from a 500 pF source.
- (4) Devices are non-detonating, non-venting, non-rupturing, and provide positive gas containment.

7. *Subsystem weight.* Weight of the pyrotechnic subsystem will not exceed 10.0 lb.

8. *Safety considerations.* The design of the pyrotechnic subsystem will adhere to the requirements of the latest revision of the AFETRM 127-1, *Range Safety Manual*. The electromechanical pyrotechnic arming device, viz., separation initiated timer and pyrotechnic arming switch, contain fail-safe arming status indication circuitry. The indication circuit is routed via the spacecraft umbilical connector to allow monitoring of the status in the launch complex blockhouse.

It is a requirement that arming circuitry be physically and electrically isolated from command circuitry to ensure that no single or common failure mode will

simultaneously arm and command a hazardous pyrotechnic event.

I. Propulsion Subsystem

The function of the propulsion subsystem is to provide directed impulses required for in-transit trajectory corrections. The propulsion subsystem is comprised of a mechanically separable module containing all necessary components and fluids to provide these impulses on command.

1. Propulsion requirements and design constraints. Propulsion propellant requirements for the *Mariner Venus/Mercury 1973* baseline mission are determined by the total impulse which is dictated by the launch date, trajectory accuracy (including injection accuracy and bias), and spacecraft weight. With modification, the requirements established for *Mariner Venus/Mercury 1973* (section V-D) can be accomplished within the perfor-

mance capability of the *Mariner Mars 1969* propulsion subsystem, assuming:

Spacecraft weight	= 750 lb
Propellant weight	= 21.4 lb
Total subsystem weight	= 50.0 lb
Total midcourse correction ΔV	= 66.0 m/sec

The propulsion subsystem will have the capability of performing as many as four trajectory correction maneuvers during the mission lifetime. The accuracy with which these maneuvers can be performed is shown in Fig. 79. This figure is based on the use of a *Mariner Mars 1969* propulsion and flight control subsystem mechanization and can meet the present requirements. The use of the *Mariner Mars 1971* mechanization in which accelerometers instead of a timer are used for integration of ΔV will result in a reduction in the ΔV errors shown in Fig. 79.

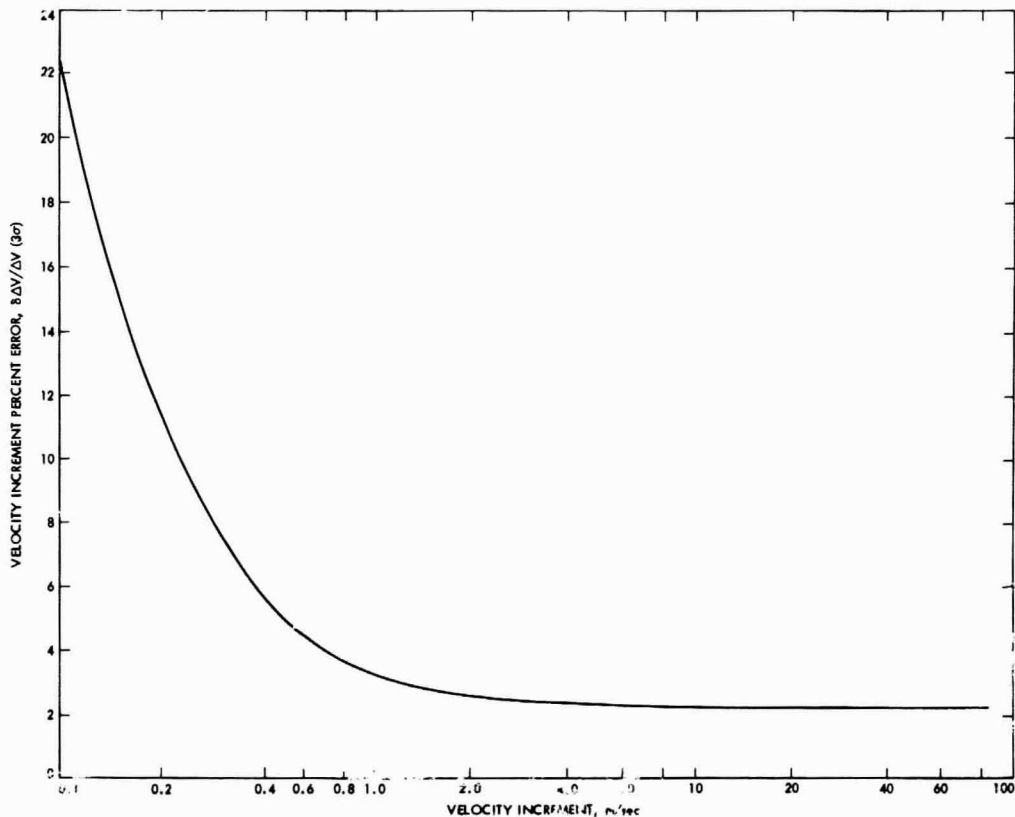


Fig. 79. Velocity increment percent error versus velocity increment for a 750-lb spacecraft

2. Subsystem description. The propulsion subsystem utilizes a liquid monopropellant, anhydrous hydrazine (N_2H_4), and develops a vacuum thrust of 50 lbf. The system is functionally a regulated gas-pressure-fed, constant-thrust rocket. The principal system components consist of a high-pressure gas reservoir, a pneumatic pressure regulator, a propellant tank and bladder, explosive valves for start and shut-off functions, and a rocket engine. The rocket engine contains a quantity of catalyst which accomplishes the spontaneous decomposition of the hydrazine. Four jet vanes are located at the exit plane of the nozzle and are used to provide spacecraft roll, yaw and pitch control during engine burn. A schematic of the system is depicted in Fig. 80.

The system concept, as developed in previous *Mariner* spacecraft and modified for the *Mariner Venus/Mercury* 1973 baseline mission, is predicated on the basis that it satisfy the long-term space-storage (approximately 180 days) and multiple start (maximum of four) requirements. Pressurization by gaseous nitrogen is used in lieu of gaseous helium; the latter being more prone to leakage. In a like manner, welded and brazed tubing and fittings are used wherever possible to minimize the number of potential leak sources. Multiple start capability is realized by the inclusion of ganged explosive valves with four parallel branches of normally closed (start)-normally open (shut-off) valve groups in the nitrogen and propellant circuits.

COMPONENT SUMMARY

No.	DESCRIPTION
1	ROCKET ENGINE
2	PROPELLANT ORIFICE
3	PROPELLANT INLET FILTER
4	PROPELLANT VALVE, START No. 1
5	PROPELLANT VALVE, START No. 2
6	PROPELLANT VALVE, START No. 3
7	PROPELLANT VALVE, START No. 4
8	PROPELLANT VALVE, SHUTOFF No. 1
9	PROPELLANT VALVE, SHUTOFF No. 2
10	PROPELLANT VALVE, SHUTOFF No. 3
11	PROPELLANT VALVE, SHUTOFF No. 4
12	FILL VALVE, PROPELLANT
13	PROPELLANT TANK
14	PROPELLANT BLADDER
15	PRESSURIZATION VALVE, NITROGEN
16	PRESSURE REGULATOR
17	NITROGEN FILTER
18	NITROGEN VALVE, START No. 1
19	NITROGEN VALVE, START No. 2
20	NITROGEN VALVE, START No. 3
21	NITROGEN VALVE, START No. 4
22	NITROGEN VALVE, SHUTOFF No. 1
23	NITROGEN VALVE, SHUTOFF No. 2
24	NITROGEN VALVE, SHUTOFF No. 3
25	NITROGEN VALVE, SHUTOFF No. 4
26	FILL VALVE, NITROGEN TANK
27	NITROGEN TANK

INSTRUMENTATION SUMMARY

PRESSURE TRANSDUCERS

P_1	NITROGEN TANK
P_2	PROPELLANT TANK
P_3	THRUST CHAMBER

TEMPERATURE TRANSDUCERS

T_1	PROPELLANT TANK
T_2	NITROGEN TANK

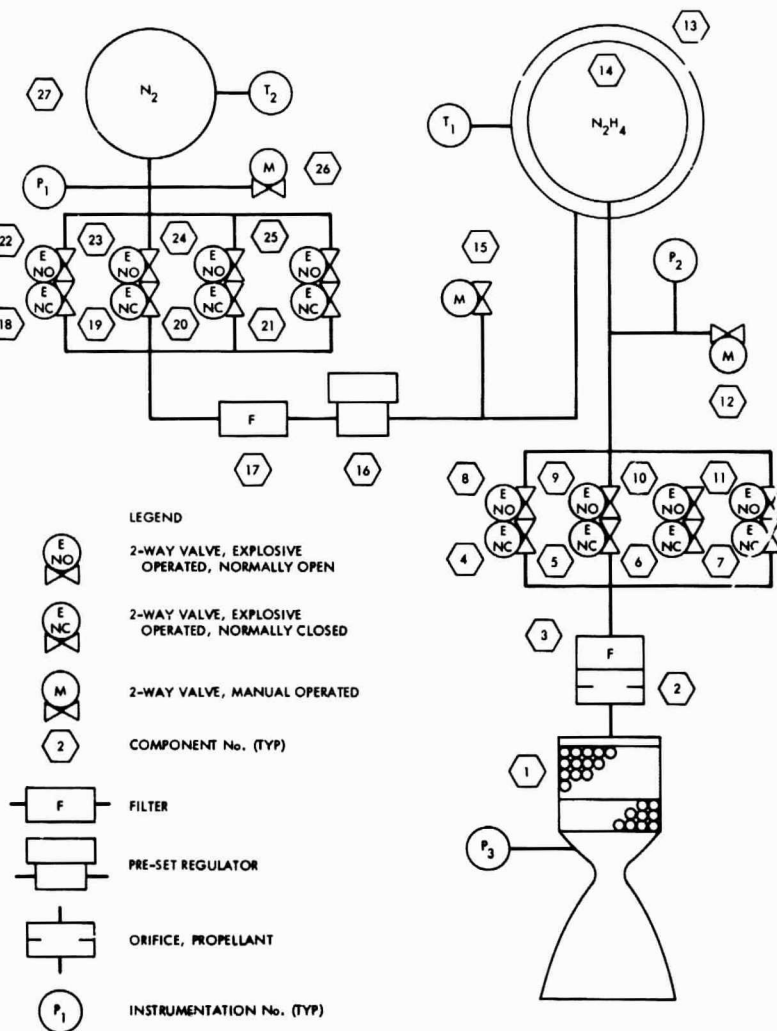


Fig. 80. Propulsion subsystem schematic

The firing of the propulsion subsystem is controlled by the CC&S. The pyrotechnic subsystem stores energy and provides the power switching for initiation of the explosive valves.

3. Modifications required for Mariner Venus/Mercury 1973. The performance required to accomplish the *Mariner Venus/Mercury 1973* baseline mission is within the capability of the *Mariner Mars 1969* propulsion subsystem. The existing tank capacity provides adequate propellant to meet the estimated three sigma trajectory corrections. The thrust level and multi-start characteristics of the rocket engine are consistent with the *Mariner Venus/Mercury 1973* needs.

Two aspects of the existing *Mariner Mars 1969* hardware require modifications based on the baseline mission requirements. The present propulsion subsystem provides the capability for only two trajectory correction maneuvers. In order to provide the capability for two additional maneuvers, the explosive valve assemblies for both the gaseous nitrogen and the monopropellant must be modified. The changes are considered to be minor.

As a consequence of the spacecraft's approach to Mercury, higher system temperatures are encountered than on previous *Mariner* missions. The increased temperatures accelerate the bladder-to-propellant reaction which results in decomposition of the hydrazine monopropellant. The present bladder material, a black butyl rubber, catalytically decomposes the hydrazine with the reaction rate strongly temperature dependent. A substitute bladder material, ethylene-propylene rubber, has undergone preliminary screening and appears to be compatible with hydrazine at elevated temperatures. The sample tests need verification utilizing a flight type configuration and pressures for long periods of time at elevated temperature.

J. Thermal Control Subsystem

1. Introduction. The *Mariner Venus/Mercury 1973* mission presents a different thermal environment from that presented to prior interplanetary spacecraft. The increased solar intensity (5.4 solar constants) during the Mercury post-encounter will result in higher equilibrium temperatures for any equipment that is exposed to direct solar radiation. The baseline spacecraft design is based on previous *Mariner* concepts with additional protection on the sunlit side. The internal temperature requirements of the spacecraft are assumed as 50°F to 90°F. External packages will need to be controlled individually to tem-

perature limits as dictated by each item of equipment. Some of the sunlit-side instruments probably will need to be redesigned to accommodate a wider temperature tolerance.

2. Baseline description. The baseline spacecraft has eight equipment mounting bays. All the bays are equipped with bimetallic controlled thermal louvers with the exception of bays II and IV. Bay II is insulated and penetrated only by the propulsion nozzle. Bay IV has no insulation in order to provide maximum heat rejection capability because of high power dissipation of the travelling wave tube (TWT).

The sunlit side of the spacecraft is protected by a high temperature insulation system. The insulation is made of multilayer metallized Kapton¹⁸ and attached to the spacecraft by a combination of Kapton tape and Vespel¹⁸ posts. The launch vehicle adapter penetrates the insulation through a self-closing cross slit so that after separation of the adapter, the spacecraft mounting feet will not be exposed to direct solar radiation. In addition, a sun shield is installed to protect the edges of the spacecraft. The shady side of the spacecraft is insulated with a multilayer metallized Mylar¹⁸ insulation system. There is a 1.2 ft² cutout in the insulation where a low-absorbing and high-emitting surface is exposed to space to provide heat dissipating capability for the spacecraft. This radiator could also transmit heat to the scan platform which will be insulated to the maximum extent possible and equipped with electrical heaters and a radiator, if necessary. The size of the heaters and radiator will be determined after the experiments are selected and the exact power dissipation is known. All externally mounted packages are individually controlled by selectively using electrical heaters and thermal control coatings.

For the solar panels, it may be necessary to increase the substrate thickness above the 5 mils (baseline weight is conservatively estimated with 20 mils) used in the *Mariner 1969/1971* design to provide a higher thermal conductivity in the case of macro-mosaic design (Appendix D). However, a final substrate thickness selection will depend on a trade-off between increased thermal conductivity and increased stresses in the solar cells and their protective cover glasses.

3. Functional description. During the prelaunch phase, the spacecraft will be provided with an air-conditioned environment and protected by a fairing during the

¹⁸Dupont trade name.

launch phase. During the early cruise phase, the temperature of the spacecraft will be maintained at approximately 50°F. This temperature is highly sensitive to the internal power dissipation of the various items of equipment.

Eight days after Venus encounter, the last nominal trajectory correction maneuver will be made. During this maneuver, the average spacecraft temperature will experience an average increase of up to 9°F because of solar radiation on parts of the spacecraft that are normally in the shade. Local temperature rises could be several times higher than the average value. However, an alternate maneuver turn sequence (Appendix C) would reduce the average temperature rise during the maneuver to a maximum of 2°F.

Near Mercury encounter the temperature of the spacecraft will reach its maximum value because of high solar radiation, which causes relatively high heat transmission into the spacecraft through the insulation, and because of high power generation internally.

4. Performance (parameters) assumptions.

- (1) The temperature T inside the spacecraft to be controlled: $50 \leq T \leq 90^\circ\text{F}$.
- (2) Louver performance capability q : (power radiated to space) 6.3 (closed) $\leq q \leq 47$ W (open) [$6.3 \leq q \leq 36$ W were assumed if the louver is located underneath a 284°F (140°C) solar panel] with 1.4 ft² effective louver area per bay.
- (3) All radiators coated to provide: α/ϵ (absorptivity/emissivity) = 0.2, and $\epsilon = 0.86$. (Figure 81 shows the heat dissipation capability of the louver system.)
- (4) Shady side insulation performance: $\epsilon_{eff} = 0.01$.
- (5) Sunlit side insulation performance: $\epsilon_{eff} = 0.01$, $\alpha/\epsilon = 0.6$.
- (6) Time of spacecraft "off the sun": as listed in section VIII-G-2.

Table 23 shows the heat balance of the spacecraft at earth and Mercury at zero cone angle (cruise attitude). The shady side radiator is sized by the internal power dissipation requirement at Mercury, which is assumed to be 304 W. The values given for earth result from the

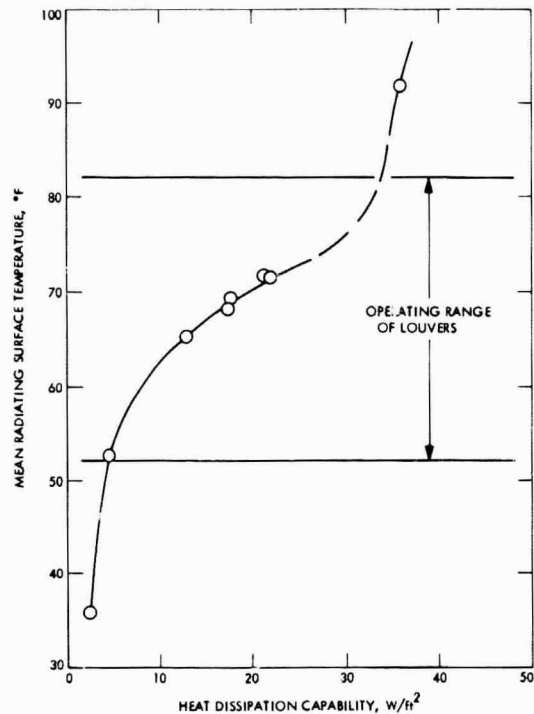


Fig. 81. Heat dissipation capability of louver system

thermal control design at Mercury. The internal power dissipated must fall within the thermal control range indicated.

The average temperature rise of the spacecraft during the last maneuver, which is at 2.18 solar constants, is

Table 23. Heat balance of Mariner Venus/Mercury 1973 spacecraft

	At earth, W	At Mercury, W
Louvers	38	240
Bare bay	59	85
Shady side insulation	4	9
Sunlit side insulation	-9	-78
Shady side radiator (1.2 ft ²)	40	48
	<u>132</u>	<u>304</u>
Thermal control modulation capability	373 to 132	304 to 63

shown in Table 24. The temperature rise is a function of heat absorbed (q) and time exposed to the sun. In computing the heating of the spacecraft during the maneuver, constant rate of pitch is assumed. Therefore the $q_{absorbed} = \alpha q_{max} \frac{2}{\pi} \int_0^\omega \cos x dx$ where ω is the pitch angle. After the pitch maneuver is completed, the spacecraft will remain in maximum q position for the remaining portion of the off-sun time.

Table 24. Average temperature rise during spacecraft maneuver at 2.18 solar constants

Position	Temperature rise
Sun at 90 deg	9°F (sun on bay IV)
Sun at 180 deg	5°F

During the sun occultation at Mercury, the average spacecraft bus temperature will not experience any change because of the short occultation duration and large spacecraft mass. However, any external objects normally facing the sun and not thermally connected to the bus will experience a severe thermal shock.

5. Thermal control problem areas. The following are problem areas that may constrain the performance of the spacecraft and influence detailed design:

(1) The thermal louver assembly used on previous *Mariner* spacecraft is not designed for operation in a high solar radiation environment. Previous tests have shown no damage or degradation of louver performance at one solar constant, but tests must be conducted at higher intensities to determine the survivability of the system during the last maneuver at greater than two

suns intensity. Some modifications in louver construction and/or surface finish may be required if problems are identified during these tests.

(2) The insulation cover sheet used on the sunlit side will be exposed to long-term, increasing solar radiation, reaching a maximum near the end of the mission. The solar ultraviolet and particulate radiation combined with the elevated temperature is expected to produce changes in the thermal properties of the insulation and may produce physical and dimensional changes as well. The magnitude of changes in thermal properties must be determined to establish the equilibrium temperature of the outer layer so that realistic boundary conditions can be simulated during subsystem and system tests. The nature and magnitude of possible physical and dimensional changes must be established so that design compensation can be provided and reliable performance assured. Table 25 shows the high temperature insulation test results as performed in a guarded hot plate calorimeter. The radiation-induced changes in the insulation cover sheet can also be expected to influence the solar pressure perturbation to spacecraft navigation in a similar but greater and less predictable manner to that observed on *Mariner V*. Radiation damage tests to support the thermal design will also provide information to reduce this uncertainty. Similarly, radiation tests on solar panel components (cover glasses and mirrors) will aid in prediction of solar pressure effects.

(3) All sun-facing equipment and sensors must be carefully examined individually to determine the effect of the high intensity solar radiation. In some instances, developmental tests must be performed in conjunction with analysis in order to achieve acceptable thermal design.

Table 25. High temperature insulation test results^a

Sample test No.	Brief description	Test temperature, °F		Heat flow, Btu/hr-ft ²	Thermal conductivity, K Btu hr-ft-°F	Effective emittance, ϵ_{eff}
		T_{hot}	T_{cold}			
3-6	20 layers gold on 1/2 mil Kapton	72	-50	0.325	8.9×10^{-5}	0.0037
3-7	20 layers gold on 1/2 mil Kapton	402	70	3.23	3.3×10^{-4}	0.0040
3-8	20 layers gold on 1/2 mil Kapton	712	70	12.4	6.4×10^{-4}	0.0040

^aTest data obtained from General Electric Company, Report DIN 69 SD 4236, Feb. 3, 1969.

Analysis of the plasma probe has shown that the interior of the Faraday cup should preferably be painted black, in which case the sensor will reach a maximum temperature of 285°F. If the interior is polished gold, the maximum temperature will reach 373°F. The cup shape is a critical factor in determining these temperatures. To hold the associated electronic equipment, located under the sensor, down to a maximum temperature of 170°F, the equipment must be located at least 4 in. away from the sensor and with minimum thermal coupling between them.

Analysis of the infrared radiometer has shown that if the sun-facing opening is no greater than 2.9 in.² and covered with a sun shield which can be removed during experimentation, and if the radiometer assembly is located immediately adjacent to the louver assembly and reasonably insulated away from any power generating equipment, the radiometer could be controlled within its temperature limits of -40 to 32°F. This instrument will reach a maximum temperature of 180°F during the post-Venus maneuver if the sun shines normal to the wide-open louver assembly.

K. Mechanical Devices

The devices used on the spacecraft are associated with latching, structural damping, and non-servo-controlled actuation. With the exception of the scan platform, its mounting and bearings, all the items in the devices subsystem are duplicates (or minor modifications) of *Mariner Mars 1971* hardware. The more important devices are described below.

1. Solar panel boost damper and deployment mechanism. Each of the four solar panels is laterally supported for launch by pairs of viscously damped struts attached to the panel tips. Each damper pair is attached to the panel through a pyrotechnic pinpuller at the interface between the dampers and a solar panel bracket. The opposite ends of the dampers attach to the adjacent panel through a bolted joint.

The solar panels are spring loaded to deploy upon actuation of the pinpullers located on the boost dampers. The spring force is sufficient to ensure proper deployment but will not cause overstressing of the panel when it is stopped in the deployed position. The spring force is supplied by a spirally wound clock spring located on one hinge of each panel. The deployment mechanism includes a viscous damper to regulate the rate of deployment.

2. Low-gain antenna dampers. The primary low-gain antenna is laterally supported by viscously damped struts. One end of each damper attaches to the antenna at approximately one-fourth its height above the octagon. The damper centerlines are approximately 90 deg from each other. The other end of each damper attaches to the basic spacecraft structure.

3. Scan platform. The planetary science scanning experiments are mounted on a platform at the edge of the octagon. The platform is a cantilevered structure supported by two bearings. The scan platform provides the instruments with cone-angle and clock-angle freedom. The scan ranges are ± 180 deg in cone and clock. The clock angle actuator is mounted on the octagon. The cone angle actuator is mounted on the scan platform. Scan control sensors may be mounted on the platform and aligned with various angular offsets to the platform reference planes if required.

4. Pyrotechnic arming switch (PAS). The PAS consists of a set of electrical switches mounted at the base of the octagon structure. The switches are actuated sequentially when the spacecraft separates from the spacecraft adapter.

5. Separation initiated timer (SIT). The SIT provides a means of time-delayed switching to back up the PAS and to provide other timed events. Spacecraft separation from the launch vehicle releases the SIT actuation plunger, initiating its sequencing function. This is accomplished by a spring-loaded, damped piston which actuates a bank of electrical switches.

6. Spacecraft separation mechanism. The spacecraft separation mechanism consists of four spring-loaded pistons mounted in the spacecraft adapter at alternate corners of the octagon and preloaded against pads on the octagon structure. These springs apply a small velocity to the spacecraft relative to the *Centaur* to accomplish separation upon V-band release.

7. Spacecraft V-band. The spacecraft V-band secures the spacecraft to the adapter by providing a radial force on eight shoes that mate the spacecraft and adapter feet in a V-shaped groove. V-band tension is controlled by turnbuckles in the band. The V-band is released by two pyrotechnic devices on opposite sides of the spacecraft. Either of the pyrotechnic devices is capable of releasing the spacecraft from the adapter. The V-band is restrained by springs and lanyards to the adapter to ensure unobstructed separation of the spacecraft and a minimum of post-separation free debris.

L. Data Storage Subsystem

The DSS is a modified *Mariner* Mars 1971 system using a digital tape recorder with associated record, playback, and control electronics. Figure 82 is a block diagram of the recorder. The storage capacity of the recorder is 1.8×10^8 bits. Four data tracks are used. Data are recorded at 175 kbits/sec, which is a modification of the *Mariner* Mars 1971 recording rate of 132.3 kbits/sec. Playback data rates are 16.2, 8.1, 4.05, 2.025 and 1.0125 kbits/sec.

Modification to the recorder logic has been considered for this baseline in order to permit a rewind feature to allow playback of the picture which has just been recorded. A second possible modification would permit the capability of recording backwards or of playback with the tape running backwards. This modification would increase flexibility in the record and playback capability, thus permitting more pictures to be taken during the encounter phase of the mission.

Doubling the capacity of the tape recorder by increasing the number of tracks from four to eight was considered but has not been included in the baseline system. This modification would approximately double the number of near-encounter pictures which could be obtained.

The DSS parameters are:

Weight: 20 lb (estimated)

Power requirements:

Ready mode: 18 W

Record mode: 22 W

Playback mode: 19 W

Search mode (fast forward): 21 W

M. Science Data Subsystem

The science data subsystem (SDS) is the data system of the science payload. The SDS controls and sequences science instruments; samples and converts the resulting data into digital form; accomplishes any necessary on-board processing; provides temporary (buffer) storage; and formats and routes the data to both the flight telemetry subsystem (FTS) and the data storage subsystem (DSS) for direct or delayed transmission to earth. The SDS exchanges commands with other subsystems aboard the spacecraft which pertain to the operation of the science payload.

The SDS produces three data streams. First, a data stream capability of up to 66% bits/sec (low-gain) or up to 166% bits/sec (high-gain) containing status, cruise science, and formatting data exists between the SDS and the flight telemetry subsystem. The high-gain mode will

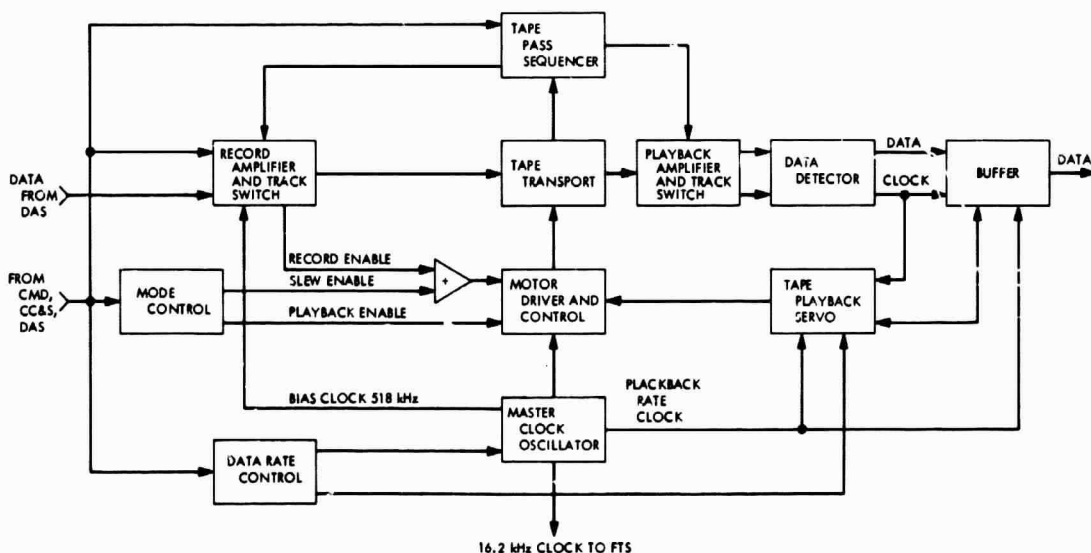


Fig. 82. Data storage system block diagram

exist after grayout. A second data stream containing high rate data (block code mode) will be provided to the FTS during encounter. This data will include portions of the TV pictures, non-TV science, and appropriate status and formatting data.

A third data stream of 175 kb/s containing TV video data, HRIR data, and fields and particles experiment data are fed to the data storage subsystem during both Venus and Mercury encounters. This data stream and the block code mode will occur at this time during the mission. The non-TV science data as well as status and formatting data is interleaved into each TV line at these times. The video output is nominally 7560 bits/line, the TV line formatting data is 74 bits/line and the non-TV science is approximately 88 bits/line (section VII-G).

Figure 83 shows a gross functional block diagram of the SDS. Table 26 indicates the *average* data output rates of the individual baseline experiments for various phases of the mission, from the low-gain cruise phase before acquisition of the high-gain antenna signal, through Venus and Mercury encounters to Mercury post-encounter. At launch +15 days, the 66% bits/sec cruise science capability of the telecommunication channel will be lost (a pre-high-gain cruise condition) until the high-gain antenna can be pointed at the earth. This break, indicated in Table 26 by an arrow, lasts for about 20 days for the reference trajectory. The *average* data rate for the TV decreases during the pre- and post-encounter modes due to the extended period between pictures. The actual time to record the pictures will remain the same.

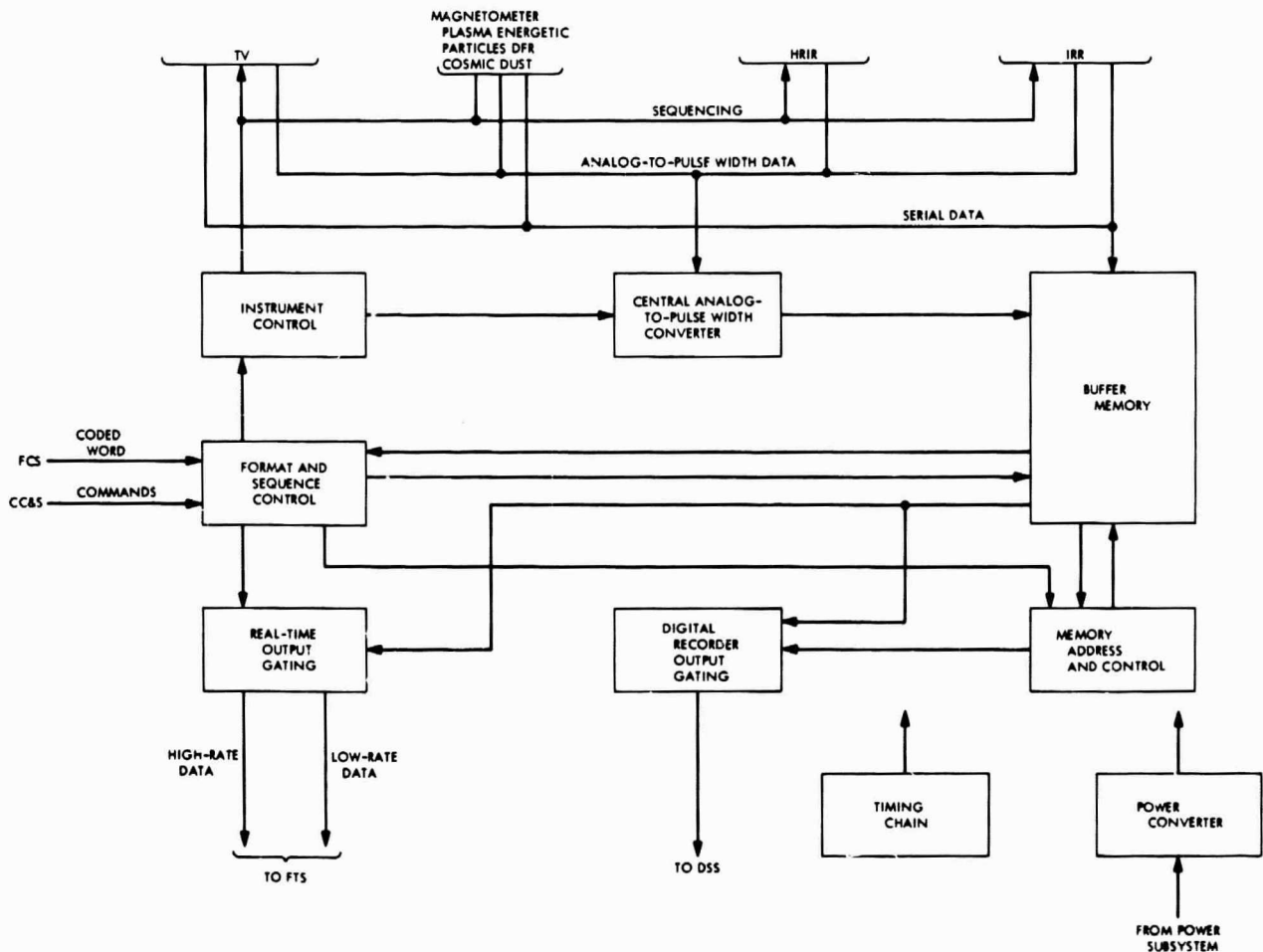


Fig. 83. Science data subsystem functional block diagram

Table 26. Science payload data summary

Subsystem	Average science data output, bits/sec								
	Grayout period ↓		Venus			Mercury			
	Low-gain cruise	High-gain cruise	Encounter	Post-encounter	Cruise	Pre-encounter	Sun occultation	Encounter	Post-encounter
TV	—	—	173.8 k ^a	≈ 20 k ^b	—	≈ 20 k ^b	—	173.8 k ^a	≈ 20 k ^b
HRIR	—	—	1000	—	—	—	—	1000	—
IRR	—	—	—	—	—	—	10	—	—
Magnetometers	5	40	40	40	40	40	40	40	40
Plasma probe	2	10	100	10	10	10	100	100	100
Energetic particles detector	≈ 1	3	3	3	3	3	3	3	3
DFR	< 10	10	10	10	10	10	10	10	10
Cosmic dust	< 1	1	1	1	1	1	1	1	1
SDS	11	11	11	11	11	11	11	11	11
Maximum Total	30	75	175 k	20 k	75	20 k	165	175 k	20 k
Transmission capability, (? channels), bits/sec	33 1/3	8 1/3 or 33 1/3	8 1/3 or 33 1/3		8 1/3 or 33 1/3	8 1/3 or 33 1/3 } engineering			
	66 2/3	166 2/3	166 2/3 or ≤ 16.2 k playback		166 2/3	166 2/3 real time (grayout) } science ≤ 8.1 k playback			
^a Effective record rate including formatting and contingency. ^b Average rate due to reduced number of pictures.									

A buffer memory similar to the 1971 design but with additional storage is used to store field and particle data during critical periods while the DSS is shut off. This occurs during earth occultation near the Venus and Mercury closest approach, during TV picture erase periods if the same camera is used repeatedly, and during the playback mode, if desired. The expected fields and particles data rate during these periods is approximately 166 bits/sec. The memory will contain a stored library of fixed formats as well as reprogrammable formats to accommodate different mission phases and contingencies. Coded commands received by the SDS to be used for controlling formats and sequencing will be routed to the buffer memory for storage and processing.

The volume required for the SDS will be approximately 600 in.³. The power requirement is about 20 W, and the weight is approximately 25 lb.

N. Science Instrument Subsystems

The representative science payload was chosen for the baseline design to provide data requirements, power requirements, and some of the salient mechanical interfaces. Instrument descriptions do not include specific implementations, with the exception of the television experiment. The instruments described here are characterized by applications in previous space missions and, therefore, can be related to qualified power, weight, and data rate requirements.

The television instrument description is more extensive than that for the other instruments because it has the largest impact on the mission and generates the major portion of the returned data.

The payload composition is consistent with the assumed importance of surface imaging data and data on the thermal properties of Mercury. A list of the payload

subsystems appears below with the assumed weight, power, and maximum data rate output:

	Weight, lb	Power, W	Maximum data rate, bits/sec
Television (TV)	49	38 ^a	175 k
High resolution infrared radiometer (HRIR)	11.3	5	1000
Infrared radiometer (IRR)	5	2.5	10
Magnetometers	6.5	5	40
Plasma probe	7	6.5	100
Energetic particle detector	3	1	3
Dual-frequency receiver (DFR)	5	2.5	10
Cosmic dust detector	2.5	3	1
SDS	25	20	11 ^b
Total	114.3	83	
^a Including 6 W for heaters ^b "Housekeeping"			

1. Television

a. *Introduction.* The baseline mission requirements for photo-imaging at the two planets are met by a television/tape recorder system optimized for a Mercury dark-side encounter. The requirements for Venus photo-imaging considered here are sufficiently compatible with those of Mercury, to be accommodated with the basic Mercury design. The basic design uses a modified *Mariner* Mars 1971 television subsystem (TVS) consisting of one wide-angle TV camera, one narrow-angle TV camera, a set of camera electronics, and one digital tape recorder. The modifications of the *Mariner* Mars 1971 TVS are (1) new lenses, (2) reduced read and erase times with higher data rates and (3) elimination of variable filtering.

b. *TVS design considerations.* The design of the television experiment is based on the following mission considerations:

(1) Spacecraft engineering constraints

- (2) Science objectives
- (3) Planetary photometric functions
- (4) Spacecraft trajectory

The spacecraft engineering constraints dictate that the camera system be limited to the same general size, shape and weight as the *Mariner* Mars 1971 TVS, which has the following characteristics. The telephoto camera is 32 in. long, with a diameter of 10 in. The total weight is 49 lb, and the total power consumption is 38 W including temperature control. The baseline tape recorder used with the TVS is a *Mariner* Mars 1971 recorder with the record data rate increased from 132.3 to 175 bits/sec. The capacity is unchanged at a nominal 1.8×10^6 bits.

The science objectives of the mission are discussed in section IV. The Mercury objectives relevant to the TVS are radii and shape determination, surface morphology and composition, and atmospheric density and composition. The Venus objective relevant to the TVS is the distribution and composition of the clouds.

The two principal photometric design considerations are brightness and required spectral response. Both are compatible with *Mariner* Mars 1971 TVS technology. The brightness of Mercury is 10 times that of Mars, and the brightness of Venus is 16 times that of Mars. Surface feature imaging of Mercury may be done anywhere in a broad spectral band since the albedo of the planet displays only small variations from near-IR (0.35μ) to near-UV (0.9μ). Imaging of large area cloud features of Venus must be done in the near-UV/blue since Venus does not display earth visible features at wavelengths longer than 0.45μ .

Principal design aspects of the spacecraft trajectory are the approach and smear velocities, the encounter altitude, and the resultant photometry of the flyby geometry. The encounter velocities are 8.3 km/sec at Venus and 15.1 km/sec at Mercury, compared to 7.5 km/sec for the *Mariner* Mars 1969 flyby. Nominal values for encounter altitudes are 2500 km at Mercury and 5000 km at Venus, compared with 3000 km for *Mariner* Mars 1969.

c. *Television subsystem.* The television subsystem consists of two camera head assemblies (identical except for optics and filters) mounted on the scan platform, and a set of electronic subassemblies mounted in the space-

craft electronic bays as characterized in Table 27. The wide angle A camera uses a lens with a focal length of 150 mm, and a focal ratio of $f/2.0$. A fixed, narrow-band, optical filter, limits spectral response to $0.30\text{--}0.35\ \mu$. The narrow-angle B camera uses a lens with a focal length of 750 mm, and a focal ratio of $f/5.6$. A fixed UV/blue attenuation filter results in overall filter/vidicon response in the visible range from 0.48 to $0.62\ \mu$. Each camera has a mechanical shutter and a 1-in. slow scan vidicon with a format size of 9.6 mm by 12.5 mm. The lens apertures are specified for a Mercury exposure resulting in a maximum smear of one TV scanning line. Venus smear is less than Mercury because of greater encounter distance, and lower encounter velocity.

Table 27. Baseline TVS characteristics

	Camera A	Camera B
Absolute photometric accuracy	15%	15%
Relative photometric accuracy	3%	3%
Spectral response with filter	$0.30\text{--}0.35\ \mu$	$0.48\text{--}0.62\ \mu$
Sensor	Slow scan vidicon	Slow scan vidicon
Focal length	150 mm	750 mm
Focal ratio	$f/2.0$	$f/5.6$
Field of view	$3^\circ 40' \times 4^\circ 50'$	$44' \times 58'$
Image size	$9.6\ \text{mm} \times 12.5\ \text{mm}$	$9.6\ \text{mm} \times 12.5\ \text{mm}$
Pixels per frame	704×945	704×945
Video quantization	8 bits	8 bits
Bits per frame	5.3×10^6 bits	5.3×10^6 bits
Exposure time, nominal	20 msec	4 msec
Smear, maximum	1 pixel	1 pixel
Record data rate, maximum	175 kbits/sec	175 kbits/sec
Frame read time	32 sec	32 sec
Erase time	10 sec	10 sec
Residual signal (nominal)	3%	3%
Size	$12'' \times 5'' \times 4''$	$22'' \times 6'' \times 6''$
Weight	32 lb on scan platform, 17 lb on bus	
Power	38-W (avg) encounter total (including 6 W of continuous temperature control power)	
Basis	Mariner Mars 1971 Television	

The wide-angle camera is designed for near-encounter, large area mapping, and for spectrally dependent measurements. It has a narrow, near-UV response in order to do Rayleigh scattering atmospheric limit studies of Mercury. The threshold of atmospheric limit detection is expected to be less than 0.2 mb. The UV spectral response does not interfere with Mercury topographic mapping, since Mercury shows little albedo variation over a wide range of wavelengths. At Venus, the wide-angle camera will be used for cloud pattern photographs. The UV response is mandatory since Venus shows little detail at wavelengths longer than $0.45\ \mu$.

The narrow-angle camera is designed for the best encounter resolution consistent with adequate far-encounter coverage. The resultant best resolution at Mercury is 55 m per TV scanning line, with a narrow-angle sequence lasting approximately 14 days. At Venus, the narrow-angle camera will be used for limb studies, for oblique-angle photographs of the upper atmosphere's cloud structure, and for phase function studies.

d. Mercury sequence. The baseline Mercury TVS encounter sequence of events is outlined in Table 28. The sequence divides into the five main operational modes of far-encounter, pre-encounter, encounter, post-encounter, and another far-encounter, spanning 14 days, and covering optical resolutions from 500 to 0.16 km. The sequence is based on a data transmission rate of 8.1 kbits/sec, and a total tape recorder storage capacity of 1.8×10^8 digital bits. It is assumed that there is no interruption of TV data recording and transmission for other instruments, except as provided by line interleaving.

The far-encounter mode starts at event 53 (section VII-C) at $E_M - 7$ days, when resolution is 500 km per optical line pair. At this time seven narrow-angle (B) and one wide-angle (A) camera frames are recorded, completing one pass of the length of the magnetic tape. Transmission is done after all eight frames are recorded. The multiple B frames provide for filling in any data dropouts, and for averaging frames for improved signal-to-noise ratio. The single A frame is recorded as engineering verification of operation, and for characterization of the A camera. The sequence of eight frames is repeated each time resolution changes by a factor of approximately two. This occurs at encounter $E_M - 7, 4, 2, 1, \frac{1}{2}$ days, for a total of five cycles.

When the field of view of the B camera is just filled, at $E_M - 6.9$ hr, the pre-encounter mode 1 is initiated (event 60). The system is operated continuously with sequential

Table 28. Mercury TVS baseline encounter sequence

Initial spacecraft event ^a	TVS operational mode	Time	Number of pictures	B camera initial optical resolution, km	B camera initial field (long side), km	Percent illuminated
53	For encounter	$E_M - 7$ days	40	500	1.8 × 10 ⁴	22
60	Pre-encounter 1	$E_M - 6.9$ hr	27	19	6400	22
63	Pre-encounter 2	$E_M - 1$ hr, 29 min	5	3.7	1200	20
70	Encounter	$E_M + 0$ hr, 3 min	32	0.1	50	41
73	Post-encounter 1	$E_M + 0.3$ hr	4	1.8	580	72
76	Post-encounter 2	$E_M + 2.0$ hr	3	5.9	1900	75
80	Far encounter	$E_M + 12$ hr	40	30.8	10 ⁴	75

^aThe spacecraft event numbers are from the sequence of events of section VII-C.

recording and transmission of one B frame each cycle. A total of 27 B frames is taken.

When there is just sufficient time to record and transmit six pictures before encounter, pre-encounter mode 2 is initiated at $E_M - 1$ hr, 29 min (event 63). Any mix of A and B frames can be taken, with one possible combination being five B frames covering most of the extent of the terminator, and one overall A frame.

The encounter mode starts at $E_M + 3$ min when 41% of the planet is illuminated and when the scan platform is at its limits of travel relative to the sun. The initial optical resolution is 160 m and the tape recorder is empty. Thirty-two frames (one full tape recorder load) are taken sequentially in the minimum possible time. The interval between frames is 32 sec for alternate A and B frames, and 42 sec for sequential A or B frames. Any programmed sequence of A and B frames can be taken. The coordinates of each successive frame can be set to arbitrary values by a preset program.

Following the encounter mode, two post-encounter modes are engaged starting at $E_M + 0.3$ hr (event 73), following the end of earth occultation, and filling of the tape recorder. In post-encounter mode 1, two frames are transmitted and one B frame is recorded. Initial B frame optical resolution is 1.8 km. The cycle is repeated immediately for a total of four times.

At $E_M + 2$ hr, post-encounter mode 2 commences when the change in resolution from between the preceding mode's cycle has dropped approximately 20%. The timing now is lengthened so that the initial change in

resolution between cycles is about 80%. The initial resolution is 5.9 km at event 76. Eight frames are transmitted and one is recorded for a total of three cycles. The tape recorder is just emptied.

When the B field of view is just filled by the planet, the second far-encounter mode is started at event 80, $E_M + 12$ hr. This mode follows the same sequence of operations (but reversed) as the initial far-encounter mode. After five cycles, when the B resolution has fallen to 500 km, the TVS operation is terminated.

e. Venus sequence. The Venus TVS sequence starts at encounter, without pre-encounter operation, principally because of the dark-side approach. After 32 frames are recorded, a playback/record mode is engaged and continued until the recorder is emptied at $E_V + 7$ to 8 hr. Picture taking is then continued an additional 8 hr before termination of the sequence. The exact timing of operation, and the sequencing of A and B frames will remain open until the Venus television mission has evolved into a more definitive form.

2. High resolution IR radiometer (HRIR). The purpose of the HRIR is to sample thermal radiation in selected wavelength bands in the general region of 1–5 μ to determine temperature and emissivity of a surface element of Mercury subtending an angle on the order of 0.5×0.5 deg. The instrument is bore sighted with the television subsystem, and is mounted on the scan platform.

3. Infrared radiometer (IRR). The IRR is used to determine the temperature on the dark side of Mercury, and is uncovered only during or near solar occultation. It

detects energy in the region of 8 to 50 μ . This instrument is body-mounted on the sun side of the spacecraft and looks toward the sun.

4. Magnetometer. The magnetometer measures magnetic fields near Mercury and Venus and in interplanetary space and has a multi-directional sensing capability. Quasi stationary magnetic fields as well as higher frequency fluctuations between 1 and 1000 Hz will be measured. The baseline magnetometer used here is a combination of a low field vector helium magnetometer and a tri-axial search coil magnetometer used with a spectrum analyzer.

5. Plasma probe. The plasma probe is postulated here in conjunction with the magnetometer to investigate the configuration and strength of the plasma bow shock produced by the interaction of the solar wind with the planet Mercury, and to study the magnetic and plasma phenomena inside the shock. The pertinent parameters of the plasma are the flux, energy spectrum, and flow direction with a time resolution that is limited only by the data rate available. A multigrad ac modulated multiple-collector Faraday cup is assumed as the baseline configuration. The energy spectrum from approximately 6 to 4000 eV will be covered. Incident fluxes in the range of 10^{10} to 10^{14} ions/cm² sec for each of 77 energy windows can be detected. Investigations of the interplanetary plasma and solar wind interaction with Venus are secondary objectives. The instrument is to be mounted on the sun side of the spacecraft with a look direction toward the sun.

6. Energetic particle detector. One major objective of the energetic particle detector is to measure the energetic electron and proton fluxes associated with Mercury. This includes a search for low energy shock-accelerated

electrons and electron fluxes in a weak magnetospheric tail. Observations are desired on the distribution of fluxes of solar protons and alpha particles as a function of spacecraft position relative to the planet and the interplanetary magnetic field direction. Measurements near Venus and in interplanetary space are secondary objectives. The energy measurements extend from several hundred keV to more than 50 MeV for nuclei and from 200 keV to more than 10 MeV for electrons. The proposed configuration is a multi-element, all silicon, solid state charged particle telescope with anticoincidence protection. The field of view for this instrument would probably be approximately normal to the spacecraft-sun line.

7. Dual-frequency receiver (DFR). This instrument will measure the integrated charge in a column between earth and the spacecraft by utilizing the dispersion by the various layers of charged particles of the radiation received from a transmitter on earth radiating to the spacecraft at several frequencies.

Frequencies in the neighborhood of 49.8, 423.3, and 1296 MHz, successively related by a factor 17:2 in this case, are heterodyned in the same IF amplifier strip, and the relative phase changes, amplitude changes, and frequency differences between them as a function of time are telemetered with other science data. Measurements on interplanetary plasma layers as well as the Mercury ionospheric charge are obtained by an earth-occluding flyby of Mercury.

8. Cosmic dust detector. A simple cosmic dust detector is postulated to measure the momentum and hemisphere of arrival of micrometeorites with components of momentum perpendicular to an impact plate greater than approximately 10^{-4} dyne-sec, the impact plate having an area in the neighborhood of 1 ft².

Appendix A

1970–1980 Mercury Opportunities (Direct and Venus Swingby)

The planets of the solar system are approximately in coplanar orbits. Therefore, mission opportunities occur once each synodic period. (The synodic period is the average time required for the difference in heliocentric longitude between two planets to go through 360°.) The earth–Venus synodic period is 583.92 days and the earth–Mercury synodic period is 115.88 days.

The beginning of each synodic period occurs at a different place in the orbits of earth and the target planet. Therefore, since the orbits are non-coplanar and each is non-circular, the geometry of each successive synodic period does not repeat exactly, and each opportunity has different trajectory characteristics. The large eccentricity of Mercury's orbit, for example, causes only one of the three opportunities per year to be attractive.

In order for trajectory characteristics to repeat themselves nearly exactly, the positions of earth and the target planet in their orbits must repeat at the same instant. In other words, an integral number of planet orbits N is equal to an integral number of earth orbits Y . Note that an earth orbit is a year. Table A-1 lists values of N for Venus and Mercury for which this equality is approximately true.

Values are shown in the table for cases where Y is different from an integer by less than 0.1. The table shows that 13 Venus orbits are very nearly equal to 8 yr, which accounts for the accurate repeat of earth–Venus trajectories every 8 yr. Also, 54 Mercury orbits are very nearly equal to 13 yr, which indicates that earth–Mercury trajectories repeat every 13 yr. Unfortunately, accurate earth–Venus repeats do not coincide with accurate earth–Mercury repeats. Therefore, earth–Venus–Mercury (EVM) missions do not repeat very accurately in a conveniently small number of years. Approximate EVM repeats occur every 8 and 13 yr. These repeats are not accurate enough to produce similar trajectory characteristics, which can be seen from differences in the 1970, 1978, and 1983 EVM opportunities. Direct missions to Mercury occur about three times per year, only one of which has launch energies as low as 50 km²/sec². The low energy trajectories all have Mercury arrival near aphelion, which is

70 × 10⁶ km from the sun as opposed to perihelion, which is 46 × 10⁶ km from the sun. Because of the 13-yr repeat of Mercury trajectories, Ref. 21 can be used to convert data for 1964–1976 to that for 1977–1989, etc.

The combined geometry for Venus/Mercury swingby missions repeats approximately every 8 yr, and to a better approximation every 32, 40, 72, 80, and 104 yr. (This results from multiples of the very exact 8-yr earth–Venus cycle.) The rapid motion and high eccentricity of Mercury in its orbit require a very precise repeat of planet configuration to duplicate mission parameters.

Reference 22 identifies Venus/Mercury missions in the 1970s. The years 1970 and 1973 provide good ballistic opportunities at low launch energies. Wallace has shown (Ref. 23) that a powered flyby is possible in 1975. The ballistic 1976 opportunity (Ref. 24) requires fairly high launch energies. Reference 25 gives data on direct and swingby missions from 1980–1999.

Tables A-2 and A-3 give a summary of mission characteristics in the 1970s. From these and other data in the references, the following comparison can be made:

<i>Direct Mercury</i>	
Advantages	Disadvantages
Shorter flight times Frequent launch opportunities Possible to reduce Mercury arrival velocity slightly in some cases	High launch energies, which implies larger launch vehicle

<i>Venus/Mercury</i>	
Advantages	Disadvantages
Low launch energies, small launch vehicle Opportunity for Venus science	More complex guidance Infrequent launch opportunities

Table A-1. Commensurate periods for earth, Venus, and Mercury

N Venus orbits = Y years		N Venus orbits = Y years	
N	Y	N	Y
5	3.076	4	0.963
8	4.922	8	1.927
13	7.998	17	4.094
18	11.074	21	5.058
21	12.919	25	6.021
26	15.995	29	6.985
31	19.072	33	7.948
		37	8.911
		46	11.079
		50	12.042
		54	13.006
		58	13.969
		75	18.064
		79	19.027
		83	19.991

Table A-2. Low-energy direct Mercury missions

Launch date	Launch energy, C_3 , km^2/sec^2	Flight time, days	Remarks
2/22/70	64.4	94	Minimum energy type I ^a
2/1/71	56.2	96	Minimum energy type I
1/13/72	49.7	98	Minimum energy type I
12/22/72	45.1	102	Minimum energy type I
12/3/73	42.3	105	Minimum energy type I
11/16/74 ^b	41.2	108	Minimum energy type I
11/13/75	55.5	97	Minimum energy type I
2/11/77	59.3	95	Minimum energy type I inferred from 1964 values
12/31/78	46.7	101	Minimum energy type I inferred from 1965 values
12/11/79	43.4	104	Minimum energy type I inferred from 1966 values
^a Type I trajectories have transfer angles less than 180 deg ^b A 15-day launch period gives the following range of parameters for this opportunity: 11/16-12/1/74 44.2 99-114 15-day launch period inferred from 1967 values. Type I; arrival speed 14.2-15.6 km/sec			

Table A-3. Venus/Mercury Missions

Launch date	Launch energy, C_3 , km^2/sec^2	Flight time, days	Remarks
7/28-8/27/70	14.0	158-182	30-day launch period. Ballistic flyby. Lowest energy in 70's. Arrival speed 11.7-13.1 km/sec
10/22 11/15/73	20.5	127-151	Current study design
6/12-7/2/75	30.0	165-185	20-day launch period. Powered flyby (100 m/sec)
8/1-8/19/78	35	140-158	High energy ballistic flyby

Appendix B

Venus Entry Considerations

I. Introduction

The possibility of including a Venus entry probe on a gravity assisted flight to Mercury has often been suggested as a means for increasing the scientific return of the mission. This appendix discusses some of the technical problems and constraints associated with such a mission. It is shown that the constraints imposed by the swingby trajectory are in conflict with scientific and communications (geometrical) requirements and with entry vehicle design and test limitations.

Entry missions at Venus have been studied by JPL and industry on several occasions (Ref. 26). The material given in this appendix is heavily based on the past work so that many of the results and conclusions of Ref. 26 and unpublished JPL works are updated and included here.

II. Geometrical Constraints

As noted in section V, flyby conditions at Venus for the 1973 Venus/Mercury mission are dictated entirely by the requirement to go on to Mercury, so that only a narrow range of geometries are available at Venus for the capsule mission. Three critical capsule-related parameters are uniquely specified: Venus approach speed, orientation of the approach asymptote with respect to the

earth, and orientation with respect to the sun. These are discussed separately below.

Venus approach speed (V_{∞}) as a function of launch date and Mercury arrival date was shown in section V, Fig. 4. Approach speeds between 7.6 and 9.2 km/sec are characteristic of this mission, and any attempt to lower the approach speed significantly would eliminate the Mercury portion of the mission. Venus approach speed translates directly into entry speed as shown in Fig. B-1, where speed at 6250 km radius is plotted versus V_{∞} . *Venera 4, 5, 6* and Venus/Mercury 1973 conditions are indicated for comparison. The figure also shows the entry speeds available for direct Venus entry missions in 1973 and 1975. Aeroshell considerations resulting from these relatively high swingby entry speeds will be discussed below.

Approach to Venus is from the dark side, and the arrival date is such that the sub-earth point is well into the dark. Figure B-2 shows typical conditions. Three types of capsule entry/communications modes are possible: dark side-direct link, dark side-relay link, and light side-relay link. Trajectories for each of these modes are indicated in Fig. B-2. Two direct link entries are shown: one landing at the sub-earth point with an entry angle γ_E of 60° and the other 30° away (in longitude) allowing

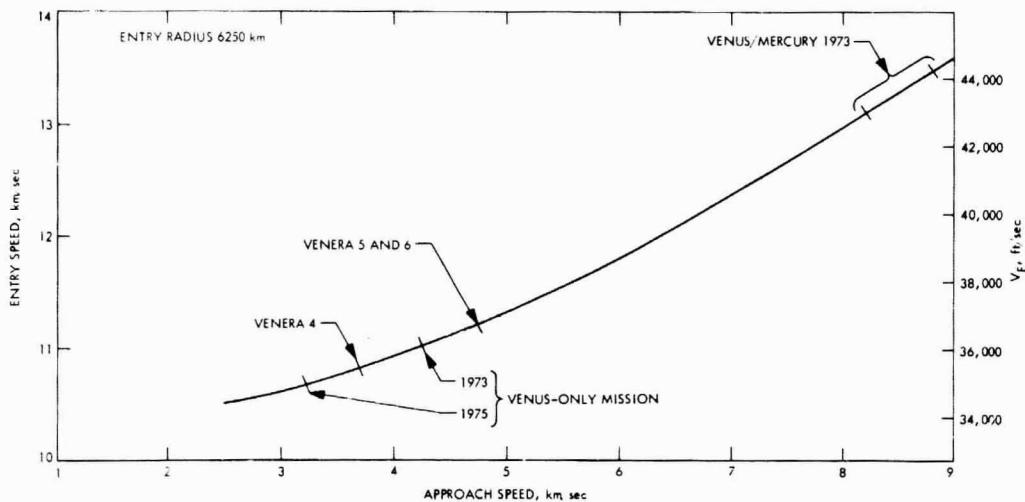


Fig. B-1. Venus entry speed versus approach speed

reduction in entry angle to $+40^\circ$ ($+$ defined as below local horizontal).

Capsule science payloads used in previous studies have concentrated on atmospheric structure and composition. These proposed payloads have often included a visual photometer to measure light levels during descent, and by this means, cloud structure might be inferred and feasibility of future TV missions could be determined. Assuming such measurements are still of interest, entry points must be on the lighted side of the terminator. Although direct capsule-to-earth communication is generally preferred for this class of Venus capsule, since it gives adequate data rate capability and generally is simpler (Ref. 26), it is clear from the geometry of Fig. B-2 that light side entries require a capsule-to-spacecraft-to-earth relay communication mode. Unfortunately, the speed and low closest approach altitude of the spacecraft limit the relay communications duration to about 20 min, which is not considered sufficient to return entry-to-surface data in real time. On the other hand, dark-side entries, with either relay or direct communications links, have steep entry angles and associated heating problems as described below.

43,000 to 44,000 ft/sec. Two basic factors in considering such a velocity increase are the effect on aeroshell structure and heat shield design, and the confidence that the resultant products will indeed survive the actual entry.

For the aeroshell structure, the maximum entry pressure loading varies as $V_E^2 \sigma \sin \gamma_E$ where σ is the ballistic coefficient. Since the entry structural weight varies as less than the square root of this imposed pressure loading, a velocity increase of 36,000 to 44,000 ft/sec would indicate a structural weight increase of less than 25%. Using these same scaling rules, a reduction in entry angle of from 45 deg to 20 deg suggests a structural weight reduction of about 40%.

In order to provide some perspective for heat shield design, entry heat transfer has been calculated for the stagnation point of a blunted-cone body over a range of entry velocities and an entry angle of 45 deg. The results are compared with calculated *Apollo*¹⁹ and USSR *Venera 4* cases in Figs. B-3 and B-4 for maximum heating rates and time integrated heating, respectively. The former relates to the severity of the environment; the latter to the time of exposure to this environment.

III. Entry Heating and Aeroshell Considerations

As evident from Fig. B-1, delivery of an entry capsule released from a Venus flyby-to-Mercury spacecraft implies a significant increase in entry velocity over a mission intended for Venus only. For a Venus-only mission in 1973, the entry velocities (V_E) can be kept below about 36,000 ft/sec, but for the Mercury-Venus-flyby they are

Regarding the maximum heating rates, the strong dependence of shock layer radiation with velocity is apparent (12th to 18th power), compared to less than the 3.5 power for convective heating. Also apparent are the relatively low *Apollo* rates. The *Venera 4* levels at a 35,000 ft/sec entry correspond roughly to 40,000 ft/sec

¹⁹Private communication, R. C. Ried, Jr., MSC, Houston, Texas.

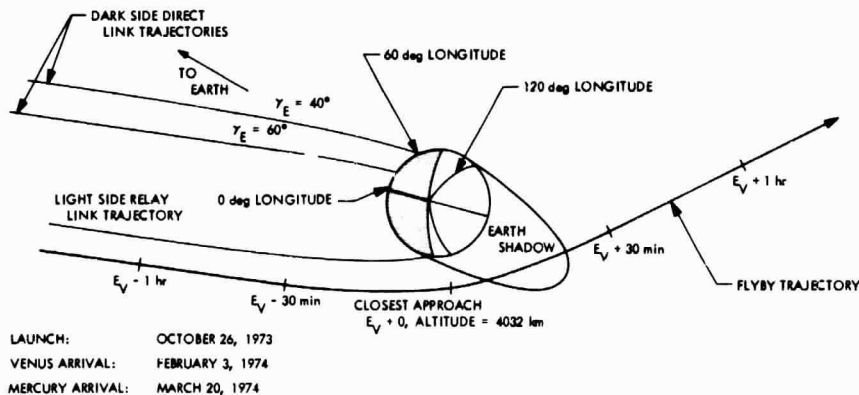


Fig. B-2. Venus capsule trajectories

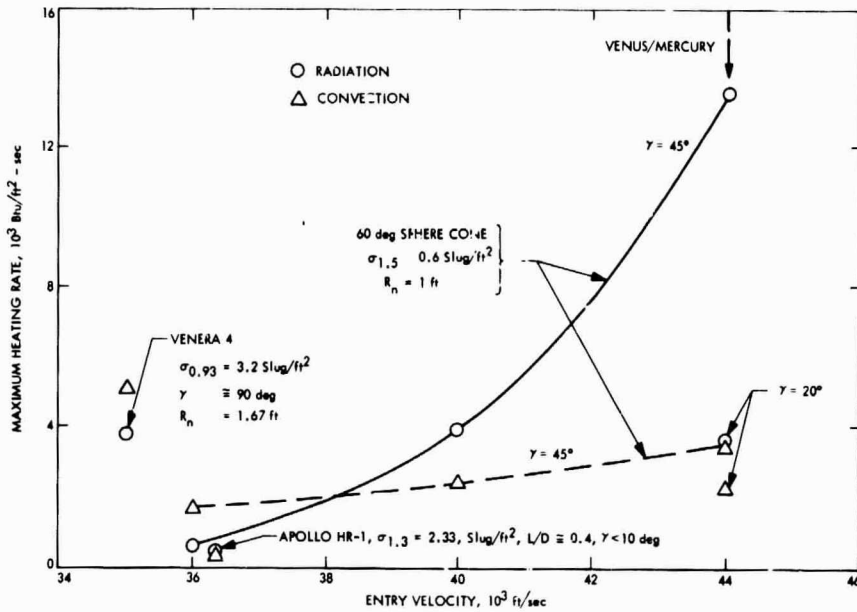


Fig. B-3. Maximum heating rates for Venus entry

for a 60-deg cone because *Venera 4* involved a nearly vertical entry with a ballistic coefficient over five times that of a cone (3.2 versus 0.6 slugs/ft²).

Figure B-4 shows integrated heating and indicates about the same trend with velocity as that for maximum heating rates (Fig. B-3). Current estimates indicate that heat shield weight increases approximately as the first to second power of the velocity; whereas, from Fig. B-4, the corresponding integrated radiative heating dependence is about the 10th power. This much weaker dependence of the heat shield weights on velocity indicates that the ablator material is performing more efficiently at the higher heating rates primarily due to the high heat absorption by char sublimation.

Recent JPL calculations (Ref. 27) for Venus entry at 44,000 ft/sec indicate that despite the relatively high radiation heat loads, the heat shield weight would not likely exceed 15% of the entry weight. The calculations also show a relatively weak sensitivity of heat shield weight to entry angle, with a 20-deg entry angle requiring about a 20% heavier shield than a 45-deg angle. Thus, the primary problem is the validation of these predictions by ground simulation as discussed below.

The environmental simulation problem can be examined by considering the entry trajectory in terms of

convective heating rate q_c , radiative heating rate q_r , and stagnation pressure P-space and comparing this space to the regions accessible with various facilities. Three such trajectories are shown in Fig. B-5 (radiative heating is normal to the paper). The 60-deg sphere-cone results of Fig. B-3 are plotted for entry angles of 45 deg (corresponding to the dark-side direct link) and 20 deg (cor-

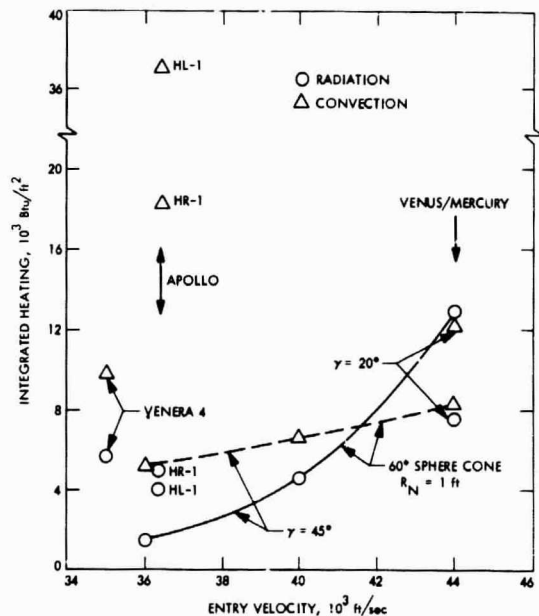


Fig. B-4. Integrated heating

responding to the light-side relay link), and the *Venera 4* conditions also are shown. Overlaid are capabilities of test facilities at NASA/Ames and NASA/MSC. Neither of the two proposed trajectories falls within the accessible regions but that reducing the entry angle from 45 to 20 deg lowers the radiative heating by about 4 times, lowers the convective heating by about 1½, and closes the simulation gap somewhat between the predicted environment and ground facilities. The preferred facility of the two shown is the Ames unit because of its radiative heating potential and larger model size (not indicated). However, the Ames facility still appears 50% low on convective simulation and somewhat less on pressure. These deficiencies could possibly be met by increasing the full scale nose radius and/or decreasing ballistic coefficient.

In summary, there appears to be no way of meeting these environmental requirements with existing or projected facilities for the 1973 Venus/Mercury mission, except for the 20-deg entry case. This case, however, is seriously limited by short descent time as discussed above.

IV. Flight Test Considerations

Because facility capabilities appear inadequate, either a large R&AD program is required or a conservative heat shield design must be adopted. In the latter case an earth reentry flight test of the heat shield material late in the program might be considered to serve as a "go, no-go"-

type decision maker. Since such an earth reentry test may appear attractive at a future time, some comments are made regarding the degree of simulation and costs. Reference 28 indicates that the response of an ablating heat shield at the stagnation point for a 36,000 ft/sec earth reentry would be well simulated if the earth reentry were vertical as compared to a 45-deg entry path angle at Venus. On a preliminary basis, it can be stated that the same factors that provide this satisfactory simulation would be expected to be present at 44,000 ft/sec. However, the capability to provide the reentry conditions for a payload of useful size and weight is expensive. For the conditions of Ref. 28, a 50-lb entry test payload on an *Athena Super H* launch vehicle is a possibility. The corresponding payload diameter would be 27 in. for a ballistic coefficient of about 0.4 slugs/ft², or 22 in. for a ballistic coefficient of 0.6 slugs/ft². The first stage of this booster is not as yet developed, but the total cost per launch (less payload) is estimated at \$0.7 million.²⁰ Existing systems that might be applicable for payloads of up to 200 lb are both costly (\$2 to 4 × 10⁶)²⁰ and, in their current state, flight tested to operate only at shallow (0 to 15 deg) entry path angles. These possible flight boosters are given in the following table. Schedules and suitability of the boosters depend on a number of factors and would require more investigation to obtain quantitative information.

²⁰Private communication, J. M. Brayshaw and W. A. Ogram, JPL.

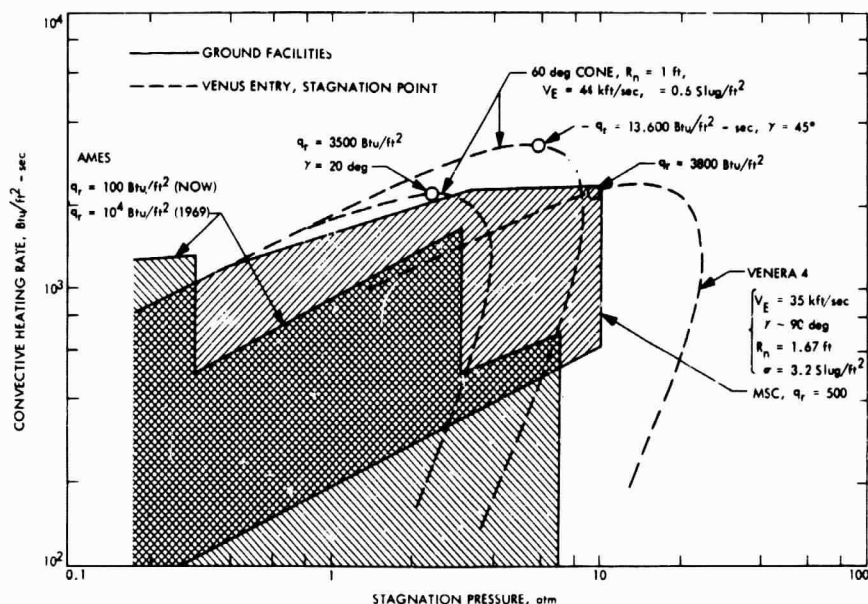


Fig. B-5. NASA ground-test simulation capability

Name	Status	Cost \$10 ⁶	Maximum velocity, ft/sec	Path angle range, deg	Payload weight, lb	Payload diameter, ft
<i>Atlas-Fire</i>	Dormant	4.1	42,000	15	200	2
<i>Thor-Delta</i>	In use	3.0	38,000	7 to 45	200	3.7
<i>Scout 5-stage</i>	Development	1.5	40,000	5 to 15	30	2.5

For payload weight and size limits less than a required Venus entry vehicle, Ref. 28 suggests that an acceptable compromise might be to truncate a full-scale entry configuration at a location that permits full-scale simulation of the stagnation region. Despite a number of shortcomings, this approach might enable a heat shield test to be made using a launch vehicle of the less expensive *Athena Super H* class.

V. Summary of Mission Characteristics

Characteristics, pro and con, of the various modes for this mission are listed in Table B-1. Note that all pos-

sible modes have substantial disadvantages; the Venus/Mercury opportunity is less than ideal for flying an entry experiment.

To compare their characteristics, a survey of Venus opportunities has been made and capsule mission launch periods have been generated for each of the Venus opportunities between 1970 and 1977. The pertinent information is summarized in Figs. B-6 and B-7 where launch energy and approach speeds are plotted for each of the opportunities. Note that 1975 stands out as having reasonably low launch energies and very low entry speeds.

Table B-1. Capsule mode summary

Dark side, direct link		Light side, relay link	
Pro	Con	Pro	Con
<p>Long descents acceptable</p> <p>No spacecraft support required after separation</p> <p>Communications distance low (43×10^4 km)</p>	<p>High entry velocity^a</p> <p>Photometry degraded</p> <p>$\gamma_E = 40$ deg (entry 30 deg from sub-earth point)^a</p> <p>$\gamma_E = 60$ deg (entry at sub-earth point)^a</p> <p>Incompatible with simultaneous relay link</p>	<p>Photometry enhanced</p> <p>$\gamma_E \approx 20-30$ deg (entry 0-15 deg on light side of terminator)</p> <p>Ground simulation may be possible</p>	<p>High entry velocity</p> <p>Spacecraft support required after separation</p> <p>Available communication times short (<20 min); entry-to-surface data not returnable in real time</p> <p>Aerodynamic staging to higher ballistic coefficient required for deepest possible atmospheric data prior to losing communications</p> <p>Entry angle-of-attack control difficult</p> <p>Entry point sensitive to guidance errors</p> <p>Incompatible with simultaneous direct link</p>
Dark side, relay link			
	<p>Spacecraft support required after separation</p> <p>High entry velocity^a</p> <p>Photometry degraded</p> <p>$\gamma_E = 60$ deg (for communication times of 90 min)^a</p> <p>Incompatible with simultaneous direct link</p>		
<p>^aGround simulation difficult.</p>			

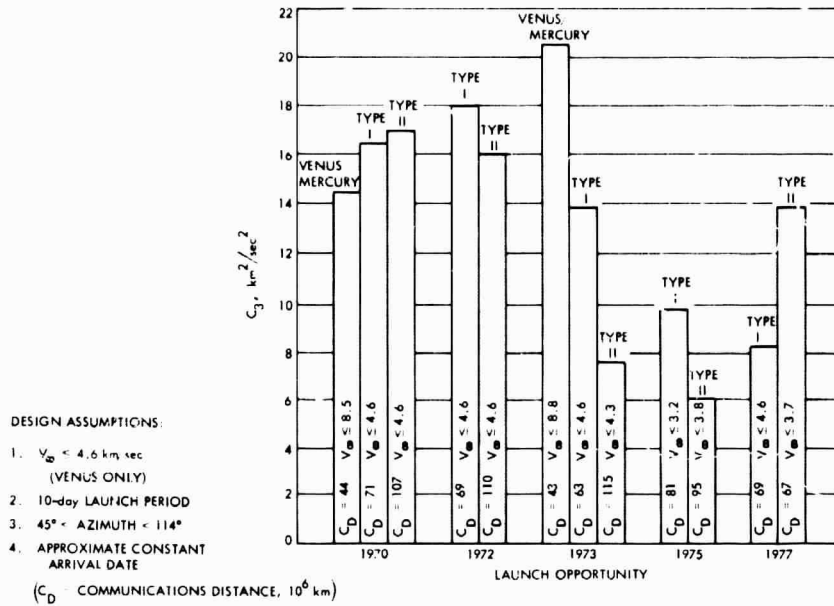


Fig. B-6. Energy requirements for Venus entry missions

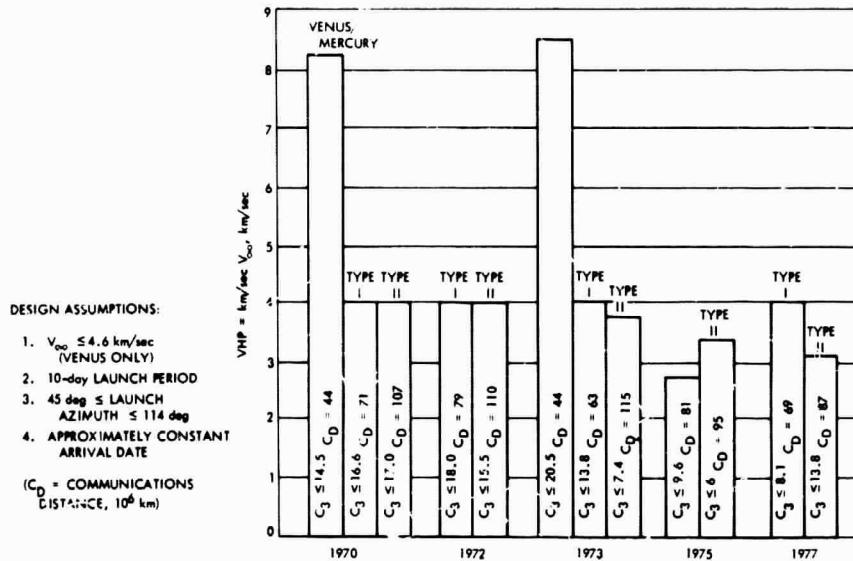


Fig. B-7. Approach speeds for Venus entry missions

Appendix C

Alternative Maneuver Turn Sequence

I. Introduction

The baseline spacecraft turn sequence described in section VIII-G uses a pitch-roll turn sequence maneuver. An alternative maneuver turn sequence (called the roll-A turn sequence), which is compatible with maneuvers performed in the vicinity of Venus and between Venus and Mercury, is discussed here.

The *Mariner* Venus/Mercury 1973 mission requires three maneuvers. A fourth maneuver has been allowed for in the baseline propulsion subsystem. The three maneuvers typically would be performed at $L+8$ days, $E_V - 3$ days, and $E_V + 8$ days. The fourth maneuver would be required if the third maneuver did not achieve the proper aim point at Mercury. Any turn sequence would have to be compatible with the above maneuvers. Maneuvers in the near-Venus environment are a new requirement since previously launched *Mariner* spacecraft have only required maneuvers to be performed near earth.

The pitch-roll maneuver sequence has been used on all *Mariner* missions with the exception of *Mariner* Venus 1962 which utilized a roll-pitch sequence. Since *Mariner* Venus/Mercury 1973 is using past *Mariner* equipment whenever possible, the pitch-roll sequence is a likely candidate as the *Mariner* Venus/Mercury 1973 maneuver turn sequence. However, the roll-A turn sequence (defined in section III of this appendix) appears to be a favorable alternative to the pitch-roll turn sequence, as certain thermal problems associated with the new maneuver environment are alleviated.

For the *Mariner* Venus/Mercury 1973 mission, as in all past missions, a certain amount of turn flexibility for any type of maneuver should be provided to satisfy possible maneuver constraints. These constraints typically would be: (1) solar-dependent, such as thermal and stray light requirements; (2) maneuver-dependent, such as low-gain antenna earth coverage; and (3) turn-accuracy-dependent, such as gyro-drift error buildup. Flexibility, as used here, is measured by the number of different ways the motor thrust vector can be rotated to point in a given direction.

II. Thermal Problems

Near-sun maneuvers will place a more severe requirement on the temperature control subsystem than those performed near earth. During the second and third maneuvers the spacecraft will be exposed to solar intensities of approximately 1.8 solar constants (260 mW/cm^2) and 2.2 solar constants (310 mW/cm^2), respectively. If a fourth maneuver had to be performed, the solar intensity would be still higher. Specific thermal considerations include:

- (1) Limiting solar panel temperatures to 285°F (140°C) during the maneuvers.
- (2) Limiting the temperature rise of the high-gain antenna feed due to focusing of the solar energy.
- (3) Establishing and limiting the maximum allowable temperature that the louver blades can tolerate when exposed to direct sunlight during the maneuver.
- (4) Maintaining the interior bus temperature within acceptable limits.
- (5) Minimizing the heating and thermal shock problem to various exposed instruments on the spacecraft, such as:
 - (a) HRIR (if there is a low temperature requirement)
 - (b) TV subsystem
 - (c) Helium axial tri-axial search magnetometers
 - (d) DFR antennas
- (6) Preventing permanent distortion of the Canopus sensor stray-light baffle and damage to the Canopus sensor.
- (7) Preventing overheating of the propulsion subsystem; the motor axis should not be within about 5° of the sun vector for extended periods of time.

As an example of the kind of problem which may be encountered, a solar illumination of 310 mW/cm^2 on a typical temperature control louver blade (made of thin hollow aluminum strips) will cause an equilibrium temperature of approximately 840°F (450°C) in 1 to 2 min. The present louver assembly will probably not survive an intensity of 2.2 solar constants.

III. Roll-A Turn Sequence Description

The roll-A sequence consists of a roll turn (spacecraft remains sun-referenced)²¹ followed by a turn about an axis perpendicular to both the engine centerline and the roll axis. This axis is called the A axis and lies halfway between the pitch and yaw axis (Fig. C-1 and C-2). The roll-A turn sequence requires some changes to the *Mariner* Mars 1969 hardware (Fig. C-3). The inertial reference unit would have to be rotated 45 deg about the roll axis, and circuits to transform the gyro signals to inputs to the pitch and yaw switching amplifiers would be required. The roll-A sequence provides a predictable sun exposure of the spacecraft during the turns. This sequence provides the required turn flexibility and is capable of pointing the engine in any desired direction.

²¹*Mariner* Mars 1971 will perform a roll turn first; however, *Mariner* Mars 1971 will use gyros rather than sun sensors, for pitch and yaw references during this turn.

IV. Comparison of Turn Sequences

With both the pitch-roll and roll-A turn sequences, there are four possible ways of turning to point the engine in a desired direction (Table C-1 shows the maximum turn ranges assumed). In the case of the pitch-roll turn sequence, either of two pitch turns will place the roll axis perpendicular to the plane formed by the engine and the desired pointing direction. Then either

Table C-1. Maximum possible turn ranges

Pitch-roll	
Maximum pitch turn range	± 180 deg
Maximum roll turn range	± 360 deg
Roll-A	
Maximum roll turn range	± 180 deg
Maximum A turn range	± 360 deg

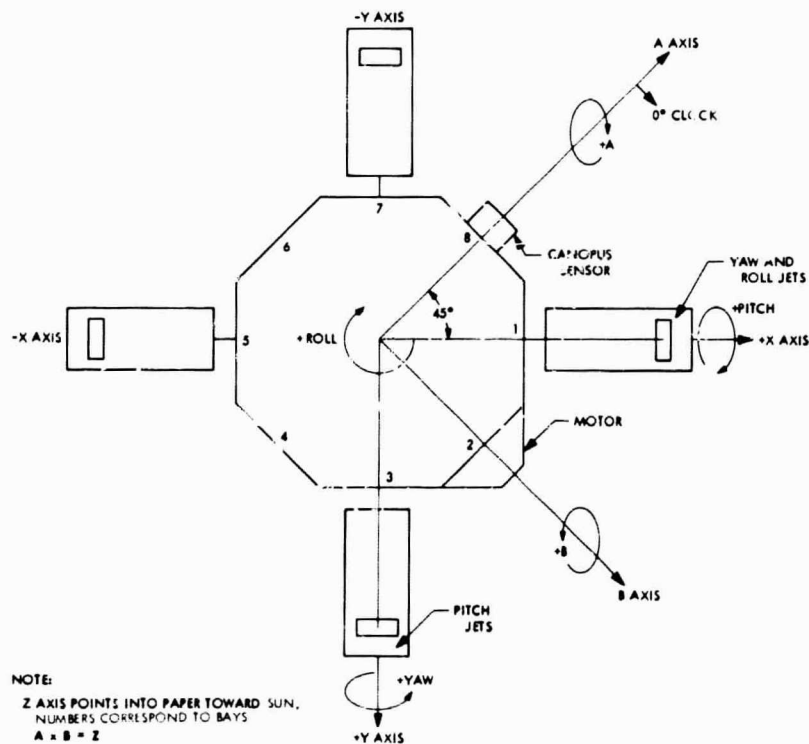
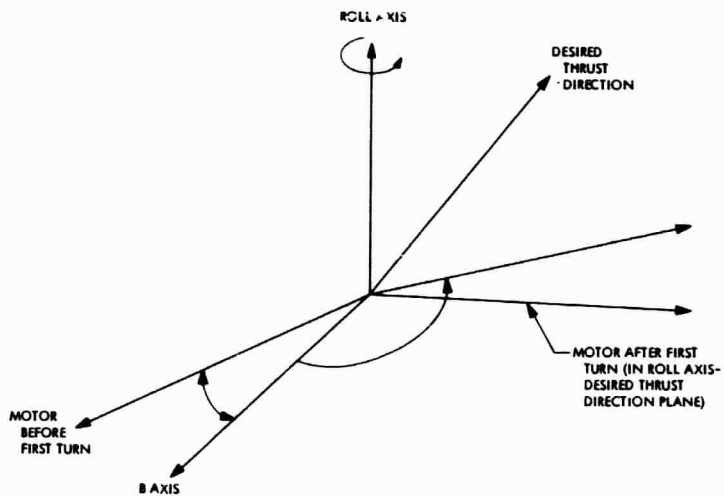
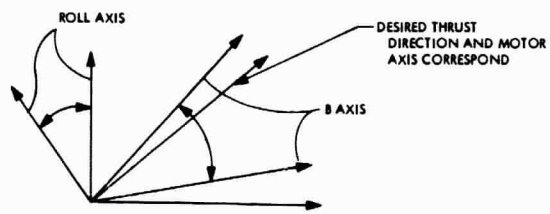


Fig. C-1. Bay configuration and axis definition as seen from shaded side



CONDITION AFTER FIRST TURN (ONE PLANE)



A AXIS COMES OUT OF PAPER

SECOND TURN THROUGH ANGLE SHOWN ABOUT A AXIS

NOTE:

B AND MOTOR AXIS DO NOT COINCIDE
 SINCE CG OF SPACECRAFT TYPICALLY
 DOES NOT LIE IN X-Y (A-B) PLANE

Fig. C-2. Arbitrary roll-A sequence

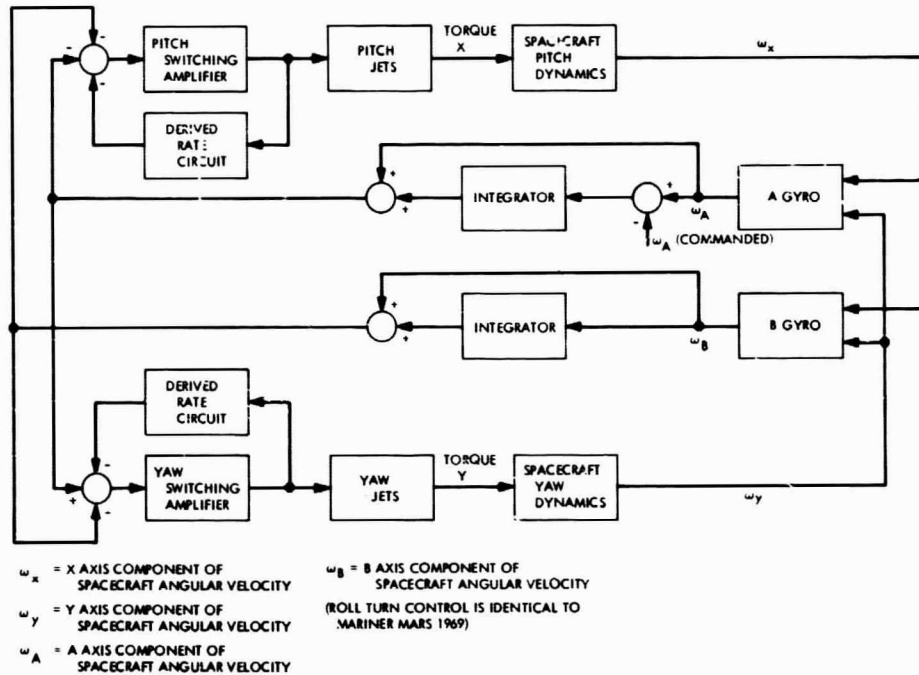


Fig. C-3. Pitch and yaw axis control for an A-axis commanded turn

of two roll turns will point the engine in the desired direction. For the roll-A turn sequence there are two different roll turns which will place the A axis perpendicular to the plane formed by the engine and the desired pointing direction; then, either of two A turns will point the engine in the desired direction.

The temperature control problems associated with the solar panels, and the internal bus temperatures, were initially thought to be reduced by selecting the turns so that the sun remains in the forward (sunny side) hemisphere of the spacecraft during the turns. Such a restriction would decrease the turn flexibility of both turn sequences. In the case of the pitch-roll sequence, there would be two possible constrained pitch turns followed by two possible roll turns which could be performed to point the engine in a desired direction. The pitch turns would have to be constrained to ± 90 deg in order to limit the sun to the forward hemisphere. In the case of the roll-A turn sequence, there would be two possible roll turns followed by two possible constrained A turns which could be performed to point the engine in the desired direction.

However, limiting the sun to the forward hemisphere (for either sequence) does not appear to be required. For example, during the third maneuver, if the sun strikes normal to the back of the solar panels, the cell temperatures are predicted to approach 260°F (130°C) if painted black, and much lower if white. This is below the maximum allowable value of 285°F (140°C).

Presumably, if a fourth maneuver were required, it would occur shortly after the third maneuver, and the thermal environment would be approximately the same. Also, interior bus temperatures would not rise excessively if the sun entered the rear hemisphere. Worst case average interior temperature rises for each sequence during the third maneuver are depicted in Table C-2. The tem-

Table C-2. Average temperature rise during spacecraft maneuver solar constants

	Pitch roll	Roll-A
Sun at 90 deg	9°F (sun on bay VIII)	2°F (sun on bay II)
Sun at 180 deg	5°F	3°F

perature rises shown for the sun at the zenith of the rear hemisphere are not deemed excessive at this time. The times assumed to generate the above temperatures are shown in Table C-3.

Table C-3. Maneuver times

Pitch Roll	
Maximum off-sun (± 180 -deg pitch, ± 360 -deg roll)	97 min
Maximum sun in rear hemisphere time	79 min
Maximum off-sun if sun is restricted to the forward hemisphere. (± 90 -deg pitch, ± 360 -deg roll)	79 min
Maximum off-sun, maximum constraints, no turn flexibility (± 90 -deg pitch, ± 180 -deg roll) (sun in forward hemisphere)	62 min
Roll-A	
Maximum off-sun (± 180 -deg A-turn)	60 min
Maximum sun in rear hemisphere	41 min
Maximum off-sun if sun is restricted to the forward hemisphere (± 90 -deg A-turn)	41 min
Maximum off-sun, maximum constraints, no turn flexibility (± 90 -deg A-turn) (same as above time)	41 min

Some advantages do accrue from limiting the sun to the forward hemisphere. For example, the baseline high-gain antenna position at the time of the third maneuver is 144 deg cone, 66 deg clock (154 deg cone, 52 deg clock at time of second maneuver). If the sun is limited to the forward hemisphere, the high-gain antenna can never look directly into the sun. If the sun were allowed to enter the rear hemisphere, the antenna might have to be repositioned so as not to look into the sun. However, coatings could partially alleviate problems associated with high-gain antenna use at high solar intensities. Because restricted maneuvers to keep the sun in the forward hemisphere reduce the turn flexibility, and unrestricted maneuvers do not cause undue temperature rises, such restricted maneuvers (for either roll-A or pitch-roll) are not recommended at this time, in spite of the advantages mentioned above. Some care in placing critical external elements will have to be applied to ensure a successful thermal design, however.

Elimination of the forward hemisphere solar restriction may allow enough turn flexibility so that optimum location of the primary and secondary low-gain antennas would allow earth communications during most, if not all, of the time of the maneuver. Another possibility is that the resulting flexibility may be utilized so that temperature-sensitive equipment would not see the sun. These possibilities must be examined in more detail at a later date.

V. Maneuver Turn Sequence Tradeoff

Either sequence without sun constraints will satisfy thermal problems (1), (2), (4), and (5) (section II of this appendix) with the present configuration and appropriate earth-based commands. However, the roll-A sequence does satisfy problems (3) and (6) more readily.

The baseline spacecraft configuration is equipped with louvers on all bays except bay II (propulsion) and bay IV (TWT). These louvers would have to be designed to look directly into the sun (for approximately 1380 sec, worst case). Present louver blades will not survive this environment. Modifications (e.g., coatings) would have to be made to existing hardware for a pitch-roll sequence. These modifications would not necessarily have to be made for a roll-A sequence (if the louvers can withstand 0.707×2.2 solar constants) since bays I, III, V and VII always would be at least 45 deg oblique to the sun. Table C-4 depicts worst case sun exposure for each bay. Utilizing a pitch-roll sequence does not guarantee that any bay does not look directly into the sun. However, a roll-A sequence does guarantee that certain bays never look into the sun, no matter what turns are performed.

Since it is not known in advance what the A turn would be, one would have to design to the combination shown in Table C-4. This table shows that the Canopus sensor

Table C-4. Worst case bay sun intensities during A-turn

A = +90 deg (-270 deg)		A = -90 deg (+270 deg)		Combined worst case	
Bay	Intensity ^a	Bay	Intensity ^a	Bay	Intensity
I	0	I	0.707	I	0.707 M
II	0	II	1.0 ^b	II	1.0 ^b
III	0	III	0.707	III	1.0
IV	0	IV	0	IV	0 ^c
V	0.707	V	0	V	1.0
VI	1.0	VI	0	VI	1.0
VII	0.707	VII	0	VII	1.0
VIII	0	VIII	0	VIII	0 ^c

^aFraction of maximum solar intensity at time of maneuver i.e., looking directly into sun).

^bBay II must never look directly into sun. The time of the maneuver has to be shifted to meet this constraint.

^cBays IV and VIII are never exposed to sun.

(bay VIII), and the TWT (bay IV) will never see the sun directly.

The constraint must be imposed that bay II (propulsion) cannot look directly into the sun (this applies to both turn sequences). The maneuver time will have to be delayed until the desired thrust direction is at least 5 deg from the sun line.

Finally, the total maneuver velocity pointing errors are approximately the same for either type of maneuver

turn sequence; these have been estimated to be 21.3 mrad, 3σ for the pitch-roll sequence and 21.7 mrad, 3σ for the roll-A sequence.

VI. Conclusion

Since the roll-A turn sequence enables worst case bay intensities to be known *a priori*, and allows two bays never to see the sun at all while not imposing additional problems, this alternate sequence appears to be a good candidate for all maneuvers for the *Mariner Venus/Mercury 1973* mission.

Appendix D

Alternate Solar Panel Configurations

I. Introduction

The solar panel configuration shown as the baseline in section VII B has the general appearance and size of the *Mariner* 1969/1971 arrangement. However, the design is considerably different and presents new problems in that two-thirds of the panel area is proposed to be highly reflecting and emitting (low α/ϵ) in order to maintain the solar cells below a prescribed upper temperature limit of about 140°C. With this design concept, termed mirror mosaic, the temperature of the solar cells near earth will be much less than with previous designs. This large earth-to-Mercury temperature excursion causes a similar large change in solar cell voltage output so that changes to previous *Mariner* power conditioning systems are also required (section VIII-D), or tiltable panels may be used as described below.

To prevent an unacceptably large voltage change with mirror mosaic flat panels the baseline power subsystem (section VIII-D) specifies that the solar panel power distribution arrangement (located in the power source logic box) would be designed to switch from a parallel to a series hookup, thus raising the voltage. For the 35 Vdc specified minimum, this switching should occur at about a panel temperature of +60°C or 0.6 AU (~ 20 days past Venus closest approach); a decreasing voltage trend would again ensue, but would not go below 45 Vdc at 20 days past closest approach to Mercury.

II. Types of Mirror Mosaic Designs

Two possible methods have been considered in a research and advanced development (R&AD) study to obtain a mirror mosaic effect as shown in Fig. D-1. One method, which is referred to as a macro-mirror mosaic, is to place second surface (back silvered) mirrors in between the solar cells (Fig. D-1a). The second, called a micro-mirror mosaic, has second surface mirror stripes, or another pattern, on each solar cell cover glass (Fig. D-1b). The macro- and micro-mosaic designs shown require about the same solar panel size for equivalent temperature control performance, and therefore, interact with the spacecraft configuration and power conditioning system similarly. However, there may be considerable differences in development costs, schedule, and reliability.

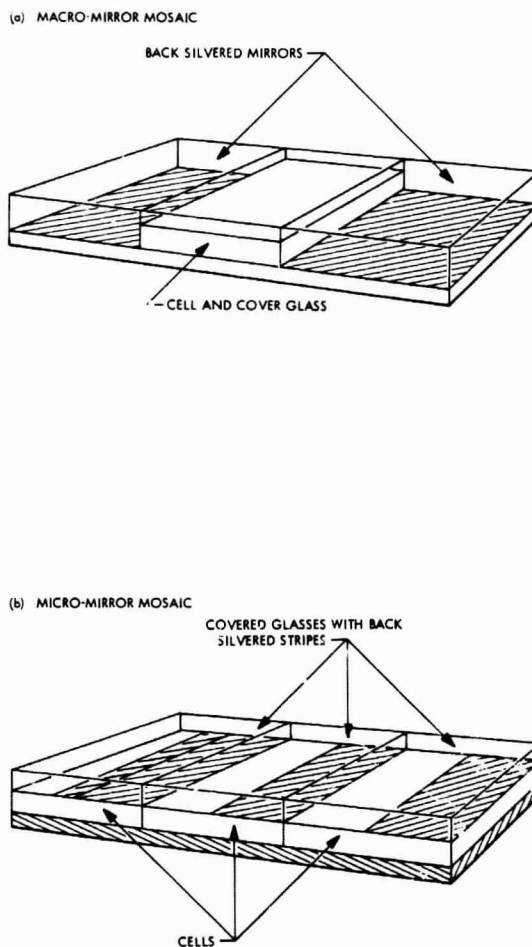


Fig. D-1. Two methods of achieving a mirror mosaic effect

III. Alternatives to Mirror Mosaic Panels

Besides the above mirror mosaic concept chosen as the baseline design, alternative approaches are also being studied under R&AD funding such as tiltable solar panels and spectrally selective narrow bandpass filters for the solar cells. Of these latter two approaches, the use of tiltable mirrorless panels appears preferable to selective filters and has some particularly attractive features, but not without introducing some problems. Also, it does not appear feasible to achieve the required temperature control with selective filters alone, but such

solar cell filters can be used to permit an increase in active solar cell area or reduce tilt angles.

IV. Tilttable Solar Panels

The primary advantages of the tilted panel approach are: (1) a much smaller temperature excursion is possible, and (2) only two *Mariner* Mars 1969-sized panels without mirrors are required. The smaller excursions of temperature and, therefore, solar cell voltage are demonstrated in Figs. D-2 and D-3. These figures give estimates of temperature and power output per 80 ft² of flat mirrored (mosaic) or mirrorless tilttable panels, as compared to flat non-mirrored panels. With a nominal maximum temperature of 140°C, a flat non-mirrored panel is clearly unacceptable shortly beyond Venus. In contrast, a four-panel, flat, 66% mirror arrangement is predicted to remain below 140°C, but very large temperature and voltage changes occur, although the power output appears acceptable.

This large temperature excursion could possibly be reduced by approximately 45% by tilting the panels 65 deg 15 days after Venus encounter at a condition where the upper temperature limit of 140°C is approached (hatched lines on Fig. D-2). The power output is sufficiently high that two panels (~ 40 ft²) rather than four would be acceptable. Figure D-3 illustrates an approximate constant temperature and maximum power operating condition which requires, in effect, continuous tilting beyond Venus.

In considering tilttable panels, it would be desirable to delay tilting of the panels until after the third maneuver because: (1) a maneuver following tilting might return a panel normal to the sunline, causing overheating, and (2) any CG shift that might affect attitude control could be avoided. Executing the third maneuver prior to panel tilting would cause the peak in the temperature curve and the dip in the power curve of Fig. D-3.

Table D-1 presents some of the factors involved in considering the flat mosaic versus the tilted panel approach. The table indicates new problems are introduced by either approach, but that tilted panels involve more system interactions than the mirror mosaic panels. Further analysis and evaluation are required to assess these interactions.

Table D-1. Tilt-mirror comparisons

Factors to be considered in a selection between flat mosaic and tilted panels

Item	Mirror mosaics	Tilttable panels
Typical power at earth, W/80 ft ²	350	850
Number of 20 ft ² panels required	4	2
Total panel weight	Similar to <i>Mariner</i> Mars 1969 (~100 lb)	Half <i>Mariner</i> Mars 1969 plus tilt mechanism (~63 lb)
Photovoltaic considerations	Uncertain cell output behavior at high solar intensities Large voltage swing from earth to Mercury	Uncertain cell/filter behavior at high tilt angles
System interface considerations	Same as previous <i>Mariners</i>	Variable spacecraft reflectivity affecting navigation (continuous tilt) Possible obstruction of instruments and antenna look angles CG shift of up to 7 in. or unbalanced solar pressure Attitude control jet placement Possible thermal interaction Last maneuver may have to be made before tilting
Thermal control considerations	Sensitivity of panel temperature to stability of mirror reflectivity	Sensitivity of panel temperature to misorientation during maneuvers
Material/fabrication considerations	New wiring for macro-mosaic Thermal shock effects	Tilt mechanism design Thermal shock effects

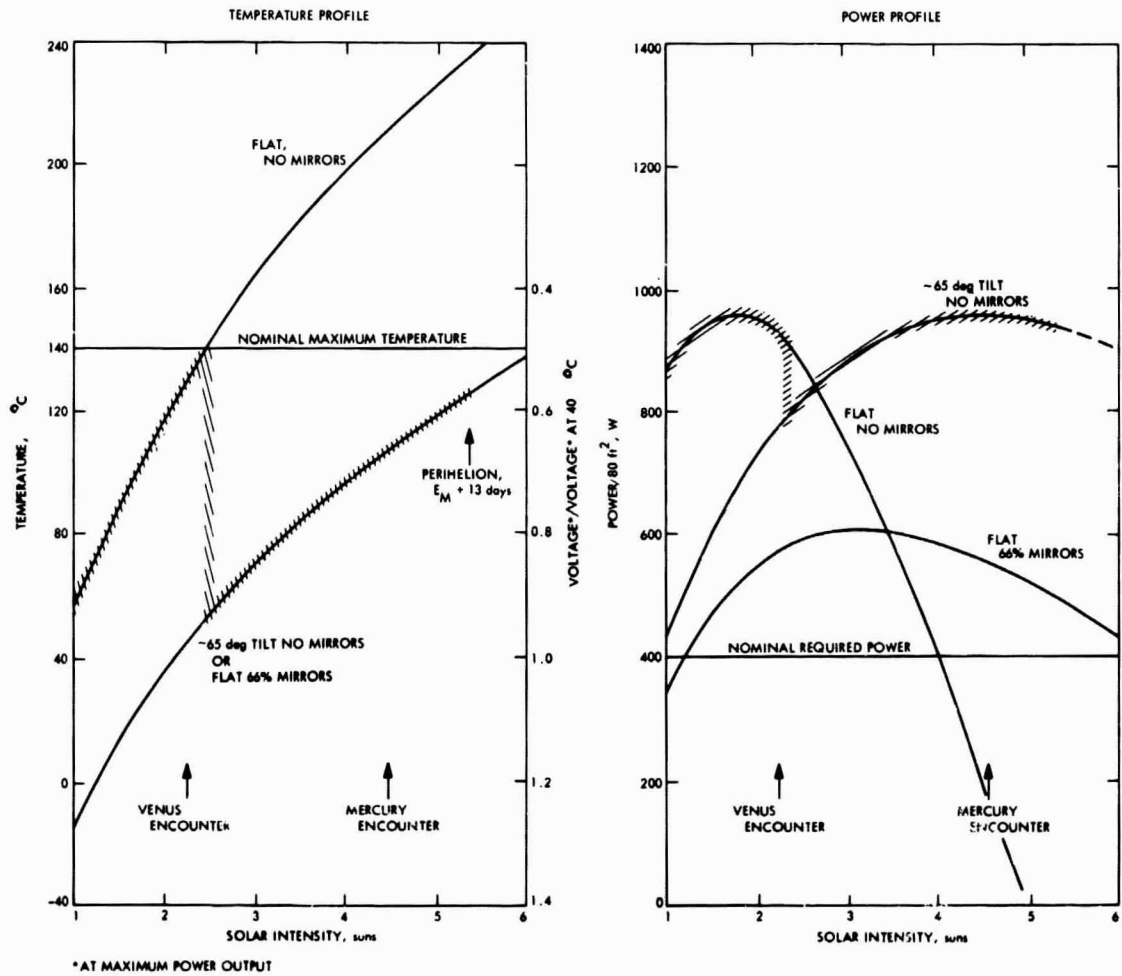


Fig. D-2. Estimated solar panel performance, one tilt to 65 deg, 15 days after Venus encounter

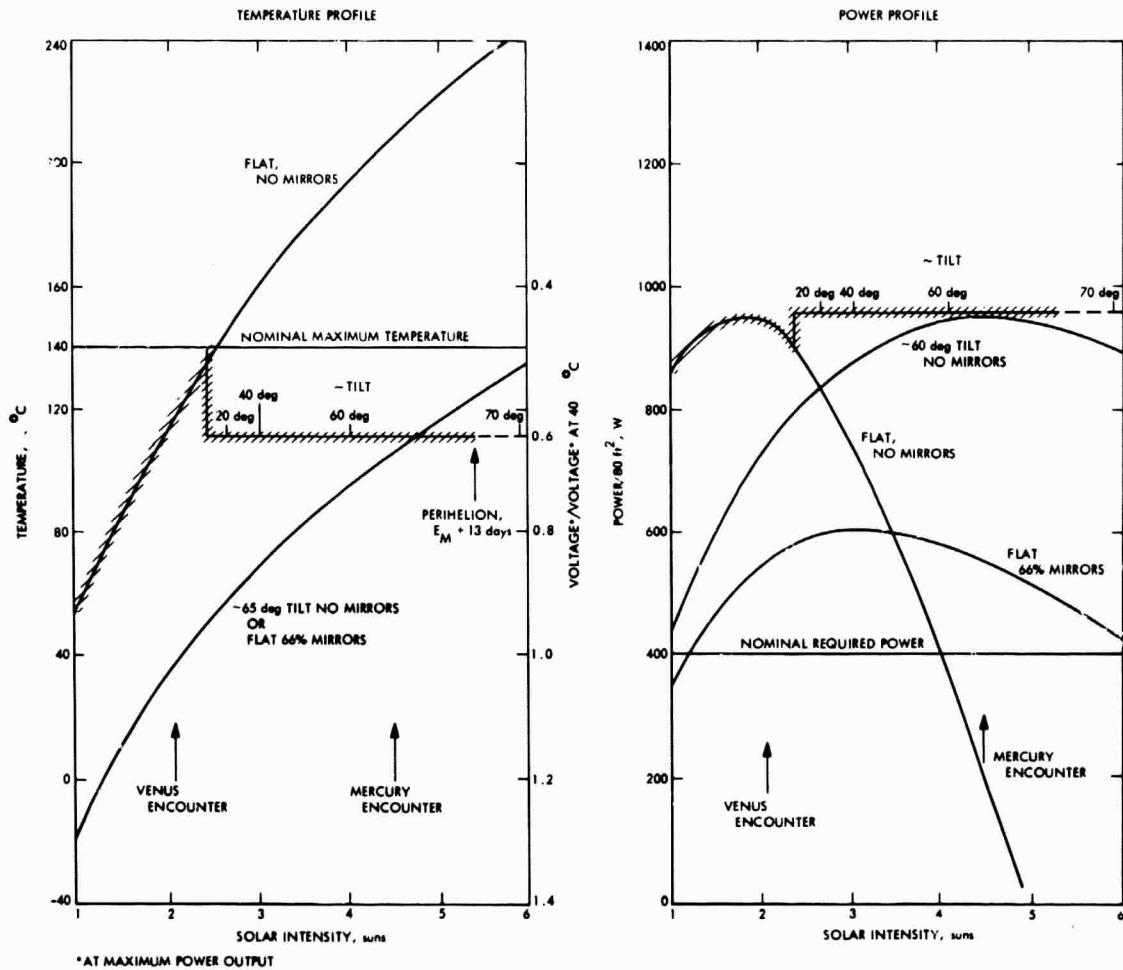


Fig. D-3. Estimated solar panel performance, increasing tilt after third maneuver for maximum power at constant temperature

Appendix E

Alternate High-Gain Antenna Positioning for Extended Missions

I. Introduction

The baseline mission terminates at $E_M + 20$ days. The principal baseline configuration constraint at that time is the high-gain antenna which cannot be pointed close enough to earth. This appendix examines alternate schemes for providing communications through at least $E_M + 90$ days ($L + 240$ days for the reference trajectory).

Two high-gain antennas are considered: a circular 40-in. paraboloid and an elliptical 33- × 66-in. paraboloid. A requirement for telemetry capability of at least 8½ bits/sec is assumed.

In any case, command capability can be provided to $L + 240$ days through the secondary low-gain antenna using the 210-ft DSIF antenna and 20 kW.

II. Circular 40-in. Paraboloid

A telemetry design control table is shown in Table E-1 which assumes:

- Cruise mode I (8½ bit/sec)
- Maximum spacecraft-earth range occurring during the first 240 days of flight of 268×10^6 km
- High power mode
- A 40-in. circular paraboloid spacecraft antenna
- An 85-ft receiving antenna

The table, which assumes no spacecraft antenna pointing loss, shows an overall performance margin of 13.4 ± 4.4 dB. Thus, the spacecraft antenna gain could be degraded by up to 9.0 dB (i.e., antenna gain of 16.6 dB would suffice) and still assure communication. Figure E-1 shows that an antenna pointing error less than 6.9 deg is required to provide this gain. If the 210-ft DSIF antenna were employed, a spacecraft antenna gain of only 7.6 dB would be required. The 40-in. spacecraft antenna must be pointed within 9.0 deg to provide this gain.

Figure E-2, which is a pointing error plot for the alternate antenna hinge axis described in section VII-F, shows that cruise mode I reception is possible through

$L + 240$ days over the 210-ft antenna. However, reception on the 85-ft antenna would be in the blackout region after about $L + 210$ days. It is possible that a slight modification to this alternate hinge orientation could be made so that telemetry could be received at $L + 240$ days on the 85-ft antenna at the expense of slightly reduced performance earlier in the mission.

The problems of mounting the 40-in. antenna to allow positioning through its full, usable range have not been investigated. However, they should be considerably less than those which are discussed for the elliptical antenna described in the next section.

III. Elliptical 33- × 66-in. Paraboloid

A possible solution to the antenna pointing problem for an extended duration mission is to use an elliptical antenna pattern with the wider beam aligned normal to the direction of antenna movement. Such a scheme has been investigated, assuming an elliptical 33- × 66-in. paraboloid, whose on-axis gain is 27 dB. Using this antenna with the alternate hinge-axis orientation described in the preceding section, cruise mode I telemetry can be received by the 85-ft DSIF antenna through $L + 240$ days; in addition, performance is improved earlier in the mission. Figure E-1 shows the major axis radiation pattern of this elliptical antenna.

Figure E-3 shows two views of the spacecraft configuration required to support this antenna. The additional field of view for the antenna requires that it be located on a boom which is deployed after launch, allowing the antenna to operate in the sun during all portions of the mission. Obstruction of the field of view of the TV could be avoided if the high-gain antenna were attached from the front face of the spacecraft and canted toward the sun such that the tip of the antenna would not interfere with the field of view of the TV over the edge of the spacecraft. The thermal problems (e.g., distortion) associated with this antenna operating at full sun intensity have not been estimated at this time. No large problems are anticipated since the high-gain antenna is primarily a passive mechanism; however, a mesh antenna may be required. The drive motor at the pivot point on the antenna might be subject to extreme environments.

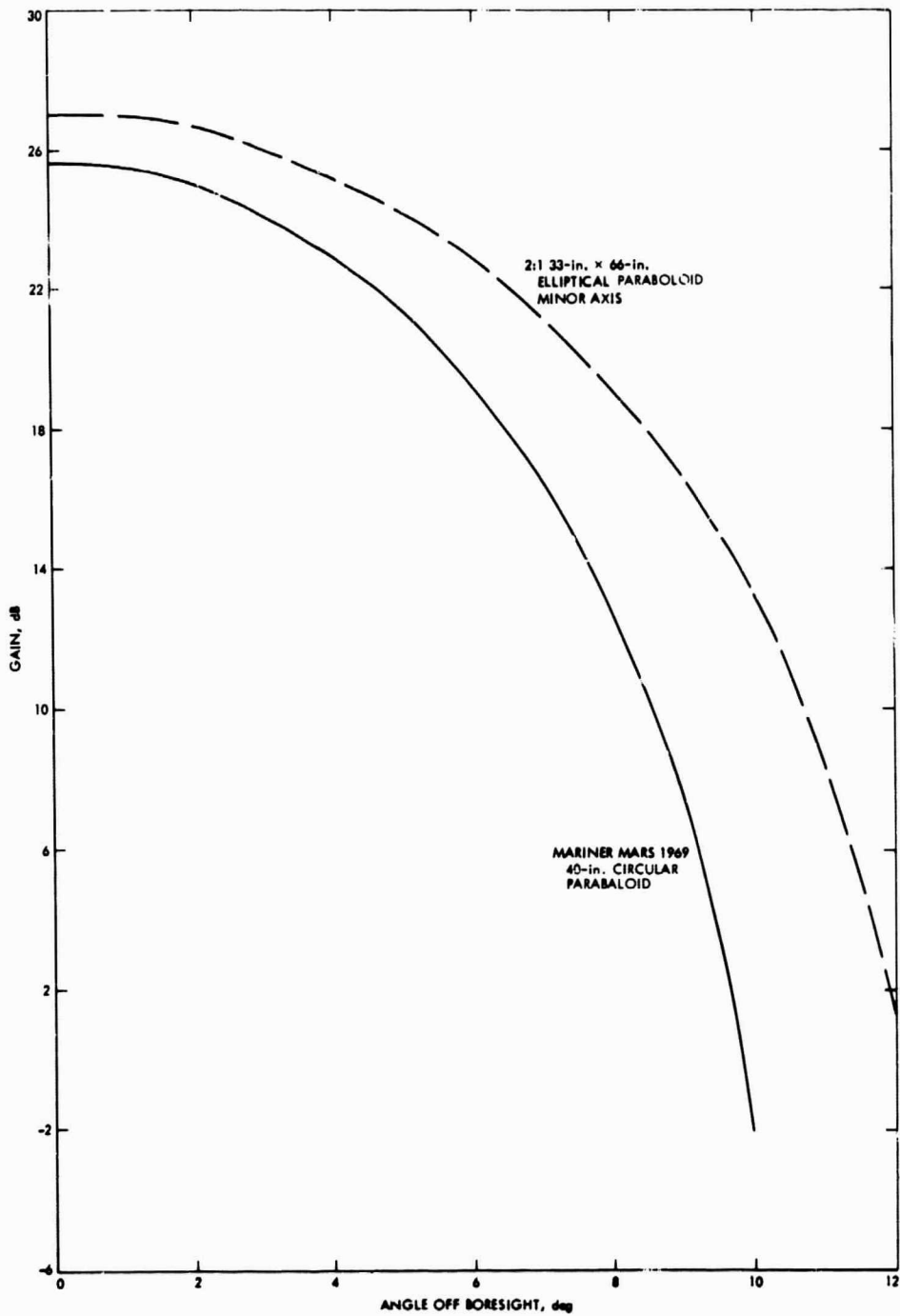


Fig. E-1. Radiation patterns of 40-in. circular paraboloid and 33-x 66-in. elliptical paraboloid (minor axis)

There are two other areas resulting from this configuration which require further study:

- (1) The attitude control gas loading, which would have to be increased because of loss of symmetry (as presented to the sun) in the spacecraft configuration.

- (2) The effect of changing reflective area on navigation ability which may degrade the measurement of general relativity effects through tracking data. (General relativity investigation may be one of the objectives of an extended-duration mission.)

Table E-1. Telemetry design control table, cruise mode I

Engineering data: $8\frac{1}{2}$ bits/sec
Science data: none

DSS: 85-ft antenna
Spacecraft: high-gain antenna

TWT: high power
Launch: 10/21/73

Arrival: 4/1/74
Time in mission: $L \pm 240$ days

No.	Parameter	Nominal value	Tolerance	
			Favorable	Adverse
1	Total transmitter power, dBmW	42.320	0.580	0.000
2	Transmitting circuit loss, dB	-1.450	0.250	-0.250
3	Transmitting antenna gain, dB	25.600	1.000	-1.200
4	Transmitting antenna pointing loss, dB	0.000	0.000	0.000
5	Space loss, dB F=2297. MHz, R=268 × 10 ⁶ km	-268.210	0.000	0.000
6	Polarization loss, dB	-0.020	0.000	-0.110
7	Receiving antenna gain, dB	53.300	0.600	-0.600
8	Receiving antenna pointing loss, dB	0.000	0.000	-0.250
9	Receiving circuit loss, dB	0.000	0.000	-0.000
10	Net circuit loss, dB (2+3+4+5+6+7+8+9)	-190.780	1.850	-2.410
11	Total received power P(T), dBmW (1+10)	-148.460	2.430	-2.410
12	Receiver noise spectral density, dBmW/Hz Noise temperature = 55 ± 10°K	-181.220	-0.872	+0.727
13	Carrier power/total power, dB	-2.440	0.560	-0.660
14	Received carrier power, dBmW (11+13)	-150.900	2.990	-3.070

No.	Parameter	Nominal value	Tolerance	
			Favorable	Adverse
15	Carrier threshold noise BW, dB/Hz	10.800	-1.000	0.000
Carrier tracking (one-way)				
16	Threshold SNR in 2B _{LO} , dB	0.000	0.000	0.000
17	Threshold carrier power, dBmW (12+15+16)	-170.420	-1.872	0.727
18	Performance margin, dB (14-17)	19.520	4.862	-3.797
Data channel B - 8 1/2 bits/sec				
19	Data power/total power, dB	-3.660	0.750	-0.880
20	Waveform distortion loss, dB	0.000	0.000	0.000
21	Loss through radio system, dB	-1.300	0.400	-0.400
22	Subcarrier demod loss, dB			
23	Bit sync/detection loss, dB			
24	Received data power, dBmW (11+19+20+21+22+23)	-153.420	3.580	-3.690
25	Threshold data power, dBmW (12+25a+25b)	-166.812	-0.872	+0.727
a	Threshold PT/N, dB (BER = 5 × 10 ⁻³)	5.200	0.000	0.000
b	Bit rate, dB bits/sec	9.208	0.000	0.000
26	Performance margin, dB (24-25)	+13.392	4.452	-4.417

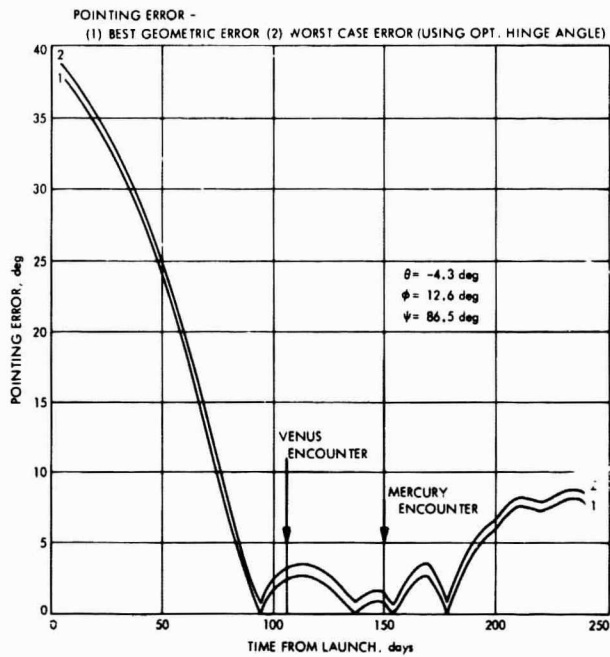
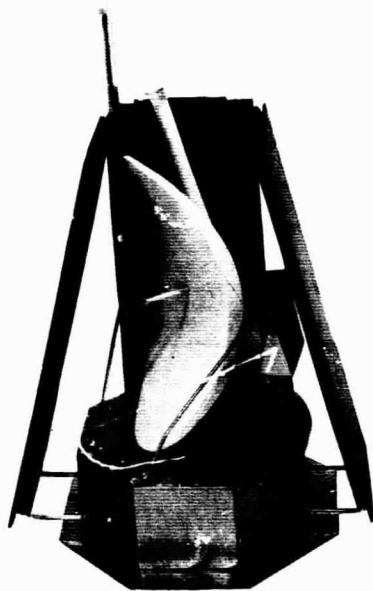
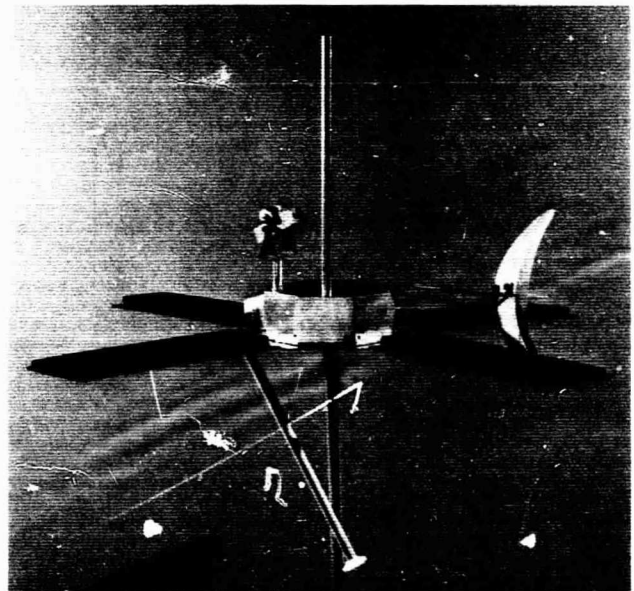


Fig. E-2. October 21, 1973 launch, pointing error, baseline antenna with alternate hinge position, L + 0 to L + 240 days



(a) Launch configuration
(one solar panel omitted)



(b) Configuration for Mercury
(post-encounter sequence)

Fig. E-3. Spacecraft configuration with 33-X 66-in. elliptical antenna

Appendix F

Solar Simulator Requirements

Because of the high solar intensity that the *Mariner Venus/Mercury 1973* spacecraft will encounter during the mission, the existing solar simulators are not adequate for the program test requirements. Therefore, a short study was conducted to determine the solar simulator requirements and to recommend facility procurement action in FY 70.

The available choice of simulator options was evaluated to determine the range of feasible options, and these are listed in Table F-1 along with the estimated costs.

The question of what sort of test program would most likely be followed, and how that program would be impacted by the facility choice was considered to determine a probable qualification and acceptance test program. These tests can be summarized as:

- (1) Some 650 hr of developmental and qualification testing at the subsystem level in a solar beam. (Note: Developmental testing of solar panels is excluded; that test program will have its own 6-in. diameter solar beam. This facility will *not* be used for thermal, qualification, or FA tests because of its small size and/or unavailability.)
- (2) A maximum of 500 hr of testing at the spacecraft system level with 120 hr of solar simulation for the PTM and 100 hr for the flight vehicle.

The solar simulator requirements for thermal control testing were evaluated. Based upon inspection of the size of the components which are exposed to the sun, it was concluded that a 1-ft solar beam would be suitable for both thermal tests of local areas of the sunlit parts of the spacecraft and development and qualification tests at the subsystem level. Such items as the sun sensors, plasma probe, sun gate, etc., would be tested in the 1-ft beam.

Using all of the above information, the total project cost for the solar simulator test program was estimated, as shown in Table F-2. This table shows a cost break-

Table F-1. Feasible simulator options

Facility options available	Estimated cost, \$ k	Time required for modification, months
I. Eight-foot beam in 25-ft simulator	100	6
A. Move existing 10-ft mirror to 25-ft simulator; make a new mixer; fix cooling on mirror		
B. New 10-ft mirror for 25-ft simulator; new mixer	250	18
Operating costs: \$330/hr with solar simulation \$225/hr without solar simulation		
II. Three-foot beam in 10-ft simulator; new mixer; fix cooling on mirror	47	6
Operating costs: \$200/hr with solar simulation \$180/hr without solar simulation		
(NOTE: <i>Mariner Mars 1971</i> decided not to use the 10-ft facility because of some \$100 k worth of modifications required to bring the chamber to first-class operational status. These costs are not included here on the assumption that these modifications will be made on yearly funds prior to <i>Mariner Venus/Mercury 1973</i> use)		
III. One-foot beam in 7- x 14-ft chamber (includes new window)		
A. Commercial design	165	12
B. JPL "in-house" design	85	6-8
Operating costs: \$32/hr with solar simulation \$20/hr without solar simulation		
IV. Six-and one-half-foot beam in 10-ft simulator; new lamps; new mixer; fix cooling on mirror	380	15
Operating costs: \$280/hr with solar simulation \$180/hr without solar simulation		

down for the same test program regardless of the facility option. While this is obviously an unrealistic assumption, it was felt to be adequate at this stage of the program. This assumption does, however, allow a qualitative esti-

Table F-2. Mariner Venus/Mercury 1973 test program costs, ~ \$k

Solar simulator options	Facility modification costs	Thermal tests ^a		With sun, PTM (120 hr)	Without sun, PTM (380 hr)	With sun, FLT (100 hr)	Without sun, FLT (400 hr)	Qualify and development tests (650 hr)	Total
		Component	TCM						
I. 8 ft only			(500 hr)						
A	100		165	40	86	33	90	214	728
B	250		165	40	86	33	90	214	878
II. ^b 3 ft	47	(280 hr)	(250 hr)						
		56	50	24	68	20	72	130	467
III. ^b 1 ft		(280 hr)	(250 hr)						
A	165	9	50	24	68	20	72	21	429
B	85	9	50	24	68	20	72	21	349
IV. 6½ ft only	380		(500 hr)	34					
			140		68	28	72	182	904
V. 8 ft + 1 ft		(280 hr)	(250 hr)						
IA + IIIB	185	9	83	40	86	33	90	21	547
IB + IIIB	335	9	83	40	86	33	90	21	697
VI. 6½ ft + 1 ft		(280 hr)	(250 hr)						
IV + IIIB	465	9	70	34	68	28	72	21	767

^aWhere a small solar beam is available, it is assumed that component tests would use the small beam and TCM test time would be reduced.

^bOptions II and III use existing Venus intensity capability in the 10-ft simulator plus electric heaters (or other techniques) for simulating Mercury level heat fluxes.

mate of where the largest costs would be accumulated and the relative size of these to the total program.

Because of a preference for a large solar beam for thermal control model (TCM) testing, possible schedule conflicts in the space simulators were evaluated considering all potential projects. Projected schedules are shown in Figure F-1. As can be seen, Venus/Mercury must be squeezed in around *Viking* and outer planet missions in 1972 and 1973. If any one program slips, the others are affected. Development and qualification testings would also have to work around *Mariner Mars* 1971 and *Viking* if only the large simulator were built.

In order to avoid potential schedule conflicts in the 25-ft space simulator if a large solar beam is required, the large solar beam should be in the 10-ft simulator. That arrangement would give *Mariner Venus/Mercury* 1973 a facility independent from *Viking* and outer planet missions.

Evaluation of the preceding information leads to the following conclusions:

- (1) A 1-ft solar beam is required at an early date for developmental testing on sun-facing equipments. That same beam would be used for qualification and for thermal testings of those components. Early funding in FY 70 is required.
- (2) The highest confidence in thermal control would be achieved if the TCM were tested in a large solar simulator.
- (3) Because of the estimated short lead time and the estimated test periods for the TCM, funding of the large solar beam can be deferred until FY 71. However, *decision* to fund should be made in the last quarter of FY 70.
- (4) The large solar beam, if built, should be in the 10-ft space simulator in order to avoid scheduling conflicts with the *Viking* and outer planet missions.

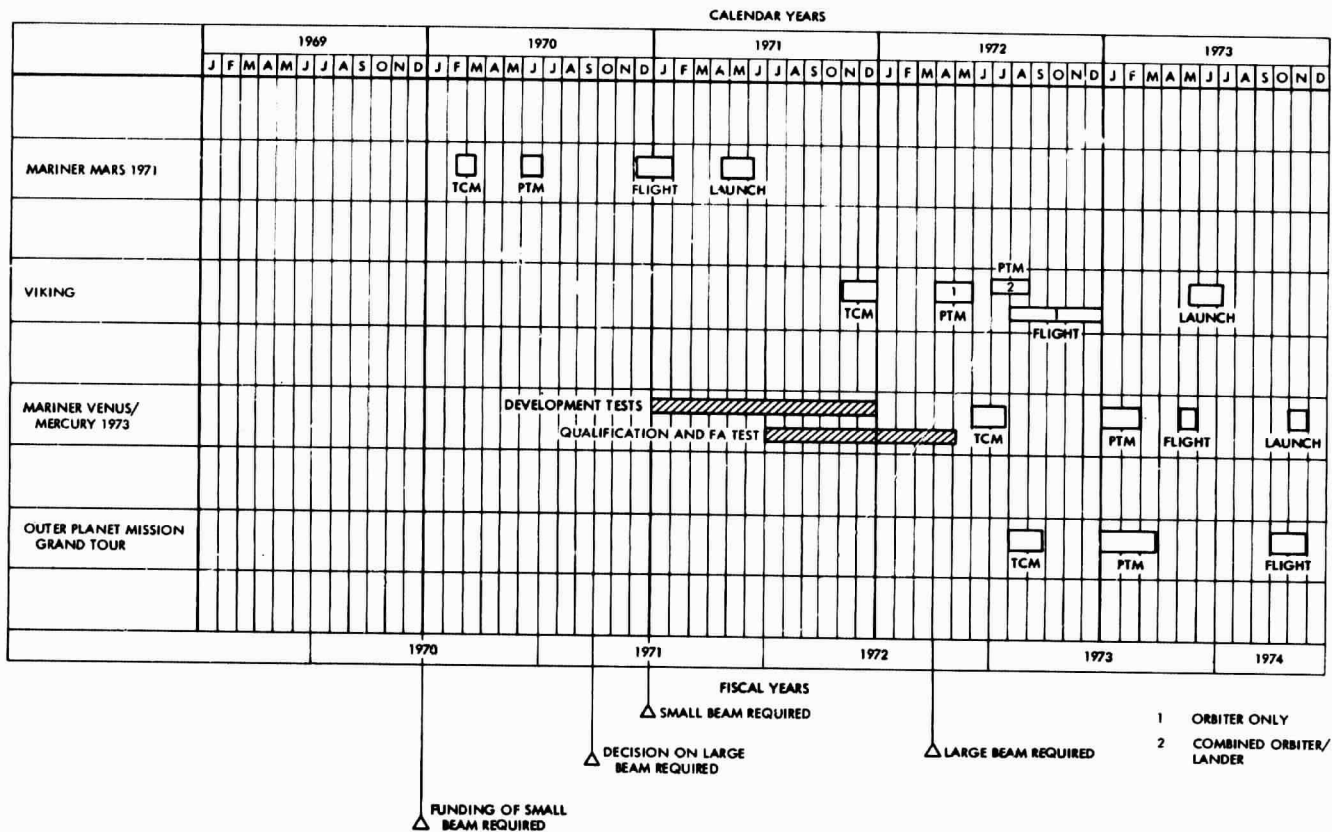


Fig. F-1. Space simulator test periods

Nomenclature

Symbols, Abbreviations, and Definitions

A,B	wide- and narrow-angle cameras, respectively; spacecraft coordinates	FY	fiscal year
ac	alternating current	GD/C	General Dynamics/Convair
ACS	attitude control subsystem	GM	universal gravitational constant
AFETR	Air Force Eastern Test Range	GMT	Greenwich Mean Time
APMT	Advanced Planetary Mission Technology	HPO, HP180	Mercury hot poles at 0°, 180° longitude
ATS	Applications Technology Satellite	HRIR	high resolution infrared radiometer
AU	astronomical unit	ID	identification
avg	average	IF	intermediate frequency
B	aiming point vector	IR	infrared
BER	bit error rate	IRR	infrared radiometer
$2B_{Lo}$	phase-locked loop threshold bandwidth	JPL	Jet Propulsion Laboratory
BW	bandwidth	K	thermal conductivity
C_s	launch energy parameter	L	launch; liftoff (2-in. rise)
CC	coded command	<i>L/D</i>	lift/drag ratio
CC&S	central computer and sequencer	LCE	launch complex equipment
CCW	counter clockwise	M_n	<i>n</i> th trajectory correction maneuver
CG	center of gravity	max	maximum
CW	clockwise	min	minimum; minutes
dc	direct current	MSC	Manned Spacecraft Center
DC	direct command	N	number of planet orbits
DFR	dual-frequency receiver	N	unit vector to generalized body
DSIF	Deep Space Instrumentation Facility	NASA	National Aeronautics and Space Administration
DSN	Deep Space Network	OAQ	Orbiting Astronomical Observatory
DSS	data storage subsystem	OD	orbit determination
<i>E</i>	encounter, i.e., time of closest approach	OGO	Orbiting Geophysical Observatory
EED	electroexplosive device	OSE	operation support equipment
eff	efficiency; effective	OSSA	Office of Space Science and Applications
ESF	explosive safe facility	P	stagnation pressure
EVM	earth-Venus-Mercury	$P(T)$	total received power
<i>f</i>	focal ratio	PAS	pyrotechnic arming switch
F	frequency	PCM	pulse code modulated
FA	flight acceptance	PM	phase modulated
FCS	flight command subsystem	PN	pseudo-random noise
FLT	flight model	PSK	phase-shift keyed
FTS	flight telemetry subsystem	PSU	pyrotechnic switching unit

Nomenclature (contd)

Symbols, Abbreviations, and Definitions (contd)

PTM	proof test model	WP90, WP270	Mercury warm poles at 90°, 270° longitude
PYRO	pyrotechnic (subsystem)	X	down-range position
q	heating rate	X, Y, Z	spacecraft coordinates
QC	quantitative command	Y	number of earth orbits
R	range; radius; radius from center of earth	α	absorptivity
R&AD	research and advanced development	$\alpha, \beta, \gamma, \delta, \epsilon$	Venus radar-identified features
R, S, T	target plane coordinate vectors	γ	atmospheric entry angle
reg	regulated; regulator	δ	incremental change
req	required; requirement	ϵ	emissivity
RF	radio frequency	Γ	flight path angle
RFS	radio frequency subsystem	ζ	angle between S and a vector to a celestial body
S	spacecraft/launch vehicle separation time	η	angle between T and projection in R-T plane of a vector to a celestial body
SCR	silicon controlled rectifier	θ	angle from T clockwise to B
SDS	science data subsystem	σ	standard deviation; ballistic coefficient
SIT	separation initiated timer	ϕ, θ, ψ	orientation angles for antenna hinge axis
SNR	signal-to-noise ratio	ω	pitch angle
ST/ N_0	signal-to-noise ratio (data channel)		
T	temperature		
TA	type approval		
TC	thermal control (subsystem)		
TCM	thermal control model		
TV	television		
TVS	television subsystem		
TWT	traveling wave tube		
UJT	unijunction transistor		
UV	ultraviolet		
V, V	inertial velocity		
V_∞	hyperbolic excess speed		
ΔV	velocity change		
W	cross range position		
\dot{W}	cross range velocity		

Subscripts and Definitions

B	generalized body
<i>c</i>	conductive; convective
<i>e</i>	execution errors
E	earth; entry
<i>h</i>	hinge angle
M	Mercury
<i>n</i>	nose cap; generalized subscript
<i>r</i>	radiative
S	sun
V	Venus

References

1. Sturms, F. M., Jr., *Trajectory Analysis of an Earth-Venus-Mercury Mission in 1973*, Technical Report 32-1062. Jet Propulsion Laboratory, Pasadena, Calif., Jan. 1, 1967.
2. Brereton, R. G., et al., *Venus/Mercury Swingby With Venus Capsule. Preliminary Science Objectives and Experiments for Use in Advanced Mission Studies*, Technical Memorandum 33-332. Jet Propulsion Laboratory, Pasadena, Calif., May 1, 1967.
3. *Study of a 1973 Venus-Mercury Mission with a Venus Entry Probe*, Document 760-1. Jet Propulsion Laboratory, Pasadena, Calif., June 15, 1967.
4. *Mariner Venus/Mercury 70 (MVM70) Mission Feasibility Study*, Document 760-14. Jet Propulsion Laboratory, Pasadena, Calif., Sept. 19, 1967.
5. *Scientific Strategy, Objectives, and Experiments for Mariner Missions from 1970 through 1973*, Document 900-94. Jet Propulsion Laboratory, Pasadena, Calif., Oct. 16, 1967.
6. Hess, H. H., "Planetary Exploration 1968-1975," Report by the Space Science Board, National Academy of Sciences, July 1968.
7. Mackin, R. J., Jr., et al., *Scientific Questions for the Exploration of the Terrestrial Planets and Jupiter: A Progress Report of the Advanced Planetary Missions Technology Program*, Technical Memorandum 33-410. Jet Propulsion Laboratory, Pasadena, Calif., Oct. 1, 1968.
8. Ash, M. E., Shapiro, I. I., and Smith, W. B., "Astronomical Constants and Planetary Ephemerides Deduced from Radar and Optical Observations," *Astron. J.*, Vol. 72, pp. 338-350, 1967.
9. Adams, J. B., Conel, J. E., Dunne, J. A., Fanale, F., Holstrom, G. B., and Loomis, A. A., "Strategy for Scientific Exploration of the Terrestrial Planets," *Rev. of Geophys.*, Vol. 7, Aug. 1969 (in press).
10. Lyttleton, R. A., "The Internal Structures of Mercury and Venus," *Astrophys. and Space Sci.*, Vol. 3, 1969 (in press).
11. Melbourne, W. B., *Constants and Related Information for Astrodynamical Calculations*, Technical Report 32-1306. Jet Propulsion Laboratory, Pasadena, Calif., July 15, 1968.
12. Anderson, J. D., *Determination of Earth-Mercury Distance from Fly-by Spacecraft Trajectories*, Technical Memorandum 311-102. Jet Propulsion Laboratory, Pasadena, Calif., Jan. 31, 1969.
13. Newburn, R., "The Exploration of Mercury, the Asteroids, the Major Planets and Their Satellite Systems, and Pluto," *Advances in Space Science and Technology*. Academic Press, 1961.
14. Minovitch, M. A., *The Determination and Characteristics of Ballistic Interplanetary Trajectories Under the Influence of Multiple Planetary Attractions*, Technical Report 32-464. Jet Propulsion Laboratory, Pasadena, Calif., Oct. 31, 1963.

References (contd)

15. Soter, S., and Ulrichs, J., "Rotation and Heating of the Planet Mercury," *Nature*, Vol. 214, June 24, 1967.
16. Goldstein, R. M., *Radar Studies of Venus*, Technical Report 32-1081. Jet Propulsion Laboratory, Pasadena, Calif., 1967.
17. Sturms, F. M., Jr., "Statistical Analysis of Three Midcourse Corrections on an Earth-Venus-Mercury Trajectory," *Space Programs Summary 37-37*, Vol. IV, pp. 1-10. Jet Propulsion Laboratory, Pasadena, Calif., Feb. 28, 1966.
18. Gates, C. R., *A Simplified Model of Midcourse Execution Errors*, Technical Report 32-504. Jet Propulsion Laboratory, Pasadena, Calif., Oct. 15, 1963.
19. Melbourne, W. G., "The Determination of Planetary Masses from Radio Tracking of Space Probes and Planetary Radar," presented at the 12th Planetary Meeting of COSPAR. Prague, Czechoslovakia, May 11-24, 1969.
20. *Engineering Study to Support Centaur Mariner '69 Missions*, Report No. GDC-BTD 67-068, General Dynamics/Convair Division, San Diego, Calif.
21. Clarke, V. C. Jr., et al, "One-Way Transfers to Mercury and Jupiter," *Design Parameters for Ballistic Interplanetary Trajectories Part II*, Technical Report 32-77. Jet Propulsion Laboratory, Pasadena, Calif., Jan. 15, 1966.
22. Sturms, F. M., "Earth-Venus-Mercury Mission Opportunities in the 1970's," *Space Programs Summary 37-38*, Vol. IV, pp. 1-5, Jet Propulsion Laboratory, Pasadena, Calif., June 30, 1966.
23. Wallace, R. Allen, *Trajectory Analysis of a 1975 Mission to Mercury via an Impulsive Flyby of Venus*, AAS Paper No. 68-113. Sept. 3-5, 1968.
24. Sturms, F. M., "An Earth-Venus-Mercury Mission Opportunity in 1978," *Space Program Summary 37-54*, Vol. III, pp. 26-29. Jet Propulsion Laboratory, Pasadena, Calif., Dec. 31, 1968.
25. Manning, Larry A., *Minimal Energy Ballistic Trajectories for Manned and Unmanned Missions to Mercury*, NASA TN D-3900. Washington, D.C., April 1967.
26. *1972 Venus Flyby/Entry Probe Mission Study*, Book I, Final Technical Report prepared for the Jet Propulsion Laboratory by AVCO Corp., AV SSD-080-68-RR, April 1968.
27. Proposed Jet Propulsion Laboratory Technical Report publication entitled *Parametric Analysis of Venus Entry Heat Shield Requirements*, by W. Jaworski and R. G. Nagler.
28. Spiegel, J. M., Wolf, F., and Zeh, D. W., *Simulation of Venus Atmospheric Entry by Earth Reentry*, AIAA Paper No. 68-1148. Williamsburg, Va., Dec. 3-4, 1968.